

BEM SOLUTIONS OF MAGNETOHYDRODYNAMIC FLOW EQUATIONS
UNDER THE TIME AND AXIAL-DEPENDENT MAGNETIC FIELD

A THESIS SUBMITTED TO
THE GRADUATE SCHOOL OF NATURAL AND APPLIED SCIENCES
OF
MIDDLE EAST TECHNICAL UNIVERSITY

BY

ELİF EBREN KAYA

IN PARTIAL FULFILLMENT OF THE REQUIREMENTS
FOR
THE DEGREE OF DOCTOR OF PHILOSOPHY
IN
MATHEMATICS

SEPTEMBER 2021

Approval of the thesis:

**BEM SOLUTIONS OF MAGNETOHYDRODYNAMIC FLOW EQUATIONS
UNDER THE TIME AND AXIAL-DEPENDENT MAGNETIC FIELD**

submitted by **ELİF EBREN KAYA** in partial fulfillment of the requirements for the degree of **Doctor of Philosophy in Mathematics Department, Middle East Technical University** by,

Prof. Dr. Halil Kalıpçılar
Dean, Graduate School of **Natural and Applied Sciences**

Prof. Dr. Yıldırım Ozan
Head of Department, **Mathematics**

Prof. Dr. Münevver Tezer-Sezgin
Supervisor, **Department of Mathematics, METU**

Examining Committee Members:

Prof. Dr. Canan Bozkaya
Department of Mathematics, METU

Prof. Dr. Münevver Tezer-Sezgin
Department of Mathematics, METU

Prof. Dr. Ömür Uğur
Institute of Applied Mathematics, METU

Prof. Dr. Gülnihal Meral
Department of Mathematics, Ankara Yıldırım Beyazıt University

Prof. Dr. Selçuk Han Aydın
Department of Mathematics, Karadeniz Technical University

Date:

I hereby declare that all information in this document has been obtained and presented in accordance with academic rules and ethical conduct. I also declare that, as required by these rules and conduct, I have fully cited and referenced all material and results that are not original to this work.

Name, Surname: Elif Ebren Kaya

Signature :

ABSTRACT

BEM SOLUTIONS OF MAGNETOHYDRODYNAMIC FLOW EQUATIONS UNDER THE TIME AND AXIAL-DEPENDENT MAGNETIC FIELD

Ebren Kaya, Elif

Ph.D., Department of Mathematics

Supervisor: Prof. Dr. Münevver Tezer-Sezgin

September 2021, 167 pages

In the thesis, four different MHD duct flow problems are solved by using the Dual Reciprocity Boundary Element Method (DRBEM) with the suitable boundary conditions according to the physics of the problem. The two-dimensional, steady or unsteady, fully-developed MHD flow of a viscous, incompressible and electrically conducting fluid is considered in a long pipe of rectangular cross-section (duct) under the effect of an externally applied magnetic field which is either uniform or time-dependent or axially changing. The inductionless MHD flow with temperature dependent viscosity and heat transfer is the first considered problem. In this problem, the induced magnetic field is neglected due to the small magnetic Reynolds number assumption. Secondly, the MHD duct flow under a time-varied external magnetic field is studied. Then, we turn our concern to MHD flow problems under an axial-dependent magnetic field varying in the streamwise direction (pipe-axis direction) in the third and the fourth problems. Specifically, the inductionless MHD flow with electric potential is considered under the effect of the axially-changing magnetic field as the third problem. Adding the induced magnetic field to the velocity and electric potential equations as a triple is the last MHD flow problem considered in the thesis.

The parametrix BEM implementation is also presented for the solution of the variable coefficient convection-diffusion type equations. The influence of the magnetic fields on the MHD flows is investigated and simulated in terms of the velocity, temperature, induced magnetic field and electric potential contours for several values of physical parameters.

Keywords: Magnetohydrodynamics, Dual Reciprocity Boundary Element Method, Parametrix BEM, Time-varied Magnetic Field, Axial-depedent Magnetic Field

ÖZ

MAGNETOHİDRODİNAMİK KANAL AKIŞLARININ KARŞILIKLI SINIR ELEMENLARI METODU İLE ÇÖZÜMÜ

Ebren Kaya, Elif

Doktora, Matematik Bölümü

Tez Yöneticisi: Prof. Dr. Münevver Tezer-Sezgin

Eylül 2021 , 167 sayfa

Bu tezde, dört farklı Magnetohidrodinamik (MHD) kanal akış problemi, problemin fiziğine göre uygun sınır koşulları ile birlikte karşılıklı sınır elemanları metodu (DR-BEM) kullanılarak çözülmüştür. Viskoz, sıkıştırılamaz ve elektrik ileten sıvının dik-dörtgen kesitli bir kanal içerisindeki iki boyutlu, zamana bağlı veya zamandan bağımsız tam gelişmiş akışı dışarıdan uygulanan bir manyetik alan etkisinde incelenmiştir. Akışı etkileyen manyetik alan ya tek düzedir ya zamana bağlıdır ya da eksenel olarak değişmektedir. Ele alınan ilk problem, sıcaklığa bağlı viskoziteye ve ısı transferine sahip indüksiyonsuz MHD akışıdır. Bu problemde, indüklenen manyetik alan küçük manyetik Reynolds sayısı varsayımından dolayı ihmal edilmiştir. İkinci problem olarak, dışarıdan uygulanan ve zamana bağlı manyetik alan etkisindeki MHD akış çalışılmıştır. Daha sonra ise, üçüncü ve dördüncü problem olarak akım yönündeki eksen boyunca değişen bir manyetik alan etkisindeki MHD akış problemleri çözülmüştür. Üçüncü problemdeki MHD akışı elektrik potansiyeline sahip fakat indüksiyonsuz bir akıştır. Dördüncü problemde ise üçüncü problemdeki MHD akışa indüklenen manyetik alan eklenerek problem denklemleri hız, elektrik potansiyel ve

indüklenen manyetik alan olarak üçlü çözülmüştür. Değişken katsayılı konveksiyon-difüzyon tipi denklemlerin çözümü için parametre sınır elemanı metodu (parametrix BEM) da kullanılmıştır. Uygulanan manyetik alanların MHD akışlarına etkisi, çeşitli fiziksel problem parametre değerleri için hız, sıcaklık, indüklenen manyetik alan ve elektrik potansiyeli açısından incelenmiş ve simülasyonları yapılmıştır.

Anahtar Kelimeler: Magnetohidrodinamik, Karşılıklı Sınır Elemanları Metodu, Parametre Sınır Elemanı Metodu, Zamana Bağlı Manyetik Alan, Eksene Bağlı Manyetik Alan

To my family

ACKNOWLEDGMENTS

Firstly, I would like to express my sincere gratitude to my supervisor Prof. Dr. Münevver Tezer for the continuous support of my Ph.D study and related research, for her patience, motivation, and immense knowledge. Her guidance encouraged me in all the time of research and writing of this thesis. I could not have imagined having a better supervisor and mentor for my Ph.D study.

Besides my supervisor, I would also like to thank my defense committee members Prof. Dr. Canan Bozkaya, Prof. Dr. Ömür Uğur, Prof. Dr. Gülnihal Meral and Prof. Dr. Selçuk Han Aydın for their valuable suggestions and guidance.

I gratefully acknowledge the financial support of The Scientific and Technological Research Council of Turkey (TÜBİTAK) with the program BİDEB 2211 (National Graduate Scholarship Programme).

Also, I would like to extend my sincerest thanks to my friends Cemre Bozyiğit and Merve Gürbüz Çaldağ for their kind friendship, honest companionship and their help while writing process of the thesis.

Moreover, I would like to express my gratitude to my mother Sevim and my father Erdoğan for their unconditional love and motivation which provide me success and happiness in my whole life. They were always with me in all the stages of my academic and social life. Words fail to express how grateful I am to both of you.

Last but not the least, I want to show my heartfelt gratitude to my husband Ruşen for his continuous encouragement and understanding.

TABLE OF CONTENTS

ABSTRACT	v
ÖZ	vii
ACKNOWLEDGMENTS	x
TABLE OF CONTENTS	xi
LIST OF TABLES	xiv
LIST OF FIGURES	xv
LIST OF ABBREVIATIONS	xx
CHAPTERS	
1 INTRODUCTION	1
1.1 Navier-Stokes equations	5
1.2 Inductionless MHD flow and heat transfer with temperature dependent viscosity	7
1.3 MHD duct flow with time-varied external magnetic field	11
1.4 Inductionless MHD flow and electric potential with variably conducting walls under axial-dependent magnetic field	17
1.5 MHD duct flow with axially-changing external magnetic field	21
1.6 Literature Survey	26
1.7 Originality of the Thesis	33
1.8 Plan of the Thesis	35

2	THE BOUNDARY AND THE DUAL RECIPROCITY BOUNDARY ELEMENT METHODS	37
2.1	The BEM procedure for the Laplace equation $\nabla^2 u = 0$	39
2.1.1	Boundary discretization with constant elements	41
2.1.2	Boundary discretization with linear elements	44
2.2	The BEM procedure for the Poisson's equation $\nabla^2 u = b(x, y)$	48
2.2.1	Composite trapezoidal rule	48
2.3	The parametrix BEM procedure for the diffusion equation containing a variable coefficient	49
2.4	DRBEM procedure for the Poisson's equation $\nabla^2 u = b(x, y)$	52
2.4.1	DRBEM procedure for the equation $\nabla^2 u = b(x, y, u)$	56
2.4.2	DRBEM procedure for the equation $\nabla^2 u = b(x, y, u, u_x, u_y)$. .	58
2.4.3	DRBEM procedure for the equation $\nabla^2 u = b(x, y, t, u, u_t, u_x, u_y)$	60
2.4.3.1	Implicit Euler method for time integration scheme	61
3	THE BEM SOLUTIONS OF THE MHD DUCT FLOW PROBLEMS	63
3.1	Parametrix BEM and DRBEM applications to inductionless MHD flow and heat transfer with temperature dependent viscosity	64
3.1.1	Parametrix BEM-DRBEM approach	65
3.1.2	DRBEM-DRBEM approach	70
3.2	DRBEM applications to MHD duct flow with time-varied external magnetic field	72
3.2.1	$R_e = 1, R_m = 1$ case	73
3.2.2	Varying R_e and R_m case	75
3.3	DRBEM applications to inductionless MHD flow and electric potential with variably conducting walls under axial-dependent magnetic field	78

3.4	DRBEM applications to MHD duct flow with axially dependent external magnetic field	83
4	NUMERICAL RESULTS OF THE MHD DUCT FLOW PROBLEMS . . .	87
4.1	Inductionless MHD flow and heat transfer with temperature dependent viscosity	88
4.2	MHD duct flow with time-varied external magnetic field	104
4.2.1	$R_e = 1, R_m = 1$ case	105
4.2.2	Effects of R_e and R_m on the MHD flow	118
4.3	Inductionless MHD flow with electric potential under axially-changing magnetic field	127
4.3.1	Uniform magnetic field	129
4.3.1.1	Uniform magnetic field: Non-conducting duct walls . .	130
4.3.1.2	Uniform magnetic field: Non-conducting side walls, variably conducting Hartmann walls	131
4.3.1.3	Uniform magnetic field: Variably conducting walls with the same conductivity ratio	132
4.3.1.4	Uniform magnetic field: Variably conducting walls with different conductivity ratios	133
4.3.2	Axial dependent magnetic field: Variably conducting walls . .	135
4.4	MHD duct flow with axially-changing external magnetic field	139
5	CONCLUSION	153
	REFERENCES	157
	CURRICULUM VITAE	165

LIST OF TABLES

TABLES

Table 4.1	Variable coefficient heat conduction problems	89
Table 4.2	Error L2 norms of the test problems for increasing number of boundary elements.	90
Table 4.3	Nusselt number, Nu , by using the pBEM-DRBEM with 100 boundary elements ($Br = 0, B = 1$).	99
Table 4.4	Nusselt number, Nu , by using the pBEM-DRBEM with 180 boundary elements ($Br = 0, B = 1$).	99
Table 4.5	Nusselt number, Nu , by using the DRBEM-DRBEM with 180 boundary elements ($Br = 0, B = 1$).	99
Table 4.6	CPU Times with 180 boundary elements ($Br = 0, B = 1$).	100
Table 4.7	The volumetric flow rate Q , $f(t) = e^t$, $M = 20$, $N = 120$, $\alpha = \pi/2$	113
Table 4.8	The volumetric flow rate Q for the step function $f(t)$, $M = 20$, $N = 120$, $\alpha = \pi/2$	117

LIST OF FIGURES

FIGURES

Figure 1.1	Physical configuration of the problem	8
Figure 1.2	Physical configuration of axially-changing MHD flow	17
Figure 2.1	Configuration of the problem domain and the boundary conditions	39
Figure 2.2	Internal angle at the boundary point i	41
Figure 2.3	Configuration for constant elements discretization	42
Figure 2.4	Configuration for linear elements discretization	44
Figure 2.5	Nodes connection of linear elements	46
Figure 3.1	Physical configuration of the problem	64
Figure 3.2	Physical configuration of the rectangular pipe	78
Figure 3.3	The boundary conditions on non-conducting duct walls	80
Figure 3.4	The boundary conditions on variably conducting duct walls . . .	80
Figure 3.5	The boundary conditions for the velocity and induced magnetic field	84
Figure 3.6	The boundary conditions of Φ on the insulated and no-slip duct walls	84
Figure 4.1	Heat conduction problems. Isotherms from parametrix BEM and Exact solutions.	89

Figure 4.2	Equavelocity and isolines for $m = 0$, $Br = 0$ and $B = 1$. (a) pBEM-DRBEM, (b) DRBEM-DRBEM	94
Figure 4.3	Equavelocity and isolines for $M = 3$, $m = 0$ and $Br = 0$. (a) pBEM-DRBEM, (b) DRBEM-DRBEM	95
Figure 4.4	Equavelocity and isolines for $M = 3$, $m = 3$ and $Br = 1$. (a) pBEM-DRBEM, (b) DRBEM-DRBEM	96
Figure 4.5	Equavelocity and isolines for $M = 3$, $Br = 0$ and $B = 1$. (a) pBEM-DRBEM, (b) DRBEM-DRBEM	97
Figure 4.6	Equavelocity and isolines for $M = 3$, $Br = 1$ and $B = 1$. (a) pBEM-DRBEM, (b) DRBEM-DRBEM	98
Figure 4.7	Midline velocity profiles at $y = 0.5$ using DRBEM-DRBEM. . .	101
Figure 4.8	Midline velocity profiles at $y = 0.5$ using DRBEM-DRBEM. . .	101
Figure 4.9	Midline temperature profiles at $y = 0.5$ using DRBEM-DRBEM.	102
Figure 4.10	Midline velocity profiles at $y = 0.5$, and $M = 3$, $m = 5$ and $Br = 1$	103
Figure 4.11	Midline velocity profiles at $y = 0.5$, and $Br = 1$, $B = 1$, $m = 3$.	103
Figure 4.12	Midline velocity profiles at $y = 0.5$, and $Br = 1$, $B = 1$, $M = 3$.	104
Figure 4.13	Midline temperature profiles at $y = 0.5$, and $Br = 1$, $B = 1$, $m = 3$	104
Figure 4.14	Velocity and induced magnetic field lines, $f(t) = 1$, $B_0(t) =$ B_0 , $M = 20$, $N = 120$, $\alpha = \pi/2$	107
Figure 4.15	Velocity and induced magnetic field lines, $f(t) = 1+t$, $M = 20$, $\alpha = \pi/2$, $t_n = 0.10$	108
Figure 4.16	Velocity and induced magnetic field lines, $f(t) = 1+t$, $M = 20$, $\alpha = \pi/2$, $t_n = 0.14$	108

Figure 4.17	Velocity and induced magnetic field lines, $f(t) = 1+t$, $M = 20$, $\alpha = \pi/2$, $t_n = 0.14$, $\Delta t = 0.01$ and $N = 140$	108
Figure 4.18	Velocity and induced magnetic field lines, $f(t) = 1+t$, $M = 20$, $\alpha = \pi/2$	109
Figure 4.19	Velocity and induced magnetic field lines, $f(t) = 1+t$, $M = 20$, $\alpha = \pi/3$	111
Figure 4.20	Velocity and induced magnetic field lines, $f(t) = 1+t$, $M = 20$, $\alpha = \pi/4$	111
Figure 4.21	Velocity and induced magnetic field lines, $f(t) = 1+t$, $M = 50$, $\alpha = \pi/2$	112
Figure 4.22	Velocity and induced magnetic field lines, $f(t) = e^t$, $M = 20$, $\alpha = \pi/2$	112
Figure 4.23	Velocity and induced magnetic field lines, $f(t) = e^t$, $M = 50$, $\alpha = \pi/2$	113
Figure 4.24	Velocity and induced magnetic field lines, $f(t) = \cos(2\pi t)$, $M = 20$, $\alpha = \pi/2$	114
Figure 4.25	Velocity and induced magnetic field lines, $f(t)$ is impulse func- tion, $M = 20$, $\alpha = \pi/2$	115
Figure 4.26	Velocity and induced magnetic field lines, step function, $M =$ 20 , $\alpha = \pi/2$	116
Figure 4.27	Velocity and induced magnetic field lines, modified step func- tion, $M = 20$, $\alpha = \pi/2$	117
Figure 4.28	Velocity contours, $f(t) = e^t$, $R_e = 1$, $R_m = 1, 3, 5$, $M = 20$, $\alpha = \pi/2$	121
Figure 4.29	Velocity contours, $f(t) = e^t$, $R_m = 1$, $R_e = 5, 10, 25$, $M = 20$, $\alpha = \pi/2$	122

Figure 4.30	Velocity and induced magnetic field, $R_e = 1$, $M = 20$, $\alpha = \pi/2$.	123
Figure 4.31	Velocity and induced magnetic field, $R_m = 1$, $M = 20$, $\alpha = \pi/2$.	123
Figure 4.32	Velocity and induced magnetic field, $R_e = 10$, $R_m = 2$, $M = 20$, $\alpha = \pi/2$.	124
Figure 4.33	Velocity and induced magnetic field, $f(t) = \cos(2\pi t)$, $R_e = R_m = 1$, $M = 20$, $\alpha = \pi/2$.	125
Figure 4.34	Velocity and induced magnetic field, at transient levels, $f(t) = \cos(2\pi t)$, $M = 20$, $\alpha = \pi/2$.	125
Figure 4.35	Velocity and induced magnetic field, $f(t) = \cos(2\pi t)$, $R_e = 5$, $R_m = 2$, $M = 20$, $\alpha = \pi/2$.	126
Figure 4.36	Flow and electric potential boundary conditions on non-conducting duct walls	128
Figure 4.37	Flow and electric potential boundary conditions on variably conducting duct walls	128
Figure 4.38	Velocity and electric potential profiles with no-slip and non-conducting duct walls. Uniform magnetic field, $\alpha = \pi/2$.	130
Figure 4.39	Velocity and electric potential profiles with no-slip and, non-conducting side walls, variably conducting Hartmann walls, uniform magnetic field, $\alpha = \pi/2$.	131
Figure 4.40	Velocity and electric potential profiles with no-slip and well-conducting duct walls, uniform magnetic field, $\alpha = \pi/2$.	133
Figure 4.41	Velocity and electric potential profiles with different conductivity ratios on the no-slip duct walls. Uniform magnetic field, $\alpha = \pi/2$.	134
Figure 4.42	Velocity profiles for axial dependent magnetic field, $M = 50$, $\alpha = \pi/2$.	137

Figure 4.43	Velocity profiles for axial dependent magnetic field, $M = 50$, $\alpha = \pi/2$	138
Figure 4.44	Flow and induced magnetic field boundary conditions on the duct walls.	139
Figure 4.45	The boundary conditions of Φ on the insulated and no-slip duct walls.	140
Figure 4.46	Velocity and induced magnetic field ($V = B = 0$ duct walls), $M = 10$, $R_m = 2$. Axially-changing magnetic field, $\alpha = \pi/2$	142
Figure 4.47	Velocity and induced magnetic field ($V = B = 0$ duct walls), $M = 30$, $R_m = 2$. Axially-changing magnetic field, $\alpha = \pi/2$	143
Figure 4.48	Velocity and induced magnetic field ($V = B = 0$ duct walls), $M = 50$, $R_m = 2$. Axially-changing magnetic field, $\alpha = \pi/2$	144
Figure 4.49	Velocity and induced magnetic field ($V = B = 0$ duct walls), $M = 30$, $R_m = 5$. Axially-changing magnetic field, $\alpha = \pi/2$	145
Figure 4.50	Velocity and induced magnetic field ($V = B = 0$ duct walls), $M = 30$, $R_m = 25$. Axially-changing magnetic field, $\alpha = \pi/2$	146
Figure 4.51	Velocity and induced magnetic field ($V = B = 0$ duct walls), $M = 30$, $R_m = 1$. Axially-changing magnetic field, $\alpha = \pi/2$	147
Figure 4.52	Velocity and induced magnetic field ($V = 0$, $B = 0$ side walls, $V = 0$, $\frac{\partial B}{\partial n} = 0$ Hartmann walls), $M = 30$, $R_m = 1$. Axially-changing magnetic field, $\alpha = \pi/2$	148
Figure 4.53	Velocity, induced magnetic field and electric current ($V = B =$ $\Phi = 0$ walls), $M = 30$, $R_m = 2$. Axially-changing magnetic field, $\alpha = \pi/2$	150
Figure 4.54	Velocity, induced magnetic field and electric current ($V = B =$ 0 , $\Phi = 0$ side walls, $\frac{\partial \Phi}{\partial n} = 0$ Hartmann walls), $M = 30$, $R_m = 2$. Axially-changing magnetic field, $\alpha = \pi/2$	151

LIST OF ABBREVIATIONS

ABBREVIATIONS

BEM	Boundary element method
DRBEM	Dual reciprocity boundary element method
CFD	Computational Fluid dynamics element method
MHD	Magnetohydrodynamics
B_0	induced magnetic field intensity
H_0	strenght of the magnetic field
B	induced magnetic field
E	electric field
J	electric current density
B	viscosity parameter
Br	Brinkmann number
f	Lorentz force
H, G	BEM matrices
F	coordinate matrix
T	temperature
L_0	characteristic length
Nu	Nusselt number
Re	Reynolds number
R_m	magnetic Reynolds number
c	conductivity ratio
c_p	specific heat capacity
m	Hall parameter
n	unit outward normal to the boundary

k	thermal conductivity
p	pressure
t	time
q	permittivity of vacuum
q'''	heat source
v_c	characteristic velocity
\mathbf{u}	velocity field
Φ	electric potential
μ	dynamic viscosity
μ_0	magnetic permeability of vacuum
σ	electric conductivity
β	Hall factor
ρ	density
ν	dynamic viscosity
Ω	problem domain
Γ	boundary of the problem domain
ϵ_0	permittivity of vacuum
κ	relaxation parameter
α	angle with the x or y -axis
x, y, z	Cartesian coordinates

CHAPTER 1

INTRODUCTION

Fluid mechanics is a branch of mechanics that examines fluids in two subsystems as fluid statics and fluid dynamics. Fluid statics studies the fluid at rest however, fluid dynamics studies the behavior of fluid in motion and the effect of forces on fluid motion which comprise both gases and liquids. Since fluid dynamics includes the study of the motion of fluid, one of the first concept is to specify that movement. The term used to describe the physical properties of the movement of liquid is flow. The flow of a fluid may be steady or unsteady, laminar or turbulent, compressible or incompressible, viscous or inviscid, uniform or non-uniform in pipe or open-channel. A flow can be one, two or three dimensional. Fluid dynamics has several subdisciplines including aerodynamics which studies air and other gases in motion and hydrodynamics studying of liquids in motion.

Fluids are integral part of our daily life. So, its application spans an extremely wide range both in human everyday activities and in the design of modern engineering systems. Primarily, fluid dynamics has a vital role in human bodies. The heart constantly pumps blood to all other part of the body through the arteries and veins. Air flows in alternating directions in the lungs. Artificial hearts, dialysis and breathing machines are designed using fluid dynamics. Similar to the piping and ducting systems of heating and air-conditioning, the piping systems for water, natural gas, and sewage are also constructed by using the basis of fluid dynamics in the houses we live in. There are numerous natural phenomena governed by the principles of the fluid dynamics such as the water flow through rivers, rising the ground water to the top of the trees, rain cycle, ocean waves, hurricanes and plate tectonics. In the design of airplanes, rockets, submarines, wind turbines and in transportation systems the analysis of fluid

motion plays an important role. From the variety of examples, it can be understood that almost every area the fluid dynamics has an application. Without fluid flows, neither life would be possible on Earth, nor technological processes that determine the high standard of our living nowadays. Therefore, flows are vital [1].

Fluid motion is governed by the Navier-Stokes equations, a set of coupled and non-linear partial differential equations that obey the three laws of conservation:

- 1) Conservation of Mass (Continuity Equation)
- 2) Conservation of Momentum (Newton's Second Law)
- 3) Conservation of Energy (First Law of Thermodynamics of Energy Equation)

Basically, these principles state that mass, momentum and energy are conserved and they are the fundamental aspects of fluid dynamics.

A fluid dynamics problem involves various properties of fluid such as the velocity, temperature, pressure and density of the fluid, as functions of space and time. The analytical solution of a fluid dynamics problem is generally impossible and scientists require to do laboratory experiments. However, the design and construction of these experiments are usually difficult and costly.

Magnetohydrodynamics (MHD) is a branch of fluid mechanics analyzing the flow of an electrically conducting fluid in the presence of a magnetic field. The magnetic field induces currents in an electrically conducting flow generating the Lorentz force. Thus, MHD is an integrated area of fluid mechanics and electrodynamics. An externally applied magnetic field has influence upon the conducting fluid such as plasma and liquid metal and so it changes motion of the fluid. This influence is mathematically expressed by adding the electromagnetic force in the equations of motion. The governing MHD equations are the continuity equation, the Navier-Stokes equations of hydrodynamics and Maxwell's equations of electromagnetism through Ohm's law [2]. The non-linear and Lorentz force terms in the MHD equations make the problems difficult to study. The interaction of an electrically conducting fluid and a magnetic field has very important industrial, biological and engineering applications such as MHD generators and pumps, fusion reactors, flowmeters, blood plasmas and etc. Therefore, the numerical methods become crucial in the study the MHD equations

with the absence of an analytical solution. MHD generators of rectangular cross-section are widespread applications of MHD flow. They are made of tubes having insulating walls which are cut with two electrodes placed parallel to each other and perpendicular to insulating walls. This configuration resembles the MHD flow in a rectangular duct [14]. In a duct, electrically conducting fluid is driven by a constant pressure gradient. In the thesis, both steady and unsteady flows of a viscous, incompressible, electrically conducting fluid are considered in a long channel of rectangular cross-section under the influence of an externally applied magnetic field.

Computational Fluid Dynamics (CFD) enables scientists to examine the physical characteristic of fluid flow by solving the mathematical equations using numerical techniques without requiring laboratory experiments. CFD is particularly dedicated to the fluids that are in motion. Nowadays, CFD has an important place as a new third discipline together with the theoretical and experimental methods due to the growth of computer power. This growth in CFD provides a qualitative prediction and analysis for the fluid flow. Moreover, even larger and more complex problems of CFD can be tackled with highly performed computer. There are many numerical methods used to simulate the behavior of the flow in CFD. Among these are the finite element method (FEM), the finite difference method (FDM), the finite volume method (FVM) and the boundary element method (BEM). The methods except the BEM, depend on domain discretization. These methods discretize the whole problem domain with element or cells having some difficulties for the curved geometries and the boundary conditions.

Indeed, FDM uses the Taylor series expansions of the derivatives in a considered problem to obtain the discrete system of equations. However, the application of FDM for a problem in complex geometries is very hard since it requires a structured grid for the method. FVM presents a discretization of the governing equations in integral form by discretizing the considered problem domain into a number of control volumes and it balances fluxes through control volumes [3]. However, fluxes computations at irregular mesh, especially near the boundary of the problem domain cause huge amount of effort. FEM discretizes the problem domain into smaller parts called as finite elements. Partial differential equation is multiplied with the shape functions and integrated over each element or the variational form of the PDE is obtained

which is to be minimized [4]. But, the computational costs of the FEM is high since the whole domain discretization requires process of very large amount of data quantities. On the other hand, BEM requires only the boundary discretization that makes it an effective alternative to domain discretization techniques such as FEM, FDM and FVM. With the help of a fundamental solution, the BEM transforms the partial differential equations to the boundary integral equations and only the discretized obtained boundary values provide a solution at once at the interior for the considered problem [5]. Therefore, its computational cost is relatively small compared to the domain type discretization methods. Generally, a fundamental solution of the whole governing equation is not available when the partial differential equation involves time derivative, convection and some nonlinear terms. In such a case, a fundamental solution that corresponds to not all but some terms of the governing equations is used. Therefore, the basic integral equations can include domain integrals due to the terms not used in the fundamental solution. For instance, in parametric BEM, these domain integrals are computed numerically [6], however in dual reciprocity BEM (DRBEM) they are approximated with the coordinate matrix [7]. The DRBEM coordinate matrix is constructed by series of radial basis functions for once and it handles the nonlinear terms in the equation easily. Furthermore, the coordinate matrix of the DRBEM procedure enables one to approximate the spatial derivatives of the unknowns in the equation and even on the boundary.

In this chapter, fundamental equations of the fluid dynamics and electrodynamics are introduced in Section 1.1 and the governing inductionless MHD duct flow equations are derived in terms of momentum, Maxwell's and energy equations in Section 1.2 where the viscosity is assumed to be temperature dependent. The velocity and the induced magnetic field equations under time varied magnetic field are obtained for rectangular channels in Section 1.3. The equations for the velocity and the electric potential are obtained for the case of axial-dependent magnetic field in Section 1.4 and lastly, the velocity, the induced magnetic field and the electric potential equations again for the case of axially changing magnetic field are given in Section 1.5. Then, in Section 1.6, literature survey related to the thesis subject takes place. Finally, the originality of the thesis is discussed and the plan of the thesis is presented in Sections 1.7 and 1.8, respectively.

1.1 Navier-Stokes equations

The fundamentals of fluid motion are formed by the Navier-Stokes equations. Most of the engineering problems such as modelling the turbulent hydrodynamic problems, motion of the star, weather movement, flow around an airfoil are characterized by the Navier-Stokes equations. The application of the conservation of mass and the Newton's second law (the conservation of momentum) to a moving medium generates the Navier-Stokes equations. These equations are non-linear partial differential equations in terms of flow velocity and pressure of the fluid which are difficult to solve. Analytical solutions are available only for some simplified physical assumptions in special type regions.

The two-dimensional, unsteady, laminar flow of an incompressible, viscous fluid without body forces are given as [8]

$$\nabla \cdot \mathbf{u} = 0 \quad (1.1)$$

$$\rho \left(\frac{\partial \mathbf{u}}{\partial t} + (\mathbf{u} \cdot \nabla) \mathbf{u} \right) = -\nabla p + \mu \nabla^2 \mathbf{u} + \rho \mathbf{f} \quad (1.2)$$

where $\mathbf{u} = (u, v, 0)$ is the velocity field of the fluid, p is the pressure of the fluid and $\rho \mathbf{f} = (\rho f_x, \rho f_y)$ denotes the body forces acting on the flow. The flow is driven by the pressure gradient ∇p , ρ and μ are the flow density and the dynamic viscosity of the fluid, respectively.

The non-dimensional variables to obtain dimensionless Navier-Stokes equations for an incompressible fluid with a constant viscosity are

$$x' = \frac{x}{L_0}, \quad y' = \frac{y}{L_0}, \quad t' = \frac{tv_c}{L_0}, \quad \mathbf{u}' = \frac{\mathbf{u}}{v_c}, \quad p' = \frac{p}{v_c^2 \rho} \quad (1.3)$$

with a characteristic length L_0 and the characteristic velocity v_c for the region fluid occupied, [9].

Substituting these quantities into equations (1.1) and (1.2) gives the non-dimensional Navier-Stokes equations (dropping the prime '' notations) as

$$\nabla \cdot \mathbf{u} = 0 \quad (1.4)$$

$$\frac{\partial \mathbf{u}}{\partial t} + (\mathbf{u} \cdot \nabla) \mathbf{u} = -\nabla p + \nu \nabla^2 \mathbf{u} + \mathbf{f} \quad (1.5)$$

where ν is the kinematic viscosity and related with the Reynolds number Re as

$$\nu = \frac{1}{Re} = \frac{\mu}{\rho v_c L_0}.$$

The dimensionless quantity Reynolds number Re characterizes the flow of the fluid. When $Re < 2100$ the viscous forces are dominant and generally the flow regime is laminar which means the fluid has a smooth behavior. Otherwise, the flow is turbulent. In this thesis, only the laminar flow will be considered.

Mathematical formulation for the velocity and pressure of a fluid flow determine the behavior of the flow under different physical conditions. This gives great importance in the designing of many technological equipments in which fluid flows. Navier-Stokes equations have aroused a great deal interest since they are the fundamental tools of the fluid flow. Therefore, the numerical solution of the Navier-Stokes equations have been studied widely in literature. Chorin [10] has used the FDM to solve the velocity and pressure of the fluid for the time-dependent equations. Pereira et al. [11] have used fourth-order-accurate scheme for the solution of the Navier-Stokes equations in the velocity-pressure form. They have performed their solution with an implicit Newton-Krylow matrix-free method for stationary problems. For the unsteady flow, they have used a standart fourth-order Runge-Kutta method. Elman [12] has described new strategies for the solution of the system arising from the discretization of the incompressible Navier-Stokes equations. Then, for the solution of the Euler and Navier–Stokes equations, discontinuous Galerkin technique has been used in [13].

When an external magnetic field \mathbf{B} acts on the fluid medium, the balance of linear momentum is written as

$$\rho \left(\frac{\partial \mathbf{u}}{\partial t} + (\mathbf{u} \cdot \nabla) \mathbf{u} \right) = -\nabla p + \mu \nabla^2 \mathbf{u} + (\mathbf{J} \times \mathbf{B}) \quad (1.6)$$

where $\mathbf{J} \times \mathbf{B}$ is the Lorentz force coupling the mechanical and electrodynamic states of the system. The interaction of the moving fluid with the magnetic field induces an electric field $\mathbf{u} \times \mathbf{B}$ driving the electric current \mathbf{J} . The current density in a moving electrically conducting fluid is given by Ohm's law $\mathbf{J} = \sigma(\mathbf{E} + \mathbf{u} \times \mathbf{B})$ where \mathbf{E} is the electrical field. Electrical field is irrotational ($\nabla \times \mathbf{E} = 0$) for a closed medium and it can be expressed by a scalar potential Φ as $\nabla \Phi = -\mathbf{E}$. Applying the curl-operator on Ohm's law for moving fluids and then substitute the electric field and

the current density by using Faraday's law $\nabla \times \mathbf{E} = -\frac{\partial \mathbf{B}}{\partial t}$ and Ampere's law for slowly varying electromagnetic processes $\nabla \times \mathbf{B} = \mu_0 \mathbf{J}$, [2] and the fact that \mathbf{B} is solenoidal $\nabla \cdot \mathbf{B} = 0$, we get the magnetic induction equation

$$\frac{\partial \mathbf{B}}{\partial t} + (\mathbf{u} \cdot \nabla) \mathbf{B} = \frac{1}{\mu_0 \sigma} \nabla^2 \mathbf{B} + (\mathbf{B} \cdot \nabla) \mathbf{u} \quad (1.7)$$

where μ_0 and σ are the magnetic permeability and the electrical conductivity of the fluid. Thus, the coupled systems of Navier-Stokes equation (1.6) including Lorentz force and the magnetic induction equation (1.7) form the basis for the magnetohydrodynamic flow.

In the thesis, all the considered MHD flows are viscous, incompressible and electrically conducting in a long pipe of rectangular cross-section. Inductionless MHD flow and heat transfer is considered in Section 1.2 in terms of the momentum and energy equations. The flow is assumed to be steady and under the influence of a uniform magnetic field. The induced magnetic field is neglected due to the small Reynolds number, however the Hall effect, viscous and Joule dissipations are taken into consideration. The MHD flow under a time-varied external magnetic field is studied in Section 1.3 in terms of the velocity and induced magnetic field equations. In this MHD flow problem, the flow is unsteady in a long pipe and it is fully-developed. In Section 1.4, inductionless MHD flow is considered under the influence of axial-dependent magnetic field. Some magnets are placed on the pipe-axis and they determine the strength of the applied magnetic field and constitute electromagnetic force in the steady flow. The induced magnetic field is neglected due to the small magnetic Reynolds number, however the electric potential from the divergence of Ohm's law is taken into consideration. Finally, the induced magnetic field equation accompanying to the velocity and electric potential equations for the case of axially changing applied magnetic field are studied in Section 1.5.

1.2 Inductionless MHD flow and heat transfer with temperature dependent viscosity

The fundamentals of the fluid motion depend on the Navier-Stokes equations. When the fluid flow applications are considered such as chemical, reactor, nuclear reactor,

cooling of electronic systems or heat exchangers for an electrically conducting fluid then, the magnetic effects together with the heat transfer must be taken into consideration. The temperature equation is more convenient form of the energy equation in fluid dynamics.

In this section, a steady flow of a viscous, incompressible, electrically conducting fluid is considered in a long channel of rectangular cross-section together with its heat transfer. The physical configuration of the flow is shown in Figure 1.1. A uniform magnetic field with intensity B_0 is applied to the duct plane perpendicular to the axis of the channel, i.e. z -axis. A constant pressure gradient $-\frac{dp}{dz}$ is applied in the z -direction and the induced magnetic field is neglected due to the small magnetic Reynolds number assumption. That means, induced magnetic field generated by motion of an electrically conducting fluid is negligible compared to externally applied magnetic field B_0 . The viscosity of the fluid is assumed to vary with the temperature. The magnetic effects on the flow together with the heat transfer must be taken into consideration in some flow applications such as chemical reactor, nuclear reactor, cooling of electronic systems and heat exchangers.

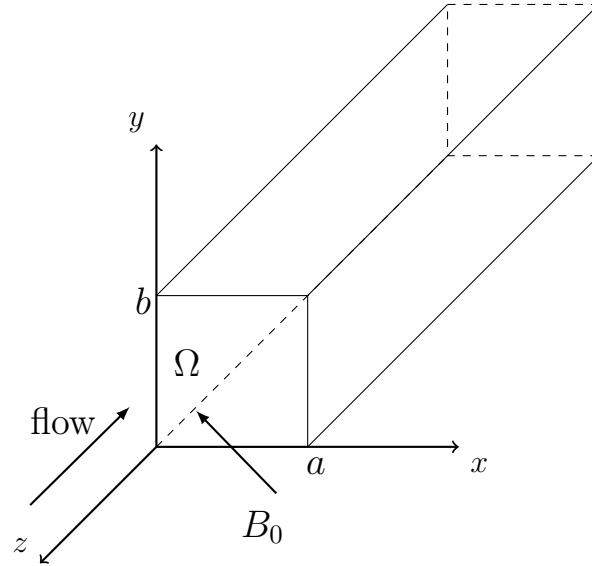


Figure 1.1: Physical configuration of the problem

Both the flow and the temperature are assumed to be steady and fully-developed along the channel. Further, the viscosity of the fluid is exponentially varying with

the temperature. The Joule and viscous dissipations are not neglected as well as the Hall effect which arises from the strong effect of magnetic force and necessarily, it must be taken into account. Consequently, the flow is only in the channel axis direction with the velocity $\mathbf{u} = (0, 0, w)$ varying in the duct as $w = w(x, y)$ for $(x, y) \in \Omega = [0, a] \times [0, b]$.

The governing equations of the problem are obtained by adding the electromagnetic Lorentz force $\mathbf{f} = \mathbf{J} \times \mathbf{B}$ [14] to the momentum equations. Thus, the Navier-Stokes equations in (1.2) with a variable viscosity is

$$\rho \left(\frac{\partial \mathbf{u}}{\partial t} + (\mathbf{u} \cdot \nabla) \mathbf{u} \right) = -\nabla p + \nabla \cdot (\bar{\mu} \nabla \mathbf{u}) + \mathbf{J} \times \mathbf{B} \quad (1.8)$$

where $\mathbf{B} = (B_x, B_y, 0)$ with intensity $B_0 = (B_x^2 + B_y^2)^{1/2}$ denotes the magnetic field perpendicular to the channel axis lying on the duct plane, and \mathbf{J} the electric current density of the fluid. A variable viscosity is included to boost the heat transfer, and the viscosity $\bar{\mu}$ is chosen depending on the temperature exponentially as given in [15]

$$\bar{\mu} = \mu_c e^{-b_0(T-T_w)} \quad (1.9)$$

where μ_c is the viscosity coefficient at $T = T_w$, and b_0 is a constant. Choosing such a dynamic viscosity in (1.9) weakens the convection dominance of the flow due to the high temperature. Adding the Hall current impact develops the physical properties of the system since the Hall current affects the magnetic force term by altering the magnitude and the direction of the current density.

Ohm's law with the Hall effect is [15]

$$\mathbf{J} = \sigma(\mathbf{u} \times \mathbf{B} - \beta(\mathbf{J} \times \mathbf{B})) \quad (1.10)$$

where σ is the electrical conductivity and β is the Hall factor of the fluid. Solving (1.10) for \mathbf{J} gives [15]

$$\mathbf{J} \times \mathbf{B} = \frac{\sigma B_0^2}{1 + m^2} w(x, y) \mathbf{k} \quad (1.11)$$

where $m = \sigma \beta B_0$ is the Hall parameter and hence $\mathbf{J} \times \mathbf{B}$ has only z component to be added to the equation (1.8). As a result, the terms on the left hand side of equation (1.8) vanish since the flow motion is steady in the z -direction and $(\mathbf{u} \cdot \nabla) = 0$. Therefore, the Navier-Stokes equations become [15]

$$\frac{\partial}{\partial x} \left(\bar{\mu} \frac{\partial w}{\partial x} \right) + \frac{\partial}{\partial y} \left(\bar{\mu} \frac{\partial w}{\partial y} \right) - \frac{\partial p}{\partial z} - \frac{\sigma B_0^2}{1 + m^2} w(x, y) = 0 \quad (1.12)$$

with the no-slip velocity assumption

$$w = 0 \quad \text{on} \quad \partial\Omega. \quad (1.13)$$

On the other hand, conservation of energy principle is taken into consideration for a general form based on the temperature as [16]

$$\rho c_p \left(\frac{\partial T}{\partial t} + \mathbf{u} \cdot \nabla T \right) = k \nabla^2 T + q''' \quad (1.14)$$

where c_p , k are the specific heat capacity, the thermal conductivity of the fluid, respectively and q''' is the heat source. A steady problem and a velocity vector having only z -component define an energy equation with viscous and Joule dissipation as [15]

$$\rho c_p w \frac{\partial T}{\partial z} = k \nabla^2 T + \bar{\mu} \left[\left(\frac{\partial w}{\partial x} \right)^2 + \left(\frac{\partial w}{\partial y} \right)^2 \right] + \frac{\sigma B_0^2}{1 + m^2} w^2 \quad (1.15)$$

where the last two terms respectively stand to represent the viscous and Joule dissipations. Further, consideration of a hydrodynamically and thermally fully-developed flow the term $\frac{\partial T}{\partial z}$ in energy equation can be represented for H1 thermal boundary condition as $\frac{\partial T}{\partial z} = \frac{dT_m}{dz}$ as in [17] and this term takes a place in the non-dimensional variable of the temperature. This condition is preferred in many applications such as heat exchanger and resistance heating. The temperature equation for our problem is considered with the boundary condition as $T = T_w$ on the duct.

The non-dimensional variables are used to nondimensionalize the equation (1.15)

$$x' = \frac{x}{a}, \quad y' = \frac{y}{a}, \quad w' = \frac{\mu_c w}{-\frac{dp}{dz} a^2}, \quad T = \frac{k(T - T_w)}{\rho c_p w_m a^2 \frac{dT_m}{dz}}, \quad \bar{\mu}' = \frac{\bar{\mu}}{\mu_c} \quad (1.16)$$

where a denotes the characteristic length of the rectangular cavity. Then, dimensionless momentum and energy equations on the domain $\Omega = [0, 1] \times [0, b/a]$ become

$$\frac{\partial}{\partial x} \left(\bar{\mu} \frac{\partial w}{\partial x} \right) + \frac{\partial}{\partial y} \left(\bar{\mu} \frac{\partial w}{\partial y} \right) = -1 + \frac{M^2}{1 + m^2} w \quad (1.17)$$

$$\nabla^2 T + Br \bar{\mu} \left[\left(\frac{\partial w}{\partial x} \right)^2 + \left(\frac{\partial w}{\partial y} \right)^2 \right] + \frac{M^2 Br}{1 + m^2} w^2 = \frac{w}{w_m} \quad (1.18)$$

where

$$w_m = \frac{1}{\mathcal{L}} \int_{\Omega} w d\Omega, \quad \bar{\mu} = e^{-BT} \quad (1.19)$$

and $\mathcal{L} = b/a$ is the aspect ratio, m , B , Br and M are the dimensionless Hall parameter, viscosity parameter, Brinkmann number and the Hartmann number, respectively and their definitions are

$$m = \sigma\beta B_0, \quad B = \frac{b_0\rho c_p w_m a^2 \frac{dT_m}{dz}}{k}, \quad Br = \frac{\frac{-dp}{dz}}{k\rho c_p \frac{dT_m}{dz} w_m} \quad \text{and} \quad M^2 = \frac{\sigma B_0^2 a^2}{\mu_c}. \quad (1.20)$$

These equations in terms of the velocity and the temperature are solved using the parametrix BEM and DRBEM approaches to examine the behavior of the inductionless MHD flow and heat transfer with temperature dependent viscosity under a vertically applied uniform magnetic field in Chapter 3, Section 3.1. The numerical results are presented in Section 4.1 of Chapter 4. Then, we turn our concern to the unsteady MHD flow equations which are derived in the following section.

1.3 MHD duct flow with time-varied external magnetic field

The unsteady MHD flow is governed by the Navier-Stokes equations including Lorentz force [18] which are coupled with Maxwell's equations of electromagnetism through Ohm's law. Maxwell's equations are

$$\begin{aligned} \nabla \cdot \mathbf{E} &= \frac{q}{\epsilon_0} && \text{Gauss's Law} \\ \nabla \cdot \mathbf{B} &= 0 && \text{Solenoidal nature of B} \\ \nabla \times \mathbf{E} &= -\frac{\partial \mathbf{B}}{\partial t} && \text{Faraday's Law} \\ \nabla \times \mathbf{B} &= \mu_0 \mathbf{J} + \mu_0 \epsilon_0 \frac{\partial \mathbf{E}}{\partial t} && \text{Ampere's Law} \end{aligned} \quad (1.21)$$

where ϵ_0 , μ_0 and q denote the permittivity of vacuum, the magnetic permeability of vacuum, and total electric charge density in the fluid, respectively. $\mathbf{E} = (E_x, E_y, E_z)$ is the electric field, $\mathbf{B} = (B_x, B_y, B_z)$ is the magnetic field.

Ohm's law expresses the current density in a moving conductor under an external magnetic field [2, 18]

$$\mathbf{J} = \sigma(\mathbf{E} + \mathbf{u} \times \mathbf{B}) \quad (1.22)$$

where σ is the electrical conductivity of the fluid.

Taking both the curl of the Ohm's law and Ampere's law, respectively brings

$$\nabla \times \mathbf{J} = \sigma(\nabla \times \mathbf{E}) + \sigma(\nabla \times (\mathbf{u} \times \mathbf{B})) \quad (1.23)$$

and

$$\nabla \times (\nabla \times \mathbf{B}) = \nabla \times (\mu_0 \mathbf{J} + \mu_0 \epsilon_0 \frac{\partial \mathbf{E}}{\partial t}). \quad (1.24)$$

Equation (1.24) equals

$$\nabla \times (\nabla \times \mathbf{B}) = \mu_0(\nabla \times \mathbf{J}) + \mu_0 \epsilon_0 (\nabla \times \frac{\partial \mathbf{E}}{\partial t}). \quad (1.25)$$

For a vector field \mathcal{A} , the curl of the curl is defined as

$$\nabla \times (\nabla \times \mathcal{A}) = \nabla(\nabla \cdot \mathcal{A}) - \nabla^2 \mathcal{A}. \quad (1.26)$$

Both the equality in (1.26) and Solenoidal nature of \mathbf{B} ($\nabla \cdot \mathbf{B} = 0$) turn equation (1.25) into

$$-\nabla^2 \mathbf{B} = \mu_0(\nabla \times \mathbf{J}) + \mu_0 \epsilon_0 (\nabla \times \frac{\partial \mathbf{E}}{\partial t}). \quad (1.27)$$

which equals

$$\nabla \times \mathbf{J} = -\frac{1}{\mu_0} \nabla^2 \mathbf{B} - \epsilon_0 (\nabla \times \frac{\partial \mathbf{E}}{\partial t}). \quad (1.28)$$

Equating (1.23) and (1.28) to each other yields

$$\sigma(\nabla \times \mathbf{E}) + \sigma(\nabla \times (\mathbf{u} \times \mathbf{B})) = -\frac{1}{\mu_0} \nabla^2 \mathbf{B} - \epsilon_0 (\nabla \times \frac{\partial \mathbf{E}}{\partial t}). \quad (1.29)$$

Then, applying Faraday's law to the first term of the above equation gives

$$\sigma(-\frac{\partial \mathbf{B}}{\partial t}) + \sigma(\nabla \times (\mathbf{u} \times \mathbf{B})) = -\frac{1}{\mu_0} \nabla^2 \mathbf{B} - \epsilon_0 (\nabla \times \frac{\partial \mathbf{E}}{\partial t}) \quad (1.30)$$

which is rearranged as

$$\frac{1}{\mu_0} \nabla^2 \mathbf{B} = \sigma(\frac{\partial \mathbf{B}}{\partial t}) - \sigma(\nabla \times (\mathbf{u} \times \mathbf{B})) - \epsilon_0 (\nabla \times \frac{\partial \mathbf{E}}{\partial t}). \quad (1.31)$$

When the time-varying magnetic field applies in x -direction B_x becomes $B_0(t) = B_0 f(t)$ where B_0 is the intensity of the applied magnetic field at $t = 0$ and $f(t)$ is the function carrying time variation. The component of the velocity, induced magnetic field and the electric potential vectors are such that $\mathbf{B} = (B_0(t), 0, B_z)$, $\mathbf{u} = (0, 0, V_z)$

and $\mathbf{E} = (0, 0, E_z)$ in two-dimensional case for a fully-developed flow ($\frac{\partial}{\partial z} = 0$). That is, the only unknowns are $V_z(x, y)$ and $B_z(x, y)$ in the pipe-axis direction (z -direction). Therefore, the last term of equation (1.31) equals

$$\nabla \times \frac{\partial \mathbf{E}}{\partial t} = \begin{vmatrix} \mathbf{i} & \mathbf{j} & \mathbf{k} \\ \frac{\partial}{\partial x} & \frac{\partial}{\partial y} & \frac{\partial}{\partial z} \\ 0 & 0 & \frac{\partial E_z}{\partial t} \end{vmatrix} = \mathbf{i} \frac{\partial}{\partial y} \left(\frac{\partial E_z}{\partial t} \right) - \mathbf{j} \frac{\partial}{\partial x} \left(\frac{\partial E_z}{\partial t} \right) + \mathbf{k} \cdot 0. \quad (1.32)$$

The curl of $(\mathbf{u} \times \mathbf{B})$ in equation (1.31) is

$$\nabla \times (\mathbf{u} \times \mathbf{B}) = \begin{vmatrix} \mathbf{i} & \mathbf{j} & \mathbf{k} \\ \frac{\partial}{\partial x} & \frac{\partial}{\partial y} & \frac{\partial}{\partial z} \\ 0 & B_0(t)V_z & 0 \end{vmatrix} = \mathbf{i} \frac{\partial}{\partial z} (-B_0(t)V_z) - \mathbf{j} \cdot 0 + \mathbf{k} (B_0(t) \frac{\partial V_z}{\partial x}) \quad (1.33)$$

since

$$\mathbf{u} \times \mathbf{B} = \begin{vmatrix} \mathbf{i} & \mathbf{j} & \mathbf{k} \\ 0 & 0 & V_z \\ B_0(t) & 0 & B_z \end{vmatrix} = \mathbf{i} \cdot 0 - \mathbf{j} (-B_0(t)V_z) + \mathbf{k} \cdot 0. \quad (1.34)$$

Therefore, the k -th component of equation (1.31)

$$\frac{1}{\mu_0} \nabla^2 B_z = \sigma \frac{\partial B_z}{\partial t} - \sigma (B_0(t) \frac{\partial V_z}{\partial x}) - 0 \quad (1.35)$$

and equally in dimensional form

$$\frac{1}{\mu_0 \sigma} \nabla^2 B_z + B_0(t) \frac{\partial V_z}{\partial x} = \frac{\partial B_z}{\partial t}. \quad (1.36)$$

To obtain the velocity equation, firstly the total force per unit volume acting on the conducting fluid is considered as

$$\mathbf{f} = q\mathbf{E} + \mathbf{J} \times \mathbf{B} \quad (1.37)$$

from which the term $q\mathbf{E}$ is disregarded since the speed of electrons in a conducting fluid is not greater than the speed of light [19]. Thus, the Lorentz force becomes

$$\mathbf{f} = \mathbf{J} \times \mathbf{B}. \quad (1.38)$$

Insertion of Ampere's law from equation (1.21) into the Lorentz force (1.38) gives

$$\begin{aligned}\mathbf{f} &= \left(\frac{1}{\mu_0} (\nabla \times \mathbf{B}) - \epsilon_0 \frac{\partial \mathbf{E}}{\partial t} \right) \times \mathbf{B} \\ &= \frac{1}{\mu_0} (\nabla \times \mathbf{B}) \times \mathbf{B} - \epsilon_0 \frac{\partial \mathbf{E}}{\partial t} \times \mathbf{B}.\end{aligned}\quad (1.39)$$

The curl of the curl of \mathbf{B} , the first term in equation (1.39) is

$$(\nabla \times \mathbf{B}) \times \mathbf{B} = \begin{vmatrix} i & j & k \\ \frac{\partial B_z}{\partial y} & -\frac{\partial B_z}{\partial x} & 0 \\ B_0(t) & 0 & B_z \end{vmatrix} = i(-B_z \frac{\partial B_z}{\partial x}) - j(B_z \frac{\partial B_z}{\partial y}) + k(B_0(t) \frac{\partial B_z}{\partial x}) \quad (1.40)$$

since

$$\nabla \times \mathbf{B} = \begin{vmatrix} i & j & k \\ \frac{\partial}{\partial x} & \frac{\partial}{\partial y} & \frac{\partial}{\partial z} \\ B_0(t) & 0 & B_z \end{vmatrix} = i \frac{\partial B_z}{\partial y} - j \frac{\partial B_z}{\partial x} + k \cdot 0. \quad (1.41)$$

Then, the second term on the Lorentz force in (1.39) is

$$\frac{\partial \mathbf{E}}{\partial t} \times \mathbf{B} = \begin{vmatrix} i & j & k \\ 0 & 0 & \frac{\partial E_z}{\partial t} \\ B_0(t) & 0 & B_z \end{vmatrix} = i \cdot 0 + j(B_0(t) \frac{\partial E_z}{\partial t}) + k \cdot 0. \quad (1.42)$$

Thus, the k -th component of the Lorentz force includes the term $\frac{1}{\mu_0} B_0(t) \frac{\partial B_z}{\partial x}$ only.

Now, the momentum equation (Navier-Stokes equation) for the unsteady flow is

$$\rho \left(\frac{\partial \mathbf{u}}{\partial t} + (\mathbf{u} \cdot \nabla) \mathbf{u} \right) = -\nabla p + \rho \nu \nabla^2 \mathbf{u} + \mathbf{J} \times \mathbf{B}. \quad (1.43)$$

The k -th component of the above momentum equation becomes with equations (1.39) and (1.40)

$$\rho \frac{\partial V_z}{\partial t} = -\frac{\partial p}{\partial z} + \rho \nu \nabla^2 V_z + \frac{1}{\mu_0} B_0(t) \frac{\partial B_z}{\partial x} \quad (1.44)$$

which equals in dimensional form

$$\rho \nu \nabla^2 V_z + \frac{1}{\mu_0} B_0(t) \frac{\partial B_z}{\partial x} = \frac{\partial p}{\partial z} + \rho \frac{\partial V_z}{\partial t}. \quad (1.45)$$

Thus, the coupled dimensional equations for the velocity V_z and induced magnetic field B_z are equations (1.45) and (1.36)

$$\rho\nu\nabla^2 V_z + \frac{1}{\mu_0} B_0(t) \frac{\partial B_z}{\partial x} = \frac{\partial p}{\partial z} + \rho \frac{\partial V_z}{\partial t} \quad (1.46)$$

$$\frac{1}{\mu_0\sigma} \nabla^2 B_z + B_0(t) \frac{\partial V_z}{\partial x} = \frac{\partial B_z}{\partial t} \quad (1.47)$$

under the applied time-varying magnetic field $B_0(t)$ in x -direction.

The velocity and induced magnetic field equations (1.46) and (1.47) are nondimensionalized by taking dimensionless variables as

$$\begin{aligned} x' &= \frac{x}{L_0}, \quad y' = \frac{y}{L_0}, \quad B' = \frac{B_z}{v_c \mu_0 \sqrt{\sigma \mu}}, \quad V' = \frac{V_z}{v_c}, \quad \frac{\partial p}{\partial z} = -\frac{\mu}{L_0^2} v_c, \\ v_c &= -\frac{L_0^2}{\mu} \frac{\partial p}{\partial z}, \quad \mu = \rho\nu, \quad t' = \frac{t}{L_0} v_c \end{aligned} \quad (1.48)$$

where L_0 and v_c are the characteristic length and characteristic velocity (mean axis velocity) of the problem.

Substituting variables (1.48) into equations (1.46)-(1.47) yields

$$\rho\nu \frac{v_c}{L_0^2} \nabla^2 V' + \frac{1}{\mu_0} B_0(t) \mu_0 v_c \frac{\sqrt{\sigma \mu}}{L_0} \frac{\partial B'}{\partial x'} = -\frac{\mu}{L_0^2} v_c + \rho v_c \frac{\partial V'}{\partial t'} \frac{v_c}{L_0} \quad (1.49)$$

$$\frac{1}{\mu_0\sigma} \mu_0 v_c \frac{\sqrt{\sigma \mu}}{L_0^2} \nabla^2 B' + B_0(t) \frac{v_c}{L_0} \frac{\partial V'}{\partial x'} = \mu_0 v_c \sqrt{\sigma \mu} \frac{\partial B'}{\partial t'} \frac{v_c}{L_0}. \quad (1.50)$$

Simplification gives

$$\nabla^2 V' + B_0(t) L_0 \frac{\sqrt{\sigma}}{\sqrt{\mu}} \frac{\partial B'}{\partial x'} = -1 + \frac{L_0}{\nu} v_c \frac{\partial V'}{\partial t'} \quad (1.51)$$

$$\nabla^2 B' + B_0(t) L_0 \frac{\sqrt{\sigma}}{\sqrt{\mu}} \frac{\partial V'}{\partial x'} = v_c L_0 \sigma \mu_0 \frac{\partial B'}{\partial t'}. \quad (1.52)$$

Finally, the non-dimensional equations take the form by dropping the prime notations in the above equations as

$$\nabla^2 V + M f(t) \frac{\partial B}{\partial x} = -1 + R_e \frac{\partial V}{\partial t} \quad (1.53)$$

$$\nabla^2 B + M f(t) \frac{\partial V}{\partial x} = R_m \frac{\partial B}{\partial t}. \quad (1.54)$$

where $R_e = \frac{v_c L_0}{\nu}$, $R_m = v_c L_0 \sigma \mu_0$ and $M = \frac{L_0 B_0 \sqrt{\sigma}}{\sqrt{\rho \nu}}$ are the Reynolds number, magnetic Reynolds number and Hartmann number, respectively.

We can equivalently write,

$$\nabla^2 V + \overline{M} \frac{\partial B}{\partial x} = -1 + R_e \frac{\partial V}{\partial t} \quad (1.55)$$

$$\nabla^2 B + \overline{M} \frac{\partial V}{\partial x} = R_m \frac{\partial B}{\partial t} \quad (1.56)$$

where $\overline{M} = Mf(t)$.

When Reynolds number R_e and magnetic Reynolds number R_m are assumed to be one (according to the physics of the problem), the MHD equations take the form

$$\nabla^2 V + \overline{M} \frac{\partial B}{\partial x} = -1 + \frac{\partial V}{\partial t} \quad (1.57)$$

$$\nabla^2 B + \overline{M} \frac{\partial V}{\partial x} = \frac{\partial B}{\partial t}. \quad (1.58)$$

When the applied magnetic field is oblique, the MHD duct flow equations can be modified by doing the necessary changes in the vector definition of the magnetic field \mathbf{B} as $\mathbf{B} = (B_0(t)\sin\alpha, B_0(t)\cos\alpha, B_z)$ where α is the angle between the applied magnetic field and the positive y -axis. Following equations from (1.37) through (1.45) and (1.22) through (1.36) bring the dimensional velocity and induced magnetic field equations as

$$\rho\nu\nabla^2 V_z + \frac{1}{\mu_0}(B_0(t)\sin\alpha\frac{\partial B_z}{\partial x} + B_0(t)\cos\alpha\frac{\partial B_z}{\partial y}) = \frac{\partial p}{\partial z} + \rho\frac{\partial V_z}{\partial t} \quad (1.59)$$

$$\frac{1}{\mu_0\sigma}\nabla^2 B_z + B_0(t)\sin\alpha\frac{\partial V_z}{\partial x} + B_0(t)\cos\alpha\frac{\partial V_z}{\partial y} = \frac{\partial B_z}{\partial t}. \quad (1.60)$$

Substituting dimensionless variables (1.48) in equations (1.59) and (1.60) and the dropping the prime notations yields

$$\nabla^2 V + Mf(t)\sin\alpha\frac{\partial B}{\partial x} + Mf(t)\cos\alpha\frac{\partial B}{\partial y} = -1 + R_e \frac{\partial V}{\partial t} \quad (1.61)$$

$$\nabla^2 B + Mf(t)\sin\alpha\frac{\partial V}{\partial x} + Mf(t)\cos\alpha\frac{\partial V}{\partial y} = R_m \frac{\partial B}{\partial t}. \quad (1.62)$$

These equations are solved by using the DRBEM. The solution is proceed iteratively until the desired time level t_n with an initial guess for the velocity and induced magnetic field as zero. This procedure is explained in detail in Section 3.2, Chapter 3. The numerical results are presented in Section 4.2, Chapter 4.

1.4 Inductionless MHD flow and electric potential with variably conducting walls under axial-dependent magnetic field

In this section, we consider the two-dimensional laminar MHD flow of a viscous and incompressible fluid in an infinitely long pipe of rectangular cross-section which is placed in a magnetic field $\mathbf{B} = (B_0(z)\cos\alpha, B_0(z)\sin\alpha, 0)$ as in Figure 1.2. The axially changing magnetic field is $B_0(z) = B_0g(z)$ where B_0 is the intensity of the applied magnetic field and $g(z)$ is the function determining the strength of the applied magnetic field along the z -axis, i.e. pipe-axis.

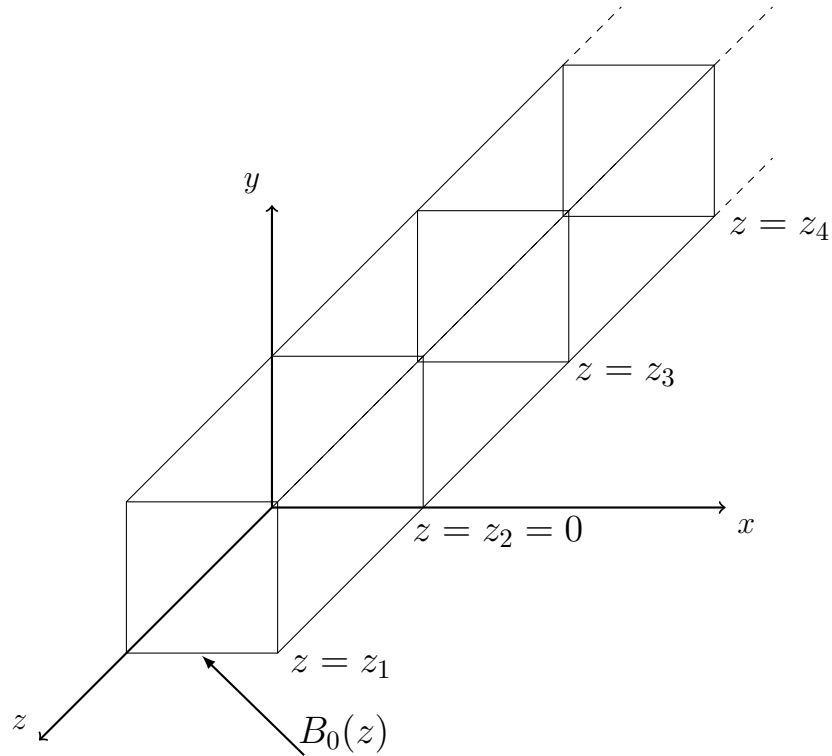


Figure 1.2: Physical configuration of axially-changing MHD flow

The MHD flow is considered in two-dimensional ducts located at some points z_1, z_2, \dots, z_n on the pipe-axis. On each cross-section at z_i , the external magnetic field $B_0(z)$ is applied as a function of z_i . The flow is assumed to be fully-developed between two fixed z -values which has only one component in the pipe-axis direction varying in the ducts xy -plane at these fixed points z_i of the axis. Physically, it may be considered as the fully-developed flow between two magnets placed on the pipe-

axis direction. The fluid is electrically conducting and it is subjected to an applied magnetic field but changing at the points where the magnets placed on the pipe-axis. However, in this section the induced magnetic field is neglected due to the small magnetic Reynolds number.

The steady MHD flow equations are derived from the Maxwell's equations and Navier-Stokes equations including Lorentz force [18]. Here, the MHD flow equations are constructed for the steady flow under externally applied axial-dependent magnetic field. Therefore, the first term which is the time derivative in equation (1.43) drops, and the continuity and momentum equations for steady flow become

$$\nabla \cdot \mathbf{u} = 0 \quad (1.63)$$

$$\rho(\mathbf{u} \cdot \nabla)\mathbf{u} = -\nabla p + \rho\nu\nabla^2\mathbf{u} + \mathbf{J} \times \mathbf{B} \quad (1.64)$$

where the velocity and the magnetic field for a two-dimensional MHD flow are represented by the velocity $\mathbf{u} = (0, 0, w(x, y))$ and the magnetic field

$\mathbf{B} = (B_0(z)\cos\alpha, B_0(z)\sin\alpha, 0)$, respectively. The external magnetic field applies with an angle α made with the positive x -axis.

The first term in (1.64), $(\mathbf{u} \cdot \nabla)$ is clearly zero since the first two components of the velocity vector are zero and $\partial w(x, y)/\partial z = 0$ for a fully-developed flow. The Lorentz force in (1.64) is computed from the Ohm's law [20] which is

$$\mathbf{J} = \sigma(-\nabla\Phi + \mathbf{u} \times \mathbf{B}) \quad (1.65)$$

by taking $\mathbf{J} \times \mathbf{B}$ since $\mathbf{E} = -\nabla\Phi$ where Φ defines a scalar electric potential and the electric field is irrotational $\nabla \times \mathbf{E} = 0$. Now,

$$\mathbf{J} = \sigma\left(-\frac{\partial\Phi}{\partial x} - (B_0(z)\sin\alpha)w, -\frac{\partial\Phi}{\partial y} + (B_0(z)\cos\alpha)w, -\frac{\partial\Phi}{\partial z}\right) \quad (1.66)$$

since

$$\begin{aligned} \mathbf{u} \times \mathbf{B} &= \begin{vmatrix} \mathbf{i} & \mathbf{j} & \mathbf{k} \\ 0 & 0 & w \\ B_0(z)\cos\alpha & B_0(z)\sin\alpha & 0 \end{vmatrix} \\ &= \mathbf{i}((-B_0(z)\sin\alpha) \cdot w) - \mathbf{j}(-(B_0(z)\cos\alpha) \cdot w) + \mathbf{k} \cdot 0. \end{aligned} \quad (1.67)$$

Thus,

$$\begin{aligned}
\mathbf{J} \times \mathbf{B} &= \begin{vmatrix} i & j & k \\ \sigma(-\frac{\partial\Phi}{\partial x} - (B_0(z)\sin\alpha)w) & \sigma(-\frac{\partial\Phi}{\partial y} + (B_0(z)\cos\alpha)w) & \sigma(-\frac{\partial\Phi}{\partial z}) \\ B_0(z)\cos\alpha & B_0(z)\sin\alpha & 0 \end{vmatrix} \\
&= \mathbf{i}((B_0(z)\sin\alpha)\sigma\frac{\partial\Phi}{\partial z}) - \mathbf{j}((B_0(z)\cos\alpha)\sigma\frac{\partial\Phi}{\partial z}) \\
&\quad + \mathbf{k}(\sigma(B_0(z)\sin\alpha)(-\frac{\partial\Phi}{\partial x} - (B_0(z)\sin\alpha)w) \\
&\quad \quad - \sigma(B_0(z)\cos\alpha)(-\frac{\partial\Phi}{\partial y} + (B_0(z)\cos\alpha)w)).
\end{aligned} \tag{1.68}$$

Then, the k -th component of the momentum equation (1.64) is

$$\rho\nu\nabla^2 w - (B_0(z))^2\sigma w = \frac{\partial p}{\partial z} + \sigma(B_0(z)\sin\alpha)\frac{\partial\Phi}{\partial x} - \sigma(B_0(z)\cos\alpha)\frac{\partial\Phi}{\partial y}. \tag{1.69}$$

In order to get non-dimensional equations, introduce the following non-dimensional parameters as

$$x' = \frac{x}{L_0}, \quad y' = \frac{y}{L_0}, \quad w' = \frac{w}{v_c}, \quad \rho\nu v_c = -L_0^2 \frac{\partial p}{\partial z}, \quad \Phi' = \frac{\Phi}{\mu_0 v_c L_0 H_0} \tag{1.70}$$

where H_0 is the strength of the magnetic field having a constitute relation with B_0 as $B_0 = \mu_0 H_0$. Substituting equation (1.70) into equation (1.69) brings

$$\begin{aligned}
\rho\nu \frac{v_c}{L_0^2} \nabla^2 w' - (B_0(z))^2 \sigma v_c w' &= -\frac{\rho\nu v_c}{L_0^2} \\
&\quad + \sigma(B_0(z)\sin\alpha)\mu_0 v_c L_0 H_0 \frac{1}{L_0} \frac{\partial\Phi'}{\partial x'} - \sigma(B_0(z)\cos\alpha)\mu_0 v_c L_0 H_0 \frac{1}{L_0} \frac{\partial\Phi'}{\partial y'}.
\end{aligned} \tag{1.71}$$

Necessary simplification and dropping prime notations yield the dimensionless velocity equation as

$$\nabla^2 w - (Mg(z))^2 w = -1 + M^2 g(z) \sin\alpha \frac{\partial\Phi}{\partial x} - M^2 g(z) \cos\alpha \frac{\partial\Phi}{\partial y} \tag{1.72}$$

since $B_0 = \mu_0 H_0$ and $M = \frac{L_0 B_0 \sqrt{\sigma}}{\sqrt{\rho\nu}}$.

Furthermore, the non-dimensional form of the electric current equation is obtained from the Ohm's law (1.65). The conservation of current $\nabla \cdot \mathbf{J} = 0$ gives the electric potential equation for the flow

$$0 = \sigma(\nabla \cdot (-\nabla\Phi) + \nabla \cdot (\mathbf{u} \times \mathbf{B})) \tag{1.73}$$

which equals

$$0 = \sigma(-\nabla^2\Phi + \nabla \cdot (\mathbf{u} \times \mathbf{B})). \quad (1.74)$$

Since the vector $(\mathbf{u} \times \mathbf{B})$ is calculated in (1.67), equation (1.74) becomes

$$\nabla^2\Phi = -B_0(z)\sin\alpha\frac{\partial w}{\partial x} + B_0(z)\cos\alpha\frac{\partial w}{\partial y}. \quad (1.75)$$

In order to get non-dimensional equation substituting equation (1.70) into equation (1.75) brings

$$\mu_0 L_0 H_0 \frac{v_c}{L_0^2} \nabla^2\Phi' = -B_0(z)\sin\alpha\frac{v_c}{L_0}\frac{\partial w'}{\partial x'} + B_0(z)\cos\alpha\frac{v_c}{L_0}\frac{\partial w'}{\partial y'}. \quad (1.76)$$

Necessary simplifications and dropping prime notations yield the dimensionless electric potential equation as

$$\nabla^2\Phi = -g(z)\sin\alpha\frac{\partial w}{\partial x} + g(z)\cos\alpha\frac{\partial w}{\partial y}. \quad (1.77)$$

Consequently, the non-dimensional flow and electric potential are

$$\nabla^2 w - (Mg(z))^2 w = -1 + M^2 g(z)\sin\alpha\frac{\partial\Phi}{\partial x} - M^2 g(z)\cos\alpha\frac{\partial\Phi}{\partial y} \quad (1.78)$$

$$\nabla^2\Phi = -g(z)\sin\alpha\frac{\partial w}{\partial x} + g(z)\cos\alpha\frac{\partial w}{\partial y}. \quad (1.79)$$

When the magnetic field is applied vertically, with an angle $\alpha = \pi/2$ with the x -axis, then the equations become

$$\nabla^2 w - (Mg(z))^2 w = -1 + M^2 g(z)\frac{\partial\Phi}{\partial x} \quad (1.80)$$

$$\nabla^2\Phi = -g(z)\frac{\partial w}{\partial x}. \quad (1.81)$$

The momentum and electric potential equations are reduced to a simplified form under a uniform applied magnetic field by taking the function $g(z)$ as 1. Then, the MHD flow equations become

$$\nabla^2 w - M^2 w = -1 + M^2 \frac{\partial\Phi}{\partial x} \quad (1.82)$$

$$\nabla^2\Phi = -\frac{\partial w}{\partial x}. \quad (1.83)$$

Both types of magnetic field either uniform or axially changing are considered in the thesis.

The obtained equations (1.80)-(1.81) and (1.82)-(1.83) are the mathematical models of the fully-developed MHD flow of a viscous and incompressible fluid along a long pipe of rectangular cross-section where the applied magnetic field changes in the pipe-axis direction. The velocity and electric potential equations are solved with suitable boundary conditions on the walls of the rectangular ducts. The no-slip velocity condition is imposed for the flow and the walls are both assumed to be electrically non-conducting and conducting (in general variably conducting). The conductance depends on the material of the duct with a ratio c which can be different at each wall. Therefore, the boundary conditions are

$$\begin{aligned} w(x, \pm 1) = w(\pm 1, y) = 0 \quad \text{no-slip velocity} \\ \text{and} \\ \frac{\partial \Phi}{\partial y}(x, \pm 1) = \frac{\partial \Phi}{\partial x}(\pm 1, y) = 0 \quad \text{non-conducting walls} \end{aligned} \tag{1.84}$$

or

$$\begin{aligned} w(x, \pm 1) = w(\pm 1, y) = 0 \quad \text{no-slip velocity} \\ \text{and} \\ \left. \begin{aligned} \pm \frac{\partial \Phi}{\partial y}(x, \pm 1) &= c \frac{\partial^2 \Phi}{\partial x^2}(x, \pm 1) \\ \pm \frac{\partial \Phi}{\partial x}(\pm 1, y) &= c \frac{\partial^2 \Phi}{\partial y^2}(\pm 1, y) \end{aligned} \right\} \text{variably conducting walls.} \end{aligned} \tag{1.85}$$

The suitable boundary conditions for the electric potential is defined by the conductivity ratio c times the second derivative of Φ , itself. This makes the solution procedure of the non-dimensional equations as iteratively to generate the required Neumann type boundary conditions of Φ , with an initial guess as $\Phi^0 = 0$. The solution is iterated till the convergence criteria is satisfied with a tolerance as explained in detail in Chapter 3, Section 3.3. The numerical results and the discussion are given in Chapter 4, Section 4.3.

1.5 MHD duct flow with axially-changing external magnetic field

In this section, finally the MHD duct flow in a long pipe of rectangular cross-section is considered under the influence of axially changing magnetic field again as in the

previous section. With the interaction of the electrically conducting fluid and magnetic field $B_0(z)$ applied vertically to the duct, an induced magnetic field $B_z(x, y)$ is introduced inside the fluid through the pipe-axis direction. Axial dependent magnetic field is written as $B_0(z) = B_0 g(z)$ where B_0 is the constant intensity and $g(z)$ denotes the function determining the strength of the applied magnetic field. The flow is laminar and steady and, the fluid is incompressible, viscous, electrically conducting and pumped through the pipe with a constant pressure gradient. The velocity \mathbf{u} and the magnetic field \mathbf{B} have unknown components only in the pipe-axis (z -axis) direction as $\mathbf{u} = (0, 0, V_z(x, y))$ and $\mathbf{B} = (0, B_0(z), B_z(x, y))$. The flow is assumed to be fully-developed between two fixed z -values, varying only in the ducts xy -plane at these z_i points of the axis. The velocity and the induced magnetic field are changing in the two-dimensional ducts but also influenced from the magnets located at the points along the pipe-axis. The pipe-axis dependent function is taken as $g(z) = \frac{1}{1 + e^{-z/0.15}}$. Thus, three-dimensional effects are caused by variations of this applied magnetic field $B_0(z)$ in the pipe-axis direction between two values of z in which the flow is assumed to be fully-developed. This case formulates and results in an extension to the equations obtained in the previous section 1.4 in the sense that induced magnetic field equation is also involved. The flow is represented by the vector $\mathbf{u} = (0, 0, V_z(x, y))$ and the electric potential is $\mathbf{E} = (0, 0, E_z(x, y))$.

To obtain the MHD flow equations in terms of velocity, induced magnetic field and electric potential, a similar procedure is used as in the previous sections as using momentum equations, Maxwell's equations and Ohm's law. Firstly, to get the induced magnetic field equation, both the curl of the Ampere's law and Ohm's law are used simultaneously for the steady flow which are respectively as

$$\nabla \times (\nabla \times \mathbf{B}) = \nabla \times (\mu_0 \mathbf{J}) \quad (1.86)$$

being equal to

$$-\nabla^2 \mathbf{B} = \mu_0 (\nabla \times \mathbf{J}) \quad (1.87)$$

and $\nabla \times \mathbf{J}$ from the Ohm's law

$$\nabla \times \mathbf{J} = \sigma (\nabla \times \mathbf{E}) + \sigma (\nabla \times (\mathbf{u} \times \mathbf{B})). \quad (1.88)$$

When $\nabla \times \mathbf{J}$'s are equated from the above two equations (1.87) and (1.88) we get

$$-\frac{1}{\mu_0} \nabla^2 \mathbf{B} = \sigma(\nabla \times \mathbf{E}) + \sigma(\nabla \times (\mathbf{u} \times \mathbf{B})). \quad (1.89)$$

Application of the Faraday's law to the first term on the right hand side of equation (1.89) which is

$$\sigma(\nabla \times \mathbf{E}) = \sigma\left(-\frac{\partial \mathbf{B}}{\partial t}\right). \quad (1.90)$$

However, since the flow is steady in the pipe-axis direction the term $\frac{\partial \mathbf{B}}{\partial t}$ drops and equation (1.89) becomes

$$-\frac{1}{\mu_0} \nabla^2 \mathbf{B} = \sigma(\nabla \times (\mathbf{u} \times \mathbf{B})). \quad (1.91)$$

Since

$$\mathbf{u} \times \mathbf{B} = \begin{vmatrix} i & j & k \\ 0 & 0 & V_z(x, y) \\ 0 & B_0(z) & B_z(x, y) \end{vmatrix} = i(-B_0(z) \cdot V_z(x, y)) - j \cdot 0 + k \cdot 0 \quad (1.92)$$

the term on the right hand side of equation (1.91) is

$$\begin{aligned} \nabla \times (\mathbf{u} \times \mathbf{B}) &= \begin{vmatrix} i & j & k \\ \frac{\partial}{\partial x} & \frac{\partial}{\partial y} & \frac{\partial}{\partial z} \\ -B_0(z) \cdot V_z(x, y) & 0 & 0 \end{vmatrix} \\ &= i \cdot 0 - j \cdot 0 + k(B_0(z) \frac{\partial V_z(x, y)}{\partial y}). \end{aligned} \quad (1.93)$$

Therefore, the k -th component of the induced magnetic field equation is

$$\frac{1}{\mu_0 \sigma} \nabla^2 B_z + B_0(z) \frac{\partial V_z}{\partial y} = 0. \quad (1.94)$$

The derivation of the velocity equation of the MHD flow is obtained from the momentum equation (1.64) where the force term is Lorentz force

$$\mathbf{f} = \frac{1}{\mu_0} (\nabla \times \mathbf{B}) \times \mathbf{B}. \quad (1.95)$$

The k -th component of the momentum equation is

$$0 = -\frac{\partial p}{\partial z} + \rho \nu \nabla^2 V_z + \frac{1}{\mu_0} (B_0(z) \frac{\partial B_z}{\partial y} - B_0(z) \frac{\partial B_0(z)}{\partial z}) \quad (1.96)$$

since

$$(\nabla \times \mathbf{B}) \times \mathbf{B} = \begin{vmatrix} i & j & k \\ \frac{\partial B_z}{\partial y} - \frac{\partial B_0(z)}{\partial z} & \frac{\partial B_z}{\partial x} & 0 \\ 0 & B_0(z) & B_z \end{vmatrix} \quad (1.97)$$

$$= \mathbf{i}(-B_z \frac{\partial B_z}{\partial x}) - \mathbf{j}(B_z(\frac{\partial B_z}{\partial y} - \frac{\partial B_0(z)}{\partial z})) + \mathbf{k}(B_0(z)(\frac{\partial B_z}{\partial y} - \frac{\partial B_0(z)}{\partial z})) \quad (1.98)$$

where

$$\nabla \times \mathbf{B} = \begin{vmatrix} i & j & k \\ \frac{\partial}{\partial x} & \frac{\partial}{\partial y} & \frac{\partial}{\partial z} \\ 0 & B_0(z) & B_z \end{vmatrix} = \mathbf{i}(\frac{\partial B_z}{\partial y} - \frac{\partial B_0(z)}{\partial z}) - \mathbf{j}(\frac{\partial B_z}{\partial x}) + \mathbf{k} \cdot 0. \quad (1.99)$$

Rearrangement of equation (1.96) is

$$\rho \nu \nabla^2 V_z + \frac{1}{\mu_0} (B_0(z) \frac{\partial B_z}{\partial y}) = \frac{\partial p}{\partial z} + \frac{1}{\mu_0} (B_0(z) \frac{\partial B_0(z)}{\partial z}). \quad (1.100)$$

To nondimensionalize the equations, introduce the following non-dimensional parameters as

$$x' = \frac{x}{L_0}, \quad y' = \frac{y}{L_0}, \quad z' = \frac{z}{L_0}, \quad V' = \frac{V_z}{v_c}, \quad B' = \frac{B_z}{\mu_0 v_c \sqrt{\mu \sigma}}, \quad v_c = -\frac{L_0^2}{\mu} \frac{\partial p}{\partial z}. \quad (1.101)$$

First, the non-dimensional form of the induced magnetic field is

$$\frac{1}{\mu_0 \sigma} \frac{v_c \mu_0 \sqrt{\sigma \mu}}{L_0^2} \nabla^2 B' + B_0 g(z) \frac{v_c}{L_0} \frac{\partial V'}{\partial y'} = 0 \quad (1.102)$$

equals to

$$\nabla^2 B' + B_0 L_0 \sqrt{\frac{\sigma}{\mu}} g(z) \frac{\partial V'}{\partial y'} = 0 \quad (1.103)$$

dropping the prime notations and using the definition of Hartmann number as $M = B_0 L_0 \sqrt{\frac{\sigma}{\mu}}$ the induced magnetic field equation becomes

$$\nabla^2 B + M g(z) \frac{\partial V}{\partial y} = 0. \quad (1.104)$$

Then, the dimensionless velocity equation is

$$\mu \frac{v_c}{L_0^2} \nabla^2 V' + \frac{1}{\mu_0} (B_0 g(z) v_c \mu_0 \frac{\sqrt{\sigma \mu}}{L_0} \frac{\partial B'}{\partial y'}) = \frac{-v_c \mu}{L_0^2} + B_0 g(z) \frac{1}{\mu_0 L_0} (B_0 \frac{\partial g(z)}{\partial z'}) \quad (1.105)$$

which equals to

$$\nabla^2 V' + \sqrt{\frac{\sigma}{\mu}} L_0 B_0 g(z) \frac{\partial B'}{\partial y'} = -1 + B_0^2 g(z) \frac{L_0}{\mu_0 v_c \mu} \frac{\partial g(z)}{\partial z'} \quad (1.106)$$

dropping the prime notations again and using the Hartmann number M bring the equation to the form

$$\nabla^2 V + M g(z) \frac{\partial B}{\partial y} = -1 + M^2 g(z) \frac{1}{R_m} \frac{\partial g(z)}{\partial z} \quad (1.107)$$

where magnetic Reynolds number R_m is $R_m = L_0 \sigma \mu_0 v_c$.

Therefore, the coupled steady MHD flow equations in terms of velocity $V(x, y)$ and induced magnetic field $B(x, y)$ is

$$\nabla^2 V + M g(z) \frac{\partial B}{\partial y} = -1 + \frac{M^2}{R_m} g(z) \frac{\partial g(z)}{\partial z} \quad (1.108)$$

$$\nabla^2 B + M g(z) \frac{\partial V}{\partial y} = 0. \quad (1.109)$$

When the electric potential $\Phi(x, y)$ is required, it can be derived by using the Ohm's law, $\mathbf{J} = \sigma(-\nabla\Phi + \mathbf{u} \times \mathbf{B})$. The conservation of the electric current $\nabla \cdot \mathbf{J} = 0$ gives the electric potential equation of the flow as

$$\nabla \cdot \mathbf{J} = 0 = \sigma(\nabla \cdot (-\nabla\Phi) + \nabla \cdot (\mathbf{u} \times \mathbf{B})). \quad (1.110)$$

Since the vector $\mathbf{u} \times \mathbf{B}$ is calculated in equation (1.92), the above equation (1.110) becomes

$$\nabla^2 \Phi = -B_0 g(z) \frac{\partial V_z}{\partial x}. \quad (1.111)$$

Using non-dimensional parameters for Φ and V_z as $\Phi' = \frac{\Phi}{\mu_0 v_c L_0 H_0}$ and $V' = \frac{V_z}{v_c}$, respectively yields

$$\mu_0 v_c L_0 H_0 \frac{1}{L_0^2} \nabla^2 \Phi' = -B_0 g(z) v_c \frac{1}{L_0} \frac{\partial V'}{\partial x'} \quad (1.112)$$

which equals to

$$\begin{aligned} \nabla^2 \Phi' &= -\frac{1}{\mu_0 H_0} B_0 g(z) \frac{\partial V'}{\partial x'} \\ &= -g(z) \frac{\partial V'}{\partial x'}. \end{aligned} \quad (1.113)$$

Dropping the prime notations yields the non-dimensional electric potential equation as

$$\nabla^2 \Phi = -g(z) \frac{\partial V}{\partial x}. \quad (1.114)$$

The obtained velocity, induced magnetic field and electric potential equations

$$\begin{aligned} \nabla^2 V + Mg(z) \frac{\partial B}{\partial y} &= -1 + \frac{M^2}{R_m} g(z) \frac{\partial g(z)}{\partial z} \\ \nabla^2 B + Mg(z) \frac{\partial V}{\partial y} &= 0 \\ \nabla^2 \Phi &= -g(z) \frac{\partial V}{\partial x} \end{aligned} \quad (1.115)$$

are studied to examine the behavior of MHD flow under axially changing applied magnetic field. Proper boundary conditions for V , B and Φ are added to equations (1.115) according to the physics of the problem and the conductivity of the material of the ducts walls. The equations are discretized with the DRBEM in Chapter 3 Section 3.4, and the numerical results are given in Chapter 4 Section 4.4.

1.6 Literature Survey

The convection–diffusion equation describes the balance between the diffusion and convection terms of a physical phenomena in which the particles, energy or other physical quantities are in motion inside a physical system. The convection-diffusion type partial differential equations may involve a variable coefficient in the diffusion term such as viscosity of the fluid. The term viscosity defines the resistance of a fluid, either liquid or gas to change its shape. From our daily life, it is a common knowledge that viscosity varies with temperature. Therefore, there are quite a number of fluid dynamics problems in which the fluid viscosity is varying with the temperature of the fluid. The governing equations for laminar flow of viscous fluids through a channel are the Navier-Stokes and the energy equations together with the continuity equation.

Understanding the importance of the temperature dependent viscosity, one can list the significant applications of the laminar flow and heat transfer through rectangular channels. Designing heat exchangers, chemical reactors, nuclear reactors, cooling of electronic systems and combustion systems are some of these application areas.

Therefore, there have been many theoretical and experimental studies and several numerical methods on the solution of the flow and heat transfer of electrically conducting fluids through rectangular channels. Xie and Hartnett [21] have conducted an experimental study of laminar flow and heat transfer in 2:1 rectangular duct filled by mineral oil since the viscosity of the mineral oil changes dramatically under the heat. They have obtained good agreement between experimental data and the analytical solution. Then, Shin et al. [22] have also investigated the influence of variable viscosity of temperature-dependent fluids on the laminar flow and heat transfer with friction factor in a rectangular duct. The governing mass, momentum and energy equations have been solved using the finite volume method (FVM). The authors have obtained an excellent agreement with the experimental results conducted by Xie and Hartnett [21]. Then, the two-dimensional, incompressible, non-Newtonian fluid between two infinite plates has been considered in [23] including the effect of viscous heating. The viscosity of the fluid depends on both temperature and shear-rate. The viscosity depending on the temperature exponentially is modeled with Arrhenius law and Chebyshev polynomials has been used for the numerical solution of the boundary value problem. Pinarbasi et al. [24] have investigated the effects of variable viscosity depending on the temperature of a non-isothermal, incompressible Newtonian fluid which flows under a constant pressure gradient. The non-linear coupled boundary value problem has been solved iteratively using Chebyshev pseudospectral method. Moreover, the effects of the temperature dependent viscosity and thermal conductivity on natural convection boundary layer flow have been studied theoretically in [25]. The authors have both used the perturbation method and FDM to compare their results and they have concluded that their solutions from both methods agreed very well. However, among the variable viscosities depending on the temperature, exponential dependence is the most suitable according to the experimental results which has been indicated in [26].

In the case of temperature dependent viscosity, a significant heat transfer enhancement is accomplished even neglecting the Hall effect, viscous and Joule dissipations. However, under a strong external magnetic field, the Hall current becomes important since it affects the current density due to the influence of the electromagnetic force. The study of MHD flows with Hall current has some important industrial applica-

tions in geophysical and astrophysical situations and in engineering problems such as Hall effect sensors, Hall accelerators, constructions of turbines, and flight magnetohydrodynamics. The investigation of the influence of Hall current on the fluid flow is essential when these applications are considered. Attia [27, 28] has solved the transient MHD flow and heat transfer equations for dusty fluid with temperature dependent viscosity. The effects of both the variable viscosity and magnetic field on the flow have been shown between parallel plates together with the heat transfer of the fluid and dust particles. Moreover, Sayed-Ahmed [29] has also investigated the effect of Hall current on MHD flow and heat transfer for Bingham fluids in a rectangular duct using FDM. Evcin et al. [30] have studied the same MHD flow and heat transfer problem with a viscosity depending on the temperature exponentially, by using mixed finite element method (FEM). They have also used optimal control techniques in order to control the system in desired velocity and temperature by the help of physically significant parameters of the system as control variables.

The magnetohydrodynamic (MHD) duct flow problem is another important application area of convection-diffusion type equations with constant convection coefficients. MHD duct flow problems can be steady or transient as depending on time. Both types of MHD flow problems are studied widely in the literature with some numerical methods used in CFD, through channels with different regular cross-sections like triangle, rectangle or circle. Singh and Lal [31] have solved steady MHD flow in a triangular pipe under the transverse magnetic field by using FDM for small values of Hartmann number. The FEM solutions for steady MHD duct flow problem for Hartmann number less than 10 have also been presented by the same authors [32]. In their study, they have extended their FEM solutions though rectangular, triangular and circular pipes with non-conducting walls. Then, Tezer-Sezgin and Köksal [33] have solved steady MHD flow problem in a duct with rectangular cross-section having arbitrarily conducting walls. The FEM has been used to obtain numerical solutions for Hartmann number values $5 \leq M \leq 100$. In the study given in [34], both polynomial based and Fourier expansion based differential quadrature methods, (PDQ) and (FDQ), for the solution of the steady MHD flow problem have been proposed for the first time with equal and unequal grid points. Moreover, Tezer-Sezgin and Gürbüz [35] have presented the linear polynomial radial basis function (RBF)

approximation to the solution of MHD convection flow in a constricted rectangular domain under a uniformly applied magnetic field in terms of the velocity, temperature and pressure of the fluid. Afterwards, the steady MHD duct flow problem through a rectangular duct has been solved by using Chebyshev collocation method for the first time in [36]. In this study the flow is under a uniform oblique magnetic field and the solutions in terms of the velocity and induced magnetic field have been obtained for large Hartmann number values, $M \leq 1000$. In the study [37], MHD flow in a straight pipe having circular cross-section has been studied under a transverse magnetic field. The wall and outside of the duct are assumed to be electrically conducting. Partial differential equations for inside region have been solved by using the DRBEM together with the PDEs for outside region of the duct. The study concludes that, as the magnetic Reynolds number of the fluid increases, MHD flow behaves as it is in a pipe with insulated walls. Apart from the above mentioned studies, MHD flow problems can be considered in irregular domains (complex geometries) rather than regular domains. Bozkaya and Tezer-Sezgin [38] have considered steady MHD pipe flow in irregular type annular-like domains with conducting walls by using the extended-domain-eigenfunction method (EDEM) and the boundary element method (BEM). However, steady MHD duct flows can be solved by using an element free method like in the study [39]. The authors have introduced a meshless method based on the element free Galerkin method (EFGM) for MHD flow in a rectangular duct having arbitrary electrical conductivity.

The researches on the unsteady MHD duct flow problems are as follows. Gupta and Singh [40] have obtained an exact solution for the unsteady MHD flow only for some special cases. The fluid flows in a circular pipe under a uniform magnetic field applied parallel to the diameter of the cross-section of pipe having insulated wall. The unsteady MHD flow in a duct having insulated walls has been solved by Tezer-Sezgin and Gürbüz [41] by using the RBF approximation. They have used the explicit Euler time integration scheme for the time derivatives and also they showed the numerical stability of the solution. In the study [42], the meshless local boundary integral equation (LBIE) method has been presented for the solution of the unsteady MHD flow through rectangular and circular pipes having non-conducting walls. The proposed method uses moving least squares (MLS) approach to approximate the unknown func-

tions. The behaviors of the velocity and the induced magnetic field have been obtained at desired time levels for Hartmann number values $5 \leq M \leq 40$. The study [43] conducted by Bozkaya and Tezer-Sezgin, unsteady convection-diffusion-type equations in two-dimension have been solved by using the boundary element method (BEM) having a fundamental solution depending on time. In this study, arbitrary wall conductivities are considered for the MHD duct flow problems along with the coupled boundary conditions. Singh and Lal [44] have presented a numerical solution for the unsteady MHD flow in a pipe having arbitrarily conducting walls. The FEM solutions have been illustrated with rectangular, circular and triangular cross-sections of the pipe. Salah et al. [45] have developed a FEM solution for the three-dimensional coupled MHD flow equations. They have presented the stability and accuracy analysis of their FEM solutions which is valid for both low and high magnetic Reynolds number. Moreover, a combination of the dual reciprocity BEM (DRBEM) and the differential quadrature method (DQM) has been proposed to obtain a numerical solution of the unsteady MHD flow in a rectangular duct having insulated walls in [46]. The authors have concluded that, a large increment for time can be used to obtain the solution at any desired time level instead of step by step computations in time. Moreover, the magnetic field can be generated by an electric current through a thin wire which is located parallel to the axis of duct with a small distance. This configuration at the each cross-section resembles the MHD flow under a point source magnetic field. Senel and Tezer-Sezgin [47] have solved both the Stokes and Navier–Stokes equations in rectangular and circular cavities under the effect of external point source magnetic field. The numerical solution of the velocity and pressure of the fluid have been obtained by using DRBEM. The biomagnetic fluid flow equations are solved under a point source magnetic field in a 3D rectangular duct by using the numerical method based on a pressure-linked pseudotransient method in [48]. The semi-implicit method for pressure linked equations (SIMPLE) has been used for the solution of electrically conducting magnetic fluid flow equations in a lid-driven cavity in [49] .

In the above mentioned studies, the MHD duct flow problems have several numerical implementations, however, they have a common property that the external magnetic field is uniformly applied in the xy -plane with a constant intensity B_0 . On the other hand, applied magnetic field can vary with time making the velocity and the

induced magnetic field time-dependent as well as the coefficients of convection terms (e.g. Hartmann number in the case of uniform applied magnetic field) depending on time. Bandaru [50] and Bandaru, et al. [51] have applied the general approach of the boundary integral procedure to the problem of turbulent magnetohydrodynamic flow in rectangular ducts as magnetic Reynolds number $R_m \approx 1$. In this case, both magnetic advection and diffusion terms have important roles in the flow behavior. The MHD flow through a pipe which is subjected to a time-varied oblique magnetic field $B_0(t) = B_0 f(t)$ where B_0 is the intensity of the applied magnetic field at the initial time level ($t = 0$) and $f(t)$ is a time varied function is considered as a second problem in the thesis. The governing transient flow and induced magnetic field equations are solved by using the DRBEM. For the function $f(t)$, several definitions have been used such as polynomial, exponential, trigonometric, impulse and step functions. Then, the MHD flow with time-dependent applied magnetic field is generalized by including the Reynolds number R_e and magnetic Reynolds number R_m influences to the time derivatives of the velocity and the induced magnetic field. Dehghan and Mirzaei [52] have solved the equations with R_e and R_m but in the case of uniform magnetic field. Thus, as a third problem of the thesis, the effects of the problem parameters R_e and R_m have been investigated on the same time-varied MHD duct flow problem under the time-dependent applied magnetic field.

Up to here, all the considered MHD duct flow problems are under the influence of an external uniform magnetic field applied in the xy -plane (in the cross section of the pipe (duct)). That means that, the strength of the applied magnetic field B_0 is constant. However, there are gradients of the applied magnetic field varying in the streamwise direction in real life applications such as in designing the self cooled liquid-metal blankets which are used for fusion reactor systems. Therefore, understanding the MHD flows under a non-uniform applied magnetic field is the key point for the development of liquid-metal blankets for future power plants. The MHD effects originated from the liquid metal flow in a pipe under a magnetic field cause a large drop on the fluid pressure [53]. Furthermore, the induced currents are closed within the flow domain for the flow in a duct with conducting walls. The currents returning through the conducting walls enhance the MHD pressure drop [54]. Therefore, the electrical conductivity of the duct walls also influences the flow behavior greatly [55]. A non-

uniform applied magnetic field especially depending on the direction of the pipe-axis causes some deviations on the fully-developed two-dimensional flow, and leads to interesting three-dimensional effects. In the thesis, we have also studied the MHD flows in a rectangular duct under the influence of an axially-changing applied magnetic field as in the third and fourth problems. The MHD duct flow studies under a non-uniform applied magnetic field are as follows. Kim [56] has studied three-dimensional liquid-metal MHD flow in a square duct under a non-uniform magnetic field. The axial-dependent magnetic field is applied perpendicularly to streamwise direction of the flow. The induced magnetic field is neglected due to small magnetic Reynolds number, and the inductionless MHD flow problem is solved in terms of the velocity and electric potential equations. Sterl [57] has also considered MHD flow in rectangular ducts in two and three dimensional regions. Firstly, he has studied two-dimensional MHD duct flow under a uniform magnetic field to examine the effect of the wall conductance ratio and several Hartmann number values on the flow behavior. Then, he has investigated three-dimensional MHD flow and shown the effects caused by axial-dependent applied magnetic field through the duct having well-conducting walls. Moreover, the MHD flow of liquid metal in thin conducting rectangular ducts under an inclined non-uniform transverse magnetic field has been studied in [58]. The aims of this study are to confine the angle between the magnetic field lines and side walls and to examine the MHD flow behavior in terms of the velocity, pressure and electric potential equations. Then, Kamamaru et al. [53] have also obtained numerical solution of the three-dimensional liquid-metal MHD flow through a circular pipe in the inlet region of the applied magnetic field. The flow is under the influence of an axially varying vertically applied magnetic field. They have considered the MHD duct flow equations in terms of velocity and induced magnetic field.

On the other hand, there are also MHD duct flow problems under the influence of spatially varying magnetic fields in the literature. Some of these studies are as follows. Klüber et al. [59] have solved the turbulent MHD flow equations in terms of the velocity and electric potential using FVM with a consistent current-conservative scheme. In their simulations, they have assumed that the magnetic field is stationary and not affected by the flow. In other words, they have considered an inductionless MHD flow since the magnetic Reynolds number is small. Then, Walker [60] has

studied a non-uniform, spatially varying magnetic field effect on the flow experimentally, again neglecting the induced magnetic field with the small magnetic Reynolds number assumption. Moreover, the steady flow of an electrically conducting fluid through a duct having rectangular cross-section with thin and electrically conducting walls has been considered in [61]. The fluid is under a non-uniform, spatially varying transverse magnetic field which is parallel to two duct walls. Furthermore, Bühler and Mistrangelo [62] have studied MHD flow under a spatially varying magnetic field. The author's main concern is to observe the MHD pressure drop and flow behavior under the influence of spatially varying magnetic field. The velocity, pressure and electric current equations are solved numerically. They have analyzed MHD flow in two entire coupled breeder units under this non-uniform strong magnetic field for the first time.

1.7 Originality of the Thesis

In the thesis, four different MHD duct flow problems are studied under the boundary conditions which are suitable according to the physics of the problem. The inductionless MHD flow with temperature dependent viscosity and heat transfer is the first considered problem. Secondly, the MHD duct flow under a time-varied external magnetic field is studied. Then, we turn our concern to MHD flow problems under an external magnetic field varying in the streamwise direction (pipe-axis direction) in the third and the fourth problems. Specifically, the inductionless MHD flow with electric potential is considered under the effect of the axially-changing magnetic field as the third problem. Adding the induced magnetic field to the velocity and electric potential equations as a triple, MHD flow equations under axial-dependent magnetic field are examined as the last problem considered throughout the thesis.

In the first problem, the diffusion term in the velocity equation contains variable coefficient in it, depending on the temperature. The parametric BEM and the DRBEM procedures are applied to solve the velocity equation while the energy equation of the MHD flow is solved by using the DRBEM in both cases. The parametric BEM procedure uses a fundamental solution which is a Levi function treating all the terms of the diffusion term in its original form. On the other hand, DRBEM procedure uses

fundamental solution of Laplace equation which is the dominant or main operator and obtaining this term requires some arrangements in the equation. However, when a PDE contains a variable coefficient, a fundamental solution which is required in the BEM applications is generally not available in explicit form. Contrarily, a Levi function is usually available in parametrix BEM. In this considered problem, our aim is to examine the behavior of the MHD flow and also to compare the efficiency of both parametrix BEM and DRBEM. In the literature, most of the BEM solutions are used with the fundamental solution of the Laplace equation. However, in this problem, the use of both a Levi function in parametrix BEM and the Laplace operator in DRBEM is deeply studied and the solutions are compared. This procedure is an original contribution to the solution of variable coefficient convection-diffusion type equations, especially to the solution of MHD flow and heat transfer with temperature dependent viscosity.

There is a wide range of steady or unsteady MHD duct flow problems under a uniform applied magnetic field. Some MHD duct flow studies with point-source magnetic field (space dependent) are also presented. On the other hand, non-uniform applied magnetic field (i.e. time dependent) studies are not given to the best knowledge of us. Thus, in the second problem of the thesis, we consider the MHD flow through a pipe having rectangular cross-section which is subjected to a time-varied oblique magnetic field. This constitutes another originality of the thesis since the governing equations are derived taking a magnetic field depending on time and they are solved by the use of DRBEM. Solving the coupled equations in terms of the velocity and induced magnetic field by choosing several definitions of time varied-function presents the first part of the numerical results for the $R_e = R_m = 1$ assumption. Then, the computations are enriched with the effects of R_e and R_m increasing values. Thus, both the effects of R_e and R_m and several choices of the time-variation on the flow behavior are discussed in the thesis.

As the third and fourth problems, the two-dimensional, laminar, MHD flow of a viscous, incompressible and electrically conducting fluid in a rectangular duct has been considered. The flow is under the influence of an axially-varying applied magnetic field $B_0(z)$. Some magnets are placed on the duct axis at fixed z -values and they are varying as a function of z . The flow is assumed to be fully-developed between two

fixed z -values. In the third problem, the flow behavior and the structure of the boundary layers influenced from the changes in the electrical conductivity of the walls, and the axial dependence of the applied magnetic field have been studied. The induced magnetic field is neglected due to small magnetic Reynolds number, and the inductionless MHD flow problem is solved in terms of velocity and electric potential equations. On the other hand, in the fourth considered problem in the thesis, the induced magnetic field with the interaction of an axially dependent applied magnetic field is introduced inside the fluid. Thus, the induced magnetic field equation along with the velocity and electric potential equations are considered for the MHD duct flow problem. Actually, the last problem is an extension of the equations obtained in the third problem in the sense that the induced magnetic field is also involved. Obtaining the DRBEM solutions of the third and fourth problems are original contribution of the thesis.

1.8 Plan of the Thesis

In this thesis, the governing equations of the considered MHD flow problems are described and the dimensionless forms are acquired in Chapter 1. Moreover, a literature survey on the thesis subject and the originality of the thesis are presented in Section 1.6 and Section 1.7, respectively.

In Chapter 2, the BEM for the Laplace and Poisson's equations and the parametric BEM for the diffusion equation containing variable coefficient are introduced. Moreover, the DRBEM which has the advantage of applying the BEM to all Poisson's type equations involving the solution itself, is also introduced. The constant and linear element discretizations for the boundary are provided since both types of discretizations are used to obtain numerical solutions of the problems considered in the thesis. Then, composite trapezoidal rule is presented to approximate the domain integral arising from the application of the BEM to Poisson's type equations. The last section of this Chapter is devoted to the Implicit Euler method which is used to approximate the time derivative in the equations by using the finite difference scheme.

In Chapter 3, the applications of BEM procedures to the MHD duct flow equations

are given. The BEM solution of the MHD flow and heat transfer with temperature dependent viscosity is presented in the first section of Chapter 3. The parametric BEM procedure which uses a Levi function to reduce the two-dimensional mixed BVPs to a boundary-domain integral equation (BDIE) together with the DRBEM procedure are explained in detail for the solution of the MHD flow equations in terms of the momentum and energy. Section 3.2 is devoted to the iterative DRBEM solution procedure for the unsteady MHD duct flow equations under a time-varied external magnetic field. The last two parts of Chapter 3 focus on the DRBEM solutions of the MHD duct flow problems under axial-dependent magnetic field. Some magnets are placed on the pipe-axis and they determine the strength of the applied magnetic field and constitute electromagnetic force in the flow. In Section 3.3 the induced magnetic field is neglected due to the small magnetic Reynolds number and so the MHD flow problem is solved in terms of the velocity and electric potential. On the other hand, the induced magnetic field equation is accompanied to the velocity and electric potential equations in Section 3.4 for the case of axial-dependent applied magnetic field.

Chapter 4 of the thesis is dedicated to the numerical results of each considered problem in Chapter 3. The detailed discussions of the results obtained for the MHD duct flow problems are given.

In Chapter 5, all the important numerical results obtained from the studies are summarized.

CHAPTER 2

THE BOUNDARY AND THE DUAL RECIPROCITY BOUNDARY ELEMENT METHODS

In this thesis, the Boundary Element Method (BEM) for the Laplace and Poisson's equations, the parametrix BEM for the diffusion equation containing variable coefficient, and the Dual Reciprocity Boundary Element Method (DRBEM) which has the advantage of applying the BEM to all Poisson's type equations involving the solution itself, are presented following the references [5], [63], [7], respectively. The BEM is a boundary-only nature technique for solving partial differential equations (PDEs). The most important feature of BEM is its unique ability to provide the problem solution by discretizing only the boundary of the problem region. In this method, a partial differential equation defined in a domain is converted to an integral equation defined on the boundary of the domain. The use of BEM reduces the dimension of the discretized system, and so it provides less computational cost compared to the other domain type discretization techniques such as Finite Element Method (FEM), Finite Difference Method (FDM) and Finite Volume Method (FVM). Especially for the homogeneous PDEs the BEM is a very suitable technique. However, the application of BEM to the non-homogeneous PDEs brings domain integrals in the integral equations and the BEM is accompanied with the computation of these domain integrals requiring internal discretization along with the boundary discretization which enlarges the dimension of the problem.

In some cases, a PDE contains a variable coefficient in its dominant operator. For this type of equation, a fundamental solution which is required in the BEM application is generally not available in explicit form. On the other hand, a parametrix (Levi function) is usually available. With the help of the parametrix, the differential equation is

reduced to a boundary-domain integral equation (BDIE). This formulation is called as parametrix BEM. Using a parametrix as a fundamental solution treats the variable coefficient in the PDE directly. When the parametrix BEM is applied to a PDE with variable coefficient in its diffusion term, a domain integral also arises besides the boundary integrals which causes again the loss of the advantages of BEM.

In order to overcome these drawbacks of BEM, new methods have been revealed. The most prominent one is the DRBEM. In this method, the Laplacian term or the main operator term of the differential equation is kept on one side of the equation and all the other terms of the differential equation are preserved on the other side. The main idea of the DRBEM is to treat these terms on the other side as inhomogeneities and approximating them by series of radial basis functions which are connected to the particular solution of the differential equation through the main, i.e. the Laplacian operator. The DRBEM procedure enables one to transform the differential equation into boundary-only integral equation. Interior computation is also included to the final system of linear equations.

In this chapter, the BEM formulation on the Laplace equation is explained in details by using both constant and linear element discretizations in Section 2.1, [5]. Then, the BEM formulation is specified on the Poisson's equation with the fundamental solution of Laplace equation in Section 2.2. Since this approach brings a domain integral in the integral equation, composite trapezoidal rule is given in Section 2.2.1 to handle this domain integral accurately. Moreover, in Section 2.3 the parametrix BEM formulation is also described for diffusion equation with a variable coefficient, [63]. Furthermore, the DRBEM formulation is presented in details on the Poisson's type equations using the fundamental solution of Laplace equation in Section 2.4. Also, the usage of DRBEM is extended further for the Poisson's type equations, containing the unknown and its derivatives with respect to space variables and time, in Sections 2.4.1- 2.4.3. Finally, a time integration scheme which is implicit Euler method is introduced for the solution of the system of ordinary differential equations resulted from the time dependent problems in Section 2.4.3.1, [7].

2.1 The BEM procedure for the Laplace equation $\nabla^2 u = 0$

The two-dimensional Laplace's equation in a domain $\Omega \subset \mathbb{R}^2$ is given as

$$\nabla^2 u = 0, \quad (x, y) \in \Omega \quad (2.1)$$

with Dirichlet and Neumann types boundary conditions

$$\begin{aligned} u(x, y) &= \bar{u}(x, y), \quad (x, y) \in \Gamma_1 \\ q(x, y) &= \frac{\partial u}{\partial n}(x, y) = \bar{q}(x, y), \quad (x, y) \in \Gamma_2 \end{aligned} \quad (2.2)$$

where $\nabla^2 = \frac{\partial^2}{\partial x^2} + \frac{\partial^2}{\partial y^2}$ denotes the Laplace operator, $\Gamma = \partial\Omega$ is the boundary with $\Gamma = \Gamma_1 \cup \Gamma_2$. The right hand side functions $\bar{u}(x, y)$ and $\bar{q}(x, y)$ are given functions and n is the unit normal vector to the boundary Γ of Ω .

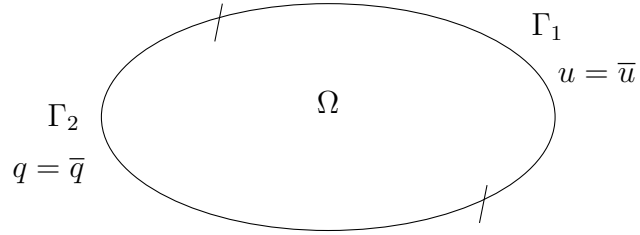


Figure 2.1: Configuration of the problem domain and the boundary conditions

The solution of equation (2.1) and its normal derivative are represented as

$$u(x, y) = \begin{cases} \bar{u}(x, y), & (x, y) \in \Gamma_1 \\ \tilde{u}(x, y), & (x, y) \in \Gamma_2 \end{cases} \quad (2.3)$$

and

$$q(x, y) = \begin{cases} \bar{q}(x, y), & (x, y) \in \Gamma_2 \\ \tilde{q}(x, y), & (x, y) \in \Gamma_1 \end{cases} \quad (2.4)$$

where $\tilde{u}(x, y)$ and $\tilde{q}(x, y)$ are the unknown values of u and q on Γ_2 and Γ_1 , respectively.

For solving the Laplace equation, the BEM uses the fundamental solution of Laplace equation which is

$$u^* = \frac{1}{2\pi} \ln\left(\frac{1}{r}\right) = \frac{1}{2\pi} \ln\left(\frac{1}{|r - r_i|}\right) \quad (2.5)$$

where $r = (x, y)$ and $r_i = (x_i, y_i)$ are the variable and fixed points in $\Gamma \cup \Omega$, respectively. The fundamental solution u^* satisfies

$$\nabla^2 u^* = -\Delta_i \quad (2.6)$$

where Δ_i is the Dirac delta function satisfying the following properties

$$\Delta_i(x) = \begin{cases} 0 & \text{if } x \neq x_i \\ \infty & \text{if } x = x_i \end{cases}, \quad \int_{\Omega} \Delta_i(x) d\Omega = 1 \quad (2.7)$$

and

$$\int_{\Omega} \phi(x) \Delta_i d\Omega = \begin{cases} \phi(x_i) & \text{if } x_i \in \Omega \\ 0 & \text{if } x_i \notin \Omega \end{cases} \quad (2.8)$$

for a continuous function ϕ at x_i .

In the BEM application of the problem (2.1)-(2.2), firstly, the weighted residual statement is obtained by multiplying both sides of equation (2.1) with the fundamental solution u^* and integrating over the domain Ω as

$$\int_{\Omega} (\nabla^2 u) u^* d\Omega = 0. \quad (2.9)$$

Applying Green's second identity two times to the equation (2.9) yields

$$\int_{\Omega} u \nabla^2 u^* d\Omega + \int_{\Gamma} \frac{\partial u}{\partial n} u^* d\Gamma - \int_{\Gamma} \frac{\partial u^*}{\partial n} u d\Gamma = 0. \quad (2.10)$$

After inserting the boundary conditions given in equation (2.2) by using the definitions (2.3) and (2.4), the following boundary-domain integral equation is obtained

$$\int_{\Omega} u \nabla^2 u^* d\Omega + \int_{\Gamma_1} \tilde{q} u^* d\Gamma_1 + \int_{\Gamma_2} \bar{q} u^* d\Gamma_2 - \int_{\Gamma_1} \bar{u} q^* d\Gamma_1 - \int_{\Gamma_2} \tilde{u} q^* d\Gamma_2 = 0 \quad (2.11)$$

where $q^* = \frac{\partial u^*}{\partial n}$ is the normal derivative of u^* .

Application of the Dirac delta function properties in (2.7)-(2.8) for the first term of equation (2.11) results in

$$\int_{\Omega} u \nabla^2 u^* d\Omega = \int_{\Omega} u (-\Delta_i) d\Omega = -c_i u_i \quad (2.12)$$

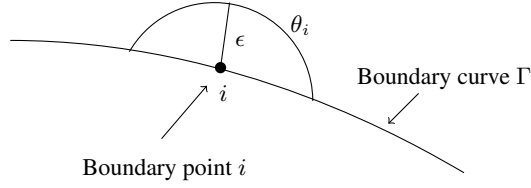


Figure 2.2: Internal angle at the boundary point i

where the coefficient c_i is given as

$$c_i = \begin{cases} \frac{\theta_i}{2\pi}, & i \in \Gamma \\ 1, & i \in \Omega \setminus \Gamma \end{cases} \quad (2.13)$$

with an internal angle θ_i at the point i as shown in Figure 2.2.

Thus, the equation (2.10) becomes

$$c_i u_i - \int_{\Gamma} q u^* d\Gamma + \int_{\Gamma} q^* u d\Gamma = 0. \quad (2.14)$$

For solving the above equation in terms of the unknown values of u on the boundary and inside the region, and normal derivative values $q = \frac{\partial u}{\partial n}$ on the boundary, discretization of the boundary Γ is the essential part. Various forms of the elements such as constant, linear, quadratic or cubic may be used for the discretization. In this thesis, constant and linear element discretizations are used and so they are presented here in details.

2.1.1 Boundary discretization with constant elements

In constant element discretization, the nodes are taken as a mid-point of each element as shown in Figure 2.3. The boundary is smooth at the nodes and the number of boundary nodes N equals to the number of constant elements on Γ .

Discretized form of the boundary-integral equation (2.14) is

$$c_i u_i - \sum_{k=1}^N \int_{\Gamma_k} u^* q d\Gamma_k + \sum_{k=1}^N \int_{\Gamma_k} q^* u d\Gamma_k = 0, \quad i = 1, \dots, N. \quad (2.15)$$

The integrands in equation (2.15) contain the unknown boundary values u and q . In this type of discretization, the function values of u and q are considered as constants

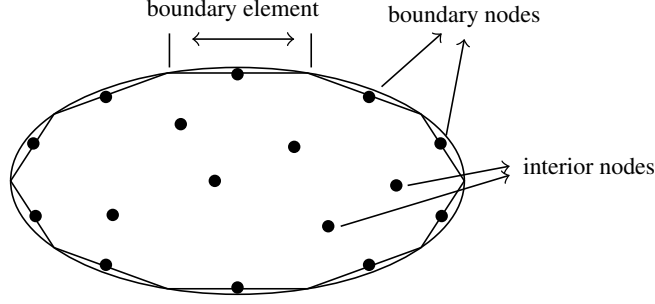


Figure 2.3: Configuration for constant elements discretization

over each element and the values of u and q are equivalent to their value only at the mid-point of each element. Therefore, u and q in equation (2.15) can be taken outside of the integral over each element k by taking the mid-point value of the element k . In other words, the nodal values of u and q are denoted by u_k and q_k , respectively. Thus, equation (2.15) is rewritten as

$$c_i u_i - \sum_{k=1}^N q_k \int_{\Gamma_k} u^* d\Gamma_k + \sum_{k=1}^N u_k \int_{\Gamma_k} q^* d\Gamma_k = 0, \quad i = 1, \dots, N. \quad (2.16)$$

The integrals over each boundary element Γ_k , $\int_{\Gamma_k} u^* d\Gamma_k$ and $\int_{\Gamma_k} q^* d\Gamma_k$ need to be computed. The evaluation of these integrals brings

$$c_i u_i + \sum_{k=1}^N \bar{H}_{ik} u_k - \sum_{k=1}^N G_{ik} q_k = 0, \quad i = 1, \dots, N \quad (2.17)$$

where the entries of the matrices $\bar{\mathbf{H}}$ and \mathbf{G} are [5]

$$\begin{aligned} \bar{H}_{ik} &= \int_{\Gamma_k} q^* d\Gamma_k = -\frac{1}{2\pi} \int_{\Gamma_k} \frac{(r - r_i) \cdot \vec{n}}{|r - r_i|^2} d\Gamma_k \quad \text{if } i \neq k \\ G_{ik} &= \int_{\Gamma_k} u^* d\Gamma_k = \frac{1}{2\pi} \int_{\Gamma_k} \ln\left(\frac{1}{|r - r_i|}\right) d\Gamma_k \quad \text{if } i \neq k. \end{aligned} \quad (2.18)$$

The vectors $\vec{r} = (x, y)$ and $\vec{r}_i = (x_i, y_i)$ are both changing depending on the position of k -th boundary element and boundary nodes, respectively.

The matrices $\bar{\mathbf{H}}$ and \mathbf{G} can be computed analytically or numerically for the case $i \neq k$. When $i = k$, \bar{H}_{ii} equals to zero due to the dot product with the normal in the definition. In this case, the difference vector $(\vec{r} - \vec{r}_i)$ is always perpendicular to the normal vector \vec{n} on the same element i . For the diagonal entries of the matrix \mathbf{G} , the singularity arises due to logarithmic function in the fundamental solution u^* . Therefore, the

diagonal entries of the matrix \mathbf{G} can be computed using exact logarithmic integration such as

$$G_{ii} = \frac{\ell_e}{2\pi} \left(\ln\left(\frac{2}{\ell_e}\right) + 1 \right) \quad (2.19)$$

where ℓ_e denotes the length of each element [7].

When, the entries of $\overline{\mathbf{H}}$ and \mathbf{G} matrices are evaluated, to solve the system of equations in (2.17) the value c_i needs to be clarified. For boundary solutions the constant c_i equals to $1/2$ since the internal angle θ_i at any node is π . The value c_i equals to 1 for the interior computations.

Thus, the discretized equation (2.17) for a node i on the boundary takes the form

$$\frac{1}{2}u_i + \sum_{k=1}^N \overline{H}_{ik}u_k - \sum_{k=1}^N G_{ik}q_k = 0, \quad i = 1, \dots, N \quad (2.20)$$

which can also be expressed as

$$\sum_{k=1}^N H_{ik}u_k - \sum_{k=1}^N G_{ik}q_k = 0, \quad i = 1, \dots, N \quad (2.21)$$

where

$$H_{ik} = \overline{H}_{ik} + \frac{1}{2}\delta_{ij}, \quad (2.22)$$

δ_{ik} representing the Kronecker delta function as

$$\delta_{ik} = \begin{cases} 1 & \text{if } i = k \\ 0 & \text{if } i \neq k. \end{cases} \quad (2.23)$$

Equation (2.21) can also be written in a matrix-vector form as

$$\mathbf{H}\mathbf{u} = \mathbf{G}\mathbf{q} \quad (2.24)$$

where \mathbf{H} and \mathbf{G} are $N \times N$ matrices with the entries defined in (2.18), (2.19) and (2.22). The vectors \mathbf{u} and \mathbf{q} have length $N \times 1$ containing the solution of the problem and its normal derivative on the boundary, respectively. After inserting the boundary conditions (2.3) and (2.4) to the matrix-vector equation (2.24), both the vectors \mathbf{u} and \mathbf{q} contain some known and unknown values. One must collect the unknown values of \mathbf{u} and \mathbf{q} on the left hand side of the equation by swapping the corresponding columns

of the matrices \mathbf{H} and \mathbf{G} as described in [5]. Thus, a linear system of algebraic equations can be obtained such as

$$\mathbf{A}\mathbf{x} = \mathbf{d} \quad (2.25)$$

where \mathbf{x} is the vector of unknowns ($\tilde{\mathbf{u}}$ on Γ_2 and $\tilde{\mathbf{q}}$ on Γ_1). Gaussian elimination or any other linear system solution scheme can be applied to obtain the unknown values of $\tilde{\mathbf{u}}$ and $\tilde{\mathbf{q}}$ on the boundary parts Γ_2 and Γ_1 , respectively. The matrix \mathbf{A} is a full matrix showing no special form although it contains lots of zero entries.

Then, these obtained boundary values are used in equation (2.17) to compute unknown values of \mathbf{u} at each interior point i by taking $c_i = 1$ which is

$$u_i = - \sum_{k=1}^N \bar{H}_{ik} u_k + \sum_{k=1}^N G_{ik} q_k, \quad i = 1, \dots, L. \quad (2.26)$$

Here, u_k and q_k represent the known values (given and already computed) on the boundary Γ of Ω . Matrices $\bar{\mathbf{H}}$ and \mathbf{G} have entries defined in equation (2.18) with the vectors r and r_i on the boundary element and at the internal nodes, respectively. L is the number of interior nodes. The vector r is measured now from the interior point i to the boundary elements.

2.1.2 Boundary discretization with linear elements

When the position of nodes are changed from the mid-point of elements to the corner points of polygon, the linear element discretization is obtained as shown in Figure 2.4.

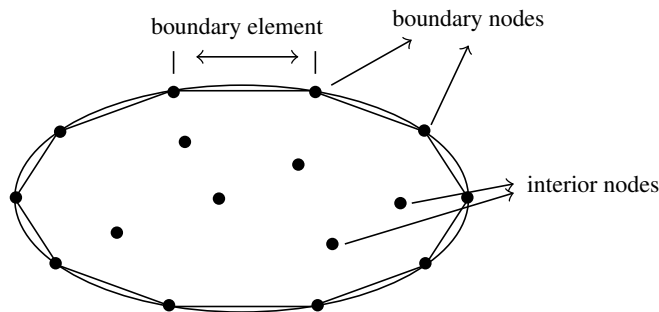


Figure 2.4: Configuration for linear elements discretization

If N number of boundary elements are used for the discretization of the boundary, we have the following discretized equation for the equation (2.14)

$$c_i u_i - \sum_{k=1}^N \int_{\Gamma_k} u^* q d\Gamma_k + \sum_{k=1}^N \int_{\Gamma_k} q^* u d\Gamma_k = 0, \quad i = 1, \dots, N. \quad (2.27)$$

Now, the u and q values are not constants anymore and they are varying linearly over each element Γ_k . Therefore, u and q can not be taken outside of the integral in equation (2.27). The values of u and q over each element vary linearly as

$$\begin{aligned} u(\xi) &= \psi_1 u_1 + \psi_2 u_2 \\ q(\xi) &= \psi_1 q_1 + \psi_2 q_2 \end{aligned} \quad (2.28)$$

where u_1 and u_2 are the values of the function u at the first and second nodes of an element, respectively. ψ_1 and ψ_2 are the linear interpolation functions and they are also referred as linear shape functions in local coordinate ξ varying from -1 to 1 .

The interpolation functions ψ_1 and ψ_2 are linear functions in local coordinate ξ

$$\begin{aligned} \psi_1 &= \frac{1}{2}(1 - \xi) \\ \psi_2 &= \frac{1}{2}(1 + \xi). \end{aligned} \quad (2.29)$$

The insertion of the functions u and q given in (2.28) into equation (2.27) results in

$$c_i u_i - \sum_{k=1}^N \int_{\Gamma_k} (\psi_1 q_1 + \psi_2 q_2) u^* d\Gamma_k + \sum_{k=1}^N \int_{\Gamma_k} (\psi_1 u_1 + \psi_2 u_2) q^* d\Gamma_k = 0, \quad (2.30)$$

which is rewritten as

$$c_i u_i - \sum_{k=1}^N \int_{\Gamma_k} \begin{bmatrix} \psi_1 & \psi_2 \end{bmatrix} u^* d\Gamma_k \begin{Bmatrix} q_1 \\ q_2 \end{Bmatrix} + \sum_{k=1}^N \int_{\Gamma_k} \begin{bmatrix} \psi_1 & \psi_2 \end{bmatrix} q^* d\Gamma_k \begin{Bmatrix} u_1 \\ u_2 \end{Bmatrix} = 0, \quad (2.31)$$

for $i = 1, \dots, N$.

With the evaluation of the integrals in equation (2.31), it is also expressed as

$$c_i u_i + \sum_{k=1}^N \begin{bmatrix} h_{ik}^1 & h_{ik}^2 \end{bmatrix} \begin{Bmatrix} u_1 \\ u_2 \end{Bmatrix} = \sum_{k=1}^N \begin{bmatrix} g_{ik}^1 & g_{ik}^2 \end{bmatrix} \begin{Bmatrix} q_1 \\ q_2 \end{Bmatrix}, \quad i = 1, \dots, N \quad (2.32)$$

with

$$\begin{aligned} h_{ik}^1 &= \int_{\Gamma_k} \psi_1 q^* d\Gamma_k, & h_{ik}^2 &= \int_{\Gamma_k} \psi_2 q^* d\Gamma_k \\ g_{ik}^1 &= \int_{\Gamma_k} \psi_1 u^* d\Gamma_k, & g_{ik}^2 &= \int_{\Gamma_k} \psi_2 u^* d\Gamma_k. \end{aligned} \quad (2.33)$$

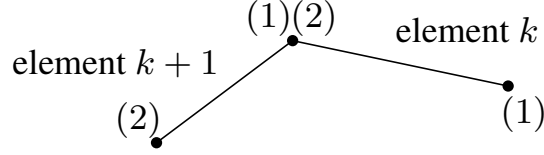


Figure 2.5: Nodes connection of linear elements

Figure 2.5 represents the linear element configuration. The nodes (1) and (2) denote the first and second nodes of an element. It can be seen from Figure 2.5 that, the first node of the element $k + 1$ is the second node of the element k . Therefore, a special arrangement called as assembly procedure is needed to evaluate the contribution of a node to an element. That is,

$$\begin{aligned}
 \bar{H}_{ik} &= h_{i(k-1)}^2 + h_{ik}^1 \quad \text{if } k = 2, 3, \dots, N \\
 \bar{H}_{i1} &= h_{iN}^2 + h_{i1}^1, \\
 G_{ik} &= g_{i(k-1)}^2 + g_{ik}^1 \quad \text{if } k = 2, 3, \dots, N \\
 G_{i1} &= g_{iN}^2 + g_{i1}^1.
 \end{aligned} \tag{2.34}$$

Then, equation (2.30) can be written in assembled form for a boundary point $i = 1, \dots, N$ as

$$c_i u_i + \begin{bmatrix} \bar{H}_{i1} & \bar{H}_{i2} & \dots & \bar{H}_{iN} \end{bmatrix} \begin{Bmatrix} u_1 \\ u_2 \\ \vdots \\ u_N \end{Bmatrix} = \begin{bmatrix} G_{i1} & G_{i2} & \dots & G_{iN} \end{bmatrix} \begin{Bmatrix} q_1 \\ q_2 \\ \vdots \\ q_N \end{Bmatrix}. \tag{2.35}$$

As in the constant element case, the same singularity arises to evaluate the diagonal entries of the matrix \mathbf{G} . In this time, G_{ii} can be computed as follows [5]

$$\begin{aligned}
 G_{ii} &= \frac{\ell_e}{2} \left(\frac{1}{2} - \ln(\ell_e) \right), \quad \text{if } i = k_1 \\
 G_{ii} &= \frac{\ell_e}{2} \left(\frac{3}{2} - \ln(\ell_e) \right), \quad \text{if } i = k_2
 \end{aligned} \tag{2.36}$$

where k_1 and k_2 denote the first and the second nodes of the element k , respectively.

Equation (2.35) is arranged for a node i as

$$c_i u_i + \sum_{k=1}^N \bar{H}_{ik} u_k - \sum_{k=1}^N G_{ik} q_k = 0, \quad i = 1, \dots, N \quad (2.37)$$

which can be transformed into the following matrix-vector equation as

$$\mathbf{H}\mathbf{u} = \mathbf{G}\mathbf{q} \quad (2.38)$$

where \mathbf{H} and \mathbf{G} are $N \times N$ matrices with $H_{ik} = c_i \delta_{ik} + \bar{H}_{ik}$. The value c_i depends on the internal angle of nodes or equivalently smoothness of the corner of each boundary element. The diagonal entries of the matrix \mathbf{H} in equation (2.38) is calculated by using the following fact; whenever a uniform potential is applied over a bounded region, all the derivative values must be zero. Consequently, equation (2.38) becomes

$$\mathbf{H}\mathbf{u} = \mathbf{0} \quad (2.39)$$

where \mathbf{u} is the vector of constant values. Hence, the sum of all elements of any row of \mathbf{H} should be zero, and the values of the diagonal entries is calculated, once the off-diagonal entries are all known as given in [5]

$$H_{ii} = - \sum_{k=1, (k \neq i)}^N H_{ik}. \quad (2.40)$$

Reconsidering equation (2.38), the $N \times 1$ vectors \mathbf{u} and \mathbf{q} have some known and unknown values after inserting the boundary conditions of the problem. By implementing the required swapping procedure, a linear system of algebraic equations $\mathbf{A}\mathbf{x} = \mathbf{d}$ can be obtained where the unknown boundary values of u and q are in the vector \mathbf{x} . The solution of this system brings all the unknown values on the boundary. Now, the values of u and q are known everywhere on the boundary. Then, the interior solution of u can be found by solving the following equation by taking the constant c_i as 1

$$u_i = - \sum_{k=1}^N \bar{H}_{ik} u_k + \sum_{k=1}^N G_{ik} q_k, \quad i = 1, \dots, L \quad (2.41)$$

where L is the interior nodes number and the matrices \bar{H} and G are computed from the above definitions given in equation (2.34) with the vectors r and r_i on the boundary element and at the internal nodes, respectively.

2.2 The BEM procedure for the Poisson's equation $\nabla^2 u = b(x, y)$

The two-dimensional boundary value problem defined by the Poisson's equation with inhomogeneity $b(x, y)$ is

$$\nabla^2 u = b(x, y), \quad (x, y) \in \Omega \quad (2.42)$$

which can be appended by the boundary conditions

$$\begin{aligned} u(x, y) &= \bar{u}(x, y), \quad (x, y) \in \Gamma_1 \\ q(x, y) &= \frac{\partial u}{\partial n}(x, y) = \bar{q}(x, y), \quad (x, y) \in \Gamma_2. \end{aligned} \quad (2.43)$$

The BEM procedure enables one to get

$$c_i u_i - \int_{\Gamma} q u^* d\Gamma + \int_{\Gamma} q^* u d\Gamma = - \int_{\Omega} b u^* d\Omega. \quad (2.44)$$

The same boundary integral terms on the left hand side of equation (2.44) are obtained as in the solution of Laplace equation, $\nabla^2 u = 0$. Along with, the domain integral over Ω arises for the solution of Poisson's equation, $\nabla^2 u = b$. To obtain accurate solution one needs to handle this domain integral carefully. A numerical integration technique has to be used to evaluate the domain integral in integration cells of Ω and the composite trapezoidal rule is one of the valuable numerical integration technique to compute this two-dimensional integral.

2.2.1 Composite trapezoidal rule

Consider a double integral

$$I = \iint_{\Omega} f(x, y) dx dy, \quad (2.45)$$

where $\Omega = \{(x, y) \in \mathbb{R}^2 : a \leq x \leq b, u(x) \leq y \leq v(x)\}$.

The iterated form is

$$I = \int_a^b \left(\int_{u(x)}^{v(x)} f(x, y) dy \right) dx. \quad (2.46)$$

To calculate the integral I , firstly the inner integral has to be approximated using the one-dimensional composite trapezoidal rule with respect to y , and x is kept as fixed. Then, the outer integral has to be evaluated in the same manner.

Hence, define $F(x)$ as

$$F(x) = \int_{u(x)}^{v(x)} f(x, y) dy \quad (2.47)$$

which converts the integral I into $I = \int_a^b F(x) dx$.

Further, I is approximated using the composite trapezoidal rule given in [64]

$$I \approx C(F, h) = \frac{h}{2} \sum_{i=1}^n (F(x_{i-1}) + F(x_i)) \quad (2.48)$$

where $x_i = x_0 + ih$ and $h = \frac{x_n - x_0}{n}$. Therefore, $F(x_i)$ can be calculated as

$$\begin{aligned} F(x_i) &= \int_{u(x_i)}^{v(x_i)} f(x_i, y) dy \approx C(f(x_i), h_i) \\ &= \frac{h_i}{2} \sum_{j=1}^{n_i} (f(x_i, y_{i,j-1}) + f(x_i, y_{i,j})) \end{aligned} \quad (2.49)$$

where $y_{i,j} = u(x_i) + jh_i$ and $h_i = \frac{v(x_i) - u(x_i)}{n_i}$.

Generally, n_i is chosen such that $h \approx h_i$ for all i for simplicity.

Thus, the general formula can be prescribed as

$$I \approx \frac{hh_i}{4} \sum_{i=0}^n \sum_{j=0}^{n_i} w_{i,j} f(x_i, y_{i,j}) \quad (2.50)$$

where $w_{i,j}$ equals to 4 in the interior and equals to 2 on the boundary, and lastly equals to 1 at the corner points of the domain Ω . The points $(x_i, y_{i,j})$ are taken as the end points of the constant elements.

In the following section, the parametrix BEM procedure which is a modified form of the BEM for Diffusion operator involving coefficient of space variables is detailed by considering a two-dimensional diffusion equation with a variable coefficient.

2.3 The parametrix BEM procedure for the diffusion equation containing a variable coefficient

The parametrix BEM gives a boundary-domain integral equation (BDIE) for the numerical solution of two-dimensional mixed boundary value problems (BVPs) of the

type, second-order, linear, elliptic PDE with variable coefficients in the elliptic operator. The method uses a parametrix (Levi function) to reduce the BVP to BDIE.

The second-order, linear, elliptic, variable coefficient partial differential equation of diffusion type is

$$Lu(x, y) = \frac{\partial}{\partial x} \left(a(x, y) \frac{\partial u}{\partial x} \right) + \frac{\partial}{\partial y} \left(a(x, y) \frac{\partial u}{\partial y} \right) = b(x, y), \quad (x, y) \in \Omega \quad (2.51)$$

with partially given boundary conditions of the unknown and flux as

$$\begin{aligned} u(x, y) &= \bar{u}(x, y), \quad (x, y) \in \Gamma_1 \\ Tu(x, y) &= a(x, y) \frac{\partial u}{\partial n}(x, y) = \bar{t}(x, y), \quad (x, y) \in \Gamma_2. \end{aligned} \quad (2.52)$$

For partial differential operators with variable coefficients as L in equation (2.51), a fundamental solution is generally not available in explicit form. However, a parametrix is often available, which is a function $P(x, x_i; y, y_i)$ as given in [6] satisfying

$$LP(x, x_i; y, y_i) = \Delta_i(x - y, x_i - y_i) + R(x, x_i; y, y_i). \quad (2.53)$$

The fundamental solution of the operator L with frozen coefficients $a(x, y) = a(x_i, y_i)$ corresponding to the equation (2.51) is used as a parametrix,

$$P(x, x_i; y, y_i) = \frac{1}{2\pi a(x_i, y_i)} \ln|r - r_i| \quad (2.54)$$

where $|r - r_i| = \sqrt{(x - x_i)^2 + (y - y_i)^2}$ for the variable and source points, $r = (x, y)$ and $r_i = (x_i, y_i)$ in $\Gamma \cup \Omega$, respectively.

Substituting equation (2.54) into equation (2.53) results in

$$\begin{aligned} \frac{\partial}{\partial x} \left(a(x, y) \frac{\partial}{\partial x} \left[\frac{1}{2\pi a(x_i, y_i)} \ln|r - r_i| \right] \right) + \frac{\partial}{\partial y} \left(a(x, y) \frac{\partial}{\partial y} \left[\frac{1}{2\pi a(x_i, y_i)} \ln|r - r_i| \right] \right) = \\ \Delta_i(x - y, x_i - y_i) + R(x, x_i; y, y_i). \end{aligned} \quad (2.55)$$

By taking $a(x, y) = a(x_i, y_i)$ and $(\frac{\partial^2}{\partial x^2} + \frac{\partial^2}{\partial y^2})(\frac{1}{2\pi} \ln|r - r_i|) = \Delta_i(x - y, x_i - y_i)$, we have

$$\Delta_i(x - y, x_i - y_i) = \frac{a(x, y)}{a(x_i, y_i)} \left(\frac{\partial^2}{\partial x^2} \left(\frac{1}{2\pi} \ln|r - r_i| \right) + \frac{\partial^2}{\partial y^2} \left(\frac{1}{2\pi} \ln|r - r_i| \right) \right) \quad (2.56)$$

and

$$\begin{aligned}
R(x, x_i; y, y_i) &= \frac{1}{a(x_i, y_i)} \frac{\partial a(x, y)}{\partial x} \frac{\partial}{\partial x} \left(\frac{1}{2\pi} \ln|r - r_i| \right) + \\
&\quad \frac{1}{a(x_i, y_i)} \frac{\partial a(x, y)}{\partial y} \frac{\partial}{\partial y} \left(\frac{1}{2\pi} \ln|r - r_i| \right) \\
&= \frac{x - x_i}{2\pi a(x_i, y_i) |r - r_i|^2} \frac{\partial a(x, y)}{\partial x} + \frac{y - y_i}{2\pi a(x_i, y_i) |r - r_i|^2} \frac{\partial a(x, y)}{\partial y}
\end{aligned} \tag{2.57}$$

which stands for $R = \frac{\partial a}{\partial n} \frac{\partial P}{\partial n}$.

For simplicity, we continue with $P(x, y)$ and $R(x, y)$ instead of $P(x, x_i; y, y_i)$ and $R(x, x_i; y, y_i)$ in the following equations.

By using Green's formula for the differential operator L ,

$$\begin{aligned}
\int_{\Omega} [u(x, y) LP(x, y) - P(x, y) Lu(x, y)] d\Omega = \\
\int_{\partial\Omega} [u(x, y) TP(x, y) - P(x, y) Tu(x, y)] d\Gamma
\end{aligned} \tag{2.58}$$

the following integral equation is obtained

$$\begin{aligned}
c_i u_i - \int_{\partial\Omega} [u(x, y) TP(x, y) - P(x, y) Tu(x, y)] d\Gamma + \\
\int_{\Omega} R(x, y) u(x, y) d\Omega = \int_{\Omega} P(x, y) b(x, y) d\Omega.
\end{aligned} \tag{2.59}$$

Therefore, the fundamental solution $P(x, y)$ treats the variable coefficient in the diffusion term directly. That means, the parametrix BEM is capable of addressing to the PDE containing a variable coefficient in its dominating operator term.

The above equation (2.59) contains two domain integrals. The one on the right hand side, $\int_{\Omega} b(x, y) P(x, y) d\Omega$ arises from the non-homogeneous term of the diffusion equation. However, the left hand side one, $\int_{\Omega} R(x, y) u(x, y) d\Omega$ is originated from the parametrix BEM procedure itself. Once more, the correct evaluation of these domain integrals is required to obtain accurate solution of the two-dimensional diffusion equation. The composite trapezoidal rule in Section 2.2.1 can be used in evaluation of these domain integrals. However, the numerical integration techniques gives at least computational and round-off errors which causes the BEM to lose its advantage. Nonetheless, the domain integral arises from the BEM procedures can be transformed

into a boundary integral by using the DRBEM which will be given in the next Section. This is the main advantage of the DRBEM over the BEM.

2.4 DRBEM procedure for the Poisson's equation $\nabla^2 u = b(x, y)$

Previously, application of the BEM procedure to the two-dimensional Poisson's equation,

$$\begin{aligned}\nabla^2 u &= b(x, y), \quad (x, y) \in \Omega \\ u(x, y) &= \bar{u}(x, y), \quad (x, y) \in \Gamma_1 \\ q(x, y) &= \frac{\partial u}{\partial n}(x, y) = \bar{q}(x, y), \quad (x, y) \in \Gamma_2\end{aligned}\tag{2.60}$$

has given the following boundary-domain integral equation

$$c_i u_i - \int_{\Gamma} q u^* d\Gamma + \int_{\Gamma} q^* u d\Gamma = - \int_{\Omega} b u^* d\Omega.\tag{2.61}$$

Now, the domain integral on the right hand side of the equation will be transformed into an equivalent boundary integral with the help of radial basis functions, [7]. For this reason, the solution of (2.60) can be written as a sum of the Laplace equation ($\nabla^2 u = 0$) and particular solution \hat{u} which satisfies

$$\nabla^2 \hat{u} = b(x, y).\tag{2.62}$$

There are generally difficulties to find out a particular solution \hat{u} in equation (2.62) especially for non-linear and time dependent problems. The DRBEM introduces the idea of using series of particular solutions \hat{u}_j instead of a single particular solution \hat{u} . The total number of these particular solutions used in DRBEM equals to the number of nodes used in the discretization of the domain [7]. Hence, the non-homogeneous term $b(x, y)$ on the right hand side of the Poisson's equation (2.62) is approximated as

$$b(x, y) = \sum_{j=1}^{N+L} \alpha_j f_j(x, y)\tag{2.63}$$

where N and L denote the number of boundary and interior nodes, respectively. The coefficients α_j 's are undetermined constants and $f_j(x, y)$'s are the radial basis functions which are connected to the particular solutions \hat{u}_j 's with the Laplace operator

$$\nabla^2 \hat{u}_j = f_j.\tag{2.64}$$

Substituting equation (2.64) into equation (2.63) gives

$$b(x, y) = \sum_{j=1}^{N+L} \alpha_j (\nabla^2 \hat{u}_j) \quad (2.65)$$

once and for all, substitution of (2.65) into equation (2.61) yields

$$c_i u_i - \int_{\Gamma} q u^* d\Gamma + \int_{\Gamma} q^* u d\Gamma = - \sum_{j=1}^{N+L} \alpha_j \int_{\Omega} (\nabla^2 \hat{u}_j) u^* d\Omega. \quad (2.66)$$

Now, the weighted residual statement is also seen on the right hand side of equation (2.66). After applying Green's second identity two times to this side of the equation, the following boundary integral equation is obtained for each source node i

$$c_i u_i + \int_{\Gamma} u q^* d\Gamma - \int_{\Gamma} q u^* d\Gamma = \sum_{j=1}^{N+L} \alpha_j (c_i \hat{u}_{ij} + \int_{\Gamma} \hat{u}_j q^* d\Gamma - \int_{\Gamma} \hat{q}_j u^* d\Gamma) \quad (2.67)$$

where $i = 1, \dots, N$, $\hat{u}_j = \hat{u}_j(x_i, y_i)$ and \hat{q}_j is the normal derivative of \hat{u}_j , explicitly as

$$\hat{q}_j = \frac{\partial \hat{u}_j}{\partial n} = \frac{\partial \hat{u}_j}{\partial x} \frac{\partial x}{\partial n} + \frac{\partial \hat{u}_j}{\partial y} \frac{\partial y}{\partial n}. \quad (2.68)$$

Here, it needs to be pointed out that equation (2.67) does not contain domain integral anymore. The domain integral involving b in (2.61) is replaced by equivalent boundary integrals. The discretized form of equation (2.67) at a source point i is

$$\begin{aligned} c_i u_i + \sum_{k=1}^N \int_{\Gamma_k} u q^* d\Gamma_k - \sum_{k=1}^N \int_{\Gamma_k} q u^* d\Gamma_k = \\ \sum_{j=1}^{N+L} \alpha_j (c_i \hat{u}_{ij} + \sum_{k=1}^N \int_{\Gamma_k} \hat{u}_j q^* d\Gamma_k - \sum_{k=1}^N \int_{\Gamma_k} \hat{q}_j u^* d\Gamma_k), \quad i = 1, \dots, N \end{aligned} \quad (2.69)$$

for N number of boundary elements. The discretization of the boundary can be done by using constant or linear elements.

Note that, the values u^* , q^* , \hat{u}_j and \hat{q}_j are defined before. Therefore, all the boundary integrals can be calculated, and as a result, the following matrix-vector equation for each node i is obtained as

$$\begin{aligned} c_i u_i + \sum_{k=1}^N \bar{H}_{ik} u_k - \sum_{k=1}^N G_{ik} q_k = \\ \sum_{j=1}^{N+L} \alpha_j (c_i \hat{u}_{ij} + \sum_{k=1}^N \bar{H}_{ik} \hat{u}_{kj} - \sum_{k=1}^N G_{ik} \hat{q}_{kj}), \quad i = 1, \dots, N \end{aligned} \quad (2.70)$$

where the definitions of \overline{H}_{ik} and G_{ik} are given previously for both constant and linear element discretizations in equations (2.18), (2.19) and (2.34), (2.36), (2.40), respectively.

To obtain the solution on the boundary, equation (2.70) becomes for a boundary point i

$$\frac{1}{2}u_i + \sum_{k=1}^N \overline{H}_{ik}u_k - \sum_{k=1}^N G_{ik}q_k = \sum_{j=1}^{N+L} \alpha_j \left(\frac{1}{2}\hat{u}_{ij} + \sum_{k=1}^N \overline{H}_{ik}\hat{u}_{kj} - \sum_{k=1}^N G_{ik}\hat{q}_{kj} \right) \quad (2.71)$$

where $i \in [1, N]$. Also, the equivalent form is

$$\sum_{k=1}^N H_{ik}u_k - \sum_{k=1}^N G_{ik}q_k = \sum_{j=1}^{N+L} \alpha_j \left(\sum_{k=1}^N H_{ik}\hat{u}_{kj} - \sum_{k=1}^N G_{ik}\hat{q}_{kj} \right) \quad (2.72)$$

where $H_{ik} = \overline{H}_{ik} + \frac{1}{2}\delta_{ij}$.

Then, the matrix-vector equation is obtained as

$$\mathbf{H}\mathbf{u} - \mathbf{G}\mathbf{q} = \sum_{j=1}^{N+L} \alpha_j (\mathbf{H}\hat{\mathbf{u}}_j - \mathbf{G}\hat{\mathbf{q}}_j). \quad (2.73)$$

When, $\hat{\mathbf{U}}$ and $\hat{\mathbf{Q}}$ matrices are constructed by considering the vectors $\hat{\mathbf{u}}_j$ and $\hat{\mathbf{q}}_j$ as columns of these matrices, respectively, the previous equation is converted into

$$\mathbf{H}\mathbf{u} - \mathbf{G}\mathbf{q} = (\mathbf{H}\hat{\mathbf{U}} - \mathbf{G}\hat{\mathbf{Q}})\boldsymbol{\alpha}. \quad (2.74)$$

The dimensions of the matrices $\hat{\mathbf{U}}$ and $\hat{\mathbf{Q}}$ are $N \times (N + L)$ and the vector $\boldsymbol{\alpha}$ has dimension $(N + L) \times 1$. The solution in terms of \mathbf{u} and \mathbf{q} on the boundary can be found by inserting the boundary conditions to equation (2.74) and applying Gaussian elimination after the required swapping procedure.

For the interior solution, the following equation need to be solved by using the obtained or given boundary values of \mathbf{u} and \mathbf{q} as well as taking the constant $c_i = 1$

$$u_i = \sum_{k=1}^N G_{ik}q_k - \sum_{k=1}^N \overline{H}_{ik}u_k + \sum_{j=1}^{N+L} \alpha_j \left(\hat{u}_{ij} + \sum_{k=1}^N \overline{H}_{ik}\hat{u}_{kj} - \sum_{k=1}^N G_{ik}\hat{q}_{kj} \right) \quad (2.75)$$

which is equivalently to the matrix-vector form

$$\mathbf{I}\mathbf{u}_i = \mathbf{G}\mathbf{q} - \overline{\mathbf{H}}\mathbf{u} + (\mathbf{I}\hat{\mathbf{U}}_i + \overline{\mathbf{H}}\hat{\mathbf{U}} - \mathbf{G}\hat{\mathbf{Q}})\boldsymbol{\alpha}, \quad i = 1, \dots, L. \quad (2.76)$$

In the above equation, \mathbf{u}_i denotes the vector evaluated at the interior nodes. Its dimension is $L \times 1$. The matrix \mathbf{I} is the identity matrix of order $L \times L$.

Therefore, all the unknowns on the boundary and inside the region can be obtained. However, in DRBEM this procedure for finding the solution over the domain Ω can be achieved at the same time by combining the linear system of algebraic equations for the boundary and inside the region. This combination in matrix-vector equation is

$$\begin{aligned} & \begin{bmatrix} \mathbf{H}^{bs} & \mathbf{0} \\ \mathbf{H}^{is} & \mathbf{I} \end{bmatrix} \begin{Bmatrix} \mathbf{u}^{bs} \\ \mathbf{u}^{is} \end{Bmatrix} - \begin{bmatrix} \mathbf{G}^{bs} & \mathbf{0} \\ \mathbf{G}^{is} & \mathbf{0} \end{bmatrix} \begin{Bmatrix} \mathbf{q}^{bs} \\ \mathbf{0} \end{Bmatrix} \\ &= \left(\begin{bmatrix} \mathbf{H}^{bs} & \mathbf{0} \\ \mathbf{H}^{is} & \mathbf{I} \end{bmatrix} \begin{Bmatrix} \hat{\mathbf{U}}^{bs} \\ \hat{\mathbf{U}}^{is} \end{Bmatrix} - \begin{bmatrix} \mathbf{G}^{bs} & \mathbf{0} \\ \mathbf{G}^{is} & \mathbf{0} \end{bmatrix} \begin{Bmatrix} \hat{\mathbf{Q}}^{bs} \\ \mathbf{0} \end{Bmatrix} \right) \boldsymbol{\alpha} \end{aligned} \quad (2.77)$$

where bs and is represent the boundary and interior nodes, respectively. $\mathbf{0}$ is the zero matrix with size $N \times N$.

Equivalently, equation (2.77) is expressed as

$$\mathbf{H}\mathbf{u} - \mathbf{G}\mathbf{q} = (\mathbf{H}\hat{\mathbf{U}} - \mathbf{G}\hat{\mathbf{Q}})\boldsymbol{\alpha}. \quad (2.78)$$

The enlarged matrices \mathbf{H} , \mathbf{G} , $\hat{\mathbf{U}}$ and $\hat{\mathbf{Q}}$ have dimension $(N + L) \times (N + L)$. The vector $\boldsymbol{\alpha}$ has size $(N + L) \times 1$ and, \mathbf{u} , \mathbf{q} contain both boundary and interior values which have sizes $(N + L) \times 1$.

Now, equation (2.78) contains the vector $\boldsymbol{\alpha}$ which has undetermined coefficients α_j in its entries. To approximate the vector $\boldsymbol{\alpha}$, firstly the coordinate matrix \mathbf{F} must be constructed by considering f_j , for $j = 1, \dots, N + L$ as columns which gives

$$\mathbf{b} = \mathbf{F}\boldsymbol{\alpha} \quad (2.79)$$

where \mathbf{F} is the coordinate matrix of size $(N + L) \times (N + L)$. The vector \mathbf{b} contains the function value of $b(x, y)$ evaluated at each $(N + L)$ nodes.

By taking the inverse of the matrix \mathbf{F} which exists, $\boldsymbol{\alpha}$ can be found

$$\boldsymbol{\alpha} = \mathbf{F}^{-1}\mathbf{b}. \quad (2.80)$$

Eventually, equation (2.78) can be written as

$$\mathbf{H}\mathbf{u} - \mathbf{G}\mathbf{q} = (\mathbf{H}\hat{\mathbf{U}} - \mathbf{G}\hat{\mathbf{Q}})\mathbf{F}^{-1}\mathbf{b}. \quad (2.81)$$

The matrices and the vector on the right hand side of equation (2.81) are known. Hence, inserting the boundary conditions into the equation and doing the necessary shuffling, one ends up with a linear system of equations such as $\mathbf{A}\mathbf{x} = \mathbf{d}$, from which the unknown values of u and q can be obtained.

At this moment, approximating function f from which the functions \hat{u} and \hat{q} are constructed is taken into consideration. Choice of the function f is unlimited and many types of function are proposed. Then, the idea of using the distance function r in the fundamental solution u^* has been selected as the most convenient type for f . Thus, the function f is well chosen as

$$f = 1 + r + r^2 + \dots + r^m \quad (2.82)$$

where $r = \sqrt{r_x^2 + r_y^2}$ in a two-dimensional region.

Inserting the polynomial form of f in equation (2.64) results in

$$\nabla^2 \hat{u} = 1 + r + r^2 + \dots + r^m \quad (2.83)$$

related particular solution \hat{u} converts in

$$\hat{u} = \frac{r^2}{4} + \frac{r^3}{9} + \dots + \frac{r^{m+2}}{(m+2)^2} \quad (2.84)$$

and the normal derivative eventually be

$$\hat{q} = (r_x \frac{\partial x}{\partial n} + r_y \frac{\partial y}{\partial n}) (\frac{1}{2} + \frac{r}{3} + \dots + \frac{r^m}{(m+2)}). \quad (2.85)$$

2.4.1 DRBEM procedure for the equation $\nabla^2 u = b(x, y, u)$

In the previous section, the application of DRBEM is shown on the Poisson type equation ($\nabla^2 u = b(x, y)$) where the non-homogeneous term is a known function depending on the position. However, in this section the inhomogeneity is no longer a known function, it is considered as containing the problem variable u in itself as

$$\nabla^2 u = b(x, y, u) \quad (2.86)$$

with the same partly essential partly natural boundary conditions given in (2.60).

Before the DRBEM procedure is applied, the non-homogeneous term b is splitted as a linear function of u as

$$b = b_1(x, y) + b_2(x, y)u \quad (2.87)$$

and then b is approximated as

$$b = b_1 + b_2u \simeq \sum_{j=1}^{N+L} \alpha_j f_j(x, y) \quad (2.88)$$

where α_j 's and f_j 's denote undetermined coefficients and approximating radial basis functions, respectively.

The DRBEM procedure emerges then

$$\mathbf{H}u - \mathbf{G}q = (\mathbf{H}\hat{\mathbf{U}} - \mathbf{G}\hat{\mathbf{Q}})\alpha \quad (2.89)$$

where

$$\alpha = \mathbf{F}^{-1}(\mathbf{b}_1 + \mathbf{B}u) \quad (2.90)$$

and \mathbf{F} is the coordinate function, \mathbf{b}_1 denotes the column vector with entries $b_1(x_i, y_i)$ at each node $i = 1, \dots, N + L$. Also, \mathbf{B} is the diagonal matrix containing $b_2(x_i, y_i)$ on the diagonal entries for $i = 1, \dots, N + L$. Since the vector α involves the unknown u itself, it can not be calculated explicitly now. Thus, it is going to be kept as unknown in the solution process.

Inserting the equality of α from (2.90) into (2.89) yields

$$\mathbf{H}u - \mathbf{G}q = (\mathbf{H}\hat{\mathbf{U}} - \mathbf{G}\hat{\mathbf{Q}})\mathbf{F}^{-1}(\mathbf{b}_1 + \mathbf{B}u). \quad (2.91)$$

Equation (2.91) can be simplified as

$$(\mathbf{H} - \mathbf{KB})u - \mathbf{G}q = \mathbf{Kb}_1 \quad (2.92)$$

where

$$\mathbf{K} = (\mathbf{H}\hat{\mathbf{U}} - \mathbf{G}\hat{\mathbf{Q}})\mathbf{F}^{-1}. \quad (2.93)$$

At this point, inserting the given boundary conditions of u and q into (2.92) and swapping procedure converts the first order partial differential equations (2.92) into a system of linear algebraic equations such as $\mathbf{A}\mathbf{x} = \mathbf{d}$ since the vector \mathbf{b}_1 can be calculated at $N + L$ points. Therefore, one ends up with the solution easily.

2.4.2 DRBEM procedure for the equation $\nabla^2 u = b(x, y, u, u_x, u_y)$

Here, the DRBEM procedure is modified for an extended form of equation (2.86) including the convection terms u_x and u_y also

$$\nabla^2 u = b(x, y, u, u_x, u_y) \quad (2.94)$$

with the same boundary conditions given in (2.60).

The non-homogeneous term b can be splitted into four functions as

$$b = b_1(x, y) + b_2(x, y)u + b_3(x, y)u_x + b_4(x, y)u_y. \quad (2.95)$$

Up to now, only a standard system is obtained in the form $\mathbf{b} = \mathbf{F}\alpha$. However, a new special approximation along with the standard one becomes requisite for this type of equation giving the relation between the nodal values of u and its coordinate derivatives with respect to x and y as $\frac{\partial u}{\partial x}$ and $\frac{\partial u}{\partial y}$.

The solution u can be approximated with the help of the same approximating functions f_j as

$$u \simeq \sum_{j=1}^{N+L} \beta_j f_j(x, y) \quad (2.96)$$

where β_j 's are undetermined coefficients and β_j 's are different from α_j 's given in equation (2.88).

The matrix-vector form of equation (2.96) is

$$\mathbf{u} = \mathbf{F}\beta \quad (2.97)$$

giving

$$\beta = \mathbf{F}^{-1}\mathbf{u} \quad (2.98)$$

since \mathbf{F} is an invertible matrix.

Taking the derivatives of both sides with respect to x and y provides

$$\begin{aligned} \frac{\partial \mathbf{u}}{\partial x} &= \frac{\partial \mathbf{F}}{\partial x} \beta \\ \frac{\partial \mathbf{u}}{\partial y} &= \frac{\partial \mathbf{F}}{\partial y} \beta. \end{aligned} \quad (2.99)$$

Substituting β in equation (2.98) gives

$$\begin{aligned}\frac{\partial \mathbf{u}}{\partial x} &= \frac{\partial \mathbf{F}}{\partial x} \mathbf{F}^{-1} \mathbf{u} \\ \frac{\partial \mathbf{u}}{\partial y} &= \frac{\partial \mathbf{F}}{\partial y} \mathbf{F}^{-1} \mathbf{u}.\end{aligned}\tag{2.100}$$

The DRBEM application ends up with the matrix-vector equation

$$\mathbf{H}\mathbf{u} - \mathbf{G}\mathbf{q} = (\mathbf{H}\hat{\mathbf{U}} - \mathbf{G}\hat{\mathbf{Q}})\boldsymbol{\alpha}\tag{2.101}$$

where $\boldsymbol{\alpha} = \mathbf{F}^{-1}\mathbf{b}$ or equivalently,

$$\mathbf{H}\mathbf{u} - \mathbf{G}\mathbf{q} = (\mathbf{H}\hat{\mathbf{U}} - \mathbf{G}\hat{\mathbf{Q}})\mathbf{F}^{-1}\mathbf{b}\tag{2.102}$$

which turns up to be

$$\mathbf{H}\mathbf{u} - \mathbf{G}\mathbf{q} = (\mathbf{H}\hat{\mathbf{U}} - \mathbf{G}\hat{\mathbf{Q}})\mathbf{F}^{-1}(\mathbf{b}_1 + \mathbf{B}\mathbf{u} + \bar{\mathbf{B}}\mathbf{u}_x + \tilde{\mathbf{B}}\mathbf{u}_y)\tag{2.103}$$

where \mathbf{B} , $\bar{\mathbf{B}}$ and $\tilde{\mathbf{B}}$ are the diagonal matrices with entries $b_2(x_i, y_i)$, $b_3(x_i, y_i)$ and $b_4(x_i, y_i)$ on their diagonals for $i = 1, \dots, N + L$, respectively. The vector \mathbf{b}_1 contains $b_1(x_i, y_i)$ at $N + L$ nodes.

Using the equalities of coordinate derivatives of \mathbf{u} from equation (2.100) in the above equation provides

$$\mathbf{H}\mathbf{u} - \mathbf{G}\mathbf{q} = (\mathbf{H}\hat{\mathbf{U}} - \mathbf{G}\hat{\mathbf{Q}})\mathbf{F}^{-1}(\mathbf{b}_1 + \mathbf{B}\mathbf{u} + \bar{\mathbf{B}}\frac{\partial \mathbf{F}}{\partial x}\mathbf{F}^{-1}\mathbf{u} + \tilde{\mathbf{B}}\frac{\partial \mathbf{F}}{\partial y}\mathbf{F}^{-1}\mathbf{u}).\tag{2.104}$$

Finally, rearrangement of the terms by keeping \mathbf{u} as unknown gives the following linear system of equations as

$$(\mathbf{H} - \mathbf{K}\mathbf{R})\mathbf{u} - \mathbf{G}\mathbf{q} = \mathbf{K}\mathbf{b}_1\tag{2.105}$$

which can be rearranged as a linear system $\mathbf{A}\mathbf{x} = \mathbf{d}$ where $\mathbf{K} = (\mathbf{H}\hat{\mathbf{U}} - \mathbf{G}\hat{\mathbf{Q}})\mathbf{F}^{-1}$ and $\mathbf{R} = (\mathbf{B} + \bar{\mathbf{B}}\frac{\partial \mathbf{F}}{\partial x}\mathbf{F}^{-1} + \tilde{\mathbf{B}}\frac{\partial \mathbf{F}}{\partial y}\mathbf{F}^{-1})$.

Therefore, the solution \mathbf{u} can be obtained easily by using Gaussian elimination from the linear system of algebraic equations, $\mathbf{A}\mathbf{x} = \mathbf{d}$. To get this system, firstly insert the boundary conditions of \mathbf{u} and \mathbf{q} into equation (2.105) together with the zero for the interior values of \mathbf{q} . Then, swap the corresponding columns of $(\mathbf{H} - \mathbf{K}\mathbf{R})$ and \mathbf{G} to obtain all the unknown values of \mathbf{u} and \mathbf{q} as \mathbf{x} on the left hand side.

2.4.3 DRBEM procedure for the equation $\nabla^2 u = b(x, y, t, u, u_t, u_x, u_y)$

In this section, the non-homogeneous term b is enlarged once more by adding the time variable t and the derivative of the solution with respect to time, $\frac{\partial u}{\partial t}$

$$\nabla^2 u = b(x, y, t, u, u_t, u_x, u_y). \quad (2.106)$$

The DRBEM solution is considered then for time-dependent Poisson's equation (Diffusion equation). Assume that, the term b contains linear combination of the unknown u , the convection terms u_x and u_y , and the time derivative u_t . Thus, the inhomogeneity b can be expressed as

$$b = u_t + b_1(x, y) + b_2(x, y)u + b_3(x, y)u_x + b_4(x, y)u_y. \quad (2.107)$$

It is estimated by using the radial basis functions f_j as

$$b = u_t + b_1 + b_2u + b_3u_x + b_4u_y \simeq \sum_{j=1}^{N+L} \alpha_j(t) f_j(x, y) \quad (2.108)$$

where $\alpha_j(t)$'s are also functions of time which makes the difference from the previously defined parameters α_j 's. The approximating functions f_j are connected to the particular solutions \hat{u}_j again through equation (2.64) with the Laplace operator.

The DRBEM application to Poisson's type equation (2.106) brings

$$\mathbf{H}u - \mathbf{G}q = (\mathbf{H}\hat{\mathbf{U}} - \mathbf{G}\hat{\mathbf{Q}})\boldsymbol{\alpha} \quad (2.109)$$

with $\boldsymbol{\alpha} = \mathbf{F}^{-1}\mathbf{b}$ which results in

$$\mathbf{H}u - \mathbf{G}q = (\mathbf{H}\hat{\mathbf{U}} - \mathbf{G}\hat{\mathbf{Q}})\mathbf{F}^{-1}\mathbf{b} \quad (2.110)$$

embedding the equality of the vector \mathbf{b} as

$$\mathbf{H}u - \mathbf{G}q = (\mathbf{H}\hat{\mathbf{U}} - \mathbf{G}\hat{\mathbf{Q}})\mathbf{F}^{-1}\left(\frac{\partial \mathbf{u}}{\partial t} + \mathbf{b}_1 + \mathbf{B}u + \bar{\mathbf{B}}\frac{\partial \mathbf{F}}{\partial x}\mathbf{F}^{-1}u + \tilde{\mathbf{B}}\frac{\partial \mathbf{F}}{\partial y}\mathbf{F}^{-1}u\right). \quad (2.111)$$

The following linear system of ordinary differential equations in time, can be obtained by rearranging the terms in (2.111)

$$\mathbf{K}\dot{u} - (\mathbf{H} - \mathbf{K}\mathbf{R})u + \mathbf{G}q = -\mathbf{K}\mathbf{b}_1 \quad (2.112)$$

with the diagonal matrices \mathbf{K} and \mathbf{R} defined in equation (2.105).

Therefore, a first order initial value problem is obtained

$$\dot{\mathbf{u}} - \mathbf{D}\mathbf{u} + \mathbf{E}\mathbf{q} = -\mathbf{b}_1 \quad (2.113)$$

where $\mathbf{D} = \mathbf{K}^{-1}\mathbf{H} - \mathbf{R}$ and $\mathbf{E} = \mathbf{K}^{-1}\mathbf{G}$.

The above system of equations can be solved for transient time levels by using any time integration scheme. However, in this thesis implicit Euler method is used for the time derivative.

2.4.3.1 Implicit Euler method for time integration scheme

The implicit Euler method is a first order numerically stable method and it is an easy finite difference approximation for the time derivative. Contrary to the other methods, a rather larger step size Δt can be used due to its unconditional stability which is the main advantage of the method. The time step represents the size between two consecutive iterations, i.e. $\Delta t = t_{m+1} - t_m$.

Introducing the notation $u(x, y, t_m) = u^m$ and using the Taylor series expansion about t_m , one can get

$$u^m = u^{m+1} - \Delta t \frac{\partial u^{m+1}}{\partial t} + \frac{\Delta t^2}{2!} \frac{\partial^2 u^{m+1}}{\partial t^2} - \dots \quad (2.114)$$

which can be rewritten as

$$\frac{\partial u^{m+1}}{\partial t} = \frac{u^{m+1} - u^m}{\Delta t} + \mathcal{O}(\Delta t). \quad (2.115)$$

Substituting this approximation into equation (2.113) and rearranging the matrix-vector system of equations in increasing time levels yields

$$\frac{\mathbf{u}^{m+1} - \mathbf{u}^m}{\Delta t} - \mathbf{D}\mathbf{u}^{m+1} + \mathbf{E}\mathbf{q}^{m+1} = -\mathbf{b}_1 \quad (2.116)$$

where \mathbf{u}^{m+1} and \mathbf{q}^{m+1} are the vectors at the $(m+1)$ -th time level. By using the initial condition for the vector \mathbf{u} , i.e. \mathbf{u}^0 , the solution can be obtained at any desired time level.

CHAPTER 3

THE BEM SOLUTIONS OF THE MHD DUCT FLOW PROBLEMS

In this chapter, the BEM solutions for convection-diffusion type PDEs are going to be presented. Mainly, three types of PDEs are solved. In the first type, the diffusion term contains variable coefficient in it depending on the space variables. Application for this type is given on the MHD flow and heat transfer with temperature dependent viscosity. The second and third convection-diffusion type PDEs considered in this chapter also contain variable coefficients but in front of the convection terms. Applications are also given for MHD flow problems in rectangular ducts. In the second problem convection coefficients are changing with respect to time t , and the third one contains axial dependent convection coefficients that is the external magnetic field applies in the streamwise direction (pipe-axis direction). Actually, in the second problem the variable coefficients depend on time due to the applied magnetic field varying with time. Similarly, axial-dependent applied magnetic field makes the variable coefficients of the convection terms depending on the streamwise direction. The common feature of these three types of PDEs is that each contains Laplace operator in their diffusion term after doing the required rearrangements. They become then, Poisson's type equations which can be treated by the techniques, parametrix BEM and DRBEM as given in Chapter 2. Thus, in this chapter, only the basic steps of the application of these numerical methods are going to be shown on these three convection-diffusion types PDEs. The outline of this chapter is as follows; the MHD flow and heat transfer problem with temperature dependent viscosity is the first convection-diffusion type PDE considered. The discretized BEM solutions for the coupled equations are given in Section 3.1. The time-dependent MHD duct flow equations in terms of the velocity and induced magnetic field constitute the second type convection-diffusion PDEs, and their DRBEM discretizations are given in Section 3.2. Then, the MHD duct flow

with streamwise direction applied magnetic field is solved in terms of the velocity and the electric potential by using the DRBEM in Section 3.3. Once and for all, the MHD duct flow equations in Section 3.3 are considered along with the induced magnetic field equation in Section 3.4 and solved by using the DRBEM.

3.1 Parametrix BEM and DRBEM applications to inductionless MHD flow and heat transfer with temperature dependent viscosity

The laminar, steady flow of a viscous, incompressible, electrically conducting fluid is considered in a long channel of rectangular cross-section (duct) in conjunction with heat transfer. A uniform magnetic field with intensity B_0 is applied to the duct perpendicular to the axis of the channel, i.e. z -axis. However, the induced magnetic field is neglected due to the assumption of small magnetic Reynolds number. The physical configuration of the flow is shown in Figure 3.1. Both the flow and the temperature are steady and fully-developed along the channel.

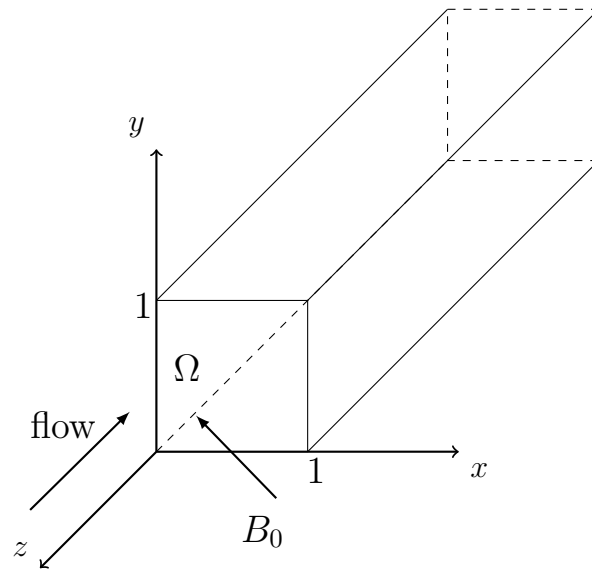


Figure 3.1: Physical configuration of the problem

The governing equations are

$$\frac{\partial}{\partial x}(\bar{\mu} \frac{\partial w}{\partial x}) + \frac{\partial}{\partial y}(\bar{\mu} \frac{\partial w}{\partial y}) = -1 + \frac{M^2}{1+m^2}w \quad (3.1)$$

$$\nabla^2 T + Br\bar{\mu}[(\frac{\partial w}{\partial x})^2 + (\frac{\partial w}{\partial y})^2] + \frac{M^2 Br}{1+m^2}w^2 = \frac{w}{w_m} \quad (3.2)$$

where B , m , M and Br denote the viscosity parameter, Hall parameter, Hartmann number and Brinkmann number, respectively. The flow has a temperature dependent viscosity $\bar{\mu} = e^{-BT}$ and w_m is the volumetric flow defined as $\int_{\Omega} w d\Omega$.

The coupled equations in terms of the velocity w and the temperature T are considered in a rectangular cross-section (duct) of a pipe with no-slip velocity and zero-temperature on the walls.

The velocity equation (3.1) is solved by using the parametrix BEM procedure first while the energy equation (3.2) is solved by using the DRBEM. In the BEM approach, the fundamental solution is going to be a parametrix and since the variable coefficient of diffusion equation is $\bar{\mu}$, the fundamental solution in Section 2.3 becomes $P(x, x_i; y, y_i) = \frac{1}{2\pi} \frac{1}{\bar{\mu}(x_i, y_i)} \ln|r - r_i|$. This fundamental solution helps one to treat the diffusion operator of the equation directly. The energy equation is rewritten by leaving $\nabla^2 T$ on the left alone and treating all the other terms as inhomogeneities. Then, it is solved by DRBEM using the fundamental solution of Laplace equation $u^* = \frac{1}{2\pi} \ln(\frac{1}{r})$. Secondly, both the velocity equation (3.1) and energy equation (3.2) are solved by using the DRBEM procedure, leaving the Laplacian terms alone on the left and using fundamental solution of Laplace equation in the application of DRBEM for both of the equations.

3.1.1 Parametrix BEM-DRBEM approach

Discretizing the boundary of Ω with N constant elements and applying the parametrix BEM and the DRBEM approaches transform the differential equations (3.1) and (3.2) into the following equivalent integral equations (3.3) and (3.4), respectively,

$$c_i w_i + \int_{\Gamma} \left[(\bar{\mu} \frac{\partial w}{\partial n}) P - (\bar{\mu} \frac{\partial P}{\partial n}) w \right] d\Gamma + \int_{\Omega} w \frac{\partial \bar{\mu}}{\partial n} \frac{\partial P}{\partial n} d\Omega = \int_{\Omega} b_1 P d\Omega \quad (3.3)$$

and

$$c_i T_i - \int_{\Gamma} \frac{\partial T}{\partial n} u^* d\Gamma + \int_{\Gamma} q^* T d\Gamma = - \int_{\Omega} b_2 u^* d\Omega \quad (3.4)$$

where the constants c_i are $c_i = \theta_i/2\pi$ with the internal angle θ_i at the source point $i = 1, \dots, N$, and

$$b_1 = -1 + \frac{M^2}{1+m^2} w \quad (3.5)$$

$$b_2 = -Br\bar{\mu} \left[\left(\frac{\partial w}{\partial x} \right)^2 + \left(\frac{\partial w}{\partial y} \right)^2 \right] - \frac{M^2 Br}{1+m^2} w^2 + \frac{w}{w_m}. \quad (3.6)$$

The integral equation obtained from the parametrix BEM procedure (3.3) contains domain integrals on both sides of equation. These domain integrals are preserved and evaluated by using numerical integration techniques. However, the domain integral resulting from the DRBEM on the right hand side of equation (3.4) is transformed into boundary integrals by using radial basis functions f_j as mentioned in the previous chapter.

Equation (3.3) with the definition of b_1 in (3.5) can be converted into the following matrix-vector equation as

$$\mathbf{H}\mathbf{w} - \mathbf{G}(\bar{\mu} \frac{\partial \mathbf{w}}{\partial n}) = \mathbf{I}_1(\mathbf{w}) - \mathbf{I}_2(\mathbf{w}) \quad (3.7)$$

where

$$\begin{aligned} I_1(w) &= \int_{\Omega} \frac{1}{2\pi\bar{\mu}(x_i, y_i)} w \frac{(r - r_i)\vec{n}}{|r - r_i|^2} \frac{\partial \bar{\mu}(x, y)}{\partial n} d\Omega \\ I_2(w) &= \int_{\Omega} \frac{1}{2\pi\bar{\mu}(x_i, y_i)} \ln|r - r_i| \left(-1 + \frac{M^2}{1+m^2} w \right) d\Omega. \end{aligned} \quad (3.8)$$

These domain integrals are evaluated by using the composite trapezoidal rule mentioned in Section 2.2.1. The rectangular domain is divided into cells with edges have equal length. That means, the cells pass from the end points of constant boundary elements.

The \mathbf{H} and \mathbf{G} are the parametrix BEM matrices with entries

$$\begin{aligned} H_{ij} &= -c_i \delta_{ij} + \frac{1}{2\pi} \int_{\Gamma_j} \frac{(r - r_i)\vec{n}}{|r - r_i|^2} \frac{\bar{\mu}(x, y)}{\bar{\mu}(x_i, y_i)} d\Gamma_j, \quad H_{ii} = - \sum_{j=1, j \neq i}^N H_{ij}, \\ G_{ij} &= \frac{1}{2\pi} \int_{\Gamma_j} \ln|r - r_i| \frac{1}{\bar{\mu}(x_i, y_i)} d\Gamma_j, \quad G_{ii} = \frac{1}{\bar{\mu}(x_i, y_i)} \frac{\ell_e}{2\pi} \left(\ln\left(\frac{\ell_e}{2}\right) - 1 \right), \end{aligned} \quad (3.9)$$

where ℓ_e represents the length of the boundary element.

The unknown values of $\frac{\partial \mathbf{w}}{\partial n}$ on the boundary can be obtained by solving the system (3.7) by using the Gaussian elimination since the velocity \mathbf{w} values are 0 everywhere on the boundary. Then, the obtained boundary values are inserted in the following equation to compute the velocity \mathbf{w} values at each interior nodes by taking the constant $c_i = 1$, as

$$\mathbf{w}_i = \bar{\mathbf{H}}\mathbf{w} - \mathbf{G}(\bar{\boldsymbol{\mu}}\frac{\partial \mathbf{w}}{\partial n}) - \mathbf{I}_1(\mathbf{w}) + \mathbf{I}_2(\mathbf{w}) \quad (3.10)$$

where $\bar{H}_{ij} = \frac{1}{2\pi} \int_{\Gamma_j} \frac{(r - r_i)\vec{n}}{|r - r_i|^2} \frac{\bar{\mu}(x, y)}{\bar{\mu}(x_i, y_i)} d\Gamma_j$, $i = 1, \dots, L$, $j = 1, \dots, N$. L denotes the number of interior nodes with the vectors r and r_i on the boundary element and at the internal nodes, respectively. The I_1 and I_2 are the same domain integrals as in (3.8) with the vector r_i at the internal nodes.

Then, the BEM discretized equation (3.4) with the definition b_2 in (3.6) is

$$\begin{aligned} c_i T_i - \int_{\Gamma} \frac{\partial T}{\partial n} u^* d\Gamma + \int_{\Gamma} q^* T d\Gamma = \\ - \int_{\Omega} (-Br\bar{\mu}[(\frac{\partial w}{\partial x})^2 + (\frac{\partial w}{\partial y})^2] - \frac{M^2 Br}{1+m^2} w^2 + \frac{w}{w_m}) u^* d\Omega \end{aligned} \quad (3.11)$$

Except the term u^* on the right hand side of equation (3.11), all other terms in the domain integral are considered as inhomogeneities and these non-homogeneous terms are approximated by a set of radial basis functions $f_j(x, y)$ linked with the particular solutions \hat{u}_j to the equation $\nabla^2 \hat{u}_j = f_j$ as mentioned in Section 2.4. Therefore, the approximation is

$$\sum_{j=1}^{N+L} \alpha_j f_j(x, y) = \sum_{j=1}^{N+L} \alpha_j \nabla^2 \hat{u}_j \quad (3.12)$$

where α_j 's are undetermined coefficients for the velocity. Inserting the approximation (3.12) in the right hand side of equation (3.11) brings the multiplication of the Laplace operator with the fundamental solution u^* . Then, applying the BEM procedure also to this side of equation gives the following DRBEM boundary integral equation

$$c_i T_i - \int_{\Gamma} \frac{\partial T}{\partial n} u^* d\Gamma + \int_{\Gamma} q^* T d\Gamma = \sum_{j=1}^{N+L} \alpha_j (c_i \hat{u}_{ij} + \int_{\Gamma} \hat{u}_j q^* d\Gamma - \int_{\Gamma} \hat{q}_j u^* d\Gamma). \quad (3.13)$$

After the boundary discretization with constant elements again, the following matrix-vector equation is achieved

$$\mathbf{H}\mathbf{T} - \mathbf{G}\frac{\partial\mathbf{T}}{\partial n} = (\mathbf{H}\hat{\mathbf{U}} - \mathbf{G}\hat{\mathbf{Q}})\mathbf{F}^{-1}\left\{-Br\bar{\boldsymbol{\mu}}\left[\left(\frac{\partial\mathbf{w}}{\partial x}\right)^2 + \left(\frac{\partial\mathbf{w}}{\partial y}\right)^2\right] - \frac{M^2Br}{1+m^2}\mathbf{w}^2 + \frac{\mathbf{w}}{w_m}\right\} \quad (3.14)$$

where $\bar{\boldsymbol{\mu}}$ is a vector constructed from the viscosity parameter $\bar{\mu} = e^{-BT}$.

The vector \mathbf{T} and $\partial\mathbf{T}/\partial n$ contain the values at $N + L$ points. The matrices \mathbf{H} and \mathbf{G} are the standard DRBEM matrices with entries

$$\begin{aligned} H_{ij} &= c_i\delta_{ij} - \frac{1}{2\pi} \int_{\Gamma_j} \frac{(r-r_i)\cdot\vec{n}}{|r-r_i|^2} d\Gamma_j, & H_{ii} &= - \sum_{j=1, j \neq i}^N H_{ij}, \\ G_{ij} &= \frac{1}{2\pi} \int_{\Gamma_j} \ln\left(\frac{1}{|r-r_i|}\right) d\Gamma_j, & G_{ii} &= \frac{\ell_e}{2\pi} \left(\ln\left(\frac{2}{\ell_e}\right) + 1\right), \end{aligned} \quad (3.15)$$

where ℓ_e represents the length of the boundary element.

The matrices $\hat{\mathbf{U}}$ and $\hat{\mathbf{Q}}$ have dimensions $(N + L) \times (N + L)$. They are constructed by taking each of the vectors \hat{u}_j and \hat{q}_j as columns, respectively as detailed in Section 2.4.

The coordinate derivatives of the velocity \mathbf{w} with respect to the variables x and y such as $\frac{\partial\mathbf{w}}{\partial x}$, $\frac{\partial\mathbf{w}}{\partial y}$ in equation (3.14) can be approximated by using the coordinate matrix \mathbf{F} which yields the following equation

$$\begin{aligned} \mathbf{H}\mathbf{T} - \mathbf{G}\frac{\partial\mathbf{T}}{\partial n} &= (\mathbf{H}\hat{\mathbf{U}} - \mathbf{G}\hat{\mathbf{Q}})\mathbf{F}^{-1}\left\{-Br\bar{\boldsymbol{\mu}}\left[\left(\frac{\partial\mathbf{F}}{\partial x}\mathbf{F}^{-1}\mathbf{w}\right)^2 + \left(\frac{\partial\mathbf{F}}{\partial y}\mathbf{F}^{-1}\mathbf{w}\right)^2\right] \right. \\ &\quad \left. - \frac{M^2Br}{1+m^2}\mathbf{w}^2 + \frac{\mathbf{w}}{w_m}\right\}. \end{aligned} \quad (3.16)$$

Up to now, the matrix-vector forms of the velocity and the energy equations have been obtained by using two methods, namely the parametrix BEM and DRBEM, respectively in (3.7)-(3.10) and (3.16). The system of the velocity equation (3.7)-(3.10) for the boundary and interior solutions, and the energy equation (3.16) for both boundary and interior solutions are going to be solved iteratively following the algorithm below.

Step 1. Pre-assign a tolerance ε for the convergence criteria.

Step 2. Define a relaxation parameter κ , $0 < \kappa < 1$ for slowing down the sharp decrease of velocity magnitude in using parametrix BEM.

Step 3. Take initial guesses for the velocity w^0 and the temperature T^0 as zero.

Step 4. Solve the following coupled equations in terms of the velocity and temperature by using the Dirichlet type boundary conditions ($w = 0$ and $T = 0$ on the boundary) as

$$\mathbf{H}\mathbf{w}^{n+1} - \mathbf{G}(\bar{\mu} \frac{\partial \mathbf{w}^{n+1}}{\partial n}) = \mathbf{I}_1(\mathbf{w}^n) - \mathbf{I}_2(\mathbf{w}^n), \quad (3.17)$$

$$w_i = \bar{\mathbf{H}}\mathbf{w} - \mathbf{G}(\bar{\mu} \frac{\partial \mathbf{w}}{\partial n}) - \mathbf{I}_1(\mathbf{w}) + \mathbf{I}_2(\mathbf{w}). \quad (3.18)$$

$$\begin{aligned} \mathbf{H}\mathbf{T}^{n+1} - \mathbf{G} \frac{\partial \mathbf{T}^{n+1}}{\partial n} &= (\mathbf{H}\hat{\mathbf{U}} - \mathbf{G}\hat{\mathbf{Q}})\mathbf{F}^{-1} \\ &\left\{ -Br\bar{\mu} \left[\left(\frac{\partial \mathbf{F}}{\partial x} \mathbf{F}^{-1} \mathbf{w}^{n+1} \right)^2 + \left(\frac{\partial \mathbf{F}}{\partial y} \mathbf{F}^{-1} \mathbf{w}^{n+1} \right)^2 \right] - \frac{M^2 Br}{1+m^2} (\mathbf{w}^2)^{n+1} + \frac{\mathbf{w}^{n+1}}{w_m} \right\}. \end{aligned} \quad (3.19)$$

Step 5. Relax the obtained velocity values using

$$w^{n+1} = \kappa w^{n+1} + (1 - \kappa)w^n, \quad 0 < \kappa < 1 \quad (3.20)$$

between n -th and $(n + 1)$ -th iterations.

Step 6. Check the convergence criteria

$$\frac{\|u^{n+1} - u^n\|_{\infty}}{\|u^n\|_{\infty}} < \varepsilon \quad (3.21)$$

where $\|u\|_{\infty} = \max\{|u_1|, |u_2|, \dots, |u_{N+L}|\}$ for the velocity w and the temperature T , and n denotes the iteration level.

Step 7. If the criteria is achieved for w and T then stop.

Step 8. If the criteria is not achieved for one of the unknowns then repeat the Steps 4-6.

Thus, the unknown problem parameters, the velocity and temperature values inside the region, and the normal derivatives of them on the boundary can be obtained along with using the normal derivatives of the velocity and the temperature as zero in the domain.

3.1.2 DRBEM-DRBEM approach

In this section, the boundary integral formulations resulted from the DRBEM formulations for the velocity and the energy equations are going to be given by discretizing the boundary of the duct with N constant elements and L interior nodes. Before applying DRBEM procedures to both equations, a rearrangement is required for the velocity equation (3.1) to leave the Laplacian term alone. Thus, the governing equations are

$$\nabla^2 w = \frac{1}{\bar{\mu}} \left(-1 + \frac{M^2}{1+m^2} w - \frac{\partial \bar{\mu}}{\partial x} \frac{\partial w}{\partial x} - \frac{\partial \bar{\mu}}{\partial y} \frac{\partial w}{\partial y} \right) \quad (3.22)$$

$$\nabla^2 T = -Br\bar{\mu} \left[\left(\frac{\partial w}{\partial x} \right)^2 + \left(\frac{\partial w}{\partial y} \right)^2 \right] - \frac{M^2 Br}{1+m^2} w^2 + \frac{w}{w_m} \quad (3.23)$$

The DRBEM procedures bring the following boundary-domain integral equations

$$\begin{aligned} c_i w_i - \int_{\Gamma} \frac{\partial w}{\partial n} u^* d\Gamma + \int_{\Gamma} q^* w d\Gamma = \\ - \int_{\Omega} \left[\frac{1}{\bar{\mu}} \left(-1 + \frac{M^2}{1+m^2} w - \frac{\partial \bar{\mu}}{\partial x} \frac{\partial w}{\partial x} - \frac{\partial \bar{\mu}}{\partial y} \frac{\partial w}{\partial y} \right) \right] u^* d\Omega \end{aligned} \quad (3.24)$$

and

$$\begin{aligned} c_i T_i - \int_{\Gamma} \frac{\partial T}{\partial n} u^* d\Gamma + \int_{\Gamma} q^* T d\Gamma = \\ - \int_{\Omega} \left(-Br\bar{\mu} \left[\left(\frac{\partial w}{\partial x} \right)^2 + \left(\frac{\partial w}{\partial y} \right)^2 \right] - \frac{M^2 Br}{1+m^2} w^2 + \frac{w}{w_m} \right) u^* d\Omega. \end{aligned} \quad (3.25)$$

The following DRBEM matrix-vector equations are obtained by considering the integrands in the domain integrals of the right hand sides as inhomogeneities, and approximating them by sets of radial basis functions given in details in Section 2.4 as

$$\mathbf{H}\mathbf{w} - \mathbf{G} \frac{\partial \mathbf{w}}{\partial n} = (\mathbf{H}\hat{\mathbf{U}} - \mathbf{G}\hat{\mathbf{Q}}) \mathbf{F}^{-1} \left\{ \frac{1}{\bar{\mu}} \left(-1 + \frac{M^2}{1+m^2} \mathbf{w} - \frac{\partial \bar{\mu}}{\partial x} \frac{\partial \mathbf{w}}{\partial x} - \frac{\partial \bar{\mu}}{\partial y} \frac{\partial \mathbf{w}}{\partial y} \right) \right\} \quad (3.26)$$

and

$$\mathbf{H}\mathbf{T} - \mathbf{G} \frac{\partial \mathbf{T}}{\partial n} = (\mathbf{H}\hat{\mathbf{U}} - \mathbf{G}\hat{\mathbf{Q}}) \mathbf{F}^{-1} \left\{ -Br\bar{\mu} \left[\left(\frac{\partial \mathbf{w}}{\partial x} \right)^2 + \left(\frac{\partial \mathbf{w}}{\partial y} \right)^2 \right] - \frac{M^2 Br}{1+m^2} \mathbf{w}^2 + \frac{\mathbf{w}}{w_m} \right\} \quad (3.27)$$

where \mathbf{H} , \mathbf{G} , $\hat{\mathbf{U}}$, $\hat{\mathbf{Q}}$ and \mathbf{F} are the standard DRBEM matrices described in (3.15).

Again, with the help of the coordinate matrix \mathbf{F} , the derivatives of the velocity \mathbf{w} and the viscosity coefficient $\bar{\mu}$ with respect to x and y are approximated. Thus, the equations (3.26) and (3.27) yield to the following equations

$$\mathbf{H}\mathbf{w} - \mathbf{G}\frac{\partial \mathbf{w}}{\partial n} = (\mathbf{H}\hat{\mathbf{U}} - \mathbf{G}\hat{\mathbf{Q}})\mathbf{F}^{-1} \left\{ \frac{1}{\bar{\mu}} \left(-1 + \frac{M^2}{1+m^2} \mathbf{w} - \frac{\partial \mathbf{F}}{\partial x} \mathbf{F}^{-1} \bar{\mu} \frac{\partial \mathbf{F}}{\partial x} \mathbf{F}^{-1} \mathbf{w} - \frac{\partial \mathbf{F}}{\partial y} \mathbf{F}^{-1} \bar{\mu} \frac{\partial \mathbf{F}}{\partial y} \mathbf{F}^{-1} \mathbf{w} \right) \right\} \quad (3.28)$$

equivalently, equation (3.28) can be written as

$$\bar{\mathbf{H}}\mathbf{w} - \mathbf{G}\mathbf{q} = (\mathbf{H}\hat{\mathbf{U}} - \mathbf{G}\hat{\mathbf{Q}})\mathbf{F}^{-1} \frac{1}{\bar{\mu}} (-1), \quad (3.29)$$

where the matrix $\bar{\mathbf{H}}$ is

$$\bar{\mathbf{H}} = \mathbf{H} - \mathbf{R}, \text{ and} \quad \mathbf{R} = (\mathbf{H}\hat{\mathbf{U}} - \mathbf{G}\hat{\mathbf{Q}})\mathbf{F}^{-1} \frac{1}{\bar{\mu}} \left(\frac{M^2}{1+m^2} - \frac{\partial \mathbf{F}}{\partial x} \mathbf{F}^{-1} \bar{\mu} \frac{\partial \mathbf{F}}{\partial x} \mathbf{F}^{-1} - \frac{\partial \mathbf{F}}{\partial y} \mathbf{F}^{-1} \bar{\mu} \frac{\partial \mathbf{F}}{\partial y} \mathbf{F}^{-1} \right) \quad (3.30)$$

and

$$\mathbf{H}\mathbf{T} - \mathbf{G}\frac{\partial \mathbf{T}}{\partial n} = (\mathbf{H}\hat{\mathbf{U}} - \mathbf{G}\hat{\mathbf{Q}})\mathbf{F}^{-1} \left\{ -Br\bar{\mu} \left[\left(\frac{\partial \mathbf{F}}{\partial x} \mathbf{F}^{-1} \mathbf{w} \right)^2 + \left(\frac{\partial \mathbf{F}}{\partial y} \mathbf{F}^{-1} \mathbf{w} \right)^2 \right] - \frac{M^2 Br}{1+m^2} \mathbf{w}^2 + \frac{\mathbf{w}}{w_m} \right\}. \quad (3.31)$$

All the terms in equations (3.28) and (3.29) are matrices while $\bar{\mu}$ and $\frac{1}{\bar{\mu}}$ are diagonal matrices constructed by taking viscosity parameter $\bar{\mu} = e^{-BT}$ and $\frac{1}{\bar{\mu}}$ as their diagonal entries, respectively.

Then, in the DRBEM procedure for the flow and temperature equations (3.29) and (3.31) are going to be solved iteratively by following the algorithm below.

Step 1. Pre-assign a tolerance ϵ for the convergence criteria.

Step 2. Take initial guesses for the velocity w^0 and the temperature T^0 as zero.

Step 3. Solve the following coupled DRBEM equations in terms of the velocity and temperature by using the Dirichlet type boundary conditions ($w = 0$ and $T = 0$ on the boundary) as

$$\bar{\mathbf{H}}\mathbf{w}^{n+1} - \mathbf{G}\mathbf{q}^{n+1} = (\mathbf{H}\hat{\mathbf{U}} - \mathbf{G}\hat{\mathbf{Q}})\mathbf{F}^{-1}\frac{1}{\mu}(-1). \quad (3.32)$$

$$\begin{aligned} \mathbf{H}\mathbf{T}^{n+1} - \mathbf{G}\frac{\partial \mathbf{T}^{n+1}}{\partial n} &= (\mathbf{H}\hat{\mathbf{U}} - \mathbf{G}\hat{\mathbf{Q}})\mathbf{F}^{-1} \\ &\left\{ -Br\bar{\mu}\left[\left(\frac{\partial \mathbf{F}}{\partial x}\mathbf{F}^{-1}\mathbf{w}^{n+1}\right)^2 + \left(\frac{\partial \mathbf{F}}{\partial y}\mathbf{F}^{-1}\mathbf{w}^{n+1}\right)^2\right] - \frac{M^2 Br}{1+m^2}(\mathbf{w}^2)^{n+1} + \frac{\mathbf{w}^{n+1}}{w_m} \right\}. \end{aligned} \quad (3.33)$$

Step 4. Check the convergence criteria

$$\frac{\|u^{n+1} - u^n\|_{\infty}}{\|u^n\|_{\infty}} < \varepsilon \quad (3.34)$$

where $\|u\|_{\infty} = \max\{|u_1|, |u_2|, \dots, |u_{N+L}|\}$ for the velocity w and the temperature T , and n denotes the iteration level.

Step 5. If the criteria is achieved for w and T , then stop.

Step 6. If the criteria is not achieved for one of the unknowns then repeat the Steps 3-4.

Therefore, all the unknown values of the velocity and temperature inside the region, and their normal derivatives on the boundary are obtained.

3.2 DRBEM applications to MHD duct flow with time-varied external magnetic field

A viscous, incompressible and electrically conducting fluid is flowing in a long pipe having a rectangular cross-section. The fully-developed flow through the pipe is subjected to a time-varied oblique magnetic field $B_0(t) = B_0 f(t)$ where B_0 is the intensity of the applied magnetic field at the initial time level ($t = 0$) and $f(t)$ is a time-varied function. The MHD equations are derived in Chapter 1 from the Navier-Stokes equations and the Maxwell's equation through Ohm's law containing the effect of time-varied applied magnetic field $B_0(t)$ [50].

The velocity $V(x, y, t)$ and the induced magnetic field $B(x, y, t)$ vary only in the duct Ω of the pipe under the effect of magnetic field changing with respect to time. The

governing equations in a domain $\Omega \times [0, \infty)$ are (equations (1.61)-(1.62))

$$\begin{aligned}\nabla^2 V + \overline{M}_x \frac{\partial B}{\partial x} + \overline{M}_y \frac{\partial B}{\partial y} &= -1 + R_e \frac{\partial V}{\partial t} \\ \nabla^2 B + \overline{M}_x \frac{\partial V}{\partial x} + \overline{M}_y \frac{\partial V}{\partial y} &= R_m \frac{\partial B}{\partial t}\end{aligned}\tag{3.35}$$

where $\Omega = \{(x, y) \in \mathbb{R}^2 : -1 \leq x, y \leq 1\}$. $\overline{M}_x = M f(t) \sin \alpha$, $\overline{M}_y = M f(t) \cos \alpha$, M is the Hartmann number and α is the angle between the applied magnetic field and the y -axis. R_e and R_m denote the Reynolds and magnetic Reynolds numbers, and defined in equations (1.53), (1.54), respectively.

The problem is considered with the following boundary conditions

$$V(x, y, t) = 0 \quad B(x, y, t) = 0 \quad (x, y) \in \Gamma, \quad t > 0\tag{3.36}$$

which means the walls of the duct have no-slip velocity and they are insulated, and initially both the velocity and induced magnetic field are zero

$$V(x, y, 0) = 0 \quad B(x, y, 0) = 0 \quad (x, y) \in \Omega.\tag{3.37}$$

3.2.1 $R_e = 1, R_m = 1$ case

In this section, the DRBEM solution for the equations in (3.35) is going to be presented. The unsteady MHD equations are in coupled form. Unless the Reynolds number R_e and magnetic Reynolds number R_m equal to 1, one must handle these PDEs in its original coupled form. However, if R_e and R_m are taken as 1 according to the physics of the problem, then they can be transformed into decoupled unsteady convection-diffusion type equations with time dependent coefficients by using the change of variables given in [65]

$$U_1 = V + B, \quad U_2 = V - B.\tag{3.38}$$

Equations in (3.35) are rewritten in decoupled form

$$\begin{aligned}\nabla^2 U_1 + \overline{M}_x \frac{\partial U_1}{\partial x} + \overline{M}_y \frac{\partial U_1}{\partial y} &= -1 + \frac{\partial U_1}{\partial t} \\ \nabla^2 U_2 - \overline{M}_x \frac{\partial U_2}{\partial x} - \overline{M}_y \frac{\partial U_2}{\partial y} &= -1 + \frac{\partial U_2}{\partial t}\end{aligned}\tag{3.39}$$

with the following boundary and initial conditions

$$\begin{aligned} U_1(x, y, t) = 0 \quad U_2(x, y, t) = 0 \quad (x, y) \in \Gamma \\ U_1(x, y, 0) = 0 \quad U_2(x, y, 0) = 0 \quad (x, y) \in \Omega \end{aligned} \quad (3.40)$$

where $(x, y, t) \in \Omega \times [0, \infty)$.

Leaving the Laplacian terms alone on one side of the equations and treating all the other terms as inhomogeneities, the application of the DRBEM procedure brings the discretized equations in the following matrix-vector form as

$$\begin{aligned} \mathbf{H}\mathbf{U}_1 - \mathbf{G}\frac{\partial \mathbf{U}_1}{\partial n} &= (\mathbf{H}\hat{\mathbf{U}} - \mathbf{G}\hat{\mathbf{Q}})\mathbf{F}^{-1} \left\{ -1 + \frac{\partial \mathbf{U}_1}{\partial t} - \bar{M}_x \frac{\partial \mathbf{U}_1}{\partial x} - \bar{M}_y \frac{\partial \mathbf{U}_1}{\partial y} \right\} \\ \mathbf{H}\mathbf{U}_2 - \mathbf{G}\frac{\partial \mathbf{U}_2}{\partial n} &= (\mathbf{H}\hat{\mathbf{U}} - \mathbf{G}\hat{\mathbf{Q}})\mathbf{F}^{-1} \left\{ -1 + \frac{\partial \mathbf{U}_2}{\partial t} + \bar{M}_x \frac{\partial \mathbf{U}_2}{\partial x} + \bar{M}_y \frac{\partial \mathbf{U}_2}{\partial y} \right\}. \end{aligned} \quad (3.41)$$

Evaluating the space derivatives of \mathbf{U}_1 and \mathbf{U}_2 with the help of the coordinate function \mathbf{F} yields

$$\begin{aligned} (\mathbf{H} + (\mathbf{H}\hat{\mathbf{U}} - \mathbf{G}\hat{\mathbf{Q}})\mathbf{F}^{-1}(\bar{M}_x \frac{\partial \mathbf{F}}{\partial x} \mathbf{F}^{-1} + \bar{M}_y \frac{\partial \mathbf{F}}{\partial y} \mathbf{F}^{-1}))\mathbf{U}_1 - \mathbf{G}\frac{\partial \mathbf{U}_1}{\partial n} &= \\ (\mathbf{H}\hat{\mathbf{U}} - \mathbf{G}\hat{\mathbf{Q}})\mathbf{F}^{-1} \left\{ -1 + \frac{\partial \mathbf{U}_1}{\partial t} \right\} \\ (\mathbf{H} + (\mathbf{H}\hat{\mathbf{U}} - \mathbf{G}\hat{\mathbf{Q}})\mathbf{F}^{-1}(\bar{M}_x \frac{\partial \mathbf{F}}{\partial x} \mathbf{F}^{-1} + \bar{M}_y \frac{\partial \mathbf{F}}{\partial y} \mathbf{F}^{-1}))\mathbf{U}_2 - \mathbf{G}\frac{\partial \mathbf{U}_2}{\partial n} &= \\ (\mathbf{H}\hat{\mathbf{U}} - \mathbf{G}\hat{\mathbf{Q}})\mathbf{F}^{-1} \left\{ -1 + \frac{\partial \mathbf{U}_2}{\partial t} \right\}. \end{aligned} \quad (3.42)$$

When the time derivatives of \mathbf{U}_1 and \mathbf{U}_2 are discretized by using the implicit Euler method and following the procedure detailed in Section 2.4.3.1, equations (3.42) become

$$\begin{aligned} \mathbf{C}(\mathbf{H} + (\mathbf{H}\hat{\mathbf{U}} - \mathbf{G}\hat{\mathbf{Q}})\mathbf{F}^{-1}(\bar{M}_x \frac{\partial \mathbf{F}}{\partial x} \mathbf{F}^{-1} + \bar{M}_y \frac{\partial \mathbf{F}}{\partial y} \mathbf{F}^{-1}))\mathbf{U}_1 - \mathbf{C}\mathbf{G}\frac{\partial \mathbf{U}_1}{\partial n} &= \\ \left\{ -1 + \frac{\mathbf{U}_1^{n+1} - \mathbf{U}_1^n}{\Delta t} \right\} \\ \mathbf{C}(\mathbf{H} + (\mathbf{H}\hat{\mathbf{U}} - \mathbf{G}\hat{\mathbf{Q}})\mathbf{F}^{-1}(\bar{M}_x \frac{\partial \mathbf{F}}{\partial x} \mathbf{F}^{-1} + \bar{M}_y \frac{\partial \mathbf{F}}{\partial y} \mathbf{F}^{-1}))\mathbf{U}_2 - \mathbf{C}\mathbf{G}\frac{\partial \mathbf{U}_2}{\partial n} &= \\ \left\{ -1 + \frac{\mathbf{U}_2^{n+1} - \mathbf{U}_2^n}{\Delta t} \right\} \end{aligned} \quad (3.43)$$

where $\mathbf{C} = ((\mathbf{H}\hat{\mathbf{U}} - \mathbf{G}\hat{\mathbf{Q}})\mathbf{F}^{-1})^{-1}$.

Rearrangement of equation (3.43) for increasing time levels results in

$$\begin{aligned} \left(\mathbf{A}_1 - \frac{1}{\Delta t}\right) \mathbf{U}_1^{n+1} - \mathbf{G}_1 \frac{\partial \mathbf{U}_1^{n+1}}{\partial n} &= \left\{-1 - \frac{\mathbf{U}_1^n}{\Delta t}\right\} \\ \left(\mathbf{A}_2 - \frac{1}{\Delta t}\right) \mathbf{U}_2^{n+1} - \mathbf{G}_2 \frac{\partial \mathbf{U}_2^{n+1}}{\partial n} &= \left\{-1 - \frac{\mathbf{U}_2^n}{\Delta t}\right\} \end{aligned} \quad (3.44)$$

where

$$\begin{aligned} \mathbf{A}_1 &= \mathbf{C}(\mathbf{H} + (\mathbf{H}\hat{\mathbf{U}} - \mathbf{G}\hat{\mathbf{Q}})\mathbf{F}^{-1}(\overline{M}_x \frac{\partial \mathbf{F}}{\partial x} \mathbf{F}^{-1} + \overline{M}_y \frac{\partial \mathbf{F}}{\partial y} \mathbf{F}^{-1})), \quad \mathbf{G}_1 = \mathbf{C}\mathbf{G} \\ \mathbf{A}_2 &= \mathbf{C}(\mathbf{H} - (\mathbf{H}\hat{\mathbf{U}} - \mathbf{G}\hat{\mathbf{Q}})\mathbf{F}^{-1}(\overline{M}_x \frac{\partial \mathbf{F}}{\partial x} \mathbf{F}^{-1} + \overline{M}_y \frac{\partial \mathbf{F}}{\partial y} \mathbf{F}^{-1})), \quad \mathbf{G}_2 = \mathbf{C}\mathbf{G}. \end{aligned} \quad (3.45)$$

Now, the equations in (3.44) can be solved separately and iteratively for increasing time levels t_n starting with the initials $U_1^0 = 0$ and $U_2^0 = 0$. The solution procedure for U_1 (or U_2) is going to be detailed as follows. The values of U_1 (or U_2) is known on the boundary as zero and the normal derivative of U_1 (or U_2) is taken as zero at the interior nodes. However, the values of U_1 (or U_2) in the region and its normal derivative on the boundary are the unknowns. Then, all the known values for the boundary and interior nodes are inserted into the corresponding matrix-vector equation in (3.44). This makes the vectors in (3.44) on both sides have some known and unknown values. All the unknown values of U_1 and $\frac{\partial U_1}{\partial n}$ (or U_2 and $\frac{\partial U_2}{\partial n}$) can be collected on one side by swapping the corresponding columns of the matrices $(\mathbf{A}_1 - \frac{1}{\Delta t})$ (or $(\mathbf{A}_2 - \frac{1}{\Delta t})$) with \mathbf{G}_1 (or \mathbf{G}_2). This shuffling procedure gives a system of linear algebraic equations such as $\mathbf{A}\mathbf{x} = \mathbf{d}$. Solving this system gives the values of U_1 (or U_2) inside the region and $\frac{\partial U_1}{\partial n}$ (or $\frac{\partial U_2}{\partial n}$) on the boundary. The iterative process is repeated until the desired time level or the preassigned convergence tolerance between two successive iterations is reached. After then, by using the back substitutions in (3.38) which is

$$V = (U_1 + U_2)/2, \quad B = (U_1 - U_2)/2 \quad (3.46)$$

the velocity $V(x, y)$ and the induced magnetic field $B(x, y)$ can be obtained at the points on which they are unknowns.

3.2.2 Varying R_e and R_m case

Without the restriction on the Reynolds number R_e and magnetic Reynolds number R_m which approximates them as 1, the coupled equations (3.35) must be solved in

their original form

$$\begin{aligned}\nabla^2 V + \overline{M}_x \frac{\partial B}{\partial x} + \overline{M}_y \frac{\partial B}{\partial y} &= -1 + R_e \frac{\partial V}{\partial t} \\ \nabla^2 B + \overline{M}_x \frac{\partial V}{\partial x} + \overline{M}_y \frac{\partial V}{\partial y} &= R_m \frac{\partial B}{\partial t}\end{aligned}\quad (3.47)$$

where $(x, y, t) \in \Omega \times [0, \infty)$.

The discretized DRBEM matrix-vector equations corresponding to the MHD flow problem (3.47) are

$$\begin{aligned}\mathbf{H}\mathbf{V} - \mathbf{G} \frac{\partial \mathbf{V}}{\partial n} &= (\mathbf{H}\hat{\mathbf{U}} - \mathbf{G}\hat{\mathbf{Q}})\mathbf{F}^{-1} \left\{ -1 + R_e \frac{\partial \mathbf{V}}{\partial t} - \overline{M}_x \frac{\partial \mathbf{B}}{\partial x} - \overline{M}_y \frac{\partial \mathbf{B}}{\partial y} \right\} \\ \mathbf{H}\mathbf{B} - \mathbf{G} \frac{\partial \mathbf{B}}{\partial n} &= (\mathbf{H}\hat{\mathbf{U}} - \mathbf{G}\hat{\mathbf{Q}})\mathbf{F}^{-1} \left\{ R_m \frac{\partial \mathbf{B}}{\partial t} - \overline{M}_x \frac{\partial \mathbf{V}}{\partial x} - \overline{M}_y \frac{\partial \mathbf{V}}{\partial y} \right\}.\end{aligned}\quad (3.48)$$

Then, the same procedures mentioned above for the special case $R_e = 1 = R_m$, which are approximating the space derivatives of \mathbf{V} and \mathbf{B} with the help of the coordinate function \mathbf{F} and evaluating the time derivatives of \mathbf{V} and \mathbf{B} by using the implicit Euler method, bring the coupled discretized system

$$\begin{aligned}\left(\mathbf{H} - \frac{R_e}{\Delta t} \mathbf{K}\right) \mathbf{V}^{n+1} - \mathbf{G} \frac{\partial \mathbf{V}^{n+1}}{\partial n} + \mathbf{P} \mathbf{B}^{n+1} + \mathbf{R} \mathbf{B}^{n+1} &= \mathbf{K} \left(-1 - \frac{R_e}{\Delta t} \mathbf{V}^n\right) \\ \left(\mathbf{H} - \frac{R_m}{\Delta t} \mathbf{K}\right) \mathbf{B}^{n+1} - \mathbf{G} \frac{\partial \mathbf{B}^{n+1}}{\partial n} + \mathbf{P} \mathbf{V}^{n+1} + \mathbf{R} \mathbf{V}^{n+1} &= \mathbf{K} \left(-\frac{R_m}{\Delta t} \mathbf{B}^n\right)\end{aligned}\quad (3.49)$$

which are solved for increasing time levels where $\mathbf{K} = (\mathbf{H}\hat{\mathbf{U}} - \mathbf{G}\hat{\mathbf{Q}})\mathbf{F}^{-1}$, $\mathbf{P} = \mathbf{K}(\overline{M}_x \frac{\partial \mathbf{F}}{\partial x} \mathbf{F}^{-1})$ and $\mathbf{R} = \mathbf{K}(\overline{M}_y \frac{\partial \mathbf{F}}{\partial y} \mathbf{F}^{-1})$.

Eventually, the equations in (3.49) can be put into the form

$$\begin{aligned}\tilde{\mathbf{H}} \mathbf{V}^{n+1} - \mathbf{G} \frac{\partial \mathbf{V}^{n+1}}{\partial n} + (\mathbf{P} + \mathbf{R}) \mathbf{B}^{n+1} &= \mathbf{b}_1 \\ \check{\mathbf{H}} \mathbf{B}^{n+1} - \mathbf{G} \frac{\partial \mathbf{B}^{n+1}}{\partial n} + (\mathbf{P} + \mathbf{R}) \mathbf{V}^{n+1} &= \mathbf{b}_2\end{aligned}\quad (3.50)$$

where $\tilde{\mathbf{H}} = \mathbf{H} - \frac{R_e}{\Delta t} \mathbf{K}$, $\check{\mathbf{H}} = \mathbf{H} - \frac{R_m}{\Delta t} \mathbf{K}$, $\mathbf{b}_1 = \mathbf{K}(-1 - \frac{R_e}{\Delta t} \mathbf{V}^n)$ and $\mathbf{b}_2 = \mathbf{K}(-\frac{R_m}{\Delta t} \mathbf{B}^n)$.

The coupled matrix-vector equations in (3.50) are solved together, by constructing

the following enlarged system

$$\begin{bmatrix} \tilde{\mathbf{H}} & (\mathbf{P} + \mathbf{R}) \\ (\mathbf{P} + \mathbf{R}) & \check{\mathbf{H}} \end{bmatrix} \begin{Bmatrix} \mathbf{V}^{n+1} \\ \mathbf{B}^{n+1} \end{Bmatrix} = \begin{bmatrix} \mathbf{G} & \mathbf{0} \\ \mathbf{0} & \mathbf{G} \end{bmatrix} \begin{Bmatrix} \frac{\partial \mathbf{V}^{n+1}}{\partial n} \\ \frac{\partial \mathbf{B}^{n+1}}{\partial n} \end{Bmatrix} + \begin{Bmatrix} \mathbf{b}_1 \\ \mathbf{b}_2 \end{Bmatrix} \quad (3.51)$$

where all the matrices and vectors in the system have sizes $(N + L) \times (N + L)$ and $(N + L) \times 1$, respectively. The $(N + L) \times (N + L)$ zero matrix is denoted by $\mathbf{0}$.

Prescribing new matrices as

$$\mathbf{H}' = \begin{bmatrix} \tilde{\mathbf{H}} & (\mathbf{P} + \mathbf{R}) \\ (\mathbf{P} + \mathbf{R}) & \check{\mathbf{H}} \end{bmatrix}, \quad \mathbf{G}' = \begin{bmatrix} \mathbf{G} & \mathbf{0} \\ \mathbf{0} & \mathbf{G} \end{bmatrix} \quad (3.52)$$

where \mathbf{H}' and \mathbf{G}' have dimensions $2(N + L) \times 2(N + L)$, the enlarged system becomes

$$\mathbf{H}' \begin{Bmatrix} \mathbf{V}^{n+1} \\ \mathbf{B}^{n+1} \end{Bmatrix} = \mathbf{G}' \begin{Bmatrix} \frac{\partial \mathbf{V}^{n+1}}{\partial n} \\ \frac{\partial \mathbf{B}^{n+1}}{\partial n} \end{Bmatrix} + \begin{Bmatrix} \mathbf{b}_1 \\ \mathbf{b}_2 \end{Bmatrix}. \quad (3.53)$$

For this considered MHD duct flow problem, the velocity and the induced magnetic field are known on the boundary. The unknowns are their values inside the region and their normal derivatives on the boundary. The normal derivatives are taken as zero in the region. After inserting all the known values of the velocity and induced magnetic field into the system of equations (3.53), the vectors on both sides contain some known and unknown values. In order to get a linear system of equations, an arrangement is required. Each unknown on the right hand side of equation (3.53) is carried to the left hand side by swapping the corresponding columns of the matrices \mathbf{H}' and \mathbf{G}' . Once all the unknown and know values are changed respectively to the left hand side and right hand side, a linear system of equations such as $\mathbf{Ax} = \mathbf{d}$ is obtained and solution of this system provides the velocity $V(x, y)$ and the induced magnetic field $B(x, y)$ values in the discretized points in the region in one stroke for increasing time levels starting from the initial values $V(x, y, 0)$ and $B(x, y, 0)$, i.e. $V^0 = 0$ and $B^0 = 0$. This solution procedure is repeated iteratively up to the desired time level or preassigned convergence tolerance is reached.

3.3 DRBEM applications to inductionless MHD flow and electric potential with variably conducting walls under axial-dependent magnetic field

In this section, the MHD flow of a viscous and incompressible fluid is considered in a long pipe of rectangular cross-section under the effect of pipe-axis direction-dependent vertically applied magnetic field $\mathbf{B} = (0, B_0(z), 0)$ and $B_0(z) = B_0 g(z)$ where B_0 is the external magnetic field intensity and $g(z)$ is the function determining the strength of the applied magnetic field along the z -axis, i.e. pipe-axis. The configuration of the MHD flow in a long pipe under streamwise-dependent applied magnetic field is seen in Figure 3.2.

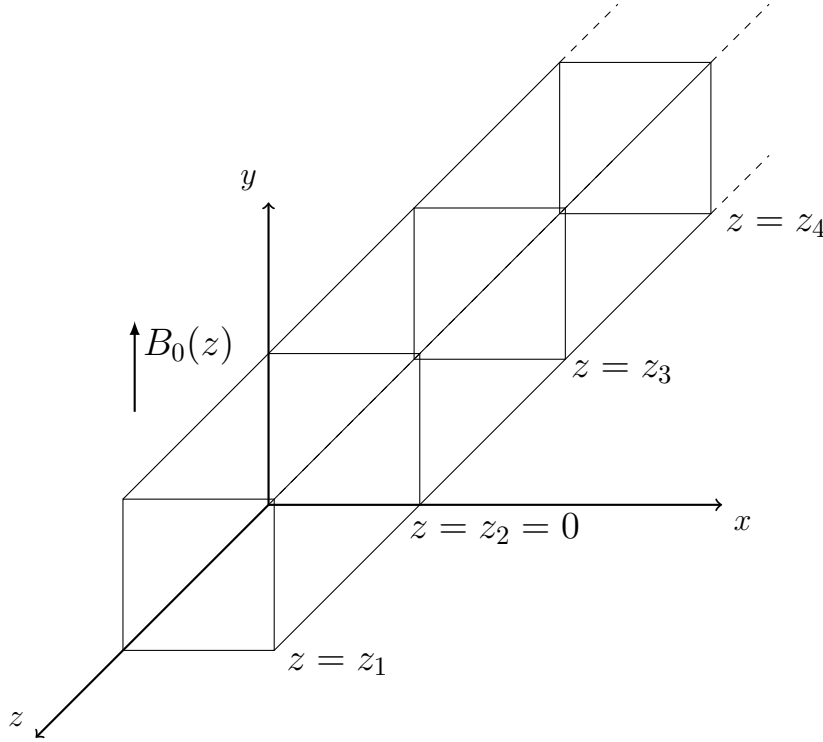


Figure 3.2: Physical configuration of the rectangular pipe

The flow is assumed to be fully developed between two fixed z -values and its velocity has only one component in the pipe-axis direction varying in the ducts xy -plane at these fixed points of the axis. Physically, it may be considered as the fully-developed flow between two magnets placed on the pipe-axis direction. The flow is considered as two-dimensional on these ducts of the xy -plane where the magnets are located.

The fluid is electrically conducting and it is subjected to a magnetic field applied vertically but changing at the points where the magnets placed on the pipe-axis. The induced magnetic field is neglected. Thus, the magnetic field $\mathbf{B} = (0, B_0(z), 0)$, the velocity $\mathbf{u} = (0, 0, w(x, y))$ and the electric potential $\Phi = \Phi(x, y)$ are varying in the ducts along with the pipe-axis.

The non-dimensional momentum and electric potential equations (divergence of current density) are coupled in Ω as

$$\begin{aligned}\nabla^2 w - (Mg(z))^2 w &= -1 + M^2 g(z) \frac{\partial \Phi}{\partial x} \\ \nabla^2 \Phi &= -g(z) \frac{\partial w}{\partial x}\end{aligned}\tag{3.54}$$

where M is the Hartmann number, $\Omega = \{(x, y) : -1 \leq x, y \leq 1\}$ and $g(z) = \frac{1}{1 + e^{-z/0.15}}$.

The no-slip velocity condition is imposed for the flow on the walls of the duct. However, the Neumann or mixed type boundary conditions are used for the electric potential depending on the conductivity of the materials of the walls. Therefore, the boundary conditions are shown in Figure 3.3 and Figure 3.4, and written as

$$\begin{aligned}w(x, \pm 1) &= w(\pm 1, y) = 0 \quad \text{no-slip velocity} \\ \text{and} \\ \frac{\partial \Phi}{\partial y}(x, \pm 1) &= \frac{\partial \Phi}{\partial x}(\pm 1, y) = 0 \quad \text{non-conducting walls}\end{aligned}\tag{3.55}$$

or

$$\begin{aligned}w(x, \pm 1) &= w(\pm 1, y) = 0 \quad \text{no-slip velocity} \\ \text{and} \\ \left. \begin{aligned}\pm \frac{\partial \Phi}{\partial y}(x, \pm 1) &= c \frac{\partial^2 \Phi}{\partial x^2}(x, \pm 1) \\ \pm \frac{\partial \Phi}{\partial x}(\pm 1, y) &= c \frac{\partial^2 \Phi}{\partial y^2}(\pm 1, y)\end{aligned} \right\} \text{variably conducting walls}\end{aligned}\tag{3.56}$$

where c denotes the wall conductance ratio of the four walls (c_t (top), c_b (bottom), c_l (left), c_r (right)) which can be taken different from each other. That is, c is a measure of the conductance of the wall compared to that of the fluid.

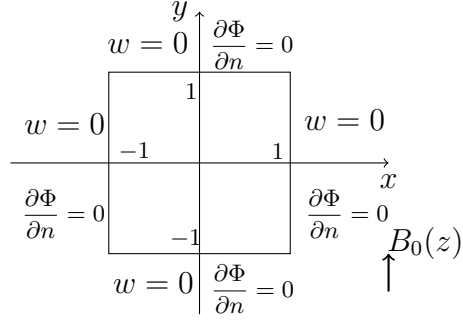


Figure 3.3: The boundary conditions on non-conducting duct walls

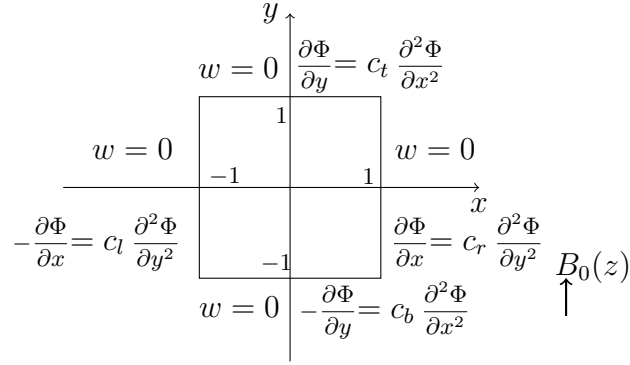


Figure 3.4: The boundary conditions on variably conducting duct walls

The discretized DRBEM equations in matrix-vector form for equation (3.54) are

$$\begin{aligned} \mathbf{H}\mathbf{w} - \mathbf{G}\frac{\partial\mathbf{w}}{\partial n} &= (\mathbf{H}\hat{\mathbf{U}} - \mathbf{G}\hat{\mathbf{Q}})\mathbf{F}^{-1}\{(Mg(z))^2\mathbf{w} - \mathbf{1} + M^2g(z)\frac{\partial\mathbf{\Phi}}{\partial x}\} \\ \mathbf{H}\mathbf{\Phi} - \mathbf{G}\frac{\partial\mathbf{\Phi}}{\partial n} &= (\mathbf{H}\mathbf{U} - \mathbf{G}\hat{\mathbf{Q}})\mathbf{F}^{-1}\{-g(z)\frac{\partial\mathbf{w}}{\partial x}\}. \end{aligned} \quad (3.57)$$

Implementing the DRBEM procedure for the space derivatives brings

$$\begin{aligned} (\mathbf{H} - \mathbf{K}(Mg(z))^2)\mathbf{w} - \mathbf{G}\frac{\partial\mathbf{w}}{\partial n} &= \mathbf{K}\{-\mathbf{1} + M^2g(z)\frac{\partial\mathbf{F}}{\partial x}\mathbf{F}^{-1}\mathbf{\Phi}\} \\ \mathbf{H}\mathbf{\Phi} - \mathbf{G}\frac{\partial\mathbf{\Phi}}{\partial n} &= \mathbf{K}\{-g(z)\frac{\partial\mathbf{F}}{\partial x}\mathbf{F}^{-1}\mathbf{w}\} \end{aligned} \quad (3.58)$$

where $\mathbf{K} = (\mathbf{H}\hat{\mathbf{U}} - \mathbf{G}\hat{\mathbf{Q}})\mathbf{F}^{-1}$.

The matrix-vector equations in (3.58) are going to be solved as a whole by construct-

ing the following enlarged system

$$\begin{bmatrix} \mathbf{H}_1 & \mathbf{H}_2 \\ \mathbf{H}_3 & \mathbf{H}_4 \end{bmatrix} \begin{Bmatrix} w \\ \Phi \end{Bmatrix} - \begin{bmatrix} \mathbf{G} & \mathbf{0} \\ \mathbf{0} & \mathbf{G} \end{bmatrix} \begin{Bmatrix} \frac{\partial w}{\partial n} \\ \frac{\partial \Phi}{\partial n} \end{Bmatrix} = \begin{Bmatrix} \mathbf{b}_1 \\ \mathbf{0} \end{Bmatrix} \quad (3.59)$$

where

$$\begin{aligned} \mathbf{H}_1 &= \mathbf{H} - \mathbf{K}(Mg(z))^2, \\ \mathbf{H}_2 &= -\mathbf{K}(M^2g(z))\frac{\partial \mathbf{F}}{\partial x}\mathbf{F}^{-1}, \\ \mathbf{H}_3 &= \mathbf{K}(g(z))\frac{\partial \mathbf{F}}{\partial x}\mathbf{F}^{-1}, \\ \mathbf{H}_4 &= \mathbf{H}, \text{ and} \\ \mathbf{b}_1 &= \mathbf{K}\{-1\}. \end{aligned} \quad (3.60)$$

Prescribing new matrices

$$\mathbf{H}' = \begin{bmatrix} \mathbf{H}_1 & \mathbf{H}_2 \\ \mathbf{H}_3 & \mathbf{H}_4 \end{bmatrix}, \quad \mathbf{G}' = \begin{bmatrix} \mathbf{G} & \mathbf{0} \\ \mathbf{0} & \mathbf{G} \end{bmatrix}, \quad (3.61)$$

the enlarged system having dimensions $2(N + L) \times 2(N + L)$ becomes

$$\mathbf{H}' \begin{Bmatrix} w \\ \Phi \end{Bmatrix} - \mathbf{G}' \begin{Bmatrix} \frac{\partial w}{\partial n} \\ \frac{\partial \Phi}{\partial n} \end{Bmatrix} = \begin{Bmatrix} \mathbf{b}_1 \\ \mathbf{0} \end{Bmatrix}. \quad (3.62)$$

In this problem, the no-slip walls of the duct are considered either electrically non-conducting or variably conducting, and/or perfectly conducting. The conductivity ratios are all zero for non-conducting walls. For the case of variably conducting walls, the conductivity ratios on the Hartmann walls are non-zero, i.e. $c_b = c_t \neq 0$. However, $c_l = c_r = c_b = c_t \neq 0$ on electrically perfectly conducting walls. The solution procedure of enlarged system of equation (3.62) for non-conducting walls with no-slip velocity as follows. Firstly, the boundary conditions of the velocity and electric potential are inserted into the system of equation (3.62) along with the known values which are the normal derivatives of the velocity and electric potential being zero inside the region Ω . Then, a linear system of equations in the form

$$\mathbf{A}\mathbf{x} = \mathbf{d} \quad (3.63)$$

is obtained after required swapping procedure is done. Lastly, by solving the system (3.63), the velocity ω and electric potential Φ values are obtained on the nodes where they are unknown. On the other hand, the solution procedure of this problem having no-slip velocity with variably or perfectly conducting walls requires iterative solution since the Neumann type boundary conditions of the electric potential Φ are not given explicitly. The normal derivatives of Φ are given in terms of the second partial derivatives of it with respect to space variables x and y . The solution can be obtained by following the algorithm described below.

Step 1. Pre-assign a tolerance ε for the convergence criteria and define a relaxation parameter κ for the electric potential.

Step 2. Take an initial guess for the electric potential, $\Phi^0 = 0$.

Step 3. Compute the Neumann type boundary conditions of the electric potential Φ by using the coordinate matrix \mathbf{F} as in [66]

$$\frac{\partial^2 \Phi^{n+1}}{\partial x^2} = \frac{\partial \mathbf{F}}{\partial x} \mathbf{F}^{-1} \frac{\partial \mathbf{F}}{\partial x} \mathbf{F}^{-1} \Phi^n \quad \frac{\partial^2 \Phi^{n+1}}{\partial y^2} = \frac{\partial \mathbf{F}}{\partial y} \mathbf{F}^{-1} \frac{\partial \mathbf{F}}{\partial y} \mathbf{F}^{-1} \Phi^n. \quad (3.64)$$

Step 4. Solve the matrix-vector equation (3.62) at $(n + 1)$ -th time level

$$\mathbf{H}' \begin{Bmatrix} \mathbf{w}^{n+1} \\ \Phi^{n+1} \end{Bmatrix} - \mathbf{G}' \begin{Bmatrix} \frac{\partial \mathbf{w}^{n+1}}{\partial n} \\ \frac{\partial \Phi^{n+1}}{\partial n} \end{Bmatrix} = \begin{Bmatrix} \mathbf{b}_1 \\ \mathbf{0} \end{Bmatrix} \quad (3.65)$$

by using the Dirichlet type boundary conditions for the velocity and Neumann type boundary conditions for the electric potential obtained from the n -th level.

Step 5. Relax the obtained electric potential values as

$$\Phi^{n+1} = \kappa \Phi^{n+1} + (1 - \kappa) \Phi^n, \quad 0 < \kappa < 1. \quad (3.66)$$

Step 6. Check the convergence criteria

$$\frac{\|u^{n+1} - u^n\|_\infty}{\|u^n\|_\infty} < \varepsilon \quad (3.67)$$

where $\|u\|_\infty = \max\{|u_1|, |u_2|, \dots, |u_{N+L}|\}$ denoting for the velocity w and the electric potential Φ , and n denotes the iteration level.

Step 7. If the criteria is achieved for w and Φ , then stop.

Step 8. If the criteria is not achieved for one of the unknowns then repeat the Steps 3-6.

3.4 DRBEM applications to MHD duct flow with axially dependent external magnetic field

In this section, the MHD duct flow in a long pipe of rectangular cross-section which is placed in a magnetic field $\mathbf{B} = (0, B_0(z), B_z(x, y))$ is considered and $B_0(z) = B_0 g(z)$ where $g(z)$ denotes the function determining the strength of the applied magnetic field along the pipe-axis, and B_0 is the uniform constant intensity in the vertical direction as shown in Figure 3.2. The flow is laminar and steady and the fluid is incompressible, viscous and electrically conducting, and it is under the effect of an axially changing magnetic field. The velocity and induced magnetic field have unknown components only in the pipe-axis (z -axis) direction. The flow is also assumed to be fully-developed between two fixed z -values varying only in the ducts xy -plane at these points of the axis as in Section 3.2. The velocity and the induced magnetic field are changing in the two-dimensional ducts but also influenced from the magnets located at the points along the pipe-axis. The applied magnetic field $B_0(z)$ in $\mathbf{B} = (0, B_0(z), B_z(x, y))$ with $B_0(z) = B_0 g(z)$ applies vertically to the duct (in the y -direction) and the pipe-axis dependent function is taken as $g(z) = \frac{1}{1 + e^{-z/0.15}}$. Thus, three-dimensional effects are caused by variations of this applied magnetic field in the pipe-axis direction between two values of z in which the flow is assumed to be fully-developed.

Firstly, the coupled MHD flow equations are considered in terms of velocity and induced magnetic field. Then, the electric potential equation is included and coupled with these MHD equations. The governing equations are

$$\begin{aligned} \nabla^2 V + M g(z) \frac{\partial B}{\partial y} &= -1 + \frac{M^2}{R_m} g(z) \frac{\partial g(z)}{\partial z} \\ \nabla^2 B + M g(z) \frac{\partial V}{\partial y} &= 0 \\ \nabla^2 \Phi &= -g(z) \frac{\partial V}{\partial x}. \end{aligned} \tag{3.68}$$

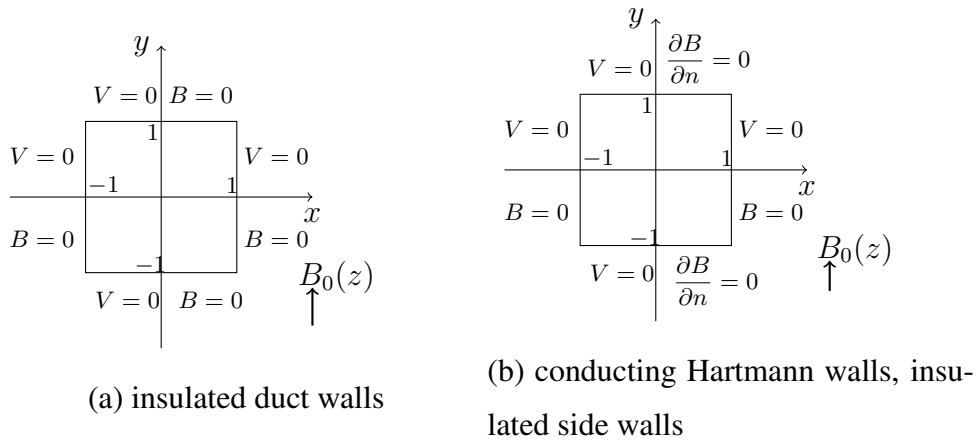


Figure 3.5: The boundary conditions for the velocity and induced magnetic field

The equations for the velocity V and the induced magnetic field B in (3.68) are considered with the boundary conditions given in Figure 3.5 (a) and (b). When the electric potential equation (3rd equation in (3.68)) is included, the problem is considered with no-slip and insulated duct walls together with the Dirichlet, and Dirichlet and Neumann type boundary conditions for Φ as in Figure 3.6 (a) and (b).

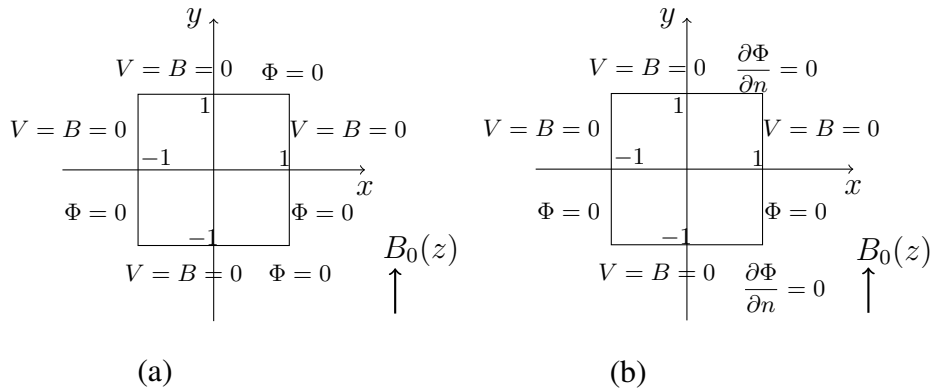


Figure 3.6: The boundary conditions of Φ on the insulated and no-slip duct walls

The DRBEM implementation to the equations (3.68) respectively bring the DRBEM

discretized system

$$\begin{aligned}
\mathbf{H}\mathbf{V} - \mathbf{G}\frac{\partial \mathbf{V}}{\partial n} &= (\mathbf{H}\hat{\mathbf{U}} - \mathbf{G}\hat{\mathbf{Q}})\mathbf{F}^{-1}\left\{-Mg(z)\frac{\partial \mathbf{B}}{\partial y} - \mathbf{1} + \frac{M^2}{R_m}g(z)\frac{\partial g(z)}{\partial z}\right\} \\
\mathbf{H}\mathbf{B} - \mathbf{G}\frac{\partial \mathbf{B}}{\partial n} &= (\mathbf{H}\hat{\mathbf{U}} - \mathbf{G}\hat{\mathbf{Q}})\mathbf{F}^{-1}\left\{-Mg(z)\frac{\partial \mathbf{V}}{\partial y}\right\} \\
\mathbf{H}\Phi - \mathbf{G}\frac{\partial \Phi}{\partial n} &= (\mathbf{H}\hat{\mathbf{U}} - \mathbf{G}\hat{\mathbf{Q}})\mathbf{F}^{-1}\left\{-g(z)\frac{\partial \mathbf{V}}{\partial x}\right\}
\end{aligned} \tag{3.69}$$

or equivalently,

$$\begin{aligned}
\mathbf{H}\mathbf{V} - \mathbf{G}\frac{\partial \mathbf{V}}{\partial n} + \mathbf{K}(Mg(z)\frac{\partial \mathbf{F}}{\partial y}\mathbf{F}^{-1}\mathbf{B}) &= \mathbf{K}\left\{-\mathbf{1} + \frac{M^2}{R_m}g(z)\frac{\partial g(z)}{\partial z}\right\} \\
\mathbf{H}\mathbf{B} - \mathbf{G}\frac{\partial \mathbf{B}}{\partial n} + \mathbf{K}(Mg(z)\frac{\partial \mathbf{F}}{\partial y}\mathbf{F}^{-1}\mathbf{V}) &= 0 \\
\mathbf{H}\Phi - \mathbf{G}\frac{\partial \Phi}{\partial n} + \mathbf{K}(g(z)\frac{\partial \mathbf{F}}{\partial x}\mathbf{F}^{-1}\mathbf{V}) &= 0
\end{aligned} \tag{3.70}$$

where $\mathbf{K} = (\mathbf{H}\hat{\mathbf{U}} - \mathbf{G}\hat{\mathbf{Q}})\mathbf{F}^{-1}$.

The solution of $\begin{Bmatrix} \mathbf{V} \\ \mathbf{B} \\ \Phi \end{Bmatrix}$ can be obtained from the following enlarged system of equations

$$\begin{bmatrix} \mathbf{H}_1 & \mathbf{H}_2 & \mathbf{H}_3 \\ \mathbf{H}_4 & \mathbf{H}_5 & \mathbf{H}_6 \\ \mathbf{H}_7 & \mathbf{H}_8 & \mathbf{H}_9 \end{bmatrix} \begin{Bmatrix} \mathbf{V} \\ \mathbf{B} \\ \Phi \end{Bmatrix} - \begin{bmatrix} \mathbf{G} & \mathbf{0} & \mathbf{0} \\ \mathbf{0} & \mathbf{G} & \mathbf{0} \\ \mathbf{0} & \mathbf{0} & \mathbf{G} \end{bmatrix} \begin{Bmatrix} \partial \mathbf{V} / \partial n \\ \partial \mathbf{B} / \partial n \\ \partial \Phi / \partial n \end{Bmatrix} = \begin{Bmatrix} \mathbf{b}_1 \\ 0 \\ 0 \end{Bmatrix} \tag{3.71}$$

where the $(N + L) \times (N + L)$ matrices are

$$\begin{aligned}
\mathbf{H}_1 &= \mathbf{H} & \mathbf{H}_4 &= \mathbf{H}_2 & \mathbf{H}_7 &= \mathbf{K}(g(z)\frac{\partial \mathbf{F}}{\partial x}\mathbf{F}^{-1}) \\
\mathbf{H}_2 &= \mathbf{K}(Mg(z)\frac{\partial \mathbf{F}}{\partial y}\mathbf{F}^{-1}) & \mathbf{H}_5 &= \mathbf{H} & \mathbf{H}_8 &= \mathbf{0} \\
\mathbf{H}_3 &= \mathbf{0} & \mathbf{H}_6 &= \mathbf{0} & \mathbf{H}_9 &= \mathbf{H}
\end{aligned} \tag{3.72}$$

and $\mathbf{b}_1 = \mathbf{K}\left(-\mathbf{1} + \frac{M^2}{R_m}g(z)\frac{\partial g(z)}{\partial z}\right)$.

Further, the solution $\begin{Bmatrix} \mathbf{V} \\ \mathbf{B} \end{Bmatrix}$ with the boundary conditions shown in Figure 3.4 can also be obtained from the same system of equations (3.71) by eliminating the last column and row of the matrices and vectors.

Prescribing new matrices as

$$\mathbf{H}' = \begin{bmatrix} \mathbf{H}_1 & \mathbf{H}_2 & \mathbf{H}_3 \\ \mathbf{H}_4 & \mathbf{H}_5 & \mathbf{H}_6 \\ \mathbf{H}_7 & \mathbf{H}_8 & \mathbf{H}_9 \end{bmatrix}, \quad \mathbf{G}' = \begin{bmatrix} \mathbf{G} & \mathbf{0} & \mathbf{0} \\ \mathbf{0} & \mathbf{G} & \mathbf{0} \\ \mathbf{0} & \mathbf{0} & \mathbf{G} \end{bmatrix} \quad (3.73)$$

the enlarged system having dimensions $3(N + L) \times 3(N + L)$ becomes

$$\mathbf{H}' \begin{Bmatrix} V \\ B \\ \Phi \end{Bmatrix} = \mathbf{G}' \begin{Bmatrix} \partial V / \partial n \\ \partial B / \partial n \\ \partial \Phi / \partial n \end{Bmatrix} + \begin{Bmatrix} \mathbf{b}_1 \\ \mathbf{0} \\ \mathbf{0} \end{Bmatrix}. \quad (3.74)$$

A linear system of equations such as $\mathbf{A}\mathbf{x} = \mathbf{d}$ can be obtained after inserting the given boundary conditions shown on Figure 3.6 into (3.74) and swapping the corresponding columns of \mathbf{H}' and \mathbf{G}' . The solution of $\mathbf{A}\mathbf{x} = \mathbf{d}$ gives the unknown values of V , B and Φ at the discretized points wherever they are unknown.

In Chapter 3, the BEM solutions for convection-diffusion type PDEs (MHD flow equations) are given. Although, mainly the MHD flow equations are solved, the differences occur in the temperature dependent viscosity coefficients in the first problem considered in Section 3.1, and time dependent or axial-dependent externally applied magnetic field cases which are treated in Sections 3.2 and 3.3-3.4, respectively. For the variable viscosity coefficients, the parametric BEM is employed as well as the DRBEM. When the applied magnetic field depends on the pipe-axis direction, MHD flow equations in terms of the velocity and electric potential are solved in Section 3.3 and, the MHD equations are also solved in Section 3.4 when the induced magnetic field is included.

CHAPTER 4

NUMERICAL RESULTS OF THE MHD DUCT FLOW PROBLEMS

The MHD flow through pipes has important application areas such as MHD generators, accelerators, MHD flow meters, blood flow measurements and nuclear reactors. In most cases, finding an analytical solution is a challenging process. Most of the convection-diffusion type PDEs including MHD flow equations do not have known analytical solutions and so finding numerical solutions becomes attractive. Since a second-order, linear, elliptic PDE with variable convection coefficients has many applications in some classes of thermostatic, elastostatic and electrostatic fields, the present chapter is devoted first to the numerical solutions of such problems. First, a heat conduction problem with variable coefficients is solved and compared with the exact solution. Then, the convection-diffusion type MHD flow problem with temperature dependent viscosity and heat transfer, is solved numerically in the absence of induced magnetic field, and the results are presented in Section 4.1. The parametric BEM and DRBEM are both used for obtaining numerical results. In the parametric BEM procedure, Levi function helps one to solve the equation in its original form, and the DRBEM uses fundamental solution of Laplace equation treating all the terms as inhomogeneities other than the Laplacian. Then, the numerical solutions of the MHD duct flow problems by using the DRBEM are presented in the rest of the chapter. In Section 4.2, the transient behaviors of the MHD duct flow are shown in terms of the velocity and induced magnetic field under the effect of a time-varied applied magnetic field $B_0(t)$. The MHD duct flow under the effect of axially changing imposed magnetic field $B_0(z)$ is solved numerically in Section 4.3. This study focuses mainly on the flow behavior and the structure of the boundary layers influenced from the changes in the electrical conductivity of the walls, and the strength of the axially changing applied magnetic field. The obtained results are displayed in terms of the

flow velocity and electric currents showing redistribution of the flow. In the latter Section 4.4, the numerical results of the MHD duct flow problem under the influence of the axial-dependent applied magnetic field are simulated in terms of the velocity, induced magnetic field and electric potential equal lines.

4.1 Inductionless MHD flow and heat transfer with temperature dependent viscosity

In this section, the steady, laminar, fully developed MHD flow and heat transfer of an incompressible, electrically conducting fluid with temperature dependent viscosity, is solved in a rectangular duct in terms of the velocity and temperature of the fluid not considering the induced magnetic field. Before dealing with the MHD flow equations, we first want to see the parametrix BEM solutions of two non-homogeneous heat conduction problems with variable coefficients as test problems as in [63] for validating our parametrix BEM code.

Test Problems :

The second-order, linear, elliptic, variable coefficient partial differential equation of diffusion type is given as (equation (2.51))

$$\frac{\partial}{\partial x} \left(a(x, y) \frac{\partial u}{\partial x} \right) + \frac{\partial}{\partial y} \left(a(x, y) \frac{\partial u}{\partial y} \right) = b(x, y), \quad (x, y) \in \Omega \quad (4.1)$$

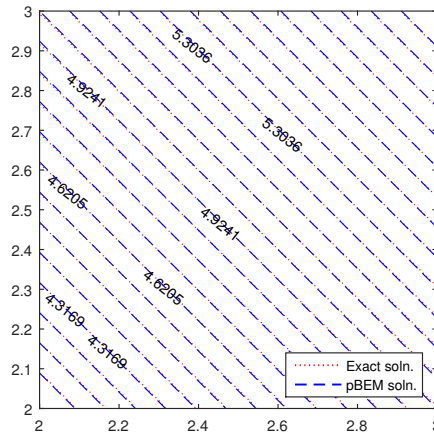
with partially given boundary conditions of the unknown and flux as

$$\begin{aligned} u(x, y) &= \bar{u}(x, y), \quad (x, y) \in \Gamma_1 \\ Tu(x, y) &= a(x, y) \frac{\partial u}{\partial n}(x, y) = \bar{t}(x, y), \quad (x, y) \in \Gamma_2. \end{aligned} \quad (4.2)$$

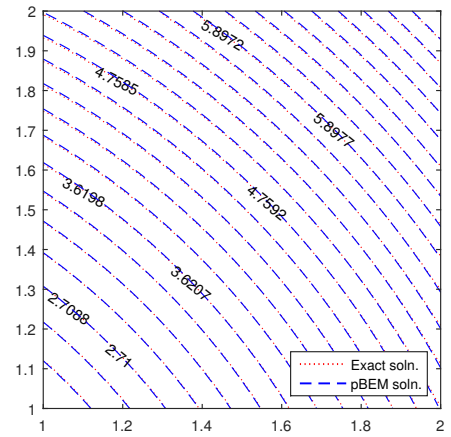
The numerical simulations are carried by solving two test problems with parametrix BEM which uses a Levi function or parametrix $P(x, x_i; y, y_i) = \frac{1}{2\pi a(x_i, y_i)} \ln|r - r_i|$ as a fundamental solution. In order to validate our numerical codes for the parametrix BEM, we particularly consider the problems for which the exact solutions are available. The variable coefficients $a(x, y)$, the non-homogeneous terms $b(x, y)$ and the exact solutions of the problems along with the problem domains and boundary conditions corresponding to the problems are given in Table 4.1

Table 4.1: Variable coefficient heat conduction problems

	Test Problem 1	Test Problem 2
$a(x, y)$	$2(x + y)$	$x^2 + y^2$
$b(x, y)$	4	$8(x^2 + y^2)$
u_{exact}	$x + y$	$x^2 + y^2$
Ω	$[2, 3] \times [2, 3]$	$[1, 2] \times [1, 2]$
$u = \bar{u}$	$x + 2$, on $y = 2$; $x \in [2, 3]$	$x^2 + 1$, on $y = 1$; $x \in [1, 2]$
$u = \bar{u}$	$x + 3$, on $y = 3$; $x \in [2, 3]$	$x^2 + 4$, on $y = 2$; $x \in [1, 2]$
$Tu = \bar{t}$	$2(x + y)$, on $x = 3$; $y \in [2, 3]$	$2x(x^2 + y^2)$, on $x = 2$; $y \in [1, 2]$
$Tu = \bar{t}$	$-2(x + y)$, on $x = 2$; $y \in [2, 3]$	$-2x(x^2 + y^2)$, on $x = 1$; $y \in [1, 2]$



(a) Test Problem 1



(b) Test Problem 2

Figure 4.1: Heat conduction problems. Isotherms from parametrix BEM and Exact solutions.

Figure 4.1 visualizes exact solutions and numerical solutions obtained from parametrix BEM for two test, variable coefficient heat conduction problems. In both solutions, the domain Ω is discretized with $N = 300$ boundary elements and $L = 5625$ interior nodes. The domain integrals arising from the parametrix BEM are computed by using composite trapezoidal rule. Figure 4.1 shows that, the parametrix BEM solutions

agree very well with the exact solutions.

Table 4.2: Error L2 norms of the test problems for increasing number of boundary elements.

	Test Problem 1	Test Problem 2
$N = 160$	0.1874	0.6353
$N = 200$	0.1828	0.6212
$N = 240$	0.1796	0.6116
$N = 300$	0.1764	0.6019

From the Table 4.2 it can be seen that, as the number boundary elements increases the error between the exact and parametrix BEM solutions of the test problems decreases in the sense of L2 norm.

Then, we continue with the non-dimensional MHD flow and heat transfer equations in which the viscosity coefficient $\bar{\mu} = e^{-BT}$ depends on the temperature T as given in equations (3.1) and (3.2) in Section 3.1 for a duct of area Ω

$$\frac{\partial}{\partial x}(\bar{\mu} \frac{\partial w}{\partial x}) + \frac{\partial}{\partial y}(\bar{\mu} \frac{\partial w}{\partial y}) = -1 + \frac{M^2}{1 + m^2} w \quad (4.3)$$

$$\nabla^2 T + Br \bar{\mu} \left[\left(\frac{\partial w}{\partial x} \right)^2 + \left(\frac{\partial w}{\partial y} \right)^2 \right] + \frac{M^2 Br}{1 + m^2} w^2 = \frac{w}{w_m}, \quad (4.4)$$

where B , Br , m , M are the viscosity parameter, Brinkmann number, Hall parameter, Hartmann number, respectively and w_m is the volumetric flow defined as $\int_{\Omega} w d\Omega$. w and T are the flow velocity and the temperature of the fluid, respectively. No-slip velocity and cold wall conditions, i.e. $w = T = 0$ on the boundary Γ of the duct Ω are specified. A uniform magnetic field with intensity B_0 is applied with an angle to the duct perpendicular to the axis of the channel, i.e. z -axis as shown in Figure 3.1.

The MHD duct flow equation (4.3) and (4.4) are solved iteratively in terms of the velocity w of the flow and the temperature T of the fluid. The momentum equation (4.3) is solved by using both the parametrix BEM and the DRBEM. Since the diffusion term contains variable viscosity parameter depending on the temperature exponentially, the Levi function is considered as a fundamental solution, $P(x, x_i; y, y_i) =$

$\frac{1}{2\pi} \frac{1}{\bar{\mu}(x_i, y_i)} \ln|r - r_i|$ which treats the variable coefficient in the equation (4.3) directly. By weighing the momentum equation with this fundamental solution converts the momentum equation into a boundary-domain integral equation. Also, by transforming the momentum equation (4.3) into Poisson equation, the DRBEM procedure is applied with the fundamental solution of Laplace's equation, $u^* = \frac{1}{2\pi} \ln(\frac{1}{r})$. Then, the energy equation (4.4) is solved by using the DRBEM keeping all the terms containing the velocity as inhomogeneities.

The discretized boundary-domain integral equations in matrix-vector form resulted from the parametrix BEM for the solution of the velocity w , and the DRBEM for the solution of the temperature T are obtained in Chapter 3 (equations (3.7), (3.14)) as

$$\begin{aligned} \mathbf{H}\mathbf{w} - \mathbf{G}(\bar{\mu} \frac{\partial \mathbf{w}}{\partial n}) &= \mathbf{I}_1(w) - \mathbf{I}_2(w) \\ \mathbf{H}\mathbf{T} - \mathbf{G} \frac{\partial \mathbf{T}}{\partial n} &= (\mathbf{H}\hat{\mathbf{U}} - \mathbf{G}\hat{\mathbf{Q}})\mathbf{F}^{-1} \left\{ -Br\bar{\mu} \left[\left(\frac{\partial \mathbf{w}}{\partial x} \right)^2 + \left(\frac{\partial \mathbf{w}}{\partial y} \right)^2 \right] - \frac{M^2 Br}{1+m^2} \mathbf{w}^2 + \frac{\mathbf{w}}{w_m} \right\} \end{aligned} \quad (4.5)$$

where from equation (3.8)

$$I_1(w) = \int_{\Omega} w \frac{\partial \bar{\mu}}{\partial n} \frac{\partial P}{\partial n} d\Omega \quad \text{and} \quad I_2(w) = \int_{\Omega} \left(-1 + \frac{M^2}{1+m^2} w \right) P d\Omega \quad (4.6)$$

and the BEM matrices \mathbf{H} , \mathbf{G} are as defined in (3.9) and (3.15), respectively for \mathbf{w} and \mathbf{T} .

When the DRBEM is applied to both the velocity and temperature equations (4.3) and (4.4), one arrives at the matrix-vector equations (equations (3.26), (3.27))

$$\begin{aligned} \mathbf{H}\mathbf{w} - \mathbf{G} \frac{\partial \mathbf{w}}{\partial n} &= (\mathbf{H}\hat{\mathbf{U}} - \mathbf{G}\hat{\mathbf{Q}})\mathbf{F}^{-1} \left\{ \frac{1}{\bar{\mu}} \left(-1 + \frac{M^2}{1+m^2} \mathbf{w} - \frac{\partial \bar{\mu}}{\partial x} \frac{\partial \mathbf{w}}{\partial x} - \frac{\partial \bar{\mu}}{\partial y} \frac{\partial \mathbf{w}}{\partial y} \right) \right\} \\ \mathbf{H}\mathbf{T} - \mathbf{G} \frac{\partial \mathbf{T}}{\partial n} &= (\mathbf{H}\hat{\mathbf{U}} - \mathbf{G}\hat{\mathbf{Q}})\mathbf{F}^{-1} \left\{ -Br\bar{\mu} \left[\left(\frac{\partial \mathbf{w}}{\partial x} \right)^2 + \left(\frac{\partial \mathbf{w}}{\partial y} \right)^2 \right] - \frac{M^2 Br}{1+m^2} \mathbf{w}^2 + \frac{\mathbf{w}}{w_m} \right\}. \end{aligned} \quad (4.7)$$

The velocity and the temperature behaviors of the fluid obtained from the solution of the coupled equations in (4.3) and (4.4) are shown in terms of equivelocity curves and isolines in Figures 4.2-4.6. In each figure part (a) belongs to the solution using parametrix BEM-DRBEM (equation (4.5)), and part (b) shows DRBEM-DRBEM results from equation (4.7). The domain of the duct $\Omega = [0, 1] \times [0, 1]$ is discretized

by using $N = 100$ and $N = 180$ constant boundary elements, and $L = 625$ and $L = 2025$ interior nodes to obtain the solution using the parametrix BEM-DRBEM. And $N = 180$ constant boundary elements and $L = 2025$ interior nodes to obtain the solution by using the DRBEM-DRBEM.

Figure 4.2 shows the velocity and temperature behaviors as Hartmann number M is increasing for $m = 0, Br = 0, B = 1$. It is observed that as Hartmann number increases, the velocity magnitude drops, due to the damping effect of the applied magnetic field with increasing intensity, this is a well-known flattening tendency of the MHD duct flow. It is observed that as Hartmann number increases, the temperature magnitude also drops. The magnitudes of the velocity obtained from the parametrix BEM-DRBEM are slightly less than the velocity magnitudes obtained with the DRBEM-DRBEM. This may be due to the errors resulting from the computations of the domain integrals.

From Figure 4.3 and also from Figure 4.4, it is also observed that, as the viscosity parameter B is increasing, the magnitudes of the velocity and the temperature drop due to the increment in the viscosity for different Hall parameter ($m = 0, m = 3$) and Brinkmann number ($Br = 0, Br = 1$) values when Hartmann number $M = 3$. The same drop in the increase of the velocity magnitudes is observed with the parametrix BEM-DRBEM computations compared to the increase of the velocity magnitudes obtained from the DRBEM-DRBEM.

From Figure 4.5 and also from Figure 4.6 for $Br = 0$ and $Br = 1$, respectively, it is seen that when the Hall parameter m increases for fixed $M = 3, B = 1$, the damping effect of the magnetic force decreases due to the term $\sigma/(1 + m^2)$. That is, the velocity magnitude increases. It is also observed that as the Hall parameter increases, the effective conductivity decreases, which reduces the Joule dissipation. Therefore, the magnitude of the temperature also increases.

The effects of the Hall parameter m and Hartmann number M on the Nusselt number, Nu , are given on Tables 4.3, 4.4 and 4.5 where $Nu = -\frac{1}{4T_m}$ and $T_m = \frac{1}{w_m} \int_0^1 \int_0^1 wT dx dy$ for $Br = 0, B = 1$ obtained from the parametrix BEM-DRBEM and the DRBEM-DRBEM procedures, respectively. It is observed that as

Hartmann number increases, the values of Nusselt number are increasing since the values of the temperature decrease. However, as the Hall parameter is increasing, the values of Nusselt number are decreasing since the temperature increases. But, it can be seen that, the effect of Hall parameter on the Nusselt number may be neglected for small values of Hartmann number ($M < 2$).

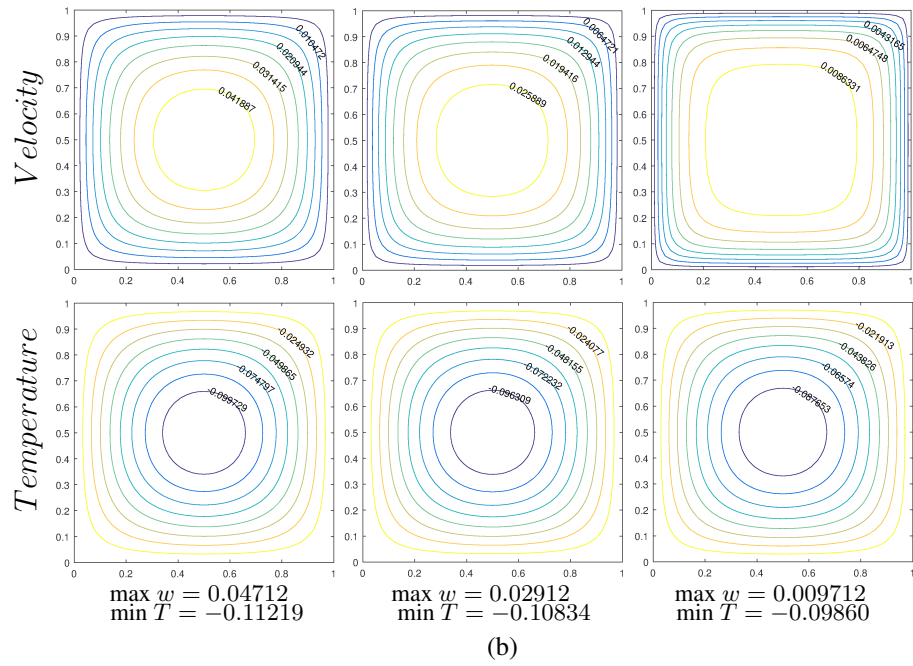
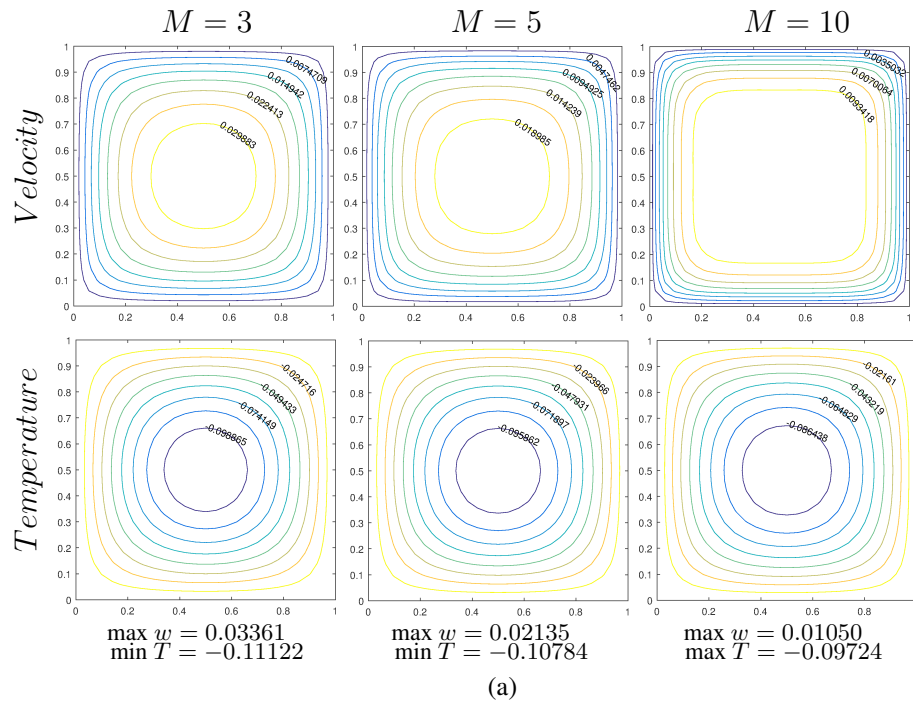


Figure 4.2: Equavelocity and isolines for $m = 0$, $Br = 0$ and $B = 1$. (a) pBEM-DRBEM, (b) DRBEM-DRBEM

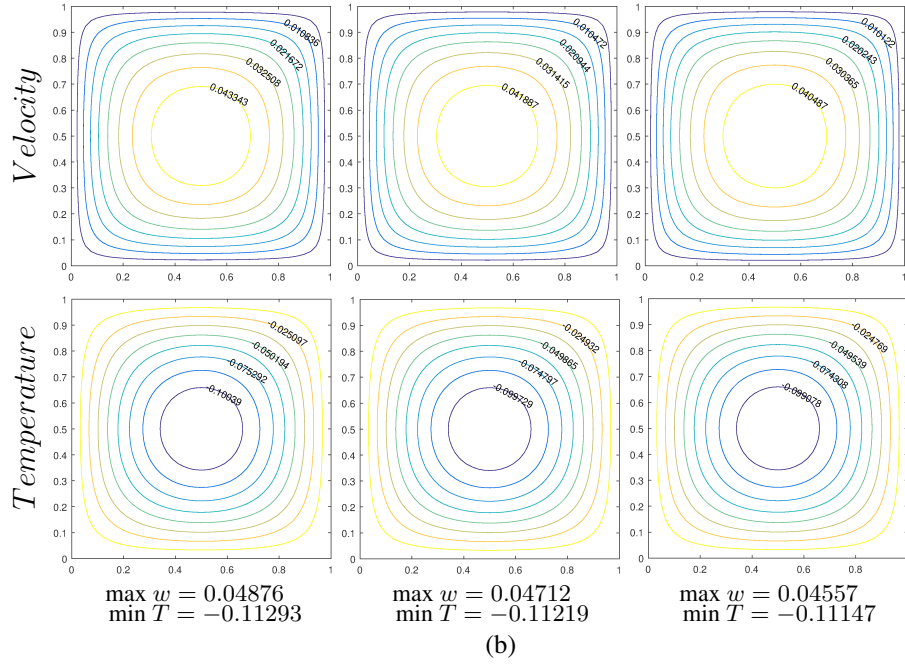
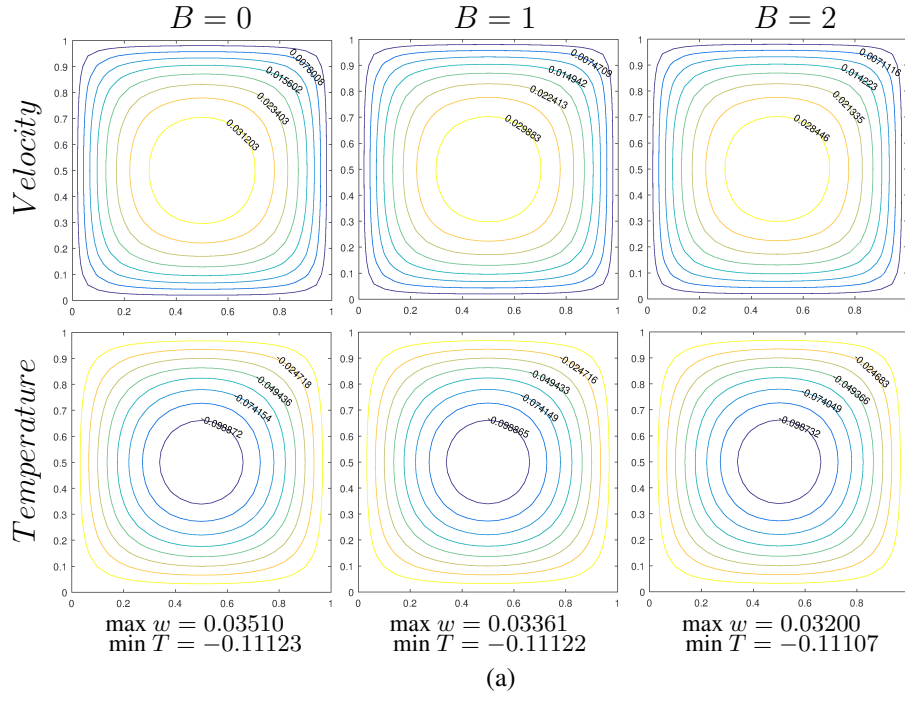


Figure 4.3: Equavelocity and isolines for $M = 3$, $m = 0$ and $Br = 0$. (a) pBEM-DRBEM, (b) DRBEM-DRBEM

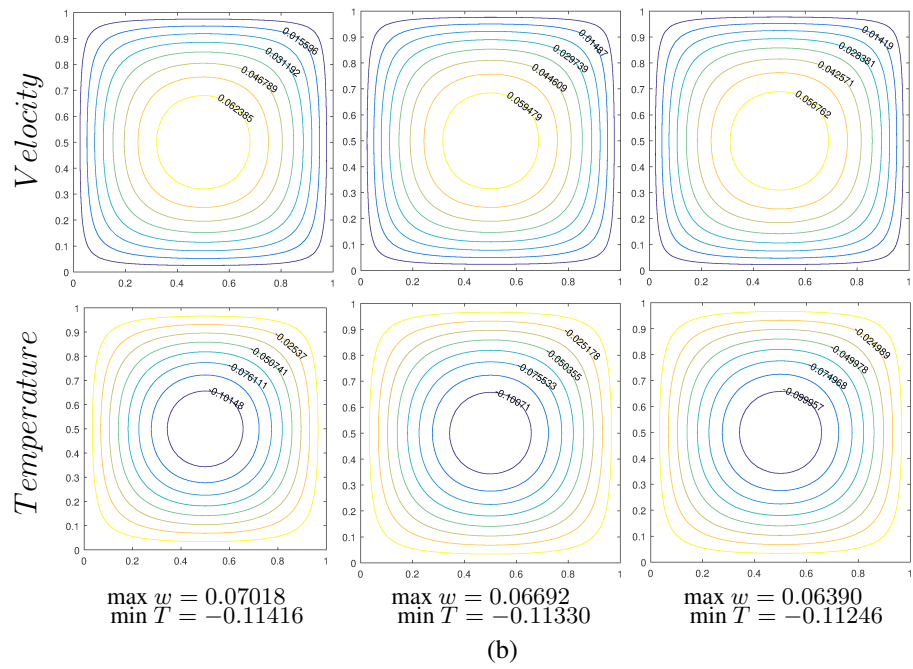
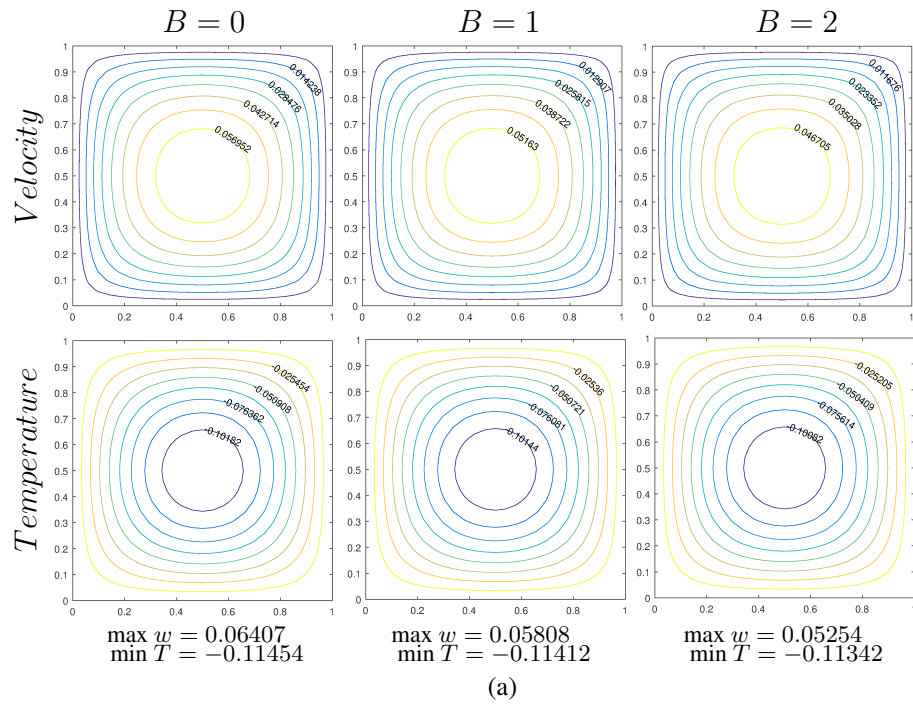


Figure 4.4: Equavelocity and isolines for $M = 3$, $m = 3$ and $Br = 1$. (a) pBEM-DRBEM, (b) DRBEM-DRBEM

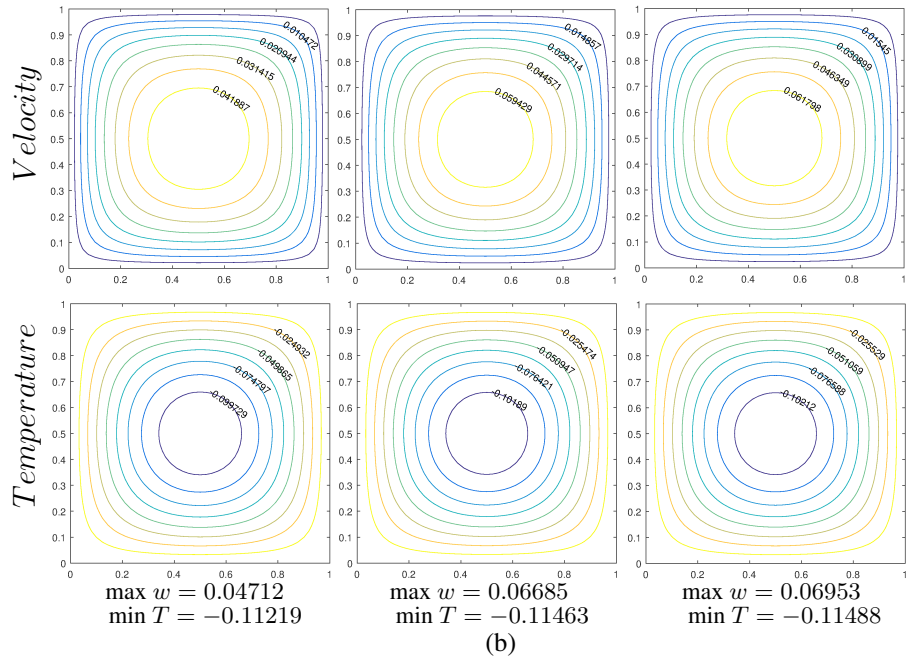
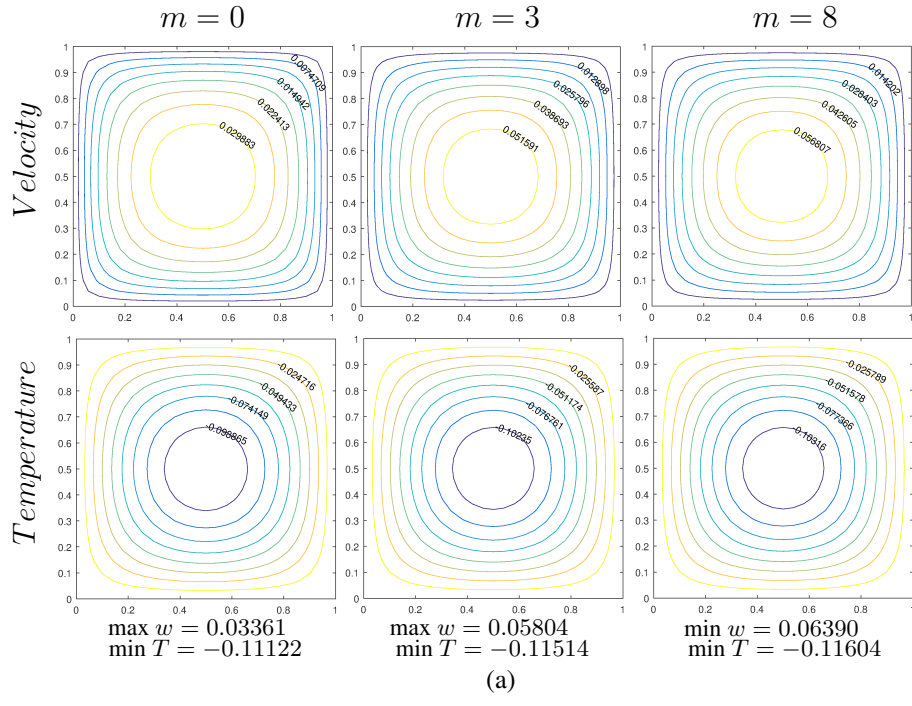


Figure 4.5: Equavelocity and isolines for $M = 3$, $Br = 0$ and $B = 1$. (a) pBEM-DRBEM, (b) DRBEM-DRBEM

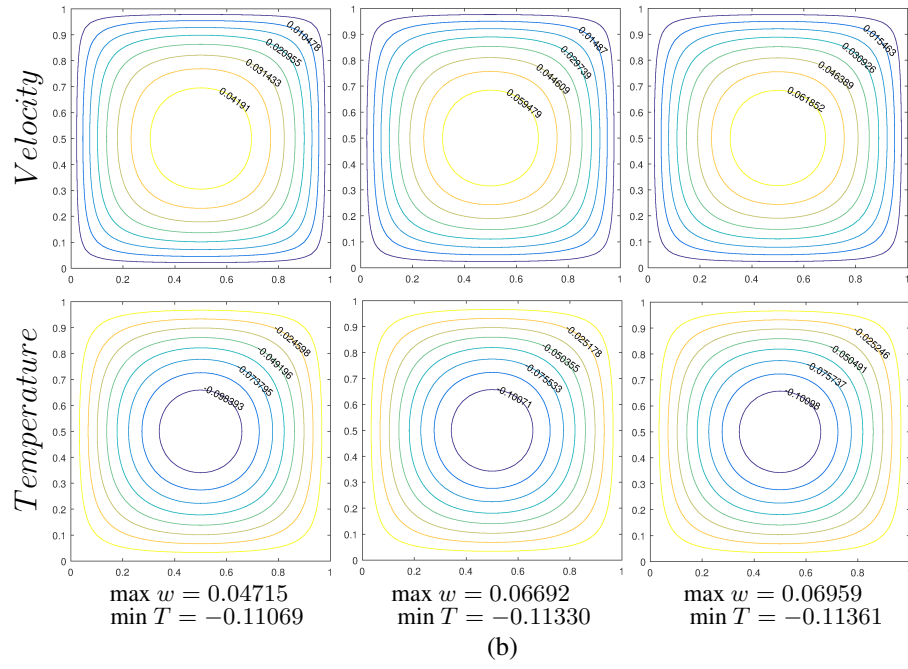
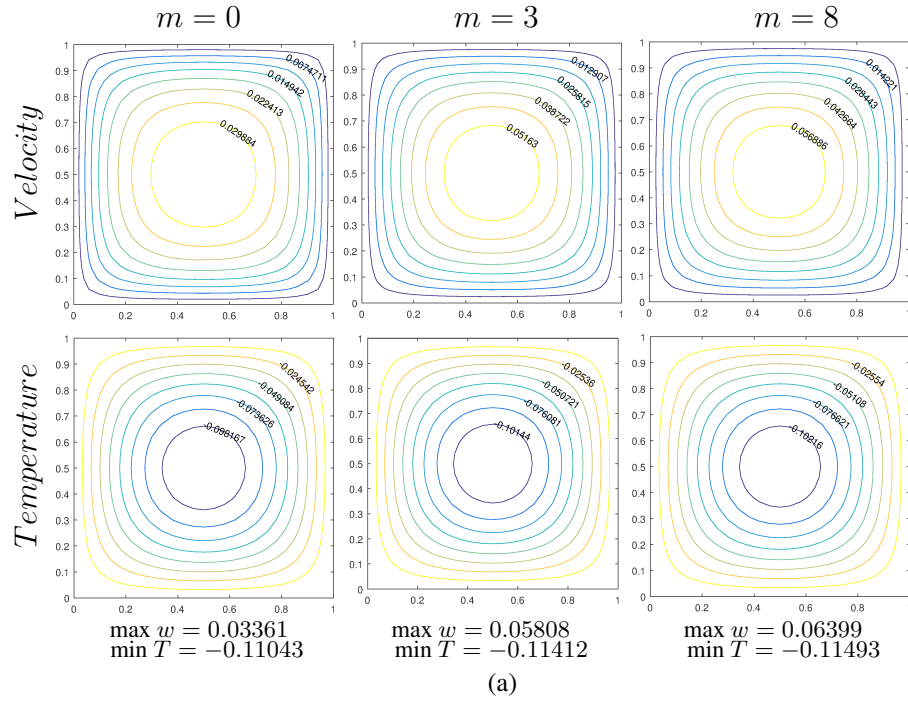


Figure 4.6: Equavelocity and isolines for $M = 3$, $Br = 1$ and $B = 1$. (a) pBEM-DRBEM, (b) DRBEM-DRBEM

Table 4.3: Nusselt number, Nu , by using the pBEM-DRBEM with 100 boundary elements ($Br = 0$, $B = 1$).

m	M	0.0	1.0	2.0	3.0	4.0	5.0
0.0		3.5662	3.6113	3.7533	3.7772	3.8586	3.9340
3.0		3.5662	3.5711	3.5896	3.6082	3.6247	3.6774
5.0		3.5662	3.5680	3.5738	3.5873	3.5981	3.6101
8.0		3.5662	3.5669	3.5692	3.5730	3.5830	3.5889

Table 4.4: Nusselt number, Nu , by using the pBEM-DRBEM with 180 boundary elements ($Br = 0$, $B = 1$).

m	M	0.0	1.0	2.0	3.0	4.0	5.0
0.0		3.6125	3.6595	3.8099	3.8342	3.9202	4.0000
3.0		3.6125	3.6176	3.6368	3.6563	3.6735	3.7294
5.0		3.6125	3.6144	3.6204	3.6344	3.6458	3.6583
8.0		3.6125	3.6132	3.6156	3.6196	3.6299	3.6361

Table 4.5: Nusselt number, Nu , by using the DRBEM-DRBEM with 180 boundary elements ($Br = 0$, $B = 1$).

m	M	0.0	1.0	2.0	3.0	4.0	5.0
0.0		3.6276	3.6417	3.6825	3.7467	3.8294	3.9250
3.0		3.6276	3.6290	3.6333	3.6403	3.6500	3.6623
5.0		3.6276	3.6282	3.6298	3.6325	3.6363	3.6411
8.0		3.6276	3.6278	3.6285	3.6296	3.6311	3.6330

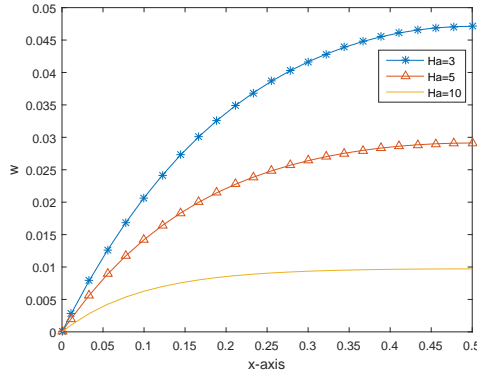
The solutions obtained by the parametrix BEM-DRBEM and the DRBEM-DRBEM in terms of w_{max} and T_{min} slightly differ (still with almost 10^{-2} accuracy) in the values, they all catch the same behaviour of the velocity and the temperature of the MHD duct flow. When the number of boundary elements is increased from 100 to 180, Nus-

selt numbers are computed more accurately than DRBEM-DRBEM when FEM results [30] are taken as a basis. As the number of boundary elements is increased from 100 to 180 in parametric BEM-DRBEM procedure, the Nusselt numbers are close with almost 10^{-2} accuracy as shown in Tables 4.3-4.5 and in agreement with FEM results given in [30]. However, when the Hall parameter is zero, $m = 0$, a relaxation parameter is needed in using parametric BEM since parametric BEM has to compute domain integrals. This is why it takes more CPU time compared to DRBEM-DRBEM procedure. Thus, the Table 4.6 shows that, solving this MHD flow problem with temperature dependent viscosity by using the DRBEM-DRBEM is more time saving than solving with the parametric BEM-DRBEM formulation due to the domain integrals computations. For this reason the DRBEM-DRBEM is preferable for solving this MHD flow problem.

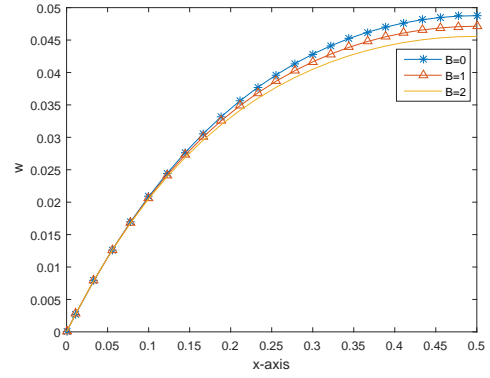
Table 4.6: CPU Times with 180 boundary elements ($Br = 0$, $B = 1$).

m	pBEM-DRBEM				DRBEM-DRBEM		
	M	3.0	5.0	10.0	3.0	5.0	10.0
0.0		139.2711	69.8268	21.2650	13.3409	13.4086	13.3453
3.0		21.7195	28.3811	132.2293	13.4548	13.3198	13.3639
5.0		21.4600	21.6551	42.2826	13.4389	13.3265	13.1714
8.0		14.6996	21.3188	21.5575	13.3785	13.2181	13.2437

Figures 4.7 and 4.8 show the velocity profiles along the midline of the rectangular duct obtained by using the DRBEM-DRBEM for increasing Hartmann number and viscosity parameter, and Brinkmann number and Hall parameter, respectively. It can be seen from Figure 4.7 (a), as Hartmann number increases, the velocity magnitude drops for fixed values of the Hall parameter, Brinkman number and viscosity parameter. From Figure 4.7 (b) it is observed that, as the viscosity parameter is increasing, the magnitude of the velocity drops for fixed values of Hartmann number, Hall parameter and Brinkman number. Also, it can be seen from Figure 4.8 (a) and 4.8 (b) that, as the Hall parameter increases, the flow magnitude also increases for Hartmann number $M = 3$, viscosity parameter $B = 1$ and Brinkman number values ($Br = 0$, $Br = 1$) taken as in the references [15] and [30].

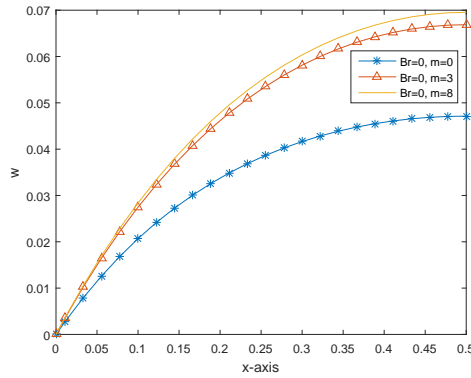


(a) $m = 0$, $Br = 0$ and $B = 1$.

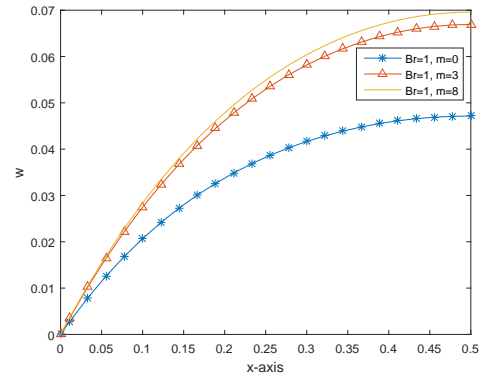


(b) $M = 3$, $m = 0$ and $Br = 0$.

Figure 4.7: Midline velocity profiles at $y = 0.5$ using DRBEM-DRBEM.



(a) $Br = 0$, $B = 1$ and $M = 3$.

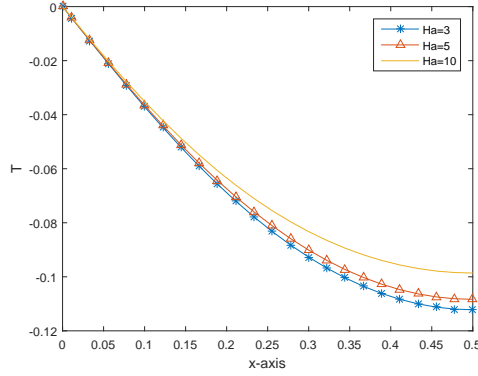


(b) $Br = 1$, $B = 1$ and $M = 3$.

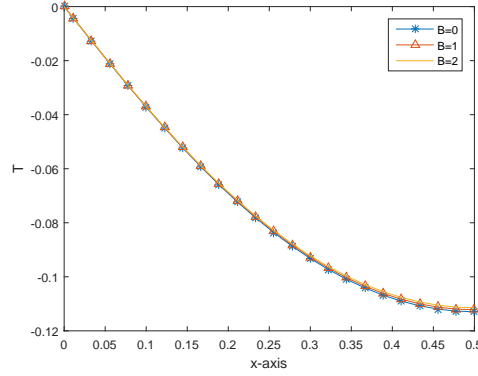
Figure 4.8: Midline velocity profiles at $y = 0.5$ using DRBEM-DRBEM.

Figure 4.9 shows the temperature profiles along the midline of the rectangular duct obtained by using the DRBEM-DRBEM for increasing Hartmann number and viscosity parameter, respectively. It can be seen from Figure 4.9 (a), as Hartmann number increases the temperature magnitude drops for fixed values of the Hall parameter, Brinkman number and viscosity parameter. This is why the terms which are multiplied by these parameters form the force term in the diffusion equation for the temperature. The effect of viscosity parameter is almost negligible in the magnitude of the temperature for fixed values of Hartmann number, Hall parameter and Brinkman

number as can be seen from Figure 4.9 (b).



(a) $m = 0$, $Br = 0$ and $B = 1$.



(b) $M = 3$, $m = 0$ and $Br = 0$.

Figure 4.9: Midline temperature profiles at $y = 0.5$ using DRBEM-DRBEM.

Finally, Figures 4.10-4.12 show the midline velocity profiles obtained from both the parametrix BEM-DRBEM and the DRBEM-DRBEM approaches for increasing viscosity parameter, Hartmann number and Hall parameter, respectively. Temperature profiles for increasing Hartmann number along the midline of the rectangular duct is shown in Figure 4.13. Although, the velocity magnitudes obtained by the parametrix BEM-DRBEM procedure is less than the velocity magnitudes from the DRBEM-DRBEM procedure, the velocity profiles show the same flattening tendency behavior of the MHD duct flow. From Figure 4.10 it is seen that, as the viscosity parameter increases, this difference between the velocity magnitudes increases due to the increment in the viscosity term $\bar{\mu} = e^{-BT}$. We can also see from Figure 4.11 that, as Hartmann number increases, the difference between the velocity magnitudes obtained from the parametrix BEM-DRBEM and the DRBEM-DRBEM increases due to the increment in the nonlinear term $\frac{M^2}{1+m^2}w$, and from Figure 4.12 when the Hall parameter is increasing, the effect of the nonlinear term decreases and so the difference between the velocity magnitudes obtained from both procedures decreases. It is expected that, the difference in the velocity magnitudes obtained from both methods results due to the extra domain integral computations in the parametrix BEM procedure. The computations of the domain integrals in parametrix BEM must be numerical, and the composite trapezoidal rule has been used. They cause at least

computational and round-off errors. This may be responsible for the discrepancies in parametrix BEM-DRBEM and DRBEM-DRBEM velocity values near the maximum. The increase of the number of constant elements, N , from 100 to 180 does not further reduce this discrepancy in the velocity values. However, from Figure 4.13, it can be seen that, the coincidence of the two methods, the parametrix BEM and the DRBEM is very well in terms of midline temperature values.

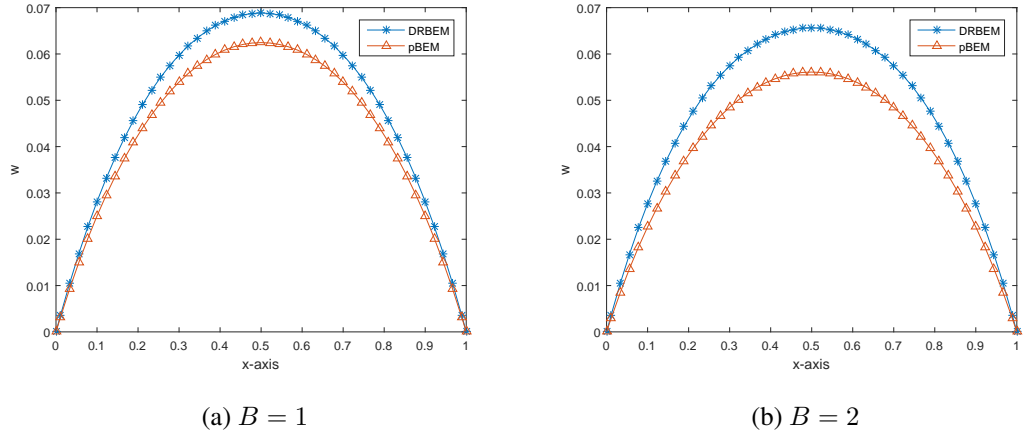


Figure 4.10: Midline velocity profiles at $y = 0.5$, and $M = 3$, $m = 5$ and $Br = 1$

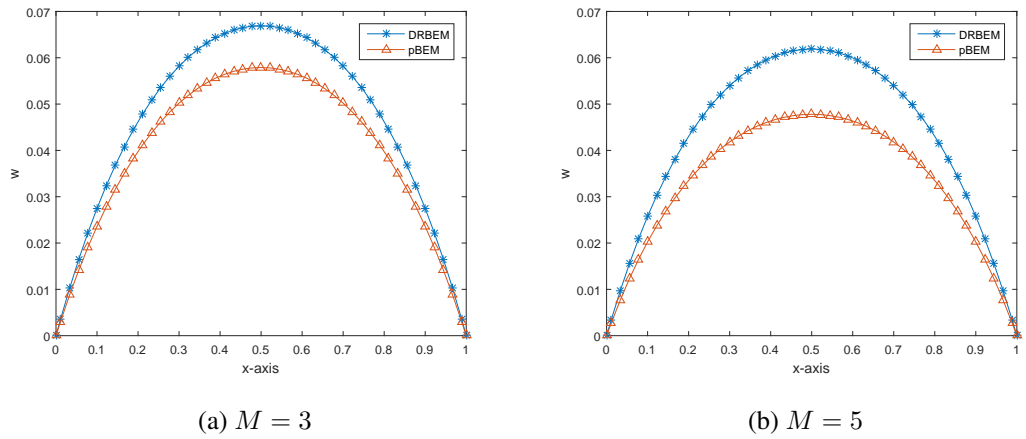
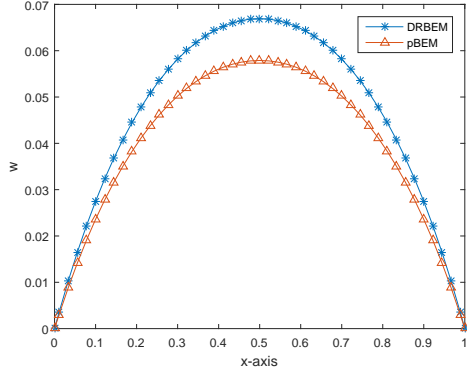
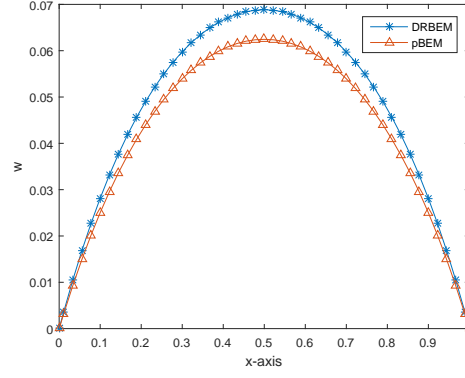


Figure 4.11: Midline velocity profiles at $y = 0.5$, and $Br = 1$, $B = 1$, $m = 3$.

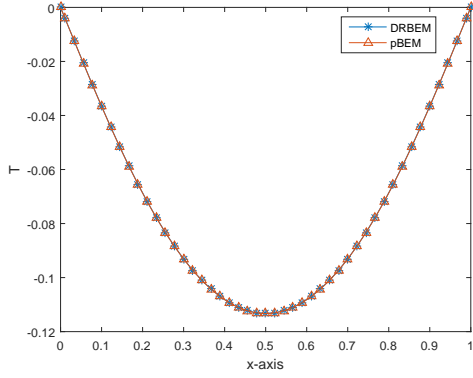


(a) $m = 3$

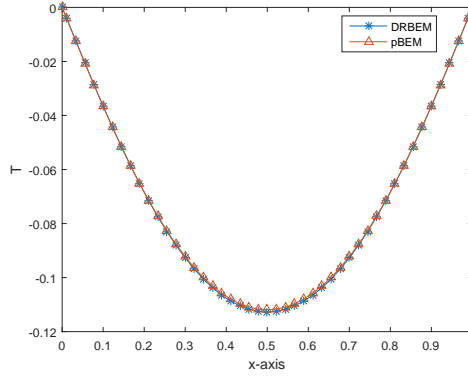


(b) $m = 5$

Figure 4.12: Midline velocity profiles at $y = 0.5$, and $Br = 1$, $B = 1$, $M = 3$.



(a) $M = 3$



(b) $M = 5$

Figure 4.13: Midline temperature profiles at $y = 0.5$, and $Br = 1$, $B = 1$, $m = 3$.

4.2 MHD duct flow with time-varied external magnetic field

In this section, the transient behavior of the MHD flow of a viscous, incompressible and electrically conducting fluid in a long pipe of rectangular cross-section (duct) is considered. The fully developed flow through the pipe is affected by a time-varied oblique magnetic field $B_0(t) = B_0 f(t)$ where B_0 is the intensity of the applied magnetic field at the initial time level, i.e. $t = 0$, and $f(t)$ is a time varied function. The governing non-dimensional flow and induced magnetic field equations are derived in

Chapter 1 (equations (1.61)-(1.62)) and also given in Section 3.2 (equation (3.35)) as

$$\begin{aligned}\nabla^2 V + \overline{M}_x \frac{\partial B}{\partial x} + \overline{M}_y \frac{\partial B}{\partial y} &= -1 + R_e \frac{\partial V}{\partial t} \\ \nabla^2 B + \overline{M}_x \frac{\partial V}{\partial x} + \overline{M}_y \frac{\partial V}{\partial y} &= R_m \frac{\partial B}{\partial t}\end{aligned}\quad (4.8)$$

in $\Omega \times [0, \infty)$ where $\Omega = \{(x, y) \in \mathbb{R}^2 : -1 \leq x, y \leq 1\}$. $\overline{M}_x = Mf(t)\sin\alpha$, $\overline{M}_y = Mf(t)\cos\alpha$, M is the Hartmann number and α is the angle between the applied magnetic field and the y -axis. R_e and R_m denote the Reynolds number and magnetic Reynolds number, respectively and given in (equations (1.53)-(1.54)). $V(x, y, t)$ and $B(x, y, t)$ are only the velocity and induced magnetic field components in the pipe-axis direction.

The boundary of the duct is considered as insulated and with no-slip velocity

$$V(x, y, t) = 0 \quad B(x, y, t) = 0 \quad (x, y) \in \Gamma, \quad t > 0 \quad (4.9)$$

where initial values of the velocity and induced magnetic field taken as zero

$$V(x, y, 0) = 0 \quad B(x, y, 0) = 0 \quad (x, y) \in \Omega. \quad (4.10)$$

4.2.1 $R_e = 1, R_m = 1$ case

Firstly, we consider the MHD duct flow problem by taking the Reynolds and magnetic Reynolds numbers as one which reduces equations (4.8) to

$$\begin{aligned}\nabla^2 V + \overline{M}_x \frac{\partial B}{\partial x} + \overline{M}_y \frac{\partial B}{\partial y} &= -1 + \frac{\partial V}{\partial t} \\ \nabla^2 B + \overline{M}_x \frac{\partial V}{\partial x} + \overline{M}_y \frac{\partial V}{\partial y} &= \frac{\partial B}{\partial t}\end{aligned}\quad (4.11)$$

where $(x, y, t) \in \Omega \times [0, \infty)$ and, the boundary and initial conditions are the same as given in (4.9) and (4.10), respectively.

Now, by using the change of variables $U_1 = V + B$ and $U_2 = V - B$, the coupled velocity and induced magnetic field equations in (4.11) are converted into decoupled equations (decoupling procedure is given in Section 3.2)

$$\begin{aligned}\nabla^2 U_1 + \overline{M}_x \frac{\partial U_1}{\partial x} + \overline{M}_y \frac{\partial U_1}{\partial y} &= -1 + \frac{\partial U_1}{\partial t} \\ \nabla^2 U_2 - \overline{M}_x \frac{\partial U_2}{\partial x} - \overline{M}_y \frac{\partial U_2}{\partial y} &= -1 + \frac{\partial U_2}{\partial t}\end{aligned}\quad (4.12)$$

with the following boundary and initial conditions

$$\begin{aligned} U_1(x, y, t) = 0 \quad U_2(x, y, t) = 0 \quad (x, y) \in \Gamma \\ U_1(x, y, 0) = 0 \quad U_2(x, y, 0) = 0 \quad (x, y) \in \Omega. \end{aligned} \quad (4.13)$$

The discretized matrix-vector equations obtained from the DRBEM application to the decoupled equations (4.12) are as given in equation (3.41)

$$\begin{aligned} \mathbf{H}U_1 - \mathbf{G}\frac{\partial U_1}{\partial n} &= (\mathbf{H}\hat{\mathbf{U}} - \mathbf{G}\hat{\mathbf{Q}})\mathbf{F}^{-1}\left\{-1 + \frac{\partial U_1}{\partial t} - \bar{M}_x \frac{\partial U_1}{\partial x} - \bar{M}_y \frac{\partial U_1}{\partial y}\right\} \\ \mathbf{H}U_2 - \mathbf{G}\frac{\partial U_2}{\partial n} &= (\mathbf{H}\hat{\mathbf{U}} - \mathbf{G}\hat{\mathbf{Q}})\mathbf{F}^{-1}\left\{-1 + \frac{\partial U_2}{\partial t} + \bar{M}_x \frac{\partial U_2}{\partial x} + \bar{M}_y \frac{\partial U_2}{\partial y}\right\}. \end{aligned} \quad (4.14)$$

Rearrangement of the above equations for increasing time levels results in

$$\begin{aligned} (\mathbf{A}_1 - \frac{1}{\Delta t})U_1^{n+1} - \mathbf{G}_1 \frac{\partial U_1^{n+1}}{\partial n} &= \{-1 - \frac{U_1^n}{\Delta t}\} \\ (\mathbf{A}_2 - \frac{1}{\Delta t})U_2^{n+1} - \mathbf{G}_2 \frac{\partial U_2^{n+1}}{\partial n} &= \{-1 - \frac{U_2^n}{\Delta t}\} \end{aligned} \quad (4.15)$$

where

$$\begin{aligned} \mathbf{A}_1 &= \mathbf{C}(\mathbf{H} + (\mathbf{H}\hat{\mathbf{U}} - \mathbf{G}\hat{\mathbf{Q}})\mathbf{F}^{-1}(\bar{M}_x \frac{\partial \mathbf{F}}{\partial x} \mathbf{F}^{-1} + \bar{M}_y \frac{\partial \mathbf{F}}{\partial y} \mathbf{F}^{-1})), \quad \mathbf{G}_1 = \mathbf{C}\mathbf{G} \\ \mathbf{A}_2 &= \mathbf{C}(\mathbf{H} - (\mathbf{H}\hat{\mathbf{U}} - \mathbf{G}\hat{\mathbf{Q}})\mathbf{F}^{-1}(\bar{M}_x \frac{\partial \mathbf{F}}{\partial x} \mathbf{F}^{-1} + \bar{M}_y \frac{\partial \mathbf{F}}{\partial y} \mathbf{F}^{-1})), \quad \mathbf{G}_2 = \mathbf{C}\mathbf{G} \end{aligned} \quad (4.16)$$

and $\mathbf{C} = ((\mathbf{H}\hat{\mathbf{U}} - \mathbf{G}\hat{\mathbf{Q}})\mathbf{F}^{-1})^{-1}$.

The decoupled equations (4.15) are solved in terms of U_1 and U_2 iteratively with a tolerance 10^{-3} as $\max_i |U_{1,i}^{n+1} - U_{1,i}^n| < 10^{-3}$ and $\max_i |U_{2,i}^{n+1} - U_{2,i}^n| < 10^{-3}$ for a time level t_n , $i = 1, \dots, N + L$. Then, the velocity V and the induced magnetic field B values are obtained using $V = \frac{U_1 + U_2}{2}$, $B = \frac{U_1 - U_2}{2}$ at transient time levels using several definitions of $f(t)$ as polynomial, exponential, trigonometric, impulse and step functions. Hartmann number values $M = 20, 50$ and the time step $\Delta t = 0.01$ are taken. This solution procedure is given in details in Section 3.2.

The cross-section of the pipe (duct), $\Omega = [-1, 1] \times [-1, 1]$ is discretized by using $N = 100, 120, 140, 160, 200$ and 300 boundary elements and $L = 625, 900, 1225, 1600, 2500$ and 5625 interior nodes. The number of boundary elements are increased for increasing Hartmann number values, and for simulating the impulse and step function behavior of induced magnetic field. The steady-state is defined for the solution of equations in (4.14) with a tolerance as given above. This tolerance is satisfied periodically at

several time levels for the solution of equations in (4.14) for trigonometric function $f(t)$. That is, the flow repeats its behavior change with a so called period. Pipe-axis velocity and the induced magnetic field are simulated at the time levels where the effect of the time-dependent applied magnetic field (i.e. $f(t)$) starts to change the flow behavior, and also the time level where the flow stabilizes which is so called the steady-state.

The proposed method is validated first for the case of horizontally applied uniform, constant magnetic field in Figure 4.14 by comparing our steady-state solution with the steady solution obtained by differential quadrature method [67]. The agreement is very well. Steady-state is taken with tolerance of 10^{-4} and 10^{-6} which occurs at $t_n = 0.20$ and $t_n = 0.30$, respectively.

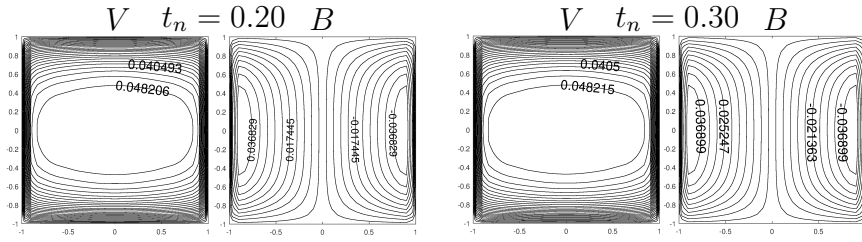


Figure 4.14: Velocity and induced magnetic field lines, $f(t) = 1$, $B_0(t) = B_0$, $M = 20$, $N = 120$, $\alpha = \pi/2$.

The effects of the time step Δt and the number of boundary elements N on the accuracy and numerical stability of the solution are also investigated in Figures 4.15 and 4.16, respectively. Since the time integration method is an explicit forward difference (Euler) method, one needs to take small Δt . From Figure 4.15 we see that at least $\Delta t = 0.01$ must be taken to capture the beginning of the flow elongation at the correct time level $t_n \approx 0.10$. Thus, the rest of the computations are carried with $\Delta t = 0.01$ on account of CPU times required since smaller Δt 's need more iterations.

One can notice from Figure 4.16 that as N increases the behavior of V and B are settled down and smoothed. Thus, we use $N = 120$ giving accurate enough results with less CPU time compared to $N = 140, 160$.

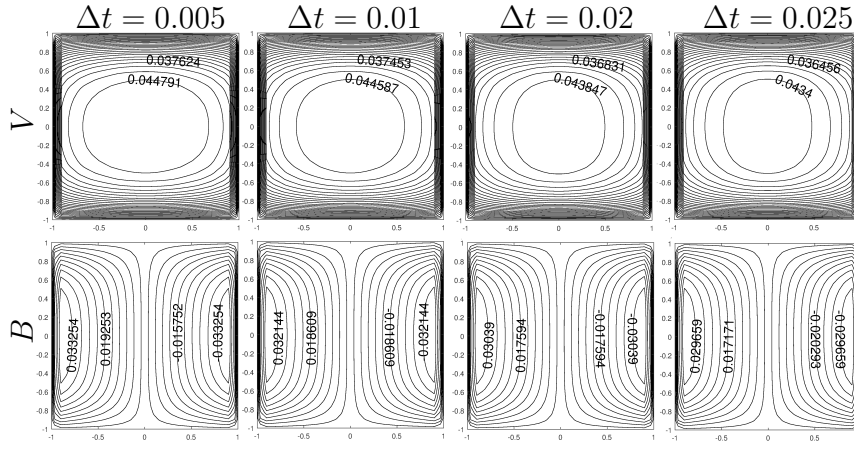


Figure 4.15: Velocity and induced magnetic field lines, $f(t) = 1 + t$, $M = 20$, $\alpha = \pi/2$, $t_n = 0.10$.

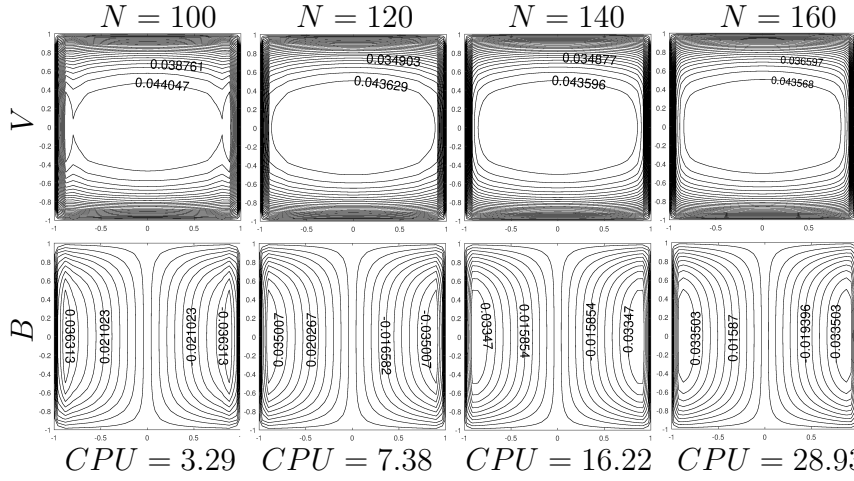


Figure 4.16: Velocity and induced magnetic field lines, $f(t) = 1 + t$, $M = 20$, $\alpha = \pi/2$, $t_n = 0.14$.

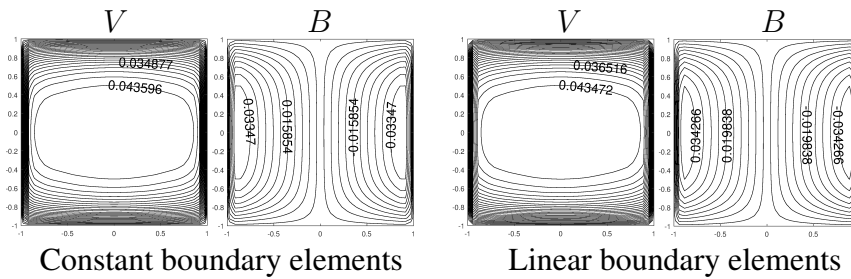


Figure 4.17: Velocity and induced magnetic field lines, $f(t) = 1 + t$, $M = 20$, $\alpha = \pi/2$, $t_n = 0.14$, $\Delta t = 0.01$ and $N = 140$.

The linear boundary element approximation is also used for comparison with the constant element approximation in terms of the accuracy of the solution. The velocity and induced magnetic field behaviors and magnitudes are the same with 10^{-3} accuracy for steady-state with $N = 140$ boundary elements as shown in Figure 4.17. Thus, the rest of the computations are carried by using constant boundary element discretization.

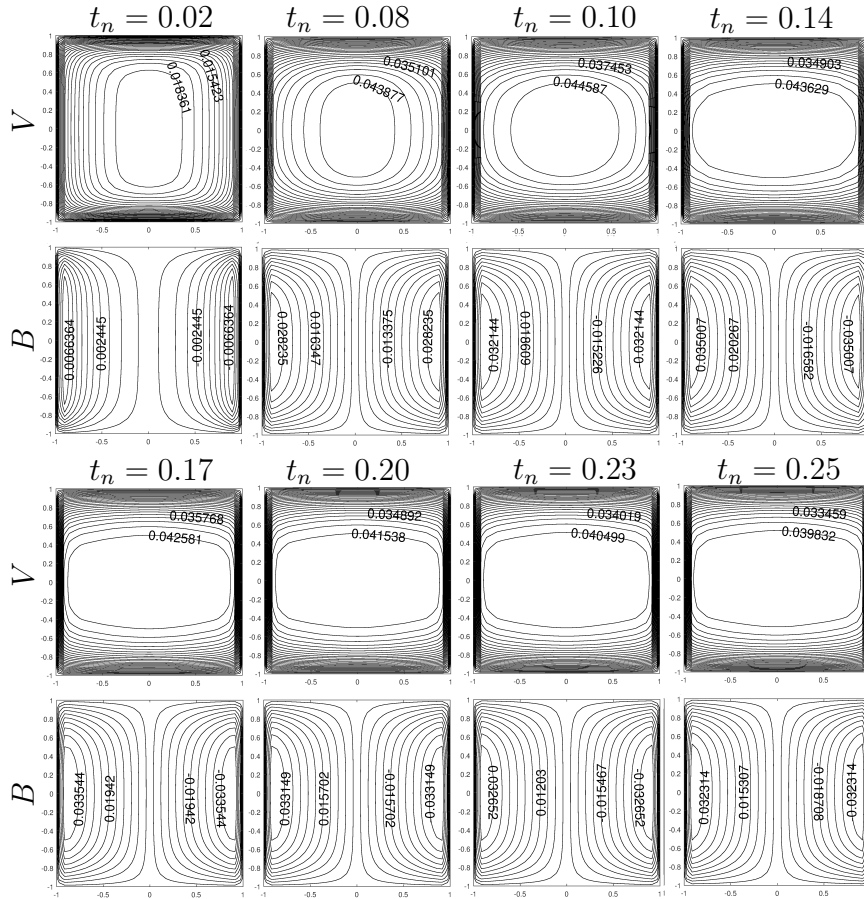


Figure 4.18: Velocity and induced magnetic field lines, $f(t) = 1 + t$, $M = 20$, $\alpha = \pi/2$.

Figure 4.18 shows the velocity and induced magnetic field behaviors when the external magnetic field varies linearly in time ($f(t) = 1 + t$) and applied with an angle $\alpha = \pi/2$ with the y -axis. The boundary is discretized by using $N = 120$ constant boundary elements, and $L = 900$ interior nodes are used. It is observed that, the flow is symmetrically distributed in the duct having a central vortex and obeying the thick-

ness of Hartmann and side layers $O(\frac{1}{M})$ and $O(\frac{1}{\sqrt{M}})$, respectively. Then, the flow shows an elliptical elongation in the direction of applied magnetic field. The thickness of Hartmann layer decreases while side layer becomes thicker. It is seen that as time t passes, the induced magnetic field magnitude increases continuously up to the time level $t_n = 0.14$ and then starts to decrease. However, the velocity magnitude increases up to a certain time level (e.g. $t_n = 0.10$) where elongation starts to occur and then slowly decreases. The so called steady-state is achieved at $t_n = 0.14$. At further time levels the behaviors of V and B stay the same with slightly decreasing magnitudes. This is an expected behavior since the coefficients of convection terms contain $f(t)$ which increases with an increase in t .

In Figures 4.19 and 4.20, the velocity and induced magnetic field are simulated for $f(t) = 1 + t$ at transient levels with an oblique applied magnetic field taking $\alpha = \pi/3$ and $\alpha = \pi/4$, respectively, for the same Hartmann number $M = 20$. The elongation of the flow starts at an earlier time level (i.e. $t_n = 0.06$) with an oblique external magnetic field compared to horizontally applied magnetic field ($\alpha = \pi/2$) aligning always in the direction of applied magnetic field, and stabilizes at again $t_n = 0.14$. Also, as a common feature for polynomial-type $f(t)$, the velocity and induced magnetic field magnitudes increase up to the flow elongation time level and then slightly decrease. The Hartmann layers are symmetrically located through the left bottom and right upper corners. Side layers are enlarged in front of the left upper and right bottom corners. The current lines also align in the direction of applied magnetic field in terms of two loops.

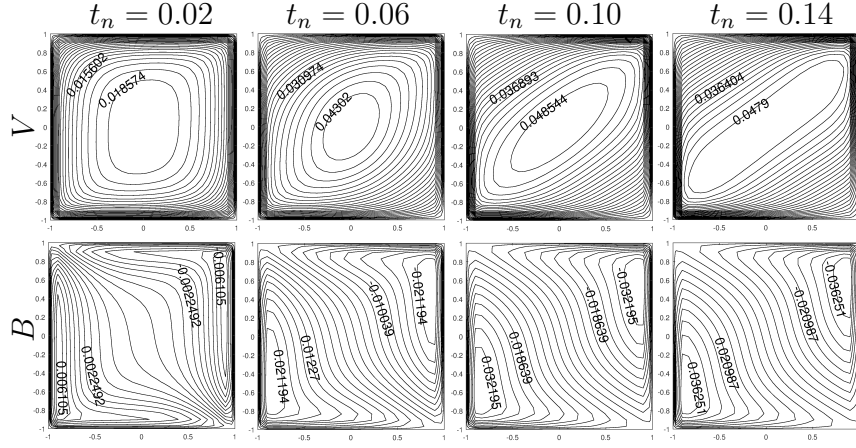


Figure 4.19: Velocity and induced magnetic field lines, $f(t) = 1 + t$, $M = 20$, $\alpha = \pi/3$.

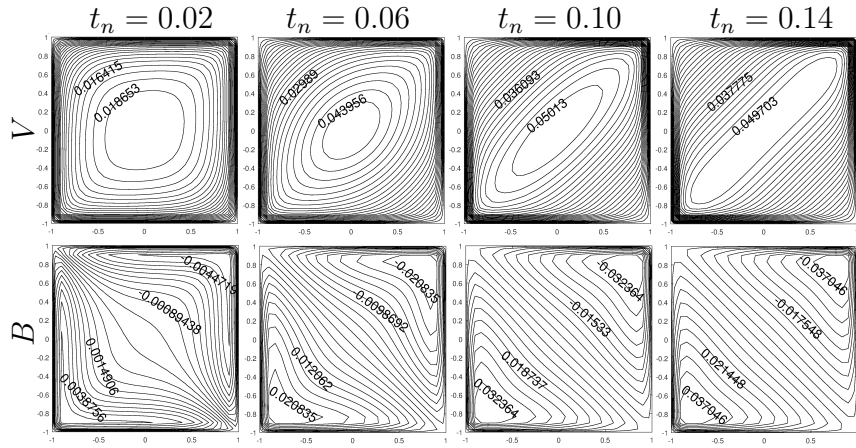


Figure 4.20: Velocity and induced magnetic field lines, $f(t) = 1 + t$, $M = 20$, $\alpha = \pi/4$.

Then, Figure 4.21 shows the effect of increased Hartmann number ($M = 50$) on the velocity and induced magnetic field at transient levels for $f(t) = 1 + t$ again. In this case, $N = 300$ constant boundary elements and $L = 5625$ interior nodes are used for the discretization of the duct and $\alpha = \pi/2$ is taken. It is seen that, when Hartmann number is increased (e.g. the strength B_0 of the applied magnetic field is increased) the elliptical elongation of the flow in the direction of applied magnetic field starts at an earlier time level, as can be seen comparing Figure 4.21 with Figure 4.18. Then,

the flow is flattened with thin Hartmann layers and side layers are enlarged. In this case, the velocity magnitude increases up to the time level (e.g. $t_n = 0.06$), and then decrease because of the increase in the strength of the applied magnetic field. The induced magnetic field magnitude shows the same behavior as in the small Hartmann number.

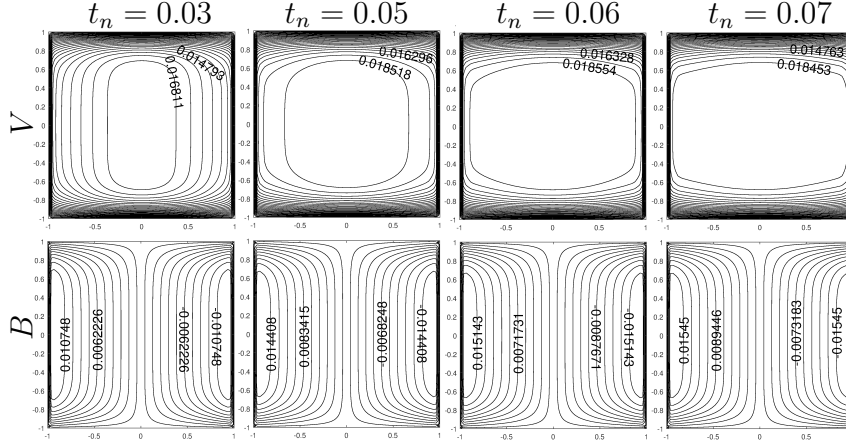


Figure 4.21: Velocity and induced magnetic field lines, $f(t) = 1 + t$, $M = 50$, $\alpha = \pi/2$.

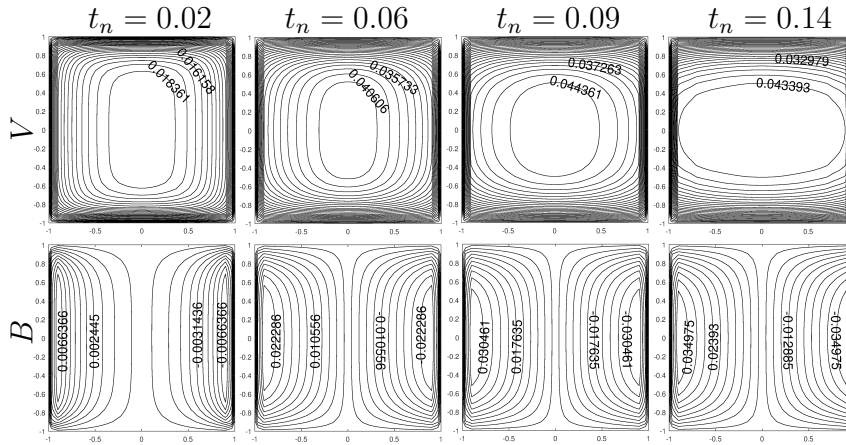


Figure 4.22: Velocity and induced magnetic field lines, $f(t) = e^t$, $M = 20$, $\alpha = \pi/2$.

Figure 4.22 depicts the velocity and induced magnetic field behaviors at transient levels for exponentially increasing applied magnetic field in time by taking $f(t) = e^t$. $N = 120$ constant boundary elements and $L = 900$ interior nodes are taken since

Hartmann number M is again 20. The magnetic field is applied horizontally ($\alpha = \pi/2$). Behavior change in the flow is similar to the case of linear $f(t)$ starting to elongate around $t_n = 0.09$ and stabilizing around $t_n = 0.14$, respectively. Again, as time increases, the velocity and induced magnetic field magnitudes increase up to the time level that nearly the flow elongates and then starts to decrease slightly. This can also be seen in terms of volumetric flow rates $Q = \int_{\Omega} V d\Omega$ in Table 4.7 which decreases slightly when the flow elongation time level is passed.

Table 4.7: The volumetric flow rate Q , $f(t) = e^t$, $M = 20$, $N = 120$, $\alpha = \pi/2$.

t_n	0.02	0.06	0.09	0.14	0.20	0.25	0.30
Q	0.0562	0.1190	0.1361	0.1390	0.1328	0.1272	0.1217

Then, Hartmann number is increased to $M = 50$ for $f(t) = e^t$. In this case, $N = 300$ boundary nodes and $L = 5625$ interior nodes are needed again for the discretization of the duct and $\alpha = \pi/2$ is taken. It is seen that, when Hartmann number is increased similar to the linear $f(t) = 1 + t$ case, the elliptical elongation of the flow in the direction of applied magnetic field starts at much earlier time level ($t_n = 0.06$) as can be seen in Figures 4.22 and 4.23. Flattening of the flow and formation of boundary layers are observed when M is increased from 20 to 50 which is the well-known behavior of MHD flow.

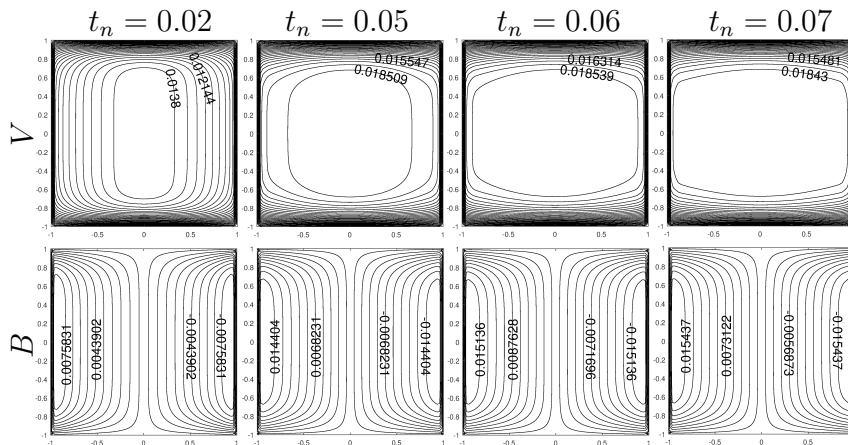


Figure 4.23: Velocity and induced magnetic field lines, $f(t) = e^t$, $M = 50$, $\alpha = \pi/2$.

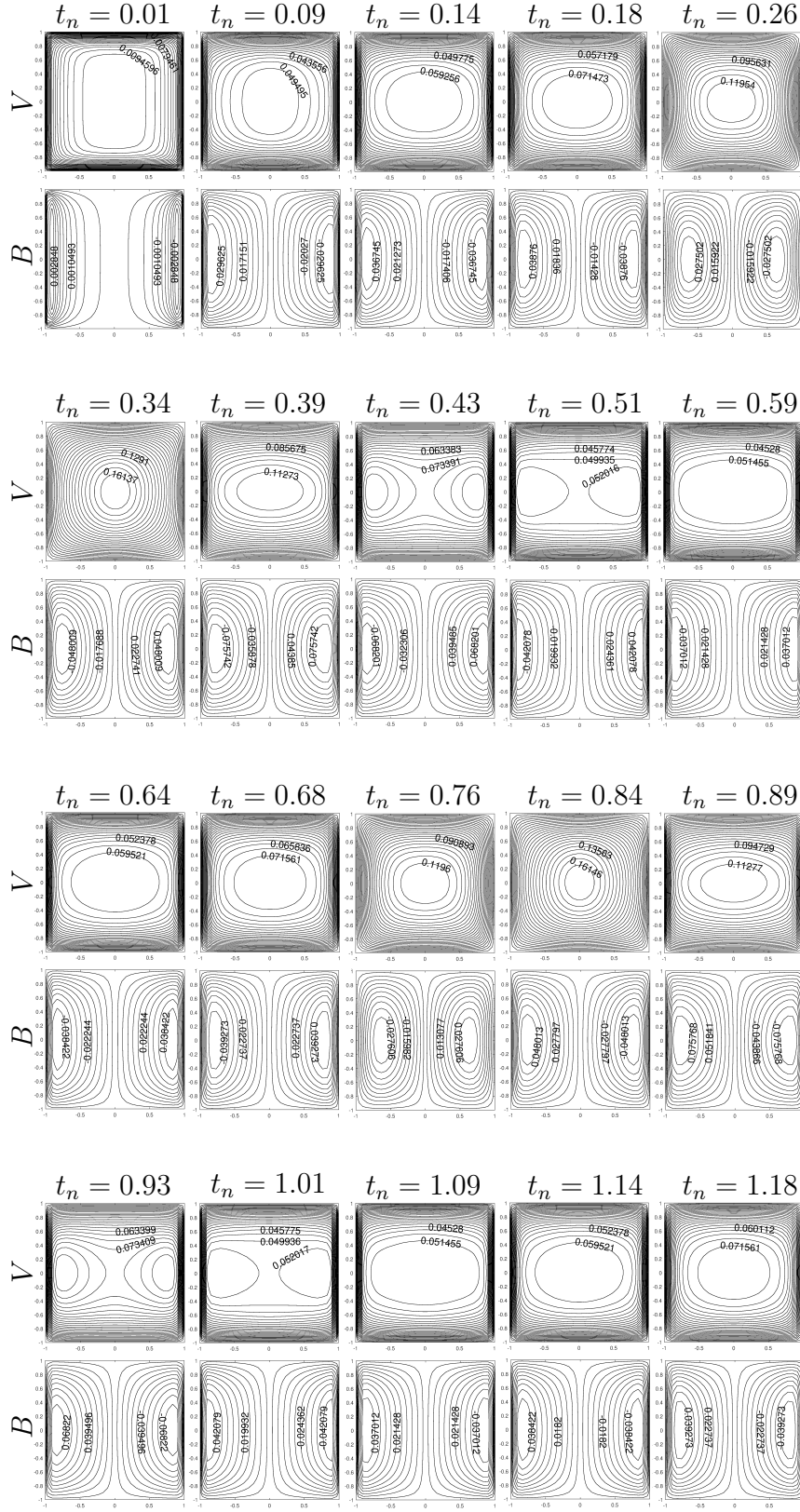


Figure 4.24: Velocity and induced magnetic field lines, $f(t) = \cos(2\pi t)$, $M = 20$, $\alpha = \pi/2$.

The velocity and induced magnetic field behaviors at transient levels for a trigonometric function $f(t) = \cos(2\pi t)$ are given in Figure 4.24 when external magnetic field applies horizontally. The boundary is again discretized by using $N = 120$ constant boundary elements and $L = 900$ interior nodes since $M = 20$. The periodic effect is observed in the flow as repeating its behavior with approximately a time period 0.5 after the elliptical elongation occurs at a time level $t_n = 0.14$ in the direction of applied magnetic field (e.g. $t_n = 0.14, 0.64, 1.14$). Also, as time increases the velocity and the induced magnetic field magnitudes show both increasing and decreasing behaviors.

An impulse function effect is visualized in Figure 4.25, on the velocity and induced magnetic field behaviors at transient levels by taking $f(t)$ as

$$f(t) = \begin{cases} 2 & t = 0.06 \\ 1 & \text{otherwise.} \end{cases}$$

In this case, the boundary is discretized by using more constant elements and interior nodes as $N = 200$ and $L = 2500$ to capture the changes due to the impulse in the applied magnetic field. The magnetic field is applied horizontally and $B_0 = 1$ is taken. The flow behavior starts to change around $t_n = 0.06$ since the applied field strength is increased suddenly. Then, it shows elliptical elongation around $t_n = 0.09$. The velocity magnitude shows a slight drop at $t_n = 0.07$ otherwise they increase. However, the induced magnetic field magnitude continues to increase and its behavior is not changed.

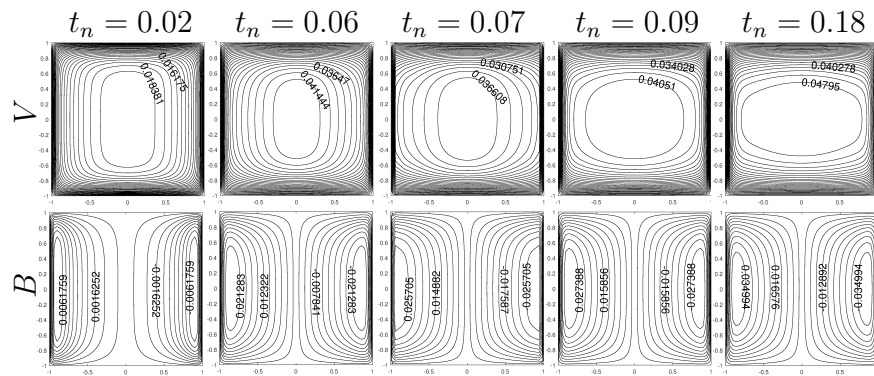


Figure 4.25: Velocity and induced magnetic field lines, $f(t)$ is impulse function, $M = 20$, $\alpha = \pi/2$.

Then, in Figure 4.26, the flow and induced magnetic field lines are presented at transient levels by taking $f(t)$ as a step function

$$f(t) = \begin{cases} 2 & t \leq 0.06 \\ t & t > 0.06. \end{cases}$$

The discretization of the duct is the same as in the case of impulse function used for $M = 20$. The magnetic field is applied horizontally and B_0 is taken as 2 in the nondimensionalization. Since the time variation of the applied magnetic field is constant before $t_n = 0.06$ and linear after $t_n = 0.06$, elongation of the flow occurs exactly at $t_n = 0.07$, then it shows the flow behavior of the case where linear $f(t) = t$ is taken. Thus, new elongation appears after the time level, $t_n = 0.33$ and exactly around $t_n = 0.98$. Then, the flow behavior does not change any more as in the case of linear function $f(t) = 1 + t$. The induced magnetic field starts to show linear function $f(t) = t$ effect after $t_n = 0.06$ forming vortices in front of the Hartmann layers and then stabilizing down.

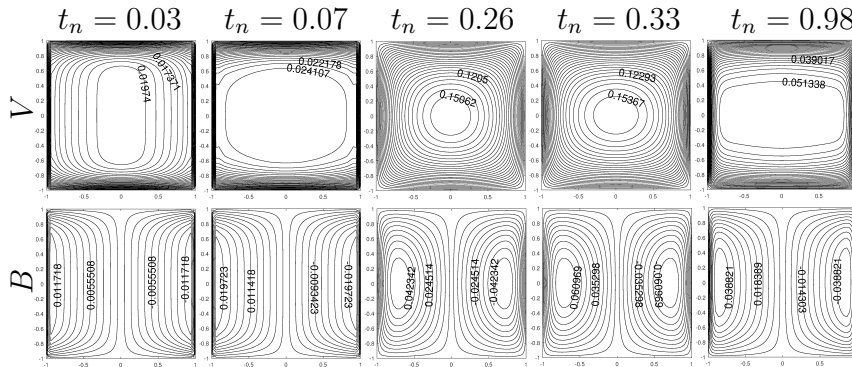


Figure 4.26: Velocity and induced magnetic field lines, step function, $M = 20$, $\alpha = \pi/2$.

Lastly, the step function $f(t)$ is rearranged (modified) by adding a constant close to 2 to its linear variation after $t > 0.06$,

$$f(t) = \begin{cases} 2 & t \leq 0.06 \\ 1.94 + t & t > 0.06. \end{cases}$$

Figure 4.27 presents the flow and induced magnetic field lines for the same Hartmann number $M = 20$ and angle $\alpha = \pi/2$ as in the previous step function case. After $t_n = 0.06$, the intensity of the applied magnetic field is greater than 2. Therefore, the flow shows only one elliptical elongation at $t_n = 0.07$ and the behavior of the flow does not change anymore. The magnitude of the velocity increases up to the time level where the flow elongates and then starts to decrease. This behavior is given in Table 4.8 in terms of volumetric flow rates showing that the flow flattens after the elongation. However, the magnitude of the induced magnetic field increases continuously till reaching steady-state.

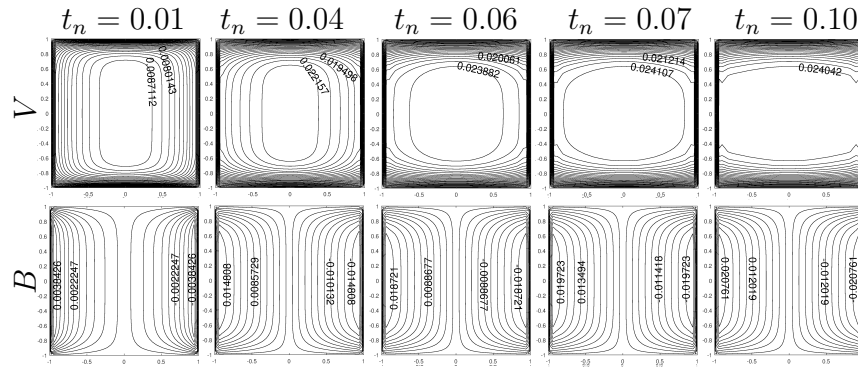


Figure 4.27: Velocity and induced magnetic field lines, modified step function, $M = 20$, $\alpha = \pi/2$.

Table 4.8: The volumetric flow rate Q for the step function $f(t)$, $M = 20$, $N = 120$, $\alpha = \pi/2$.

t_n	0.01	0.04	0.06	0.07	0.10	0.15	0.20
Q	0.0282	0.0719	0.0807	0.0825	0.0834	0.0819	0.0802

4.2.2 Effects of R_e and R_m on the MHD flow

Then, the same MHD duct flow equations (4.8) are solved by taking the effect of Reynolds R_e and magnetic Reynolds R_m numbers into account, so we eliminate the restriction taking these number as one. The MHD flow in a rectangular duct is assumed to be under the effect of a horizontally ($\alpha = \pi/2$) applied magnetic field. The governing equations are

$$\begin{aligned} \nabla^2 V + \overline{M}_x \frac{\partial B}{\partial x} &= -1 + R_e \frac{\partial V}{\partial t} \\ \nabla^2 B + \overline{M}_x \frac{\partial V}{\partial x} &= R_m \frac{\partial B}{\partial t} \end{aligned} \quad \text{in } \Omega \times [0, \infty) \quad (4.17)$$

with the same no-slip velocity and insulated wall conditions, and initial conditions

$$\begin{aligned} V(x, y, t) = 0 \quad B(x, y, t) = 0 \quad (x, y) \in \Gamma \\ V(x, y, 0) = 0 \quad B(x, y, 0) = 0 \quad (x, y) \in \Omega. \end{aligned} \quad (4.18)$$

The discretized matrix-vector equations obtained from the DRBEM procedure are (given in equation (3.48))

$$\begin{aligned} \mathbf{H}\mathbf{V} - \mathbf{G} \frac{\partial \mathbf{V}}{\partial n} &= (\mathbf{H}\hat{\mathbf{U}} - \mathbf{G}\hat{\mathbf{Q}})\mathbf{F}^{-1} \left\{ -\mathbf{1} + R_e \frac{\partial \mathbf{V}}{\partial t} - \overline{M}_x \frac{\partial \mathbf{B}}{\partial x} \right\} \\ \mathbf{H}\mathbf{B} - \mathbf{G} \frac{\partial \mathbf{B}}{\partial n} &= (\mathbf{H}\hat{\mathbf{U}} - \mathbf{G}\hat{\mathbf{Q}})\mathbf{F}^{-1} \left\{ R_m \frac{\partial \mathbf{B}}{\partial t} - \overline{M}_x \frac{\partial \mathbf{V}}{\partial x} \right\}. \end{aligned} \quad (4.19)$$

The duct $\Omega = [-1, 1] \times [-1, 1]$ is discretized by using $N = 200$ constant boundary elements and $L = 2500$ interior nodes. The velocity and induced magnetic field values are obtained at transient time levels using several definitions of $f(t)$ such as polynomial, exponential and trigonometric function, with Hartmann number value $M = 20$, and the time step Δt is taken as 0.01. Pipe-axis velocity $V(x, y, t)$ and the induced magnetic field $B(x, y, t)$ are simulated at transient time levels to show the effect of the problem parameters R_e and R_m . The solution of these coupled equations in (4.19) must be iteratively by constructing the enlarged system of equations as

$$\begin{aligned} \left(\mathbf{H} - \frac{R_e}{\Delta t} \mathbf{K}\right) \mathbf{V}^{n+1} - \mathbf{G} \frac{\partial \mathbf{V}^{n+1}}{\partial n} + \mathbf{P} \mathbf{B}^{n+1} &= \mathbf{K} \left(-\mathbf{1} - \frac{R_e}{\Delta t} \mathbf{V}^n\right) \\ \left(\mathbf{H} - \frac{R_m}{\Delta t} \mathbf{K}\right) \mathbf{B}^{n+1} - \mathbf{G} \frac{\partial \mathbf{B}^{n+1}}{\partial n} + \mathbf{P} \mathbf{V}^{n+1} &= \mathbf{K} \left(-\frac{R_m}{\Delta t} \mathbf{B}^n\right) \end{aligned} \quad (4.20)$$

for increasing time levels where $\mathbf{K} = (\mathbf{H}\hat{\mathbf{U}} - \mathbf{G}\hat{\mathbf{Q}})\mathbf{F}^{-1}$ and $\mathbf{P} = \mathbf{K}(\overline{M}_x \frac{\partial \mathbf{F}}{\partial x} \mathbf{F}^{-1})$.

The enlarged system of equations in (4.20) are constructed by approximating the space derivatives of \mathbf{V} and \mathbf{B} with respect to x , $\frac{\partial \mathbf{V}}{\partial x}$ and $\frac{\partial \mathbf{B}}{\partial x}$ by using the coordinate matrix \mathbf{F} , and the time derivatives of \mathbf{V} and \mathbf{B} , $\frac{\partial \mathbf{V}}{\partial t}$ and $\frac{\partial \mathbf{B}}{\partial t}$ in equation (4.19) are calculated by using the Euler's method as detailed in Section 3.2.

Figure 4.28 shows the flow behavior at several time levels for increasing values of magnetic Reynolds number R_m as 1, 3, 5 when $R_e = 1$. The external magnetic field varies exponentially in time, i.e. $f(t) = e^t$. The time levels t_n where the flow elongation (central vortex turns to be aligned in the direction of the applied magnetic field) occurs for each value of R_m are included. Actually, the flow elongates at $t_n = 0.10, 0.15, 0.19$ for the values of magnetic Reynolds number $R_m = 1, 3$ and 5, respectively. One can deduce from Figure 4.28 that, as R_m increases the time level where the elongation occurs is postponed to a further time level and also the magnitude of the flow increases as the value of R_m increases. The effect of increasing R_m ($R_m \neq 1$) is seen after the elongation, that is, the flow circulates in front of the Hartmann walls and then settles down in the applied magnetic field direction dropping its magnitude.

From Figure 4.29 the effect of the increase in Reynolds number R_e on the flow behavior can be seen when the time-varied function is $f(t) = e^t$. The Reynolds number values are taken as $R_e = 5, 10, 25$ and magnetic Reynolds number is fixed as $R_m = 1$. The flow behaviors are presented at the time levels t_n where the elongation occurs as well as the time levels before and after the elongations for increasing values of Reynolds number R_e . The time levels $t_n = 0.20, 0.30, 0.50$ are the values where the flow elongates for Reynolds number $R_e = 5, 10$ and 25, respectively. The increase in R_e postpones the elongation of the flow to a further time level. Moreover, as R_e increases the magnitude of the flow decreases which is an opposite effect on the behavior compared to the increase in R_m .

Figure 4.30 depicts the velocity and induced magnetic field when the external magnetic field varies linearly and exponentially in time ($f(t) = 1 + t$ and $f(t) = e^t$, respectively) for increasing values of magnetic Reynolds number R_m as 1, 3, 5 and $R_e = 1$ at the time levels where the elongation of the flow occurs. The first row in Figure 4.30 where $R_e = R_m = 1$ shows an agreement with the solution of the de-

coupled MHD equations in which it is possible only for the values $R_e = R_m = 1$ as shown in Section 4.2.1. The flow elongates almost at the same time levels for both linear and exponential functions for the same R_e and R_m values. Although, the behavior of the induced magnetic field does not change as R_m increases, its magnitude increases as well as the increase in the flow magnitude.

Figure 4.31 shows the flow and induced current profiles for $f(t) = 1+t$ and $f(t) = e^t$, keeping $R_m = 1$ and for increasing values of Reynolds number R_e as 5, 10 and 25. The magnitude of the induced magnetic field decreases similar to the decrease in the flow magnitudes as R_e increases.

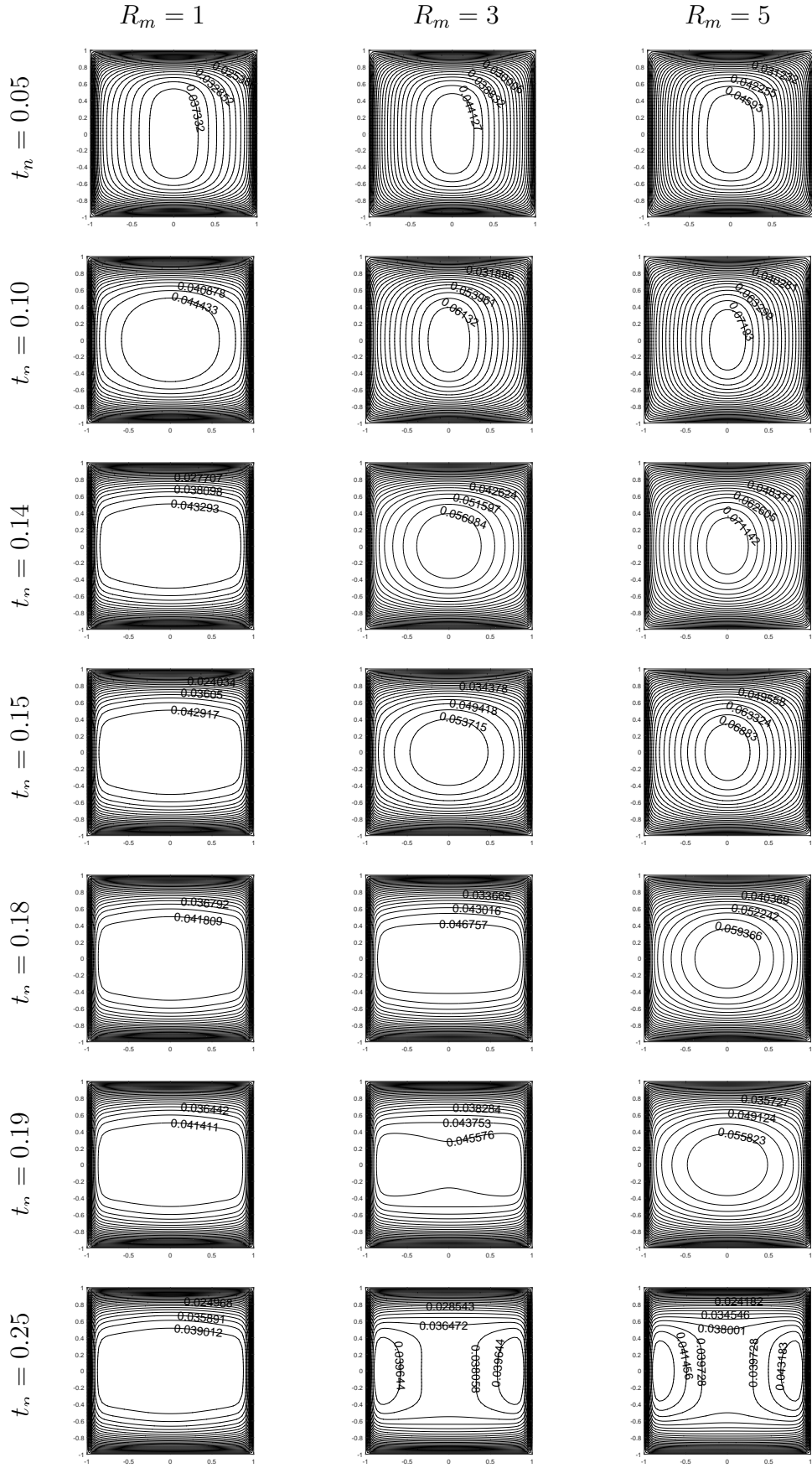


Figure 4.28: Velocity contours, $f(t) = e^t$, $R_e = 1$, $R_m = 1, 3, 5$, $M = 20$, $\alpha = \pi/2$.

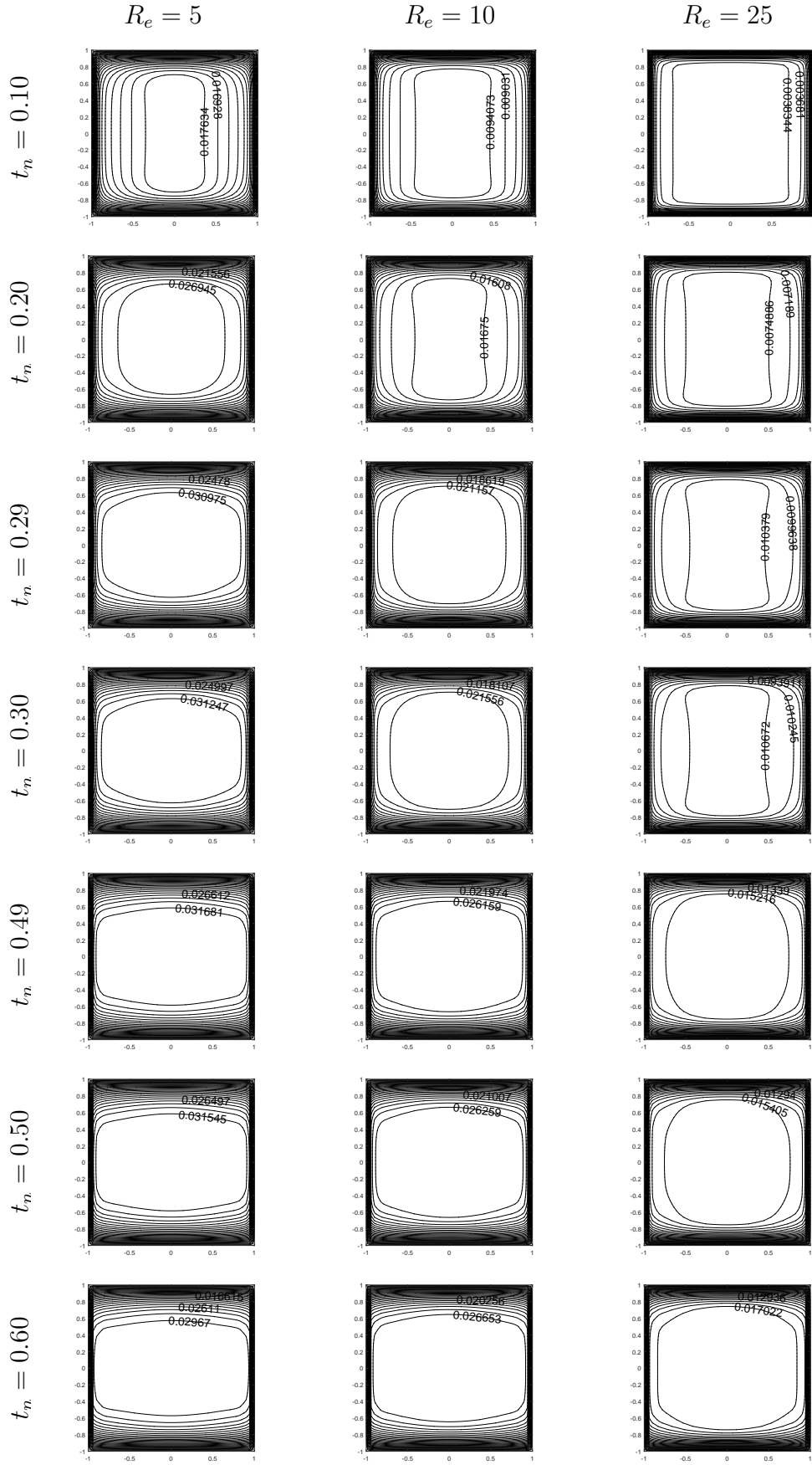


Figure 4.29: Velocity contours, $f(t) = e^t$, $R_m = 1$, $R_e = 5, 10, 25$, $M = 20$, $\alpha = \pi/2$.

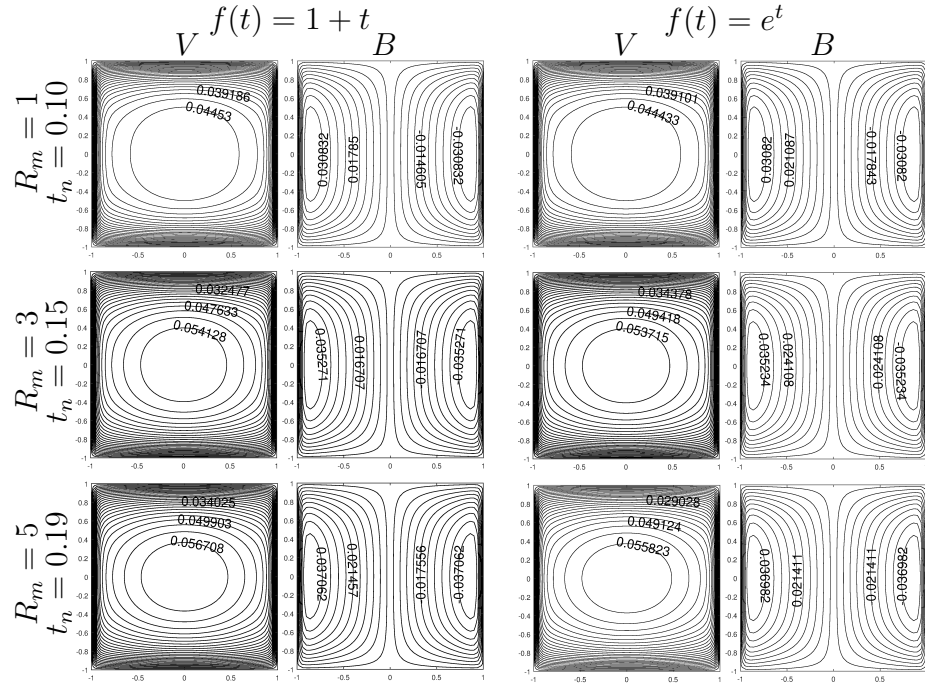


Figure 4.30: Velocity and induced magnetic field, $R_e = 1$, $M = 20$, $\alpha = \pi/2$.

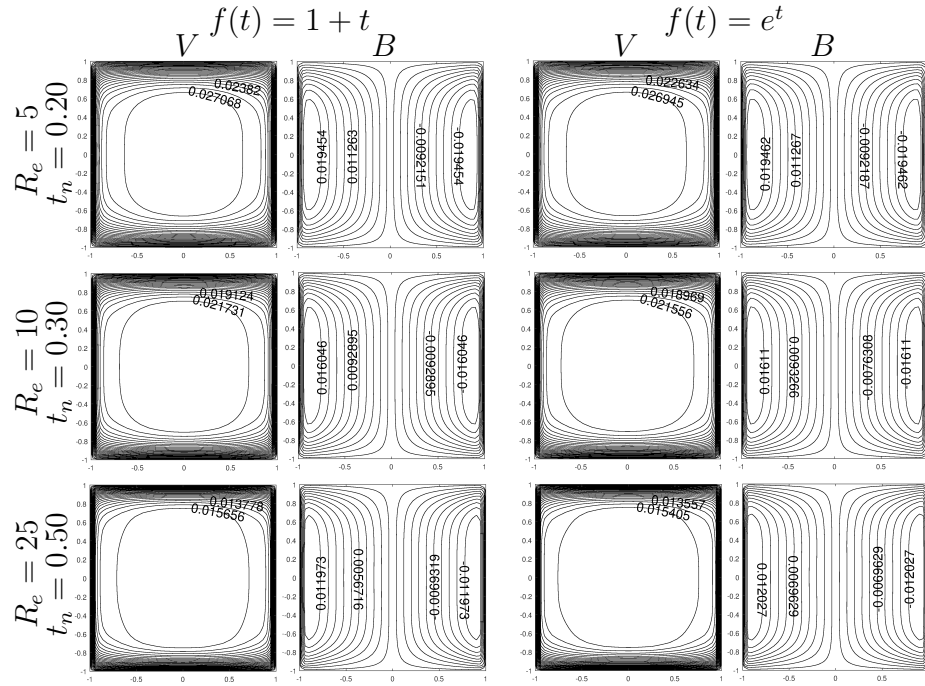


Figure 4.31: Velocity and induced magnetic field, $R_m = 1$, $M = 20$, $\alpha = \pi/2$.

In Figure 4.32, the Reynolds and magnetic Reynolds number values are taken different than one as $R_e = 10$, $R_m = 2$. It can be seen that, the flow elongation occurs at

$t_n = 0.40$ for $R_e = 10$ and $R_m = 2$ which is a postponed time level, with the effect of the increase in R_m , compared to the case $R_e = 10$ and $R_m = 1$ given in Figure 4.31. Since the elongation occurs around small time levels (e.g. $t_n = 0.40$) the effects of the functions $f(t) = 1 + t$, $f(t) = e^t$ are almost the same. They may differ for larger values of t but the behavior of the flows do not change after the elongations.

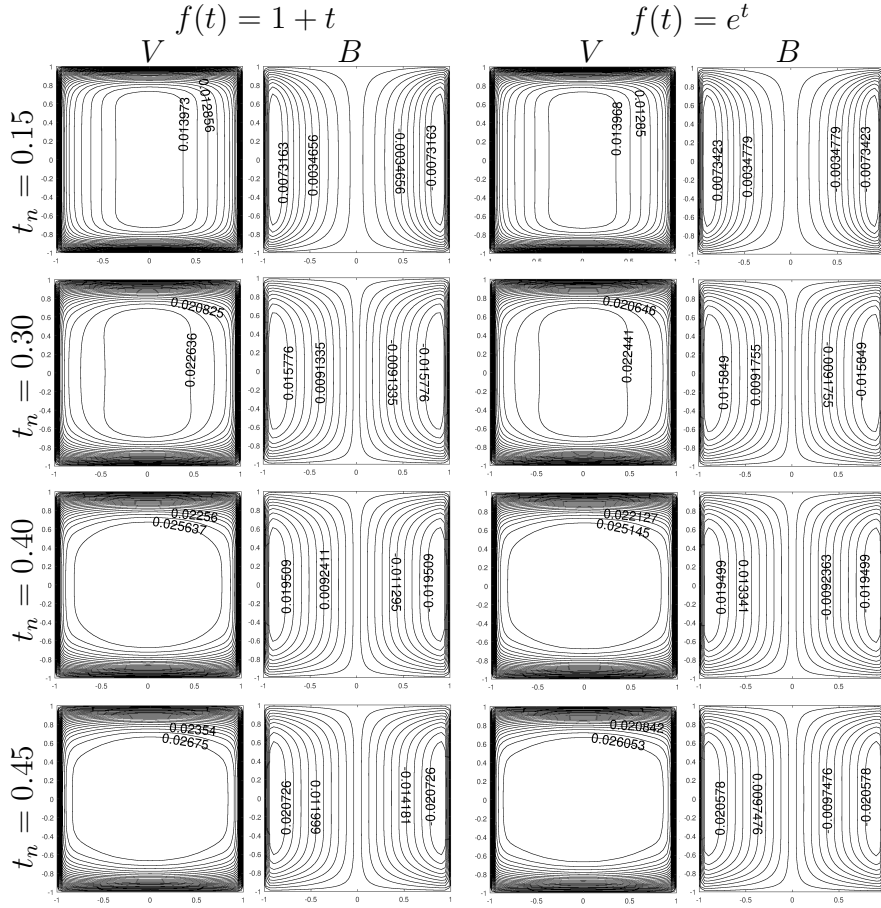


Figure 4.32: Velocity and induced magnetic field, $R_e = 10$, $R_m = 2$, $M = 20$, $\alpha = \pi/2$.

Figure 4.33 stands to validate again the solution of the MHD flow equations solved in coupled form for $R_e = R_m = 1$ with $f(t) = \cos(2\pi t)$, with the solution in [68] obtained from the decoupled MHD equations. The flow repeats its behavior with a period 0.5. Then, Figure 4.34 depicts the profiles of the velocity and induced magnetic field for $R_e = 1$, $R_m = 2$ and $R_e = 5$, $R_m = 1$, respectively. In both cases, the first

time level exhibits where the flow shows an elliptical elongation for the first time. Once more, the time level where the elongation occurs is postponed when compared to Figure 4.33. The period of $f(t) = \cos(2\pi t)$ does not change with the changes in the values of the problem parameters R_e and R_m staying again 0.5.

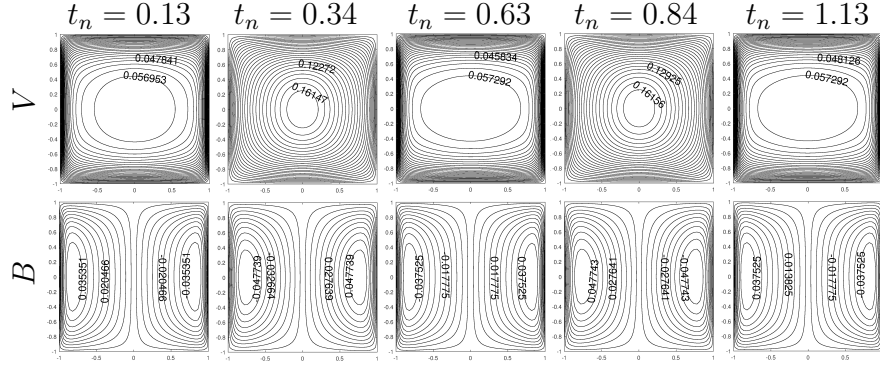


Figure 4.33: Velocity and induced magnetic field, $f(t) = \cos(2\pi t)$, $R_e = R_m = 1$, $M = 20$, $\alpha = \pi/2$.

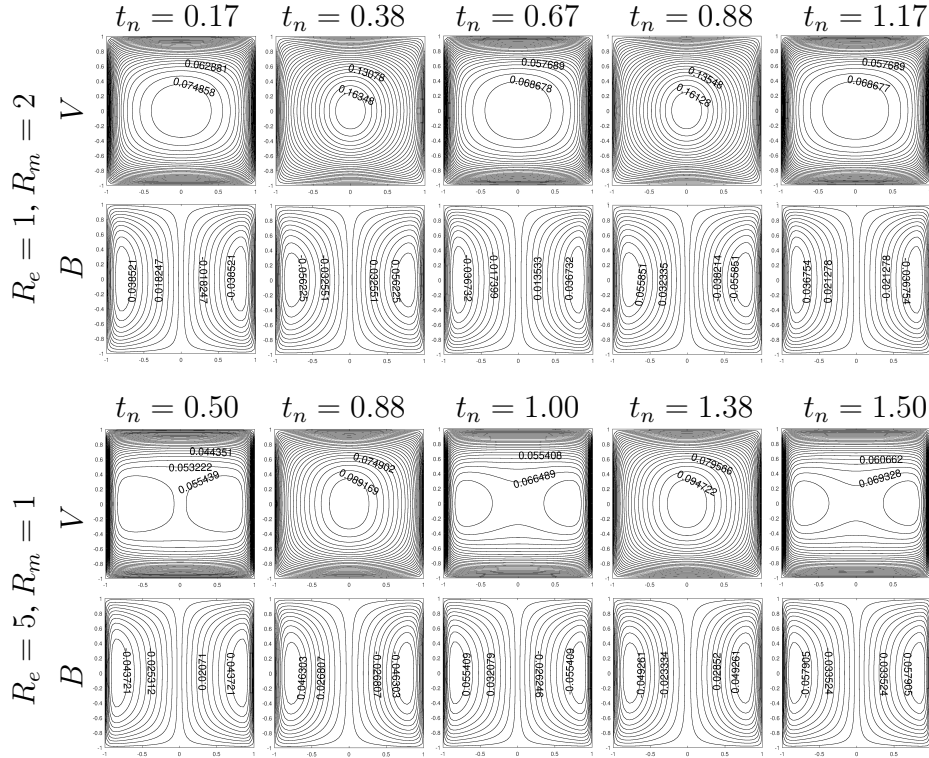


Figure 4.34: Velocity and induced magnetic field, at transient levels, $f(t) = \cos(2\pi t)$, $M = 20$, $\alpha = \pi/2$.

The flow and induced magnetic field profiles are demonstrated at further transient time levels for $f(t) = \cos(2\pi t)$, when $R_e = 5$ and $R_m = 2$ in Figure 4.35. It is confirmed that the period of the flow for the elongation is really 0.5. The periodic effect of the function $f(t)$ in the applied magnetic field, can be seen on the flow behavior in Figure 4.33, Figure 4.34 and Figure 4.35 as the flow is repeating itself.

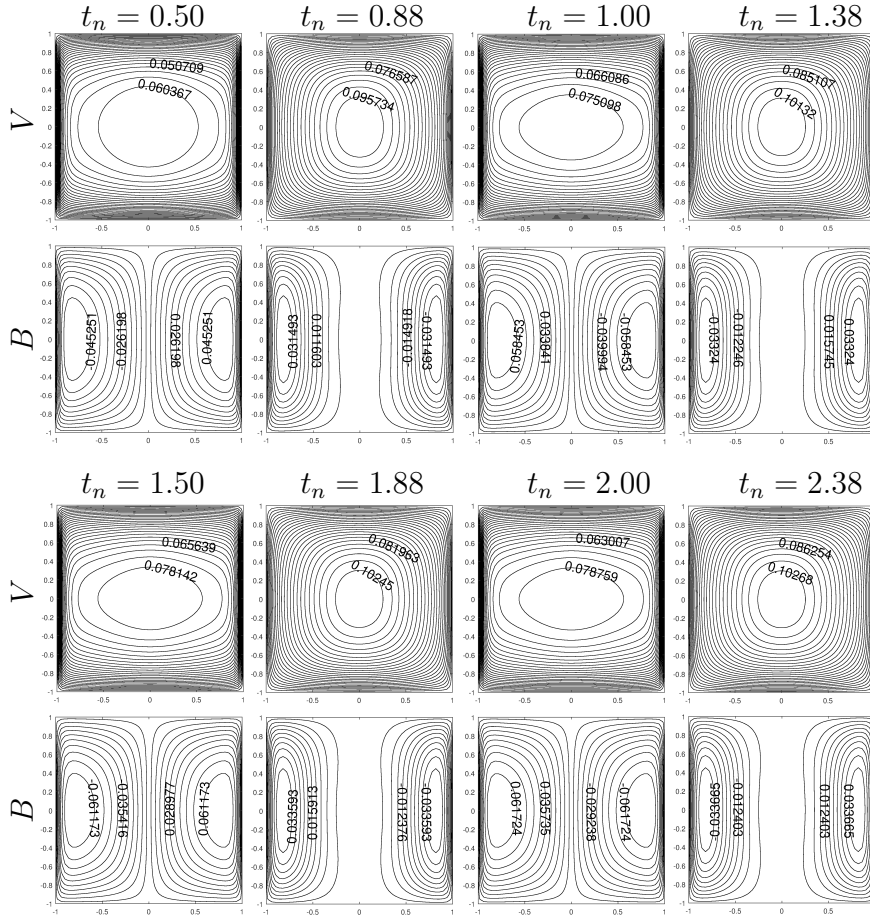


Figure 4.35: Velocity and induced magnetic field, $f(t) = \cos(2\pi t)$, $R_e = 5$, $R_m = 2$, $M = 20$, $\alpha = \pi/2$.

4.3 Inductionless MHD flow with electric potential under axially-changing magnetic field

The two-dimensional steady, fully developed MHD flow of a viscous and incompressible fluid is considered along a long pipe of rectangular cross-section $\Omega = \{(x, y) : -1 \leq x, y \leq 1\}$. The flow is under the effect of axial-dependent, vertically imposed ($\alpha = \pi/2$ with the positive x -axis) magnetic field $\mathbf{B} = (0, B_0(z), 0)$ and $B_0(z) = B_0 g(z)$ where B_0 denotes the external magnetic field intensity, and $g(z)$ is the function determining the strength of the applied magnetic field along the pipe-axis. The governing non-dimensional flow and electric potential equations are given in equation (3.54)

$$\begin{aligned} \nabla^2 w - (Mg(z))^2 w &= -1 + M^2 g(z) \frac{\partial \Phi}{\partial x} \\ \nabla^2 \Phi &= -g(z) \frac{\partial w}{\partial x} \end{aligned} \quad (4.21)$$

where M is the Hartmann number.

The walls on the duct Γ have no-slip velocity. However, the Neumann or mixed type boundary conditions depending on the conductivity of the materials of the walls are imposed for the electric potential. Therefore, the boundary conditions can be written as

$$\begin{aligned} w(x, \pm 1) &= w(\pm 1, y) = 0 \quad \text{no-slip velocity and} \\ \frac{\partial \Phi}{\partial y}(x, \pm 1) &= \frac{\partial \Phi}{\partial x}(\pm 1, y) = 0 \quad \text{non-conducting walls} \end{aligned} \quad (4.22)$$

or

$$\begin{aligned} w(x, \pm 1) &= w(\pm 1, y) = 0 \quad \text{no-slip velocity and} \\ \left. \begin{aligned} \pm \frac{\partial \Phi}{\partial y}(x, \pm 1) &= c \frac{\partial^2 \Phi}{\partial x^2}(x, \pm 1) \\ \pm \frac{\partial \Phi}{\partial x}(\pm 1, y) &= c \frac{\partial^2 \Phi}{\partial y^2}(\pm 1, y) \end{aligned} \right\} \text{variably conducting walls} \end{aligned} \quad (4.23)$$

where c denotes the wall conductance ratio of the four walls (c_t (top), c_b (bottom), c_l (left), c_r (right)) which can be taken as different values. That is, c is a measure of the conductance of the wall compared to that of the fluid. The figure corresponding to the boundary conditions respectively are

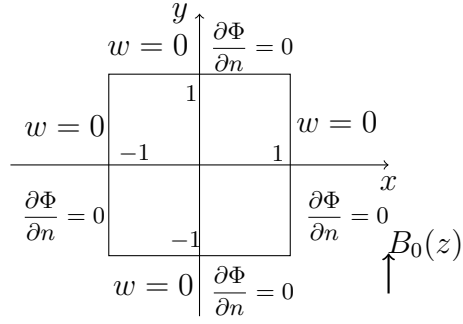


Figure 4.36: Flow and electric potential boundary conditions on non-conducting duct walls

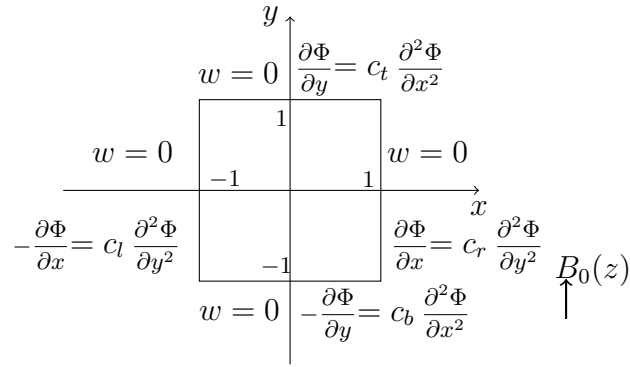


Figure 4.37: Flow and electric potential boundary conditions on variably conducting duct walls

This study investigates the flow behavior and the structure of the boundary layers influenced from the changes in the electrical conductivity of the walls, and the axial dependence and the strength of the applied magnetic field. Firstly, the effects of variably conducting duct walls are deeply studied and simulated in terms of the flow and electric potential for the case of uniform vertically applied magnetic field. Then, numerical results are obtained for the redistribution of flows when the magnetic field applies vertically but changes with respect to the streamwise (pipe-axis) direction in the following subsections, respectively.

4.3.1 Uniform magnetic field

As a basic case, we have considered a vertically applied uniform magnetic field by taking the function $g(z) = 1$ in the equations (4.21) to examine the effect of Hartmann number M with different wall conductance. Therefore, the equations take the form

$$\begin{aligned}\nabla^2 w - M^2 \omega &= -1 + M^2 \frac{\partial \Phi}{\partial x} \\ \nabla^2 \Phi &= -\frac{\partial w}{\partial x}\end{aligned}\tag{4.24}$$

with the given boundary conditions given in (4.22) and (4.23).

The DRBEM implementation gives the following discretized matrix-vector equations

$$\begin{aligned}\mathbf{H}\mathbf{w} - \mathbf{G}\frac{\partial \mathbf{w}}{\partial n} &= (\mathbf{H}\hat{\mathbf{U}} - \mathbf{G}\hat{\mathbf{Q}})\mathbf{F}^{-1}\left\{M^2\mathbf{w} - \mathbf{1} + M^2\frac{\partial \Phi}{\partial x}\right\} \\ \mathbf{H}\Phi - \mathbf{G}\frac{\partial \Phi}{\partial n} &= (\mathbf{H}\hat{\mathbf{U}} - \mathbf{G}\hat{\mathbf{Q}})\mathbf{F}^{-1}\left\{-\frac{\partial \mathbf{w}}{\partial x}\right\}.\end{aligned}\tag{4.25}$$

The matrix-vector equations in (4.25) are solved for the velocity w and electric potential Φ values by constructing enlarged system of equations as in (3.59). The numerical results of this study with a uniform applied magnetic field are given in the following Sections 4.3.1.1-4.3.1.4. When the problem is considered with no-slip and non-conducting ($c = 0$) duct walls, the matrix-vector equations in (4.25) are solved at once by using the boundary conditions given in equation (4.22). On the other hand, the solution procedure of the matrix-vector equations in (4.25) must be iterative starting with initial guess $\Phi^0 = 0$ if one of the duct wall is conducting with a non-zero conductivity ratio, i.e. $c \neq 0$. In this case, at least one of the boundary condition is not given explicitly however, it is depending on the second order partial space derivative of the unknown Φ itself. These boundary conditions for conducting duct walls are computed by using the coordinate matrix \mathbf{F} . Then, the values of w^1 and Φ^1 are obtained and the solution procedure is repeated until the convergence criteria is satisfied. This solution process requires to relax the electric potential Φ as described in Section 3.3.

4.3.1.1 Uniform magnetic field: Non-conducting duct walls

First, the coupled equations in matrix-vector form (4.25) are solved in a duct with no-slip and non-conducting walls ($c = 0$, $\frac{\partial \Phi}{\partial n} = 0$) as shown in Figure 4.36 on which the boundary conditions written on the walls. The effect of Hartmann number M on the flow has been demonstrated by taking M as 30, 50, 100. For $M = 30$ and 50, $N = 200$ constant boundary elements are used, but $M = 100$ requires $N = 300$ boundary elements since the first equation in (4.24) becomes reaction dominant.

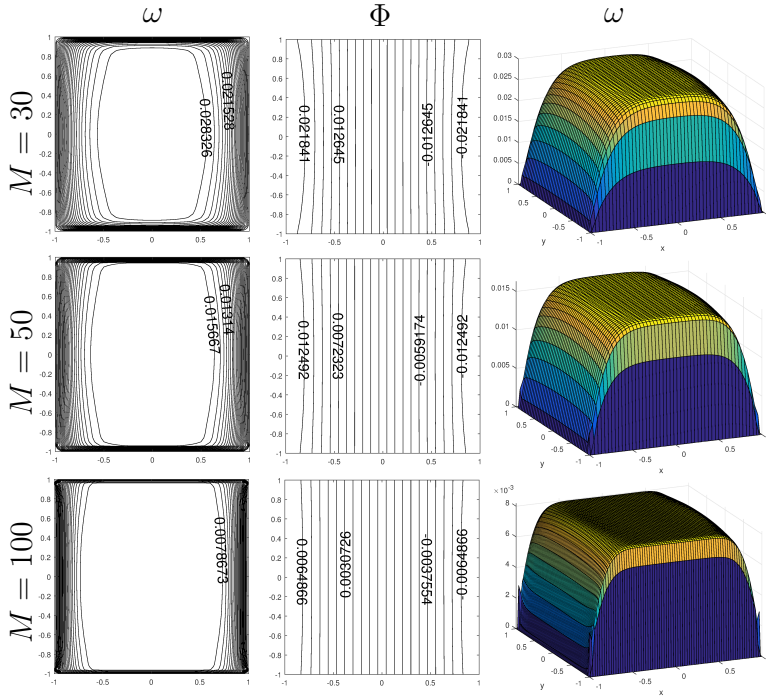


Figure 4.38: Velocity and electric potential profiles with no-slip and non-conducting duct walls. Uniform magnetic field, $\alpha = \pi/2$.

Increasing N for large M increases accuracy of the solution since more clustered point are used close to the walls capturing boundary layer profiles. Figure 4.38 shows the contour plots of the velocity and electric potential and the velocity level curves. It is observed from Figure 4.38 that, as M increases boundary layers are formed (Hartmann and side layers on perpendicular and parallel walls to the vertically applied magnetic field, respectively) and the magnitude of the velocity drops. This is the well-known behavior of MHD flow, that is the flow is flattened as M increases. The

magnitude of electric potential also drops. Electric potential always aligns in the direction of applied magnetic field, the flow is maximum at the centre of the duct when M is small and its velocity drops to zero at the walls, this drop becomes sudden for large M and the centre becomes stagnant for the fluid. This behavior is observed as parabolic velocity profile in the level curves as is also observed in [57].

4.3.1.2 Uniform magnetic field: Non-conducting side walls, variably conducting Hartmann walls

Then, we have solved MHD equations with vertically applied uniform magnetic field by considering non-conducting side walls and variably conducting Hartmann walls (i.e $c_l = c_r = 0$ and $c_b = c_t = 0.1$), and with no-slip velocity everywhere to examine the behavior of the flow for increasing Hartmann number values. The coupled equa-

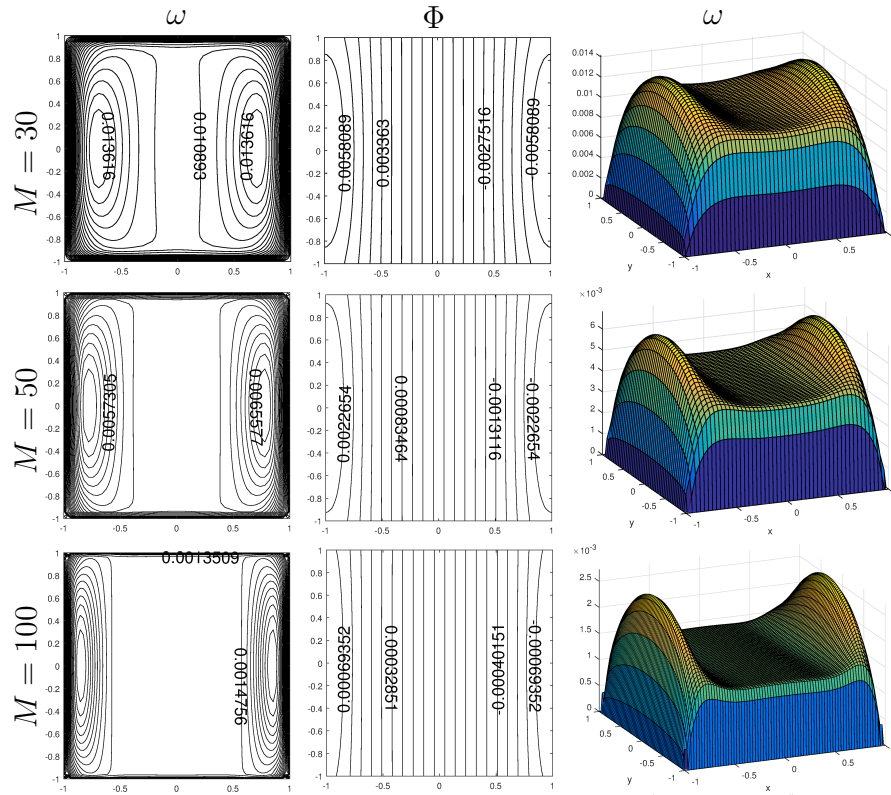


Figure 4.39: Velocity and electric potential profiles with no-slip and, non-conducting side walls, variably conducting Hartmann walls, uniform magnetic field, $\alpha = \pi/2$.

tions (4.25) for uniform magnetic field are solved iteratively for w and Φ using the initial value Φ^0 as zero. The results are obtained with a tolerance $\max_i |w_i^{n+1} - w_i^n| < 10^{-4}$ and $\max_i |\Phi_i^{n+1} - \Phi_i^n| < 10^{-4}$ for $i = 1, \dots, N + L$ and the electric potential Φ is relaxed using the equation $\Phi^{n+1} = (1 - \kappa)\Phi^n + \kappa\Phi^{n+1}$ with a relaxation parameter taken as $\kappa = 0.01$. The obtained results are shown in Figure 4.39 in terms of velocity, electric potential contours and level curves of velocity.

The flow aligns in terms of two loops parallel to applied magnetic field in front of the side walls. That means, the fluid mainly flows in front of the side walls. As M increases the velocity and electric potential behaviors stay the same with a decrease in magnitudes. The magnitudes of the velocity and electric potential are smaller than the ones in the case of non-conducting duct walls. This means that the increase in the conductivity of the top and bottom walls causes the drop of the magnitudes. The fluid is nearly stagnant in the centre of the duct. Due to the peaks with higher velocity values occurring on the side layers, the flow form M-shape profile for increasing Hartmann number values. This case is the validation of the numerical results obtained by the proposed method with the finite difference results given in [57].

4.3.1.3 Uniform magnetic field: Variably conducting walls with the same conductivity ratio

Then, the MHD flow in the duct is solved with well-conducting walls for again Hartmann number values $M = 30, 50, 100$. The number of boundary elements are the same as in the previous cases of conductivity of the walls. In this case, electric potential satisfies mixed type boundary conditions as given in equation (4.23) for variably conducting walls with $c = 0.1$ (i.e $c_t = c_b = c_t = c_r = 0.1$). Again, it is required to solve the coupled matrix-vector equations in (4.25) for w and Φ iteratively with the initial values $\Phi^0 = 0$. The results are demonstrated with the same tolerance and relaxation parameter used in the case of non-conducting side walls and variably conducting Hartmann walls given in Section 4.3.1.2. The velocity level curves as well as the contour plots of w and Φ are shown in Figure 4.40. It can be deduced that, the magnitudes of the velocity and electric potential slightly drop compared to the case when the side walls are non-conducting as given in Section 4.3.1.2. Also, the increase

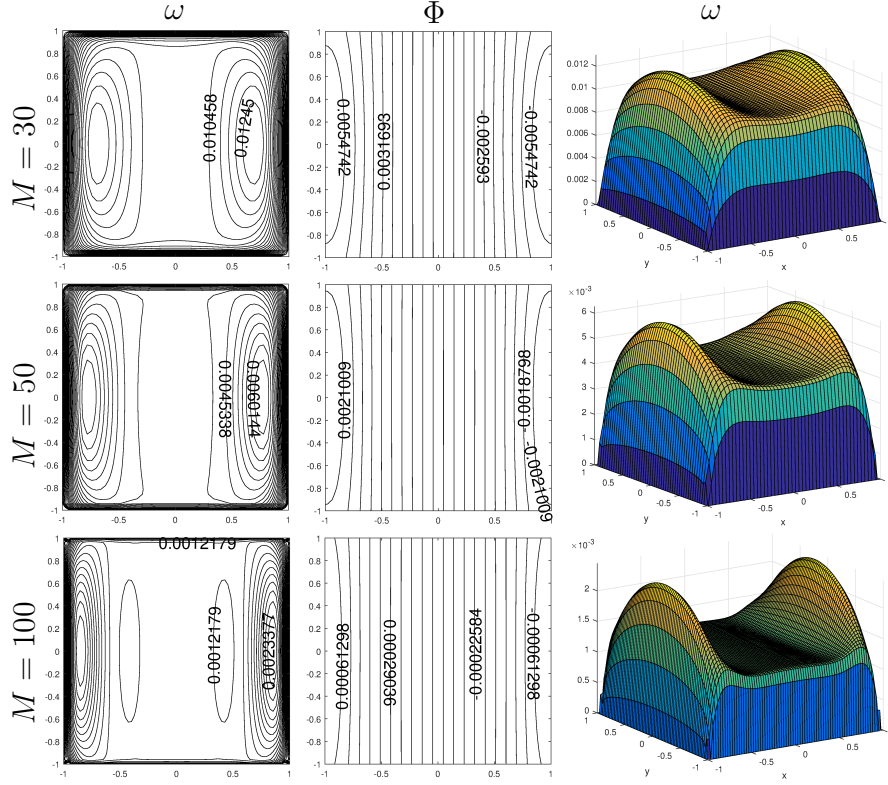


Figure 4.40: Velocity and electric potential profiles with no-slip and well-conducting duct walls, uniform magnetic field, $\alpha = \pi/2$.

in the conductivity ratio at all the walls accelerates the formation of boundary layers and the M-shape of the flow. Thus, the increase in both the M and walls conductivities cause the slow motion of the fluid in the pipe.

4.3.1.4 Uniform magnetic field: Variably conducting walls with different conductivity ratios

In this section, the effect of different wall conductivities such as $c_b = c_t = c_l = 0.1$ and $c_r = 5 \times 10^{-3}$ are examined with the same Hartmann number M values 30, 50 and 100. The three walls of the duct have high electrical conductivity whereas the left wall has a small electrical conductivity. The obtained results are shown in Figure 4.41. The coupled matrix-vector equations for w and Φ are solved iteratively using the same N , tolerance, relaxation parameter and initial values as in the previous cases

of wall conductivities. It is seen that, the flow turbulence occurs with the effect of the increasing Hartmann number M and this turbulence effect is not symmetric since the side walls have different conductivities. Magnitudes of w and Φ slightly increase compared to the magnitudes when all the walls have the same high conductivity ($c = 0.1$). This is due to the drop of the conductivity on the right side wall. Velocity shows a minimum between core and right side wall distorting slightly the M-shape as in the study [57]. Therefore, it can be deduced from the Figure 4.41 that, the conductivities of the walls determine the structure of the boundary layers significantly.

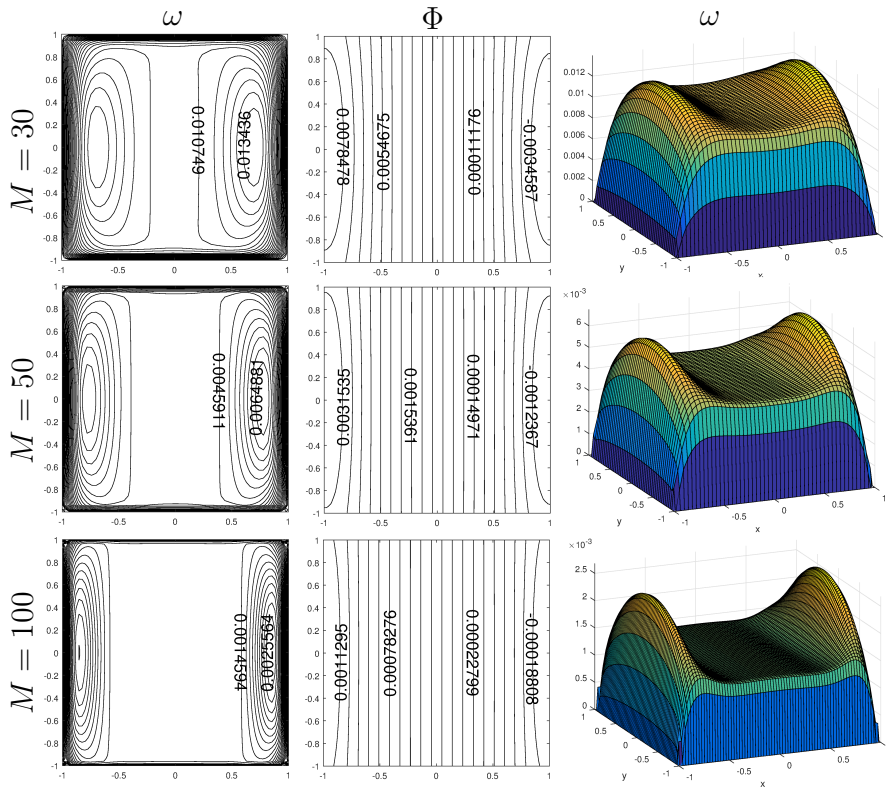


Figure 4.41: Velocity and electric potential profiles with different conductivity ratios on the no-slip duct walls. Uniform magnetic field, $\alpha = \pi/2$.

The effects of Hartmann number M and wall conductivity ratio on the flow behavior under uniform applied magnetic field have been visualized in Sections 4.3.1.1-4.3.1.4. In the following section, we present the effect of axially changing applied magnetic field when $g(z) \neq 1$, $B_0(z) = B_0 g(z)$ on the flow.

4.3.2 Axial dependent magnetic field: Variably conducting walls

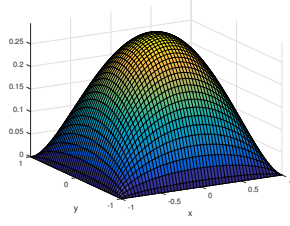
The DRBEM discretized matrix-vector equation of the coupled equations (4.21) gives

$$\begin{aligned} \mathbf{H}\mathbf{w} - \mathbf{G}\frac{\partial \mathbf{w}}{\partial n} &= (\mathbf{H}\hat{\mathbf{U}} - \mathbf{G}\hat{\mathbf{Q}})\mathbf{F}^{-1}\{(Mg(z))^2\mathbf{w} - \mathbf{1} + (M^2g(z))\frac{\partial \Phi}{\partial x}\} \\ \mathbf{H}\Phi - \mathbf{G}\frac{\partial \Phi}{\partial n} &= (\mathbf{H}\mathbf{U} - \mathbf{G}\hat{\mathbf{Q}})\mathbf{F}^{-1}\{-g(z)\frac{\partial \mathbf{w}}{\partial x}\}. \end{aligned} \quad (4.26)$$

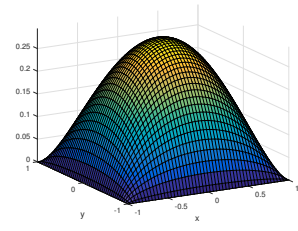
The external magnetic field with strength $Mg(z)$ is applied vertically. The function $g(z)$ in equations (4.26) is chosen as $\frac{1}{1 + e^{-z/z_0}}$ where $z_0 = 0.15$ as given in [57]. The distance between two consecutive z_i and z_{i+1} values are assumed to be long enough that, the flow is considered fully developed between these z values. Since z_0 is positive $B_0(z)$ rises from zero to one. The magnitude of z_0 governs the gradient of the field. The reason for choosing $z_0 = 0.15$ is to keep the streamwise extension of the computational domain as small as possible in order to obtain good resolution. Figures 4.42-4.43 show the velocity level curves at different positions of z -axis along the pipe by taking $M = 50$ and $N = 200$. The strength of the magnetic field $B_0(z)$ is also displayed. The no-slip velocity and high electrical conductivity such as $c_b = c_t = c_r = c_l = 0.1$ are inserted as boundary conditions for w and Φ , respectively. The velocity and electric potential profiles are obtained by solving the equations in (4.26) iteratively with a tolerance $\max_i |w_i^{n+1} - w_i^n| < 10^{-4}$ and $\max_i |\Phi_i^{n+1} - \Phi_i^n| < 10^{-4}$ for $i = 1, \dots, N + L$. The electric potential Φ is relaxed with a parameter κ using the equation $\Phi^{n+1} = (1 - \kappa)\Phi^n + \kappa\Phi^{n+1}$ where κ is taken in the range $0.0001 \leq \kappa \leq 0.01$ appropriately chosen for the z -values on the axis that the magnetic field $B_0(z)$ is changing. In Figure 4.42, flow behavior for negative z -values is shown along with the corresponding increase in the magnitude of the applied magnetic field $B_0(z)$. The first velocity profile in (a) shows the flow behavior when $z = -1.13$ and $B_0(z) = 5.34 \times 10^{-4}$ which is not a strong enough magnetic field. In this case, the velocity has a parabolic shape which is almost purely hydrodynamic profile. The velocity profiles in Figure 4.42 (b)-(f) show the effects of increasing strength of the applied magnetic field from $B_0(z) = 0.00669$ to $B_0(z) = 0.1192$. The increasing strength of the magnetic field causes a decrease in the magnitude of the velocity keeping still the parabolic profile since the strength of $B_0(z)$ is still weak. Then, the velocity profiles in Figures 4.42 (g)-(h) are obtained at $z = -0.20$ and $z = -0.10$, and the strength of the applied magnetic field is increased to $B_0(z) = 0.2086$ and $B_0(z) = 0.3392$,

respectively. An increase in the strength of the applied magnetic field flattens the flow. When z -value approaches through the origin the formation of M-shape profile slightly starts as in (i). The M-shape grows when z is at the origin which can be seen in Figure 4.42 (j).

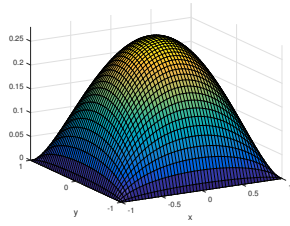
The velocity profiles in Figure 4.43 are obtained when z values pass the origin. The M-shape profile of the flow is getting deeper and deeper. Moreover, the fluid is driven towards the side walls parallel to $B_0(z)$ which can be seen from the Figures 4.43 (k)-(s). The value of z where M-shape reaches its maximum, the applied magnetic field is also maximum. Then, the M-shape profile of the flow is preserved for further z values since the strength of the applied magnetic field is no longer changed as can be seen from Figure 4.43 (t). Therefore, the applied magnetic field varying through the pipe-axis direction as if the magnets of different strengths are placed in the stream-wise direction results in three-dimensional effects on the flow. The MHD equations are solved in two-dimensional ducts where the magnets are placed. Between the two magnets (applied magnetic fields of different strength) the flow is assumed to be fully-developed. The changes in the flow behavior through the pipe are due to the velocity magnitude depending on the z -values and the M-shape due to the conducting duct walls. The transition of the flow from fully-developed hydrodynamic to the fully-developed magnetohydrodynamic occurs through several states as can be seen in Figures 4.42 and 4.43. The flow shows a highly M-shape profile due to the side layers developed. The same flow behavior has been seen in Sterl's study [57] when the three-dimensional MHD flow equations were solved.



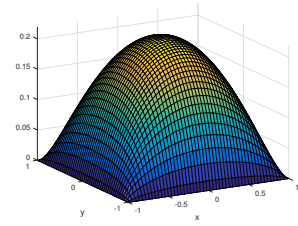
(a) $z = -1.13$, $B_0(z) = 5.34 \times 10^{-4}$



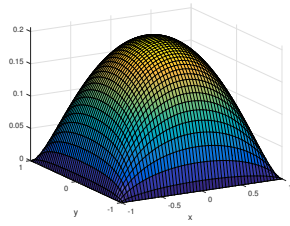
(b) $z = -0.75$, $B_0(z) = 0.00669$



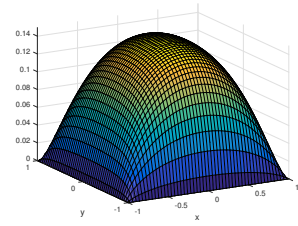
(c) $z = -0.55$, $B_0(z) = 0.0249$



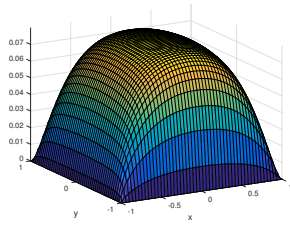
(d) $z = -0.40$, $B_0(z) = 0.0649$



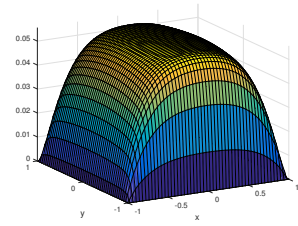
(e) $z = -0.38$, $B_0(z) = 0.0736$



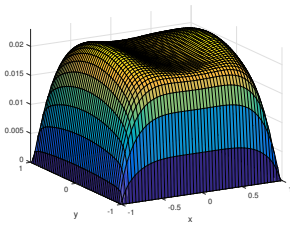
(f) $z = -0.30$, $B_0(z) = 0.1192$



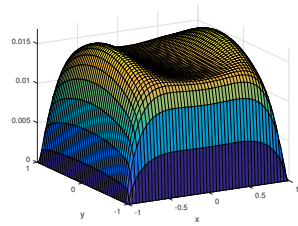
(g) $z = -0.20$, $B_0(z) = 0.2086$



(h) $z = -0.10$, $B_0(z) = 0.3392$

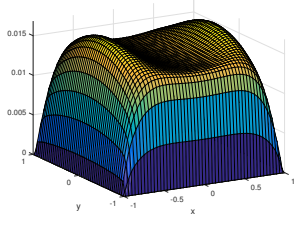


(i) $z = -0.06$, $B_0(z) = 0.4013$

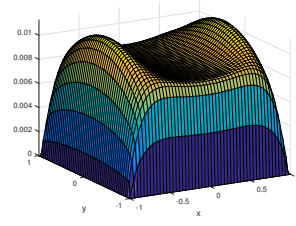


(j) $z = 0$, $B_0(z) = 0.50$

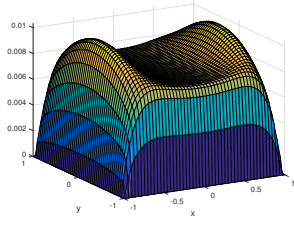
Figure 4.42: Velocity profiles for axial dependent magnetic field, $M = 50$, $\alpha = \pi/2$.



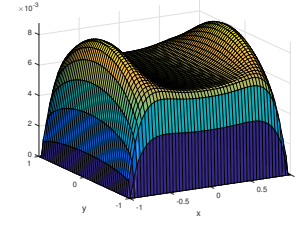
(j) $z = 0, B_0(z) = 0.50$



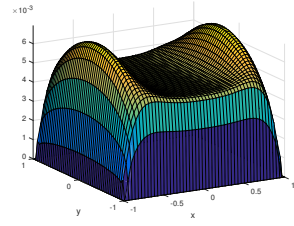
(k) $z = 0.10, B_0(z) = 0.6607$



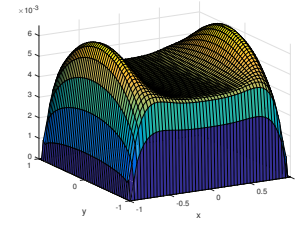
(l) $z = 0.13, B_0(z) = 0.7040$



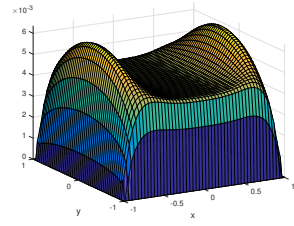
(m) $z = 0.20, B_0(z) = 0.7914$



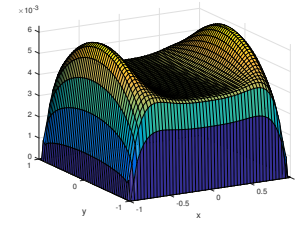
(n) $z = 0.38, B_0(z) = 0.9264$



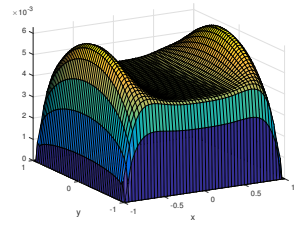
(o) $z = 0.55, B_0(z) = 0.9750$



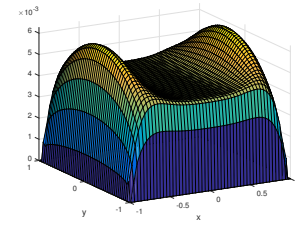
(p) $z = 0.75, B_0(z) = 0.9933$



(r) $z = 1.00, B_0(z) = 0.9987$



(s) $z = 1.13, B_0(z) = 0.9995$



(t) $z = 1.50, B_0(z) = 0.9999$

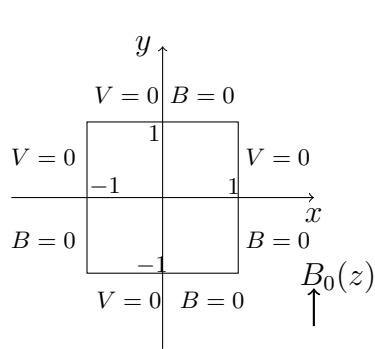
Figure 4.43: Velocity profiles for axial dependent magnetic field, $M = 50, \alpha = \pi/2$.

4.4 MHD duct flow with axially-changing external magnetic field

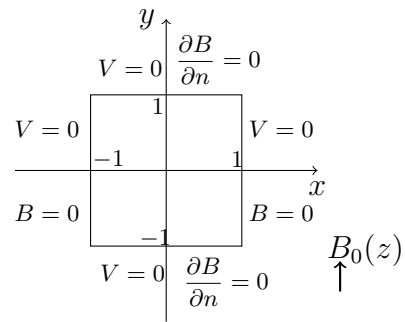
The laminar, fully-developed MHD flow of a viscous and incompressible fluid has been considered between consecutive magnets placed on the pipe-axis. The flow is under the effect of an axial-dependent vertically applied magnetic field. The MHD flow equations in terms of the velocity, induced magnetic field and electric potential are (Section 3.4, equations (3.68))

$$\begin{aligned} \nabla^2 V + Mg(z) \frac{\partial B}{\partial y} &= -1 + \frac{M^2}{R_m} g(z) \frac{\partial g(z)}{\partial z} \\ \nabla^2 B + Mg(z) \frac{\partial V}{\partial y} &= 0 \\ \nabla^2 \Phi &= -g(z) \frac{\partial V}{\partial x}. \end{aligned} \quad -1 \leq x, y \leq 1 \quad (4.27)$$

The coupled equations of the velocity V and the induced magnetic field B in (4.27) are considered with the boundary conditions given in Figure 4.44 (a) and (b). The coupled equations along with the electric potential equation (3rd equation) are considered with no-slip and insulated duct walls together with the Dirichlet, and Dirichlet and Neumann type boundary conditions for Φ as given in Figure 4.45 (a) and (b).



(a) insulated duct walls



(b) conducting Hartmann walls, insulated side walls

Figure 4.44: Flow and induced magnetic field boundary conditions on the duct walls.

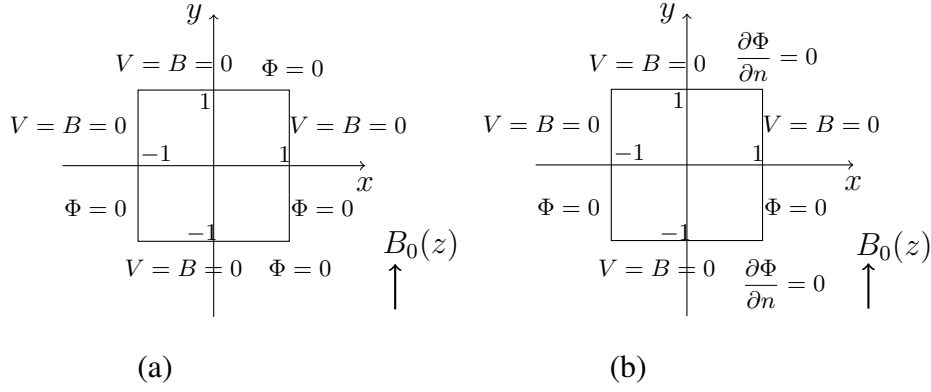


Figure 4.45: The boundary conditions of Φ on the insulated and no-slip duct walls.

The DRBEM implementation to equations (4.27) bring the following DRBEM discretized system, (equations (3.69))

$$\begin{aligned}
 \mathbf{H}\mathbf{V} - \mathbf{G}\frac{\partial \mathbf{V}}{\partial n} &= (\mathbf{H}\hat{\mathbf{U}} - \mathbf{G}\hat{\mathbf{Q}})\mathbf{F}^{-1}\left\{-Mg(z)\frac{\partial \mathbf{B}}{\partial y} - 1 + \frac{M^2}{R_m}g(z)\frac{\partial g(z)}{\partial z}\right\} \\
 \mathbf{H}\mathbf{B} - \mathbf{G}\frac{\partial \mathbf{B}}{\partial n} &= (\mathbf{H}\hat{\mathbf{U}} - \mathbf{G}\hat{\mathbf{Q}})\mathbf{F}^{-1}\left\{-Mg(z)\frac{\partial \mathbf{V}}{\partial y}\right\} \\
 \mathbf{H}\Phi - \mathbf{G}\frac{\partial \Phi}{\partial n} &= (\mathbf{H}\hat{\mathbf{U}} - \mathbf{G}\hat{\mathbf{Q}})\mathbf{F}^{-1}\left\{-g(z)\frac{\partial \mathbf{V}}{\partial x}\right\}
 \end{aligned} \tag{4.28}$$

where the BEM matrices are given in (3.15).

The equations in (4.28) are either solved by considering coupled equations in terms of the velocity V and induced magnetic field B values with the boundary conditions given in Figure 4.44 or the equations in (4.28) are solved for the velocity V , induced magnetic field B and the electric potential Φ values with the boundary conditions given in Figure 4.45.

The ducts $\Omega_i = [-1, 1] \times [-1, 1]$ are discretized at the locations z_i on the pipe-axis by using $N = 200$ constant boundary elements and $L = 2500$ interior nodes. The pipe-axis dependent function in $B_0(z)$ is taken as $g(z) = \frac{1}{1 + e^{-z/0.15}}$. The z_i values (positions of the magnets) are considered between $-2.13 \leq z \leq 2.13$ (a section of length 4.26 around the origin in the pipe-axis direction). First, the velocity V and induced magnetic field B are obtained by solving the discretized matrix-vector equations (4.28) with no-slip and insulated duct walls as shown in Figure 4.44 (a) for increasing values of Hartmann number M as 10, 30 and 50 by taking magnetic

Reynolds number fixed as $R_m = 2$. The velocity and induced current contours and velocity level curves at several locations in $[-2.13, 2.13]$ along the pipe are presented in Figures 4.46, 4.47 and 4.48. The fluid flows in the positive pipe-axis direction first and then it reverses its direction at a certain z -value, and then the flow becomes positive again in that interval. It can be seen from these figures that, as M increases the reversed flow occurs much earlier, and then the flow turns to the pipe-axis direction (positive z -axis) much later. That is, the length of the interval on the pipe-axis on which the flow is reversed is increasing (i.e. for $M = 10$ the length of the interval for reversed flow is 1.30, for $M = 30$ it is 1.80 and for $M = 50$ it is 2.03). The flattening tendency of the flow is also observed as M increases at the same location of the pipe (i.e. at $z = 2.13$).

Figures 4.47, 4.49 and 4.50 depict the behavior of the flow and induced current for increasing values of magnetic Reynolds number as $R_m = 2, 5, 25$ for a fixed Hartmann number $M = 30$ in the interval $-2.13 \leq z \leq 2.13$ again for the case of no-slip and insulated duct walls. It is observed that, as R_m increases the flow reverses much later however, reversing back to the pipe-axis direction occurs much earlier. That is, the length of the interval for the reverse flow is getting shorter as R_m increases. The lengths are 1.80, 1.59 and 1.22 for R_m as 2, 5 and 25, respectively. This opposite effects of the increase in the values of Hartmann number and magnetic Reynolds number, on the lengths of the sections of the pipes for the reversed flow can be explained physically. For the same fluid of constant viscosity μ and electric conductivity σ , Hartmann number increases when the intensity of the applied magnetic field B_0 is strong. Its effect is also strong on the fluid and the flow reversion occurs on a longer interval on the pipe-axis. But, the magnetic Reynolds number R_m increases when magnetic permeability μ_0 increases. Thus, the flow changes direction quickly on the pipe-axis.

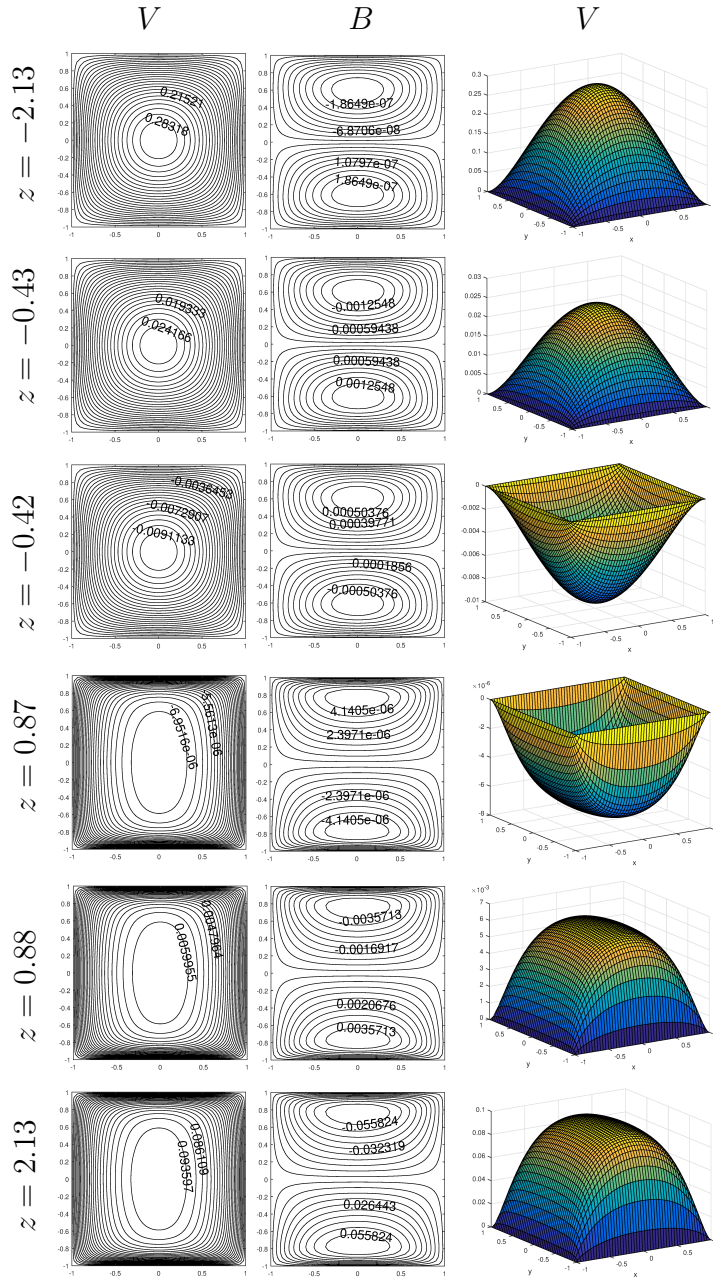


Figure 4.46: Velocity and induced magnetic field ($V = B = 0$ duct walls), $M = 10$, $R_m = 2$. Axially-changing magnetic field, $\alpha = \pi/2$.

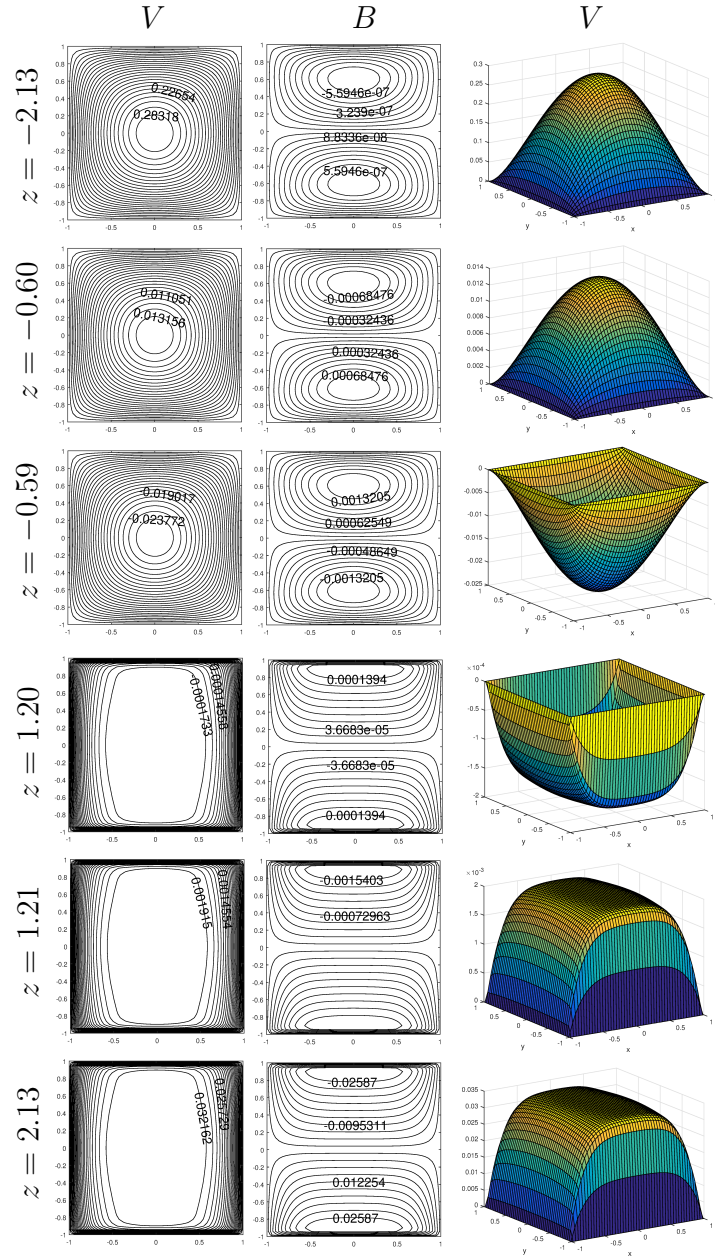


Figure 4.47: Velocity and induced magnetic field ($V = B = 0$ duct walls), $M = 30$, $R_m = 2$. Axially-changing magnetic field, $\alpha = \pi/2$.

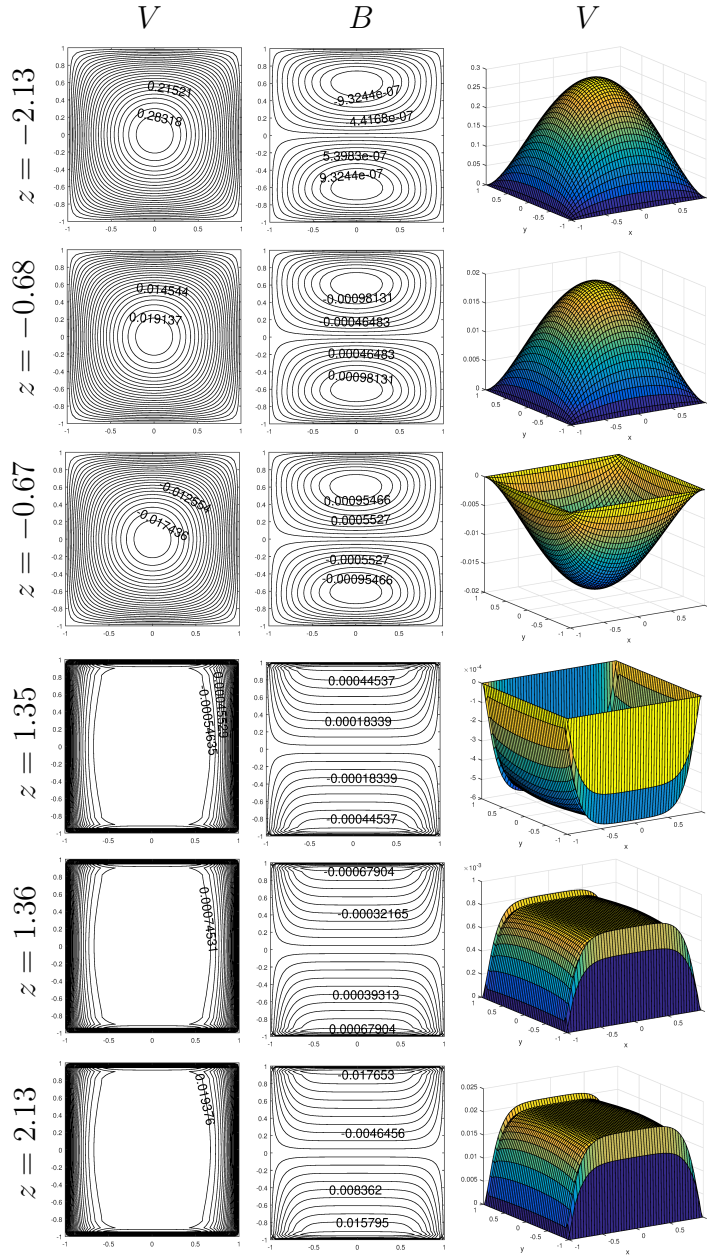


Figure 4.48: Velocity and induced magnetic field ($V = B = 0$ duct walls), $M = 50$, $R_m = 2$. Axially-changing magnetic field, $\alpha = \pi/2$.

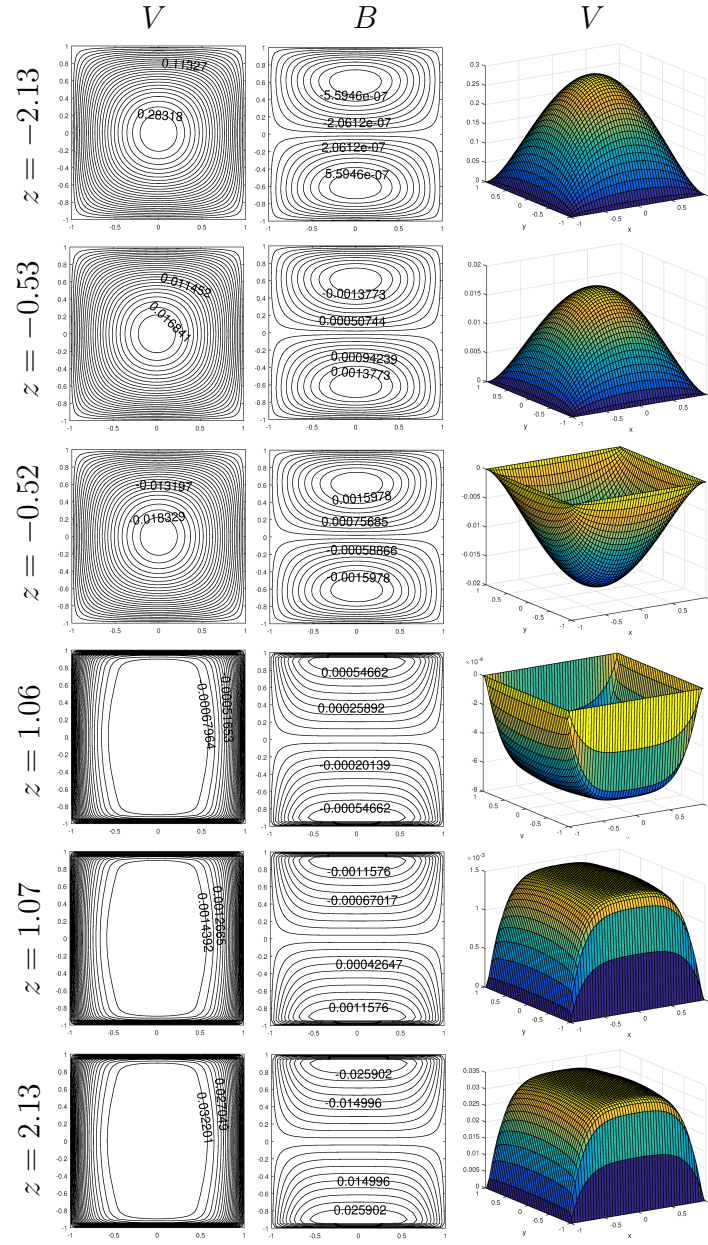


Figure 4.49: Velocity and induced magnetic field ($V = B = 0$ duct walls), $M = 30$, $R_m = 5$. Axially-changing magnetic field, $\alpha = \pi/2$.

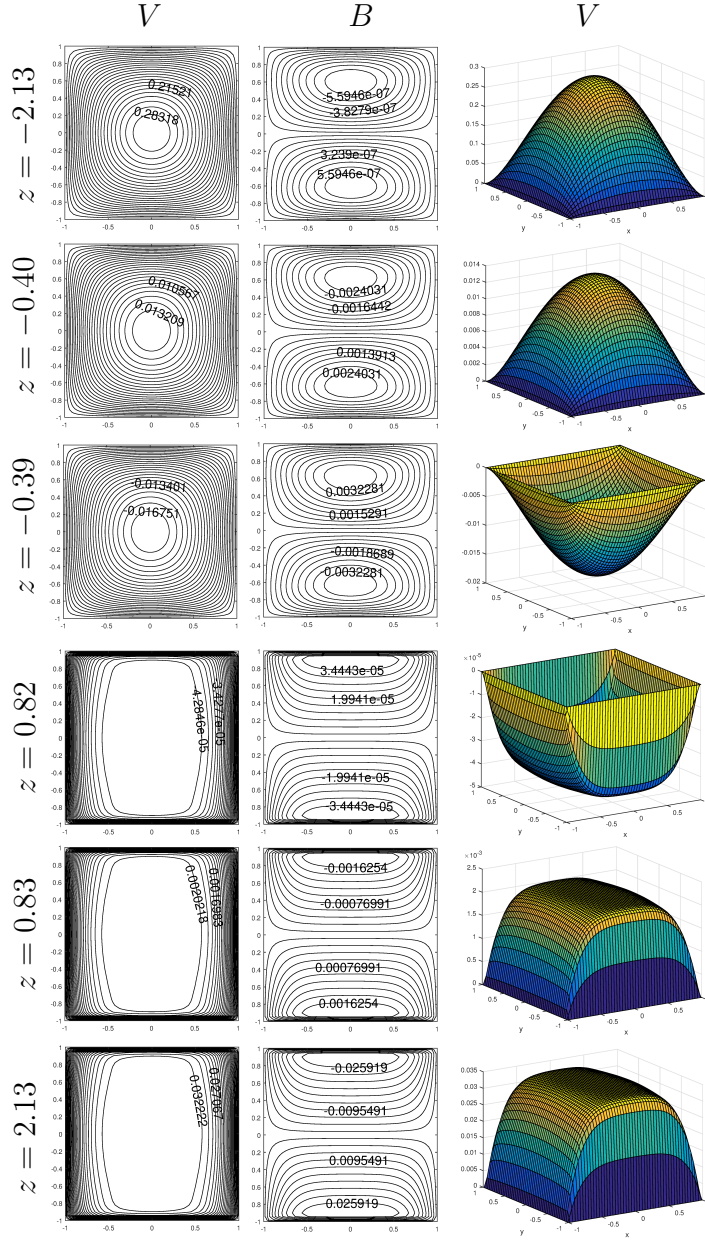


Figure 4.50: Velocity and induced magnetic field ($V = B = 0$ duct walls), $M = 30$, $R_m = 25$. Axially-changing magnetic field, $\alpha = \pi/2$.

When the Hartmann walls (walls perpendicular to the applied magnetic field, top and bottom walls) are changed from insulated to perfectly conducting (Figure 4.44 (b)), the points on the pipe-axis where the flow is reversed are not changed. This can be seen from Figures 4.51 and 4.52 which are drawn for $M = 30$ and $R_m = 1$ where

Figure 4.51 is still with the $V = B = 0$ wall conditions. On the other hand, the flow is greatly affected aligning in terms of two loops in front of side walls parallel to applied magnetic field. The current lines do not close themselves in front of the Hartmann walls anymore due to the $\frac{\partial B}{\partial n} = 0$ boundary conditions.

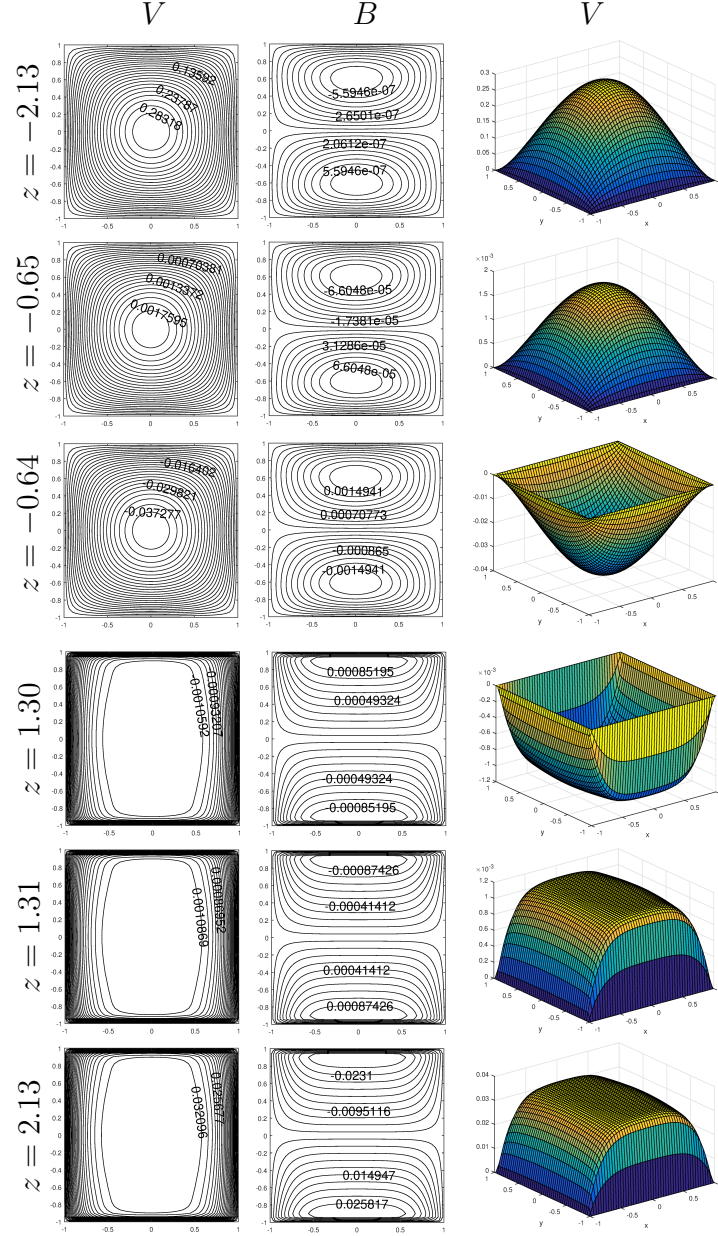


Figure 4.51: Velocity and induced magnetic field ($V = B = 0$ duct walls), $M = 30$, $R_m = 1$. Axially-changing magnetic field, $\alpha = \pi/2$.

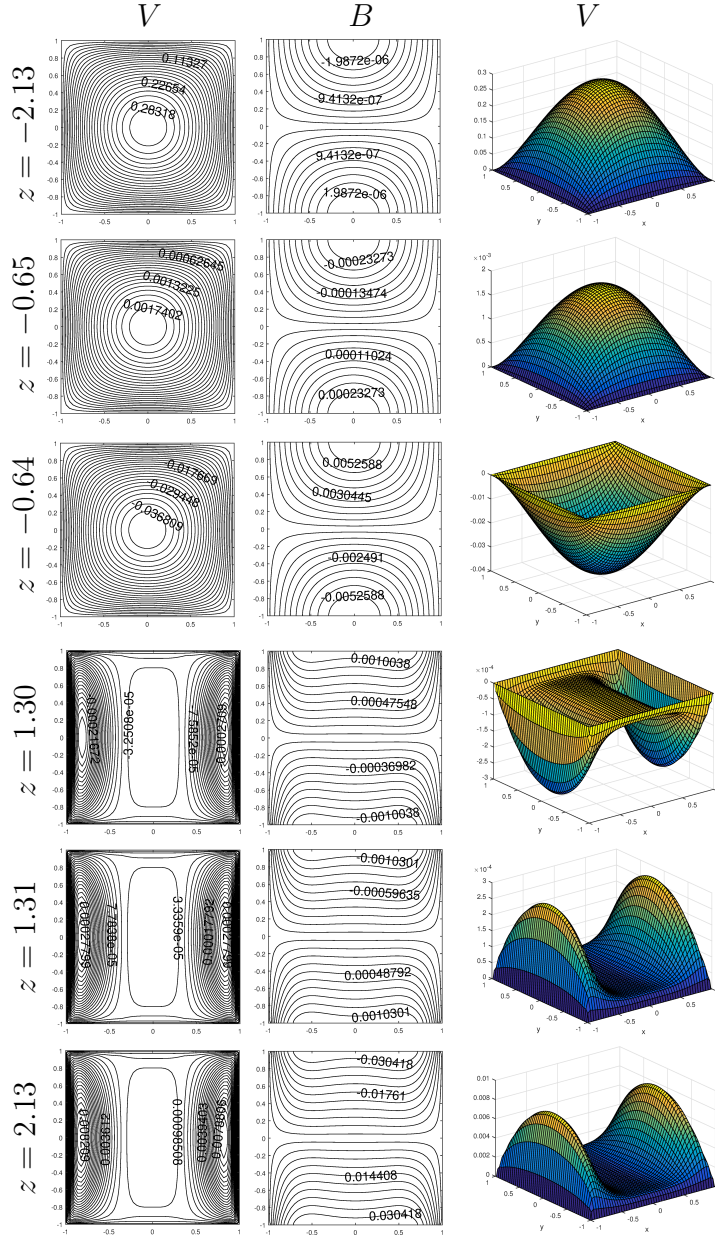


Figure 4.52: Velocity and induced magnetic field ($V = 0$, $B = 0$ side walls, $V = 0$, $\frac{\partial B}{\partial n} = 0$ Hartmann walls), $M = 30$, $R_m = 1$. Axially-changing magnetic field, $\alpha = \pi/2$.

The inclusion of electric potential Φ requires the solution of discretized DRBEM equations (4.28). When the unknowns V , B and Φ are obtained numerically for the case $M = 30$, $R_m = 2$, we see from Figures 4.53 and 4.54 that, the velocity and

induced magnetic field contours stay exactly the same since velocity and induced magnetic field equations do not contain Φ . Thus, the flow reversion locations are also the same. For Dirichlet type boundary condition for Φ , $\Phi = 0$ and $V = B = 0$, electric potential curves show the same behavior in opposite direction with induced current B curves but in different magnitude. For the Neumann boundary conditions $\frac{\partial \Phi}{\partial n} = 0$ on the top and bottom walls, the flow and the induced current profiles are again the same, only the electric potential lines do not close in front of the Hartmann walls anymore.

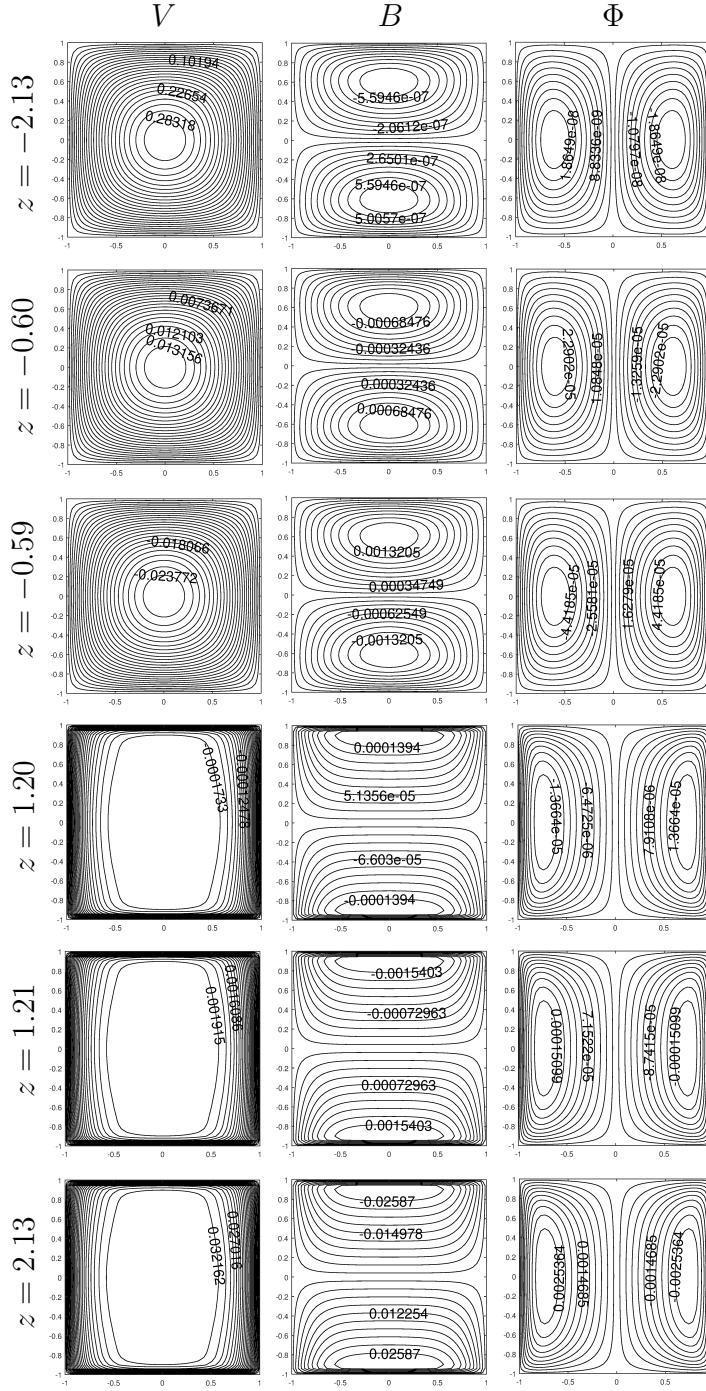


Figure 4.53: Velocity, induced magnetic field and electric current ($V = B = \Phi = 0$ walls), $M = 30$, $R_m = 2$. Axially-changing magnetic field, $\alpha = \pi/2$.

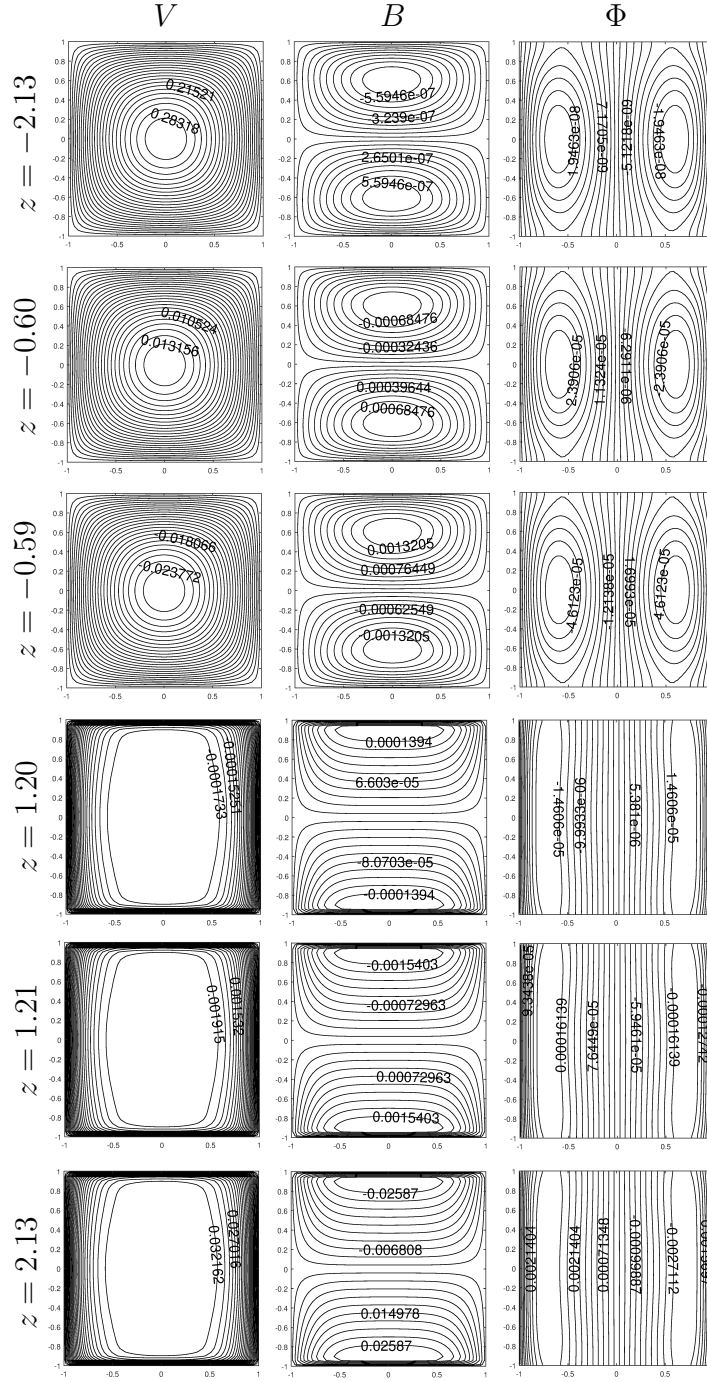


Figure 4.54: Velocity, induced magnetic field and electric current ($V = B = 0$, $\Phi = 0$ side walls, $\frac{\partial \Phi}{\partial n} = 0$ Hartmann walls), $M = 30$, $R_m = 2$. Axially-changing magnetic field, $\alpha = \pi/2$.

In Chapter 4, the numerical results of the MHD duct flow problems are simulated in four different parts. In Section 4.1, the numerical result are presented for the MHD

flow and heat transfer equations containing variable viscosity coefficient. Then, unsteady MHD duct flow under the influence of a time-varied applied magnetic field $B_0(t)$ is considered with different types of time-varied functions $f(t)$ in Section 4.2. Furthermore, in Sections 4.3 and 4.4 the numerical results of the MHD duct flow problems under the effect of axially changing applied magnetic field $B_0(z)$ are displayed. Sections 4.3 and 4.4 are also supplied with electric potential equation giving flow and electric potential profiles in Section 4.3 whereas Section 4.4 presents the full problem solutions as the velocity, induced magnetic field as well as electric potential.

CHAPTER 5

CONCLUSION

This thesis provides the numerical solutions of four kinds of two-dimensional, steady or unsteady, fully-developed MHD problems. The electrically conducting fluid inside the rectangular duct is influenced by a uniform magnetic field in the first problem, a time-varied magnetic field in the second problem and an axial-dependent magnetic field in the third and fourth problems. Mainly, the BEM is applied for the solution of the MHD duct flow equations, differing as the parametric BEM or the DRBEM according to the dominating operator of the equations. The parametric BEM procedure is carried out with the help of a Levi function which treats the variable viscosity in the diffusion term directly to reduce the differential equation into a boundary-domain integral equation, while the DRBEM is used with the fundamental solution of Laplace equation to transform the boundary value problems into the system of boundary integral equations. The linear radial basis function approximation is used for the inhomogeneity in the usage of DRBEM. In most of the simulations, constant boundary elements are used to discretize the boundaries of the problem domains.

First, the numerical solution of the convection-diffusion type MHD flow problem with temperature dependent viscosity and heat transfer is obtained in the absence of induced magnetic field. The parametric BEM and DRBEM are both used for obtaining numerical results. The momentum and energy equations are solved iteratively. The use of the parametric BEM makes it possible to treat the diffusion operator of the equation in its original form. Although, the obtained results from parametric BEM and DRBEM differ slightly in maximum values of the velocity and temperature magnitudes, both methods capture the well known flattening property of the MHD duct flow as Hartmann number increases. The numerical results also show that, parametric

BEM with the same number of boundary elements requires more CPU time than the one in DRBEM.

Then, the transient behavior of the MHD duct flow is presented in terms of the velocity and induced magnetic field when the flow is subjected to a time-varied oblique magnetic field. The implicit forward finite difference approximation is used for the time derivatives. This MHD flow problem is solved in two cases. In the first case, the Reynolds and magnetic Reynolds number are taken as 1 which enables to write the MHD flow equations in decoupled form. The simulations of the flow behavior are obtained by using several definitions of time-dependent functions such as polynomial, exponential, trigonometric, step and impulse type functions. Increasing Hartmann number and the orientation of the magnetic field affect the flow behavior for each type of functions. Then, in the second case, Reynolds and magnetic Reynolds numbers are involved forcing the MHD flow equations to be solved in coupled form. Capturing an elliptical elongation for the flow in the direction of applied magnetic field at a certain time level is the common feature for all the type of functions considered. The flow elongation repeats itself periodically if trigonometric function is used. The elongation starts at an earlier time level in the flow when the Hartmann number increases or the applied magnetic field is oblique rather than being horizontal. As time passes, the Hartmann layers are more pronounced while the side layers get thinner due to the elongation of the flow. The well-known behavior of the MHD flow, drop in the velocity magnitude and the formation of the boundary layers are observed. Also, an increase in Reynolds or magnetic Reynolds numbers postpones the time level where the flow elongates.

Afterwards, the DRBEM solution of the MHD duct flow under the effect of an axially changing imposed magnetic field is obtained. The induced magnetic field is neglected due to small magnetic Reynolds number, however the electric potential from the divergence of Ohm's law is taken into consideration. The influences of the Hartmann number and the electrical conductivity of the walls on the flow are presented. The results show that, the Hartmann number controls the thickness of the boundary layers, while the wall conductivity determines the structure of the flow. The maximum value of the velocity occurs on the non-conducting or conducting side walls instead of the centre of the duct causing M-shape for the flow. Moreover, an increase in the Hart-

mann number leads to stronger fluctuation on the flow behavior on the side layers for the case of variably conducting walls. The three-dimensional effects of the MHD flow are obtained in the pipe when axially varying magnetic field is applied at consecutive two points for which the flow is fully-developed. MHD flow shows a highly M-shape profile due to the side layers developed. Therefore, the structure a redistribution of the flow greatly depend on the strength of the axially changing applied magnetic field throughout the pipe.

Furthermore, the DRBEM solution of the MHD duct flow under the effect of an axially changing magnetic field is presented taking also into consideration of the induced magnetic field in ducts where the magnets are located at several points through the pipe. The MHD flow equations are solved in terms of velocity, induced magnetic field and electric potential with the fully-developed flow assumption between these points. This way, the three-dimensional effects on the MHD flow are obtained throughout the pipe. The flow behavior is investigated for increasing values of problem parameters, Hartmann number and magnetic Reynolds number. The numerical results show that, axially changing magnetic field makes the flow to change its direction at a certain position of the pipe-axis. But then, the flow turns back to the pipe-axis direction after traveled a shorter distance for the case of increasing Hartmann number than the case of increasing magnetic Reynolds number.

To conclude, the DRBEM is the most effective numerical method for the solution of the MHD duct flow problems through pipes or channels in the presence or absence of induced magnetic field for the most general form of wall conductivity conditions. It provides both the unknown (velocity, temperature, induced magnetic field, electric potential) itself and its normal derivative at once on the duct walls by only discretizing the boundary of the considered problem which reduces the dimension of the final discretized system. Thus, the numerical solutions are obtained with a low computational cost compared to the other domain type discretization techniques.

REFERENCES

- [1] F. Durst, *Fluid Mechanics: An Introduction to the Theory of Fluid Flows*. Springer Science & Business Media, 2008.
- [2] U. Müller and L. Bühler, *Magnetofluidynamics in Channels and Containers*. Springer, 2001.
- [3] O. Kolditz, *Computational Methods in Environmental Fluid Mechanics*. Springer Science & Business Media, 2002.
- [4] J. N. Reddy, *An Introduction to the Finite Element Method*. McGraw-Hill, New York, 2006.
- [5] C. A. Brebbia and J. Dominguez, *Boundary Elements - An Introductory Course*. WIT Press, 1996.
- [6] S. E. Mikhailov, “Localized boundary-domain integral formulations for problems with variable coefficients,” *Engineering Analysis with Boundary Elements*, vol. 26, no. 8, pp. 681-690, 2002.
- [7] P. W. Partridge, C. A. Brebbia, and L. C. Wrobel, *The Dual Reciprocity Boundary Element Method*. Computational Mechanics Publications, Southampton, Boston, 1992.
- [8] D. J. Tritton, *Physical Fluid Dynamics*. Oxford Science Publications, 1988.
- [9] D. L. Young, C. W. Chen, C. M. Fan, K. Murugesan and C. C. Tsai, “The method of fundamental solutions for Stokes flow in a rectangular cavity with cylinders,” *European Journal of Mechanics. B Fluids*, vol. 24, no. 6, pp. 703-716, 2005.
- [10] A. J. Chorin, “Numerical solution of the Navier-Stokes equations,” *Mathematics of Computation*, vol. 22, no. 104, pp. 745-762, 1968.
- [11] J. M. C. Pereira, M. H. Kobayashi and J. C. F. . Pereira, “A Fourth-order-accurate

- finite volume compact method for the incompressible Navier–Stokes solutions,” *Journal of Computational Physics*, vol. 167, no. 1, pp. 217-243, 2001
- [12] H. C. Elman, “Preconditioning strategies for models of incompressible flow,” *Journal of Scientific Computing*, vol. 25, no. 112, pp. 347-366, 2005
- [13] C. E. Baumann and J. T. Oden, “A discontinuous hp finite element method for the Euler and Navier–Stokes equations,” *International Journal for Numerical Methods in Fluids*, vol. 31, no. 1, pp. 79-95, 1999.
- [14] L. Dragoş, *Magnetofluid Dynamics*. Abacus Press, 1975.
- [15] M. E. Sayed-Ahmed and H. A. Attia, “MHD flow and heat transfer in a rectangular duct with temperature dependent viscosity and Hall effect,” *International Communications in Heat and Mass Transfer*, vol. 27, no. 8, pp. 1177-1187, 2000.
- [16] F. M. White, *Viscous Fluid Flow*. 2nd Ed., McGraw-Hill, 1991.
- [17] G. L. Morini, “Analytical determination of the temperature distribution and Nusselt numbers in rectangular ducts with constant axial heat flux,” *International Journal of Heat and Mass Transfer*, vol. 43, no. 5, pp. 741-755, 2000.
- [18] J. Shercliff, *A Textbook of Magnetofluidynamics*. Pergamon Press, 1965.
- [19] P. A. Davidson, *An Introduction to Magnetohydrodynamics*. Cambridge University Press, 2001.
- [20] J. P. Garandet, T. Alboussiere and R. Moreau, “Buoyancy driven convection in a rectangular enclosure with a transverse magnetic field ,” *International Journal of Heat and Mass Transfer*, vol. 35, no. 4, pp. 741-748, 1992.
- [21] C. Xie and J. P. Hartnett, “Influence of variable viscosity of mineral oil on laminar heat transfer in a 2:1 rectangular duct,” *International Journal of Heat and Mass Transfer*, vol. 35, no. 3, pp. 641-648, 1992.
- [22] S. Shin, Y. I. Cho, W. K. Gingrich and W. Shyy, “Numerical study of laminar heat transfer with temperature dependent fluid viscosity in a 2:1 rectangular duct,” *International Journal of Heat and Mass Transfer*, vol. 36, no. 18, pp. 4365-4373, 1993.

- [23] A. Pinarbasi and M. Imal, "Nonisothermal channel flow of a non-newtonian fluid with viscous heating," *International Communications in Heat and Mass Transfer*, vol. 29, no. 8, pp. 1099-1107, 2002.
- [24] A. Pinarbasi, C. Ozalp and S. Duman, "Influence of variable thermal conductivity and viscosity for nonisothermal fluid flow," *Physics of Fluids*, vol. 17, no. 3, pp. 038109, 2005.
- [25] M. A. Hossain and M. S. Munir, "Natural convection flow of a viscous fluid about a truncated cone with temperature dependent viscosity and thermal conductivity," *International Journal of Numerical Methods for Heat & Fluid Flow*, vol. 11, no. 6, pp. 494-510, 2001.
- [26] D. R. Jenkins, "Rolls versus squares in thermal convection of fluids with temperature-dependent viscosity," *Journal of Fluid Mechanics*, vol. 178, pp. 491-506, 1987.
- [27] H. A. Attia, "Influence of temperature dependent viscosity on the MHD-channel flow of dusty fluid with heat transfer," *Acta Mechanica*, vol. 151, pp. 89-101, 2001.
- [28] H. A. Attia, "Influence of temperature-dependent viscosity on the MHD Couette flow of dusty fluid with heat transfer," *Differential Equations and Nonlinear Mechanics*, vol. 2006, pp. 1-14, 2006.
- [29] M. E. Sayed-Ahmed, "Numerical solution of power law fluids flow and heat transfer with a magnetic field in a rectangular duct," *International Communications in Heat and Mass Transfer*, vol. 33, no. 9, pp. 1165-1176, 2006.
- [30] C. Evcin, Ö. Uğur and M. Tezer-Sezgin, "Determining the optimal parameters for the MHD flow and heat transfer with variable viscosity and Hall effect," *Computers & Mathematics with Applications*, vol. 76, no. 6, pp. 1338-1355, 2018.
- [31] B. Singh and J. Lal, "MHD axial flow in a triangular pipe under transverse magnetic field," *Indian Journal of Pure and Applied Mathematics*, vol. 9, no. 2, pp. 101-115, 1978.

- [32] B. Singh and J. Lal, "Finite element method in magnetohydrodynamic channel flow problems," *International Journal for Numerical Methods in Engineering*, vol. 18, no. 7, pp. 1104-1111, 1982.
- [33] M. Tezer-Sezgin and S. Köksal, "Finite element method for solving MHD flow in a rectangular duct," *International Journal for Numerical Methods in Engineering*, vol. 28, pp. 445-459, 1989.
- [34] M. Tezer-Sezgin, "Solution of magnetohydrodynamic flow in a rectangular duct by differential quadrature method," *Computers & Fluids*, vol. 33, no. 4, pp. 533-547, 2004.
- [35] M. Tezer-Sezgin and M. Gürbüz, "MHD convection flow in a constricted channel," *Analele Stiintifice ale Universitatii Ovidius Constanta-Seria Matematica*, vol. 26, no. 2, pp. 267-283, 2018.
- [36] İ. Çelik, "Solution of magnetohydrodynamic flow in a rectangular duct by Chebyshev collocation method," *International Journal for Numerical Methods in Fluids*, vol. 66, no. 10, pp. 1325-1340, 2011.
- [37] S. H. Aydın and M. Tezer-Sezgin, "A DRBEM solution for MHD pipe flow in a conducting medium," *Journal of Computational and Applied Mathematics*, vol. 259, pp. 720-729, 2014.
- [38] C. Bozkaya and M. Tezer-Sezgin, "Magnetohydrodynamic pipe flow in annular-like domains," *European Journal of Computational Mechanics*, vol. 26, no. 4, pp. 394-410, 2017.
- [39] S. L. L. Verardi, J. M. Machado and J. R. Cardoso, "The element-free Galerkin method applied to the study of fully developed magnetohydrodynamic duct flows," *IEEE Transactions on Magnetics*, vol. 38, no. 2, pp. 941-944, 2002.
- [40] S. C. Gupta and B. Singh, "Unsteady magnetohydrodynamic flow in a circular pipe under a transverse magnetic field," *Physics of Fluids*, vol. 13, no. 2, pp. 346-352, 1970.
- [41] M. Tezer-Sezgin and M. Gürbüz, "Numerical solution and stability analysis of transient MHD duct flow," *Journal of Balikesir University Institute of Science and Technology*, vol. 20, no. 3, pp. 53-61, 2018.

- [42] M. Dehghan and D. Mirzaei, "Meshless local boundary integral equation (LBIE) method for the unsteady magnetohydrodynamic (MHD) flow in rectangular and circular pipes," *Computer Physics Communications*, vol. 180, no. 9, pp. 1458-1466, 2009.
- [43] N. Bozkaya and M. Tezer-Sezgin, "Time-domain BEM solution of convection-diffusion-type MHD equations," *International Journal for Numerical Methods in Fluids*, vol. 56, no. 11, pp. 1969-1991, 2008.
- [44] B. Singh and J. Lal, "Finite element method for unsteady MHD flow through pipes with arbitrary wall conductivity," *International Journal for Numerical Methods in Fluids*, vol. 4, no. 3, pp. 291-302, 1984.
- [45] N. B. Salah, A. Soulaïmani and W. G. Habashi, "A finite element method for magnetohydrodynamics," *Computer Methods in Applied Mechanics and Engineering*, vol. 190, no. 43-44, pp. 5867-5892, 2001.
- [46] C. Bozkaya and M. Tezer-Sezgin, "Boundary element solution of unsteady magnetohydrodynamic duct flow with differential quadrature time integration scheme," *International Journal for Numerical Methods in Fluids*, vol. 51, no. 5, pp. 567-584, 2006.
- [47] P. Senel and M. Tezer-Sezgin, "DRBEM solutions of Stokes and Navier–Stokes equations in cavities under point source magnetic field," *Engineering Analysis with Boundary Elements*, vol. 64, pp. 158-175, 2016.
- [48] E. E. Tzirtzilakis, V. D. Sakalis, N. G. Kafoussias and P. M. Hatzikonstantinou, "Biomagnetic fluid flow in a 3D rectangular duct," *International Journal for Numerical Methods in Fluids*, vol. 44, pp. 1279-1298, 2004.
- [49] E. E. Tzirtzilakis and M. A. Xenos, "Biomagnetic fluid flow in a driven cavity," *Meccanica*, vol. 48, pp. 187-200, 2013.
- [50] V. Bandaru, "Magnetohydrodynamic duct and channel flows at finite magnetic reynolds numbers," Ph.D. Thesis, Fakultät für Maschinenbau der Technischen Universität Ilmenau, 2015.
- [51] V. Bandaru, T. Boeck, D. Krasnov and J. Schumacher, "A hybrid finite difference-boundary element procedure for the simulation of turbulent MHD

- duct flow at finite magnetic Reynolds number,” *Journal of Computational Physics*, vol. 304, pp. 320-339, 2016.
- [52] M. Dehghan and D. Mirzaei, “Meshless local petrov–galerkin (MLPG) method for the unsteady magnetohydrodynamic (MHD) flow through pipe with arbitrary wall conductivity,” *Applied Numerical Mathematics*, vol. 59, pp. 1043–1058, 2009.
- [53] H. Kamamaru, K. Shimoda and K. Itoh, “Three-dimensional numerical calculations on liquid-metal magneto-hydrodynamic flow through circular pipe in magnetic-field inlet-region,” *Journal of Nuclear Science and Technology*, vol. 44, no. 5. pp. 714-722, 2007.
- [54] D. Sarma, G. C. Hazarika and P. N. Deka, “Numerical study of liquid metal MHD flow through a square duct under the action of strong transverse magnetic field,” *International Journal of Computer Applications*, vol. 71, no. 8. pp. 29-32, 2013.
- [55] X. Cai, H. Qiang, S. Dong, J. Lu and D. Wang, “Numerical simulations on the fully developed liquid-metal MHD flow at high Hartmann numbers in the rectangular duct,” *In 2nd International Conference on Applied Mathematics, Modelling and Statistics Application (AMMSA) 2018*, vol. 143, pp. 68-71, Atlantis Press, 2018.
- [56] C. N. Kim, “Numerical analysis of a magnetohydrodynamic duct flow with flow channel insert under a non-uniform magnetic field,” *Journal of Hydrodynamics*, vol. 30, no. 6. pp. 1134-1142, 2018.
- [57] A. Sterl, “Numerical simulation of liquid-metal MHD flows in rectangular ducts,” *Journal of Fluid Mechanics*, vol. 216, pp. 161-191, 1990.
- [58] T. Q. Hua and J. S. Walker, “MHD flow in rectangular ducts with inclined non-uniform transverse magnetic field,” *Fusion Engineering and Design*, vol. 27, pp. 703-710, 1995.
- [59] V. Klüber, L. Bühler and C. Mistrangelo, “Numerical simulation of 3D magnetohydrodynamic liquid metal flow in a spatially varying solenoidal magnetic field,” *Fusion Engineering and Design*, vol. 156, pp. 111659, 2020.

- [60] J. S. Walker, "Liquid-metal flow in a rectangular duct with a non-uniform magnetic field," *Argonne Nat. Lab. Rep. ANL/FPP/TM-207*, 1986.
- [61] A. Ting, T. Q. Hua, J. S. Walker and B. F. Picologlou, "Liquid-metal flow in a rectangular duct with thin metal walls and with a non-uniform magnetic field," *International Journal of Engineering Science*, vol. 31, no. 3, pp. 357-372, 1993.
- [62] L. Bühler and C. Mistrangelo, "Magnetohydrodynamic flows in breeder units of a HCLL blanket with spatially varying magnetic fields," *Fusion Engineering and Design*, vol. 88, pp. 2314-2318, 2013.
- [63] M. A. Al-Jawary and L. C. Wrobel, "Numerical solution of two-dimensional mixed problems with variable coefficients by the boundary-domain integral and integro-differential equation methods," *Engineering Analysis with Boundary Elements*, vol. 35, no. 12, pp. 1279-1287, 2011.
- [64] L. W. Johnson and R. D. Riess, *Numerical Analysis*. Addison-Wesley Publishing Company, 1977.
- [65] M. Tezer-Sezgin, "Boundary element method solution of MHD flow in a rectangular duct," *International Journal for Numerical Methods in Fluids*, vol. 118, no. 10, pp. 937-952, 1994.
- [66] B. Pekmen, "DRBEM applications in fluid dynamics problems and DQM solutions of hyperbolic equations," Ph.D. Thesis, Middle East Technical University, 2014.
- [67] M. Tezer-Sezgin, "Solution of magnetohydrodynamic flow in a rectangular duct by differential quadrature method," *Computers & Fluids*, vol. 33, no. 4, pp. 533-547, 2004.
- [68] E. Ebrek Kaya and M. Tezer-Sezgin, "DRBEM solution of MHD flow in a rectangular duct with time-varied external magnetic field," *Engineering Analysis with Boundary Elements*, vol. 117, pp. 242-250, 2020.

CURRICULUM VITAE

PERSONAL INFORMATION

Surname, Name: Ebren Kaya, Elif

Nationality: Turkish (TC)

Date and Place of Birth: 13.06.1990, Ankara

Marital Status: Married

E-mail:: elifebren90@gmail.com

EDUCATION

Degree	Institution	Year of Graduation
Ph.D.	Department of Mathematics, Middle East Technical University	2021
B.S.	Department of Mathematics, Middle East Technical University	2013

PROFESSIONAL EXPERIENCE

Year	Place	Enrollment
2014-2021	Department of Mathematics, Middle East Technical University	Research Assistant
2021-Present	TÜBİTAK	Specialist

PROGRAMMING LANGUAGES

C, Matlab, LaTeX

FOREIGN LANGUAGES

English (fluent), Italian (beginner)

PUBLICATIONS

International Journal Publications

1. E. Ebren Kaya, M. Tezer-Sezgin, *The BEM solutions of MHD flow and heat transfer in a rectangular duct with temperature dependent viscosity*, European Journal of Computational Mechanics, vol. 28, no. 1-2, pp. 97-122, 2019.
2. E. Ebren Kaya, M. Tezer-Sezgin, *DRBEM solution of MHD flow in a rectangular duct with time-varied external magnetic field*, Engineering Analysis with Boundary Elements, vol. 117, pp. 242-250, 2020.
3. E. Ebren Kaya, M. Tezer-Sezgin, *DRBEM solution of MHD flow in a rectangular duct under axial-dependent external magnetic field*, Progress in Computational Fluid Dynamics, (submitted).

International Conference Proceedings

1. E. Ebren Kaya, M. Tezer-Sezgin, *The application of BEM to MHD flow and heat transfer in a rectangular duct with temperature dependent viscosity*, Advances in Boundary Element & Meshless Techniques XIX-BETEQ 2018, Malaga, Spain, 9-11 July 2018, pp. 83-89.
2. E. Ebren Kaya, M. Tezer-Sezgin, *DRBEM solutions of magnetohydrodynamic duct flow under time-varied obliqu magnetic field*, Advances in Boundary Element & Meshless Techniques XX-BETEQ 2019, Palermo, Italy, 22-24 July 2019, pp. 25-32.

AWARDS

- Middle East Technical University, Honor student degree, 2013

- The Scientific and Technological Research Council of Turkey (TÜBİTAK), National Ph.D. Fellowship Programme (2211-A), 2014-2018